

APPLICATIONS OF THE MULTIFUNCTIONAL MAGNETIC
NANOPARTICLES FOR DEVELOPMENT OF MOLECULAR THERAPIES FOR
THE BREAST CANCER

A THESIS SUBMITTED TO
THE GRADUATE SCHOOL OF NATURAL AND APPLIED SCIENCES
OF
MIDDLE EAST TECHNICAL UNIVERSITY

BY

ELİF AŞIK

IN PARTIAL FULFILLMENT OF THE REQUIREMENTS
FOR
THE DEGREE OF DOCTOR OF PHILOSOPHY
IN
BIOTECHNOLOGY

NOVEMBER 2015

Approval of the Thesis;

**APPLICATIONS OF THE MULTIFUNCTIONAL MAGNETIC
NANOPARTICLES FOR DEVELOPMENT OF MOLECULAR THERAPIES
FOR BREAST CANCER**

submitted by **ELİF AŞIK** in a partial fulfillment of the requirements for the degree of
**Doctor of Philosophy in Biotechnology Department, Middle East Technical
University** by

Prof. Dr. Gülbin Dural Ünver
Dean, Graduate School of **Natural and Applied Sciences**

Prof. Dr. Filiz B. Dilek
Head of **Department, Biotechnology**

Prof. Dr. N.Tülin Güray
Supervisor, **Biology Dept., METU**

Prof. Dr. Mürvet Volkan
Co-Supervisor **Chemistry Dept., METU**

Examining Committee Members:

Prof. Dr. İhsan Gürsel
Molecular Biology and Genetic Dept., Bilkent University

Prof. Dr. N.Tülin Güray
Biology Dept., METU

Assoc.Prof.Dr. Can Özen
Biotechnology Dept., METU

Assoc.Prof.Dr. Bulent Ozpolat
Experimental Therapeutics Dept., Texas University (USA)

Assoc.Prof.Dr. Elif Erson Bensan
Biology Dept., METU

Date: 19 / 11 / 2015

I hereby declare that all information in this document has been obtained and presented in accordance with academic rules and ethical conduct. I also declare that, as required by these rules and conduct, I have fully cited and referenced all materials and results that are not original to this work.

Name, Last name: Elif Aşık

Signature:

ABSTRACT

APPLICATIONS OF THE MULTIFUNCTIONAL MAGNETIC NANOPARTICLES FOR DEVELOPMENT OF MOLECULAR THERAPIES FOR BREAST CANCER

Aşık, Elif

Ph.D., Department of Biotechnology

Supervisor: Prof. Dr.N.Tülin Güray

Co-supervisor: Prof.Dr.Mürvet Volkan

November 2015, 181 pages

The understanding of how magnetic nanoparticles (MNPs) interact with living system is one of the prerequisite pieces of information needed to be obtained before any further development for desired biomedical applications. In this study, Cobalt Ferrite magnetic nanoparticles (CoFe-MNPs) in their naked and silica-coated forms were characterized. In vitro cell culture for their likely cytotoxicity and genotoxicity potential were examined. The apoptosis, lipid peroxidation, ROS formation and oxidative stress related gene expression levels of some drug metabolizing enzymes in human cancer (MDA-MB-231, MCF-7) and non-cancer (MCF-10A) breast cell lines were analyzed in response to MNPs treatment. Our results revealed that, uptake of the highest amounts of CoFe-MNPs was observed in metastatic cells and the uptake of the silica coated CoFe-MNPs were higher than the naked ones in all cells. Naked CoFe-MNPs represented higher levels of cytotoxicity, genotoxicity and ROS generation compared to silica coated CoFe-MNPs. Silica coated CoFe-MNPs were functionalized with COOH groups for further modifications. 2-amino-2-deoxy-glucose (2DG), which is a potential targeting molecule for cancer treatment, was conjugated on silica coated CoFe-MNPs surface through -

COOH groups. Internalization and accumulation of both -COOH modified (COOH-MNPs) and 2DG conjugated (2DG-MNPs) were studied in MDA-MB-231 and MCF-7 cancer and MCF-10A non-cancer breast cells by transmission electron microscopy (TEM), Prussian blue staining and Inductively Coupled Plasma Optical Emission Spectroscopy (ICP-OES). According to our results, it was apparent that 2DG-MNPs were internalized more efficiently than COOH-MNPs under same conditions, in all cell types studied. Moreover, the highest amount of uptake was observed in MDA-MB-231 cells, which is followed by MCF-7 and normal MCF-10A for both MNPs.

The apoptotic effects of 2DG-MNPs was further evaluated, and it was found that apoptosis was not induced at low concentration of 2DG-MNPs, regardless of the cell types, whereas dramatic cell death was observed at higher concentrations. In addition, the gene expression levels of some drug metabolizing enzymes, two Phase I (CYP1A1, CYP1B1) and two Phase II (GSTM3, GSTZ1) were also seen to increase at high concentration of 2DG-MNPs, whereas at low concentration no induction was observed. Eukaryotic elongation factor-2 kinase (eEF2K) is gaining potential as a prognostic marker and therapeutic target to treat breast cancer. Hence, eEF2K siRNA was decorated on silica coated CoFe-MNPs through -COOH groups and the expression and role of this gene investigated in the BRCA1 mutated breast cancer cells (MDA-MB-436, HCC-1937). According to our results, the silencing of eEF2K using siRNA decorated MNPs inhibited colony formation; proliferation, migration and invasion of BRCA1 mutated cells. Furthermore, the down modulation of eEF2K was investigated in an orthotopic model of BRCA1 mutated breast cancer in nude mice *in vivo* by through systematically administration of eEF2K siRNA decorated MNPs.

In vivo silencing of eEF2K lead to inhibition of molecules and pathways that are involved in migration/invasion (Src/FAK/paxillin), angiogenesis (VEGF), proliferation (c-Myc), cell cycle (CyclinD1), survival/drug resistance (PI3K/Akt) translational regulation (4E-BP1). Taken together, our data suggest, for the first time, which eEF2K is associated with tumorigenesis and progression of BRCA1 mutated breast cancer and may be a novel potential therapeutic target in this cancer.

Keywords: Breast cancer, uptake, cytotoxicity, genotoxicity, ROS generation, silica coating, CoFe-MNP, 2-amino-2-deoxy-glucose, targeting therapy, 2DG-MNP BRCA1 mutated cells, eEF2 kinase, proliferation, invasion/metastasis, angiogenesis, tumorigenesis, apoptosis nanotechnology, siRNA

ÖZ

ÇOK FONKSİYONLU MANYETİK NANOPARÇACIKLARIN MEME KANSERİ İÇİN MOLEKÜLER TEDAVİLERİN GELİŞTİRİLMESİNDE UYGULANMASI

Aşık, Elif

Doktora, Biyoteknoloji Bölümü

Tez Yöneticisi: Prof.Dr.N.Tülin Güray

Ortak Tez Yöneticisi: Prof. Dr. Mürvet Volkan

Kasım 2015, 181 sayfa

Manyetik nanoparçacıkların (MNP), biyolojik uygulamalarda kullanılabilmesi için öncelikle canlı sistemlerle ilişkisini anlamak gereklidir. Bu nedenle, bu çalışmada Kobalt ferrite manyetik nanoparçacıkların silika kaplı ve kapsız formlarının sitotoksiteleri, genotoksiteleri, apoptoz, lipid peroksidasyon, reaktif oksijen türleri oluşturma potansiyelleri ve bazı ilaç metabolize eden enzimlerin gen ekspresyon düzeyleri kanserli (MDA-MB-231 ve MCF-7) ve kanserli olmayan (MCF-10A) insan meme hücrelerinde değerlendirildi. Kobalt ferrit MNP'ların metastatik hücrelerde alımının daha fazla olduğu ve silika kaplı kobalt ferrit MNP'ların kapsız olanlara göre bütün hücrelere daha fazla girdiği gözlemlenmiştir. Yüzeyi kapsız Kobalt ferrit MNP'lar silika kaplı olanlara göre daha fazla sitotoksite genotoksite göstermiş ve reaktif oksijen türleri oluşumunu artmıştır. Silikalı yüzey, bu etkilerin önemli ölçüde azaltmış ve parçacıkların hücre içine girmesi arttırmıştır.

Silika kaplı kobalt ferrit MNP'lar, daha sonraki modifikasyonlar için -COOH grupları ile fonksiyonel hale getirilmiştir. 2-amino-2-deoksi glikoz, kanser tedavisi için potansiyel hedefleme molekülü olarak, silika kaplı MNP'ların COOH yüzeylerinden bağlanmıştır. Her iki COOH modifiye ve 2DG bağlı MNP'ların hücre içine alımı ve birikmesi, geçirimli electron mikroskopu, Prussian mavisi, ICP-OES yöntemi ile MDA-MB-231, MCF-7 ve MCF-10A hücrelerinde araştırılmıştır. Elde edilen sonuçlara göre 2DG-

MNP'lar, COOH-MNP'lara göre daha fazla hücrelerin içine alındığı ve en fazla alımın MDA-MB-231 hücrelerinde olduğu, bunu MCF-7 ve MCF-10A hücrelerinin takip ettiği bulunmuştur. 2DG-MNP'ların, hücre tipi fark etmeksizin düşük konsantrasyonlarda apoptozu tetiklemediği fakat yüksek konsantrasyonda tetiklediği gözlemlenmiştir. Ayrıca dört ilaç metabolize eden iki faz 1 (CYP1A1, CYP1B1) ve iki faz 2 (GSTM3, GSTZ1) enzimlerin gen ekspresyon düzeyleri düşük konsantrasyonda artmazken yüksek konsantrasyonda arttığı bulunmuştur.

Ekaryotik elongasyon factor 2-kinaz, meme kanseri tedavisi de prognostik işaret ve terapötik hedef olarak artan bir potansiyeli vardır. Bu nedenle eEF2k siRNA, öncelikle silika kaplı CoFe MNP'ların COOH gruplarından bağlanmıştır. Daha sonra bu genin rolü BRCA1+ mutant meme kanseri hücrelerinde (MDA-MB-436, HCC-1937) araştırılmıştır. Sonuçlarımıza göre, eEF2 kinazın siRNA bağlı MNP'lar kullanılarak susturulması, koloni oluşumunu, proliferasyonu, migrasyonu ve invazyonu bu hücrelerde anlamlı bir şekilde inhibe edildiği bulunmuştur. Ayrıca, siRNA bağlı MNP'lar kullanılarak eEF2 kinazın susturulması, in vivo orthotropic model nude farelerde de uygulanmıştır. eEF2 kinazın susturulması, migrasyon/invazyon (Src/FAK/paxillin), angiogenez (VEGF), proliferasyon (c-myc), hücre döngüsü (CyclinD1), sağkalım/ilaç dirençliliği (PI3K/Akt) transkripsiyon düzenleme (4E-BP1) yollarını inhibe etmiştir. Sonuç olarak ilk kez eEF2K tümör geniz ve BRCA1+ mutant kanser tedavisinde özgün terapötik hedef olarak kullanılabiliceği gösterilmiştir.

Anahtar Kelimeler Meme kanseri, alım, sitotoksitesite, genotoksitesite, ROS oluşumu, silika kaplama, CoFe-MNP, 2-amino-2-deoksi-glukoz, hedefleyici terapi, 2DG-MNP, BRCA1 mutant hücre, eEF2 kinaz, proliferasyon. Invasion/migrasyon, angiogenez, tümör geniz apoptoz, nanoteknoloji, siRNA,

*Dedicated to my family Nuray and Ahmet Ařık,
and
in memory of Prof.Dr.Mesude İřcan...*

ACKNOWLEDGEMENTS

This thesis is a result of the support I have received from numerous people throughout my graduate studies. It is a great pleasure for me to have this opportunity to express my deep sense of gratitude.

First and foremost I would like to thank Prof.Dr.Mesude İşcan for her immense guidance, support and motivation throughout my graduate studies. “Or else in a laboratory in your white coat and safety glasses, you can die for people-even for people whose faces you have never seen” Whenever I read this poem written by Nazım Hikmet- I remember her. She gave me lot of liberty and vision to plan my work, implement my ideas. She allowed me to develop as a researcher and taught how to be a better one. She was a true mentor as well as great person. She understood me without speaking just looking at my eyes most of the times. She made us feel so special as individually for all her graduate students and gave us her so valuable time without complain.

I would like to express my deepest gratitude to my supervisor, Prof. Dr. Tülin Güray for her patient guidance and warm encouragement that made this thesis possible. I really appreciate for accepting me to her lab and for her support throughout my graduate studies. She has always been there for me to give her suggestions and ideas I needed to complete this degree.

I would like to express my sincere gratitude to co-supervisor, Prof. Dr. Mürvet Volkan for her guidance, insight, encouragement and valuable suggestions throughout this study. She has helped me to carry out this thesis by keeping warmness of the love of science in my heart; I feel really lucky for having such a scientist model like her. It is a big honor to have two supervisors with such wonderful personality.

I would like to express my sincere appreciation to especially Assoc. Prof. Dr. Bülent Özpolat (MD Anderson Cancer Center, USA) and to Prof. Dr. Gabriel Lopez Berestein (MD Anderson Cancer Center, USA) for accepting me as a fellow researcher in their

laboratory and their support and helps during the time I worked in their laboratory. I have always been grateful for the opportunity to study in their lab. In addition to the research training, I also learnt a lot of other skills from them such as technical writing and presentation skills.

I thank the members of the thesis committee Prof. Dr. İhsan Gürsel, Assoc. Prof. Dr. Can Özen and Assoc. Prof. Dr. Elif Erson Bensan for their valuable time, suggestions and assistance.

I would like to thank Prof. Dr. Sema Burgaz and, Assoc. Prof. Dr. Gonca Çakmak Demircigil, Assoc. Prof. Dr. Ela Kadioğlu and Dr. Esra Emerce open not only their laboratory but also their office and home. I am grateful to their trust and support. I would like to special thanks to Assoc. Prof. Dr. Gonca Çakmak Demircigil for genotoxicity experiments.

I would also like to acknowledge Assoc. Prof. Dr. A. Elif Erson Bensan for the donation of Human mammary epithelial cell lines and Assoc. Prof. Dr. Mayda Gürsel and her kind lab members for the flow cytometer measurements and Prof. Dr. Nursen Çoruh for fluorescent spectroscopy measurement and Dr. Nizamettin Özdoğan for his support. He was there whenever I need to talk.

There is no way I can appreciate Tuğba Nur Aslan, she has been a great partner for me throughout the experiments. We really shared hard times while working and run not only in the lab but also her home until morning and countless cheerful times. I want to thank to her husband Fuat Aslan for his support and kindness. I am really lucky to meet him.

Huge thanks all former and Prof. Güray laboratory members, especially to Dr. Can Yılmaz, Dr. Pembegül Uyar, Dr. Metin Konuş, M.Sc. Selis Yılmaz, M.Sc. Elif Sakallı, M.Sc. Emilia Qomi, M.Sc. Deniz Hisarlı and Dr. Deniz İrtem Kartal. I am grateful for their helps and warm friendship.

I would like to thank to my labmates from C-50 laboratory for their friendships during this study. Special thanks come for Yeliz Akpınar, Ceren Uzun for their friendship and support. They always helped me whenever I need.

My deepest thanks and gratitude go to Prof. Dr. Lopez - Assoc. Prof. Dr. Özpolat lab members Dr. Burcu Aslan who shared her experience about Ph.D. journey and motivated me during this study. Nermin Mak Kahraman, Recep and Emine Bayraktar, Nashwa Kabil, Mehmet Reşit Asoğlu, Pınar Ünaldı and Merve Denizli for making my graduate journey very enjoyable and helping me during western and *in vivo* experiments. Mohammed Helmy, He was always with me whenever I need help. Gülnihal Özcan always inspired me that show us how a woman makes not only life but also science so beautiful. Cristian Rodriguez Aguayo, His knowledge and experience in cancer biology are so impressive. It was big honor to work with him in the same lab.

My special thanks go to Yeşim Kümbet, Şule Şahin, Dr. Tuba Çulcu, Dr. Aslıgül Kurt and Emrah Sağır for their great friendship, endless support and for all the fun we have had during all my Ph.D. years. I would like to special thanks to Ahmet Altay, and his family. I would never go to USA without their support. I consider them as my real brother and sister. I am very lucky to have such good friends, they are always with me whenever I laughed, I cried and I needed them. Without them this thesis would not be possible.

Last but certainly not least; I cannot express my deep feelings in words towards my family for their sacrifice, motivation and unconditional love. Grateful thanks go to my family; my mother Nuray Aşık, my father Ahmet Aşık, for their endless love during every step of my life, they always believe in me and support me under each situation. They always make me feel so lucky to have them. They have been with me during the hard as well as the cheerful times.

I also wish to thank all in Biological Sciences and Chemistry Department of METU.

This study was supported by a grant Project number: 113Z557 and 2214-A International Doctoral Research Fellowship from The Scientific and Technological Research Council

of Turkey Research Project Fund (TUBITAK) and Middle East Technical University Research Project Fund (Project number: METU BAP-07-02-2011-004) and I would like to acknowledge for a scholarship Project number: SBAG 109S419 to TUBITAK.

TABLE OF CONTENTS

ABSTRACT.....	v
ÖZ.....	viii
ACKNOWLEDGEMENTS.....	xi
TABLE OF CONTENTS.....	xv
LIST OF FIGURES	xxi
LIST OF TABLES	xxix
LIST OF EQUATIONS	xxx
ABBREVIATIONS	xxxii
CHAPTERS	1
1.INTRODUCTION	1
1.1 An Introduction to Nanomaterial	1
1.1.1 Physico-chemical and surface properties of nanoparticles	2
1.1.2 Overview of different classes of nanoparticles	3
1.2 Magnetic Nanoparticles	4
1.2.1 Surface modifications.....	4
1.2.2 Silica coating.....	5
1.3 Applications of Magnetic Nanoparticles.....	6
1.3.1 Cancer theranostics	6
1.3.2 Drug/Gene Delivery	6
1.3.3 Active targeting.....	8
1.3.4 Cancer diagnostics	10
1.4 Nanoparticle/cell interaction	10
1.4.1 Transport of nanoparticles	10
1.4.2 The Biology of Particle-Induced Oxidative Stress.....	12

1.5 Cancer	14
1.5.1 Breast Cancer	15
1.5.2 Treatment Strategies for BRCA1 mutated Breast Cancer	18
1.5.3 Possible targeted therapies	18
1.5.4 PARP inhibitors	19
1.5.5 Mechanism of siRNA-mediated gene silencing.....	20
1.5.6 Eukaryotic elongation factor 2 kinase.....	22
1.5.7 eEF2K in cancer therapeutics	23
1.6 Aim of This Study.....	25
2. MATERIALS AND METHODS.....	27
2.1. Materials	27
2.2. Methods.....	29
2.2.1. Preparation, and silica coating of cobalt ferrite nanoparticles	29
2.2.2 Cell Culture.....	30
2.2.2.1 Cell culturing and treatments	30
2.2.2.2 Cell Thawing.....	30
2.2.2.3 Cell Passaging.....	31
2.2.2.4 Cell Freezing.....	31
2.2.2.5 Cell counting.....	31
2.2.3 Visualization of intracellular MNP	32
2.2.3.1 Cellular Uptake by TEM.....	32
2.2.3.2 Cellular Uptake of MNPs by ICP-OES	33
2.2.3.3 Cellular uptake of MNPs by Prussian blue staining	34
2.2.3.4 Cellular uptake of MNPs by Flow cytometry	34
2.2.4 Cytotoxicity Assay.....	35
2.2.4.1 XTT assay	35
2.2.4.2 Trypan Blue Exclusion Method	35
2.2.5 Genotoxicity Assay.....	36
2.2.5.1 Single-Cell Gel Electrophoresis (SCGE, Comet)	36
2.2.5.2 Cytokinesis-blocked micronucleus (CBMN) assay	37

2.2.6 Measurement of intracellular ROS.....	38
2.2.6.1 Assay of Reactive oxygen species (ROS).....	38
2.2.6.2 Lipid peroxidation assay	39
2.2.7 Apoptosis Assay.....	40
2.2.7.1 Annexin-V-FITC / PI staining	40
2.2.7.2 Gene Expression Analysis.....	40
2.2.8 The preparation of 2-amino-2-deoxy-glucose labeled cobalt ferrite magnetic nanoparticles (2DG-MNPs)	41
2.2.8.1 Functionalization of silica coated cobalt ferrite nanoparticles.....	41
2.2.8.2 Modification of COOH-MNPs with 2-amino-2-deoxy-glucose (2DG). 41	
2.2.8.3 Spectrophotometric determination of 2DG on COOH-MNPs.....	42
2.2.9.1 Cellular uptake of 2DG-MNPs by TEM	42
2.2.9.2 Cellular uptake of 2DG-MNPs by ICP-OES	42
2.2.9.3 Cellular uptake of 2DG-MNPs by Prussian blue staining	43
2.2.10 The cytotoxicity of 2DG-MNPs.....	43
2.2.10.1 Cell viability (XTT) assay.....	43
2.2.11 Apoptosis Assay.....	43
2.2.11.1 Annexin-V-FITC/PI staining	43
2.2.11.2 Gene expression analysis	43
2.2.12 The conjugation of EF2K siRNA to cobalt ferrite magnetic nanoparticle (MNP-EF2K siRNA)	43
2.2.12.1 Cell Lines and culture	43
2.2.12.2 Transfections with siRNA.....	44
2.2.12.3 EDC/s-NHS Coupling Reactions	44
2.2.12.4 <i>In vitro</i> cellular uptake	45
2.2.12.5 Prussian blue staining.....	45
2.2.12.6 Clonogenic survival assay.....	45
2.2.12.7 Matrigel invasion assay.....	46
2.2.12.8 Migration assay	46
2.2.12.9 Western blot analysis	47

2.2.12.10 Orthotopic xenograft tumor model of breast cancer	47
2.2.12.11 <i>In vivo</i> tissue distribution of MNP-siRNA nanoparticles	48
2.2.12.12 Immunohistochemical analysis	48
2.2.12.13 Immunohistochemical analysis Proliferation and microvessel density CD31	49
2.2.12.14 MTS assay for combination Olaparib (AZD2281) and MNP-EF2K siRNA	49
2.2.12.15 Statistical analysis	50
3.RESULTS AND DISCUSSION.....	51
3.1 Characterization of naked and silica coated CoFe MNPs.....	51
3.2 Visualization of intracellular MNP	54
3.2.1 Cellular uptake by TEM.....	54
3.2.2 Cellular Uptake of MNPs by ICP-OES	56
3.2.3 Cellular Uptake of MNPs by Prussian Blue Staining	61
3.2.4 Cellular Uptake of MNPs by Flow cytometry	62
3.3 XTT Assay	64
3.4 Genotoxicity assay	66
3.4.1 Evaluation of genotoxicity by the alkaline comet assay	66
3.4.2 Evaluation of the genotoxicity by CBMN assay.....	68
3.5 Measurement of intracellular ROS	72
3.5.1 Assay for Reactive oxygen species (ROS)	72
3.5.2 Lipid Peroxidation (TBARS) Assay	77
3.6 Apoptosis Assay.....	79
3.6.1 Annexin-V-FITC / PI Assay	79
3.6.2 Effect of naked and silica coated MNPs on Apoptotic Gene Expressions.....	82
3.7 mRNA Expression Analysis of Phase I and Phase II Enzymes.....	85
3.7.1 Effect of naked and silica coated MNPs on CYP1A1 and CYP1B1 Gene Expressions.....	85
3.7.2 Effect of naked and silica coated MNPs on GSTZ1 and GSTM3	

Gene Expressions.....	86
3.8 The conjugation of 2-amino-2-deoxy-glucose to cobalt ferrite magnetic nanoparticle (2DG-MNPs).....	90
3.8.1. Characterization of modified CoFe MNPs.....	90
3.8.2. Cellular uptake of 2DG-MNPs.....	92
3.8.2.1 Cellular uptake of 2DG-MNPs by TEM	92
3.8.2.2 Cellular uptake of 2DG-MNPs by (ICP-OES).....	93
3.8.2.2 Cellular uptake of 2DG-MNPs by Prussian blue staining	94
3.8.3. Cell viability (XTT) Assay	95
3.8.4 Apoptosis Assay.....	97
3.8.4.1 Annexin-V-FITC / PI Assay	97
3.8.4.2 Effect of 2DG-MNPs on Apoptotic Gene Expressions.....	100
3.8.5 mRNA Expression Analysis of Phase I and Phase II enzymes.....	102
3.8.5.1 Effect of 2DG-MNPs on CYP1A1 and CYP1B1 Gene Expression	102
3.8.5.2 Effect of 2DG-MNPs on GSTZ1 and GSTM3 Gene Expressions.....	103
3.9.1 EF2K is overexpressed in BRCA1 mutated and triple negative breast cancer	106
3.9.2 Knockdown of EF2K by MNP- siRNA in BRCA1 mutated breast cells	107
3.9.3 Knockdown of EF2K inhibits migration and invasion of BRCA1 mutated breast cancer cells.....	112
3.9.4 Targeting eEF2K impairs BRCA1 mutated cell invasion and migration through inhibition of SRC/FAK/Paxillin.....	114
3.9.5 <i>In vivo</i> Targeting of EF2K leads to antitumor activity in BRCA1 xenograft models.....	125
3.9.6 <i>In vivo</i> inhibition of eEF2K inhibits tumor cell proliferation, microvessel density and induces apoptosis in BRCA1 mutated tumor xenografts.....	127
3.9.7 MNP-EF2K siRNA nanoparticles accumulate in BRCA1 mutated tumor tissues	129
3.9.8 <i>In vivo</i> Targeting of EF2K inhibits cyclin D1, autophagy and impairs	

the activity of c-Src/ FAK/ Paxillin complex	132
3.9.9 Knockdown eEF2K leads to decrease the expression level of MCP-1 in BRCA1 mutated tumors.....	133
3.9.10 Targeting eEF-2K inhibits PI3K/AkT/mTOR/ 4EBP1 in BRCA1 mutated tumors.....	133
3.9.11 Targeting eEF-2K leads a decrease Stem Cell like markers in BRCA1 mutated tumors.....	135
3.9.12 Combination of PARP inhibitors with eEF2K siRNA enhance the BRCA1 mutated breast cancer proliferation.....	136
4.CONCLUSION.....	141
5.REFERENCES.....	145
APPENDICES	161
A. DETECTION OF MYCOPLASMA	161
B. PRIMER SEQUENCES	165
C. AMPLIFICATION CURVES, MELT CURVES, STANDARD CURVES.....	167
VITA	177

LIST OF FIGURES

FIGURES

Figure 1. Size case.....	2
Figure 2. A schematic diagram of multifunctional silica coated MNPs	5
Figure 3. A Schematic diagram of magnetic drug delivery system	7
Figure 4. Representations of MNPs tumor-targeting modalities.	8
Figure 5. Possible cellular uptake mechanisms for nanomaterials.....	11
Figure 6. The oxidative stress model.	13
Figure 7. To better understand the so-called “Angelina Jolie effect”	17
Figure 8. Candidate targets and pathways in triple-negative breast cancer.	19
Figure 9. The RNA-interference process in mammalian cells.....	21
Figure 10. Targeting eEF-2K leads tumorigenesis in breast cancer cells.	24
Figure 11. The EDX results of A) naked CoFe-MNPs and B) silica coated CoFe-MNPs.	52
Figure 12. FTIR results of (a)(blue line) naked cobalt ferrite (CoFe-MNPs) and (b) (red line) silica coated cobalt ferrite magnetic nanoparticles (CoFe-MNPs).....	53
Figure 13. Representative TEM microphotographs of MDA-MB-231 cells treated with MNPs.	54
Figure 14. Internalization of MNPs in MDA-MB-231 cells observed with TEM...	55
Figure 15. TEM images of ultrathin sections of MCF-10A cells.	56
Figure 16. ICP-OES measurements and comparison of intracellular uptake of naked and silica coated CoFe-MNPs in MDA-MB-231 vs MCF-10A for 24 h.	57

Figure 17. ICP-OES measurements of intracellular uptake of naked and silica coated in MDA-MB-231 and MCF-10A cells after 2 h, 4 h, 8 h and 24 h of CoFe-MNPs (250 $\mu\text{g}/\text{mL}$) incubation.....	58
Figure 18. Uptake of CoFe-MNPs (compared to the controls at 37°C) in the presence of different endocytic inhibitors in MDA-MB-231 4°C, sucrose (0.45 M), NaN_3 (0.1%), and chlorpromazine (CLPZ) (6 $\mu\text{g}/\text{mL}$).	59
Figure 19. Uptake of CoFe-MNPs (compared to the controls at 37°C) in the presence of different endocytic inhibitors in MCF-10A 4°C, sucrose (0.45 M), NaN_3 (0.1%), and chlorpromazine (CLPZ) (6 $\mu\text{g}/\text{mL}$).	60
Figure 20. Light microscopy images of MDA-MB-231, MCF-7 and MCF-10A cells that are stained with Prussian blue, followed by counterstain nuclear fast red. The cells were treated with naked and silica coated MNPs at concentrations of 125 $\mu\text{g}/\text{mL}$ for 24 h.	61
Figure 21. Uptake of MNPs into (A) normal epithelium (MCF10A) and (B) breast cancer cells (MDA-MB-231). Real images after treatments with different sized MNPs (50 and 100 $\mu\text{g}/\text{mL}$) are shown for 24 h and given in the flow cytometry histograms.63	63
Figure 22. DNA damage in MDA-MB-231 cells after 4 and 24 h of exposure to different concentrations of naked and silica coated CoFe-MNP; olive tail moment (arbitrary unit); cell viability.....	67
Figure 23. DNA damage in MCF-10A cells after 4 and 24 h of exposure to different concentrations of naked and silica coated CoFe-MNPs; olive tail moment (arbitrary unit); cell viability.....	68
Figure 24. Micronucleus frequency ($\%$) of MDA-MB-231 treated with CoFe-MNPs showing binucleated cell and CBPI (cytokinesis block proliferation index).	69
Figure 25. Micronucleus frequency ($\%$) of MCF-10A treated with CoFe-MNPs showing binucleated cell and CBPI (cytokinesis block proliferation index).....	70

Figure 26. Effects of naked and silica coated MNPs on the generation of reactive oxygen species (ROS) in (A) MCF-10A cells for 4 and 24 h. The % DCF fluorescence of the control cells was considered 100 %. (B) Representative images of production of ROS using DCFDA dye in MCF-10A cells (a) Control cells, (b-d) Cells exposed to naked MNPs (62 µg/mL, 125 µg/mL and 500 µg/mL, respectively) (e) positive control: H₂O₂ treatment, (f-h) Cells exposed to silica coated MNPs (62 µg/mL, 125 µg/mL and 500 µg/mL respectively) for 24 h showing increase in fluorescence 74

Figure 27. Effects of naked and silica coated MNPs on the generation of reactive oxygen species (ROS) in (A) MCF-7 cells for 4 and 24 h. The % DCF fluorescence of the control cells was considered 100 %. (B) Representative images of production of ROS using DCFDA dye in MCF-7 cells (a) Control cells; (b-d) Cells exposed to naked MNPs (62 µg/mL, 125 µg/mL and 500 µg/mL respectively) (e) positive control; H₂O₂ treatment; (f-h) Cells exposed to silica coated MNPs (62 µg/mL, 125 µg/mL and 500 µg/mL respectively) for 24h showing increase in fluorescence 75

Figure 28. Effects of naked and silica coated MNPs on the generation of reactive oxygen species (ROS) in (A) MDA-MB-231 cells for 4 and 24 h. The % DCF fluorescence of the control cells was considered 100%. Representative images of production of ROS using DCFDA dye in MDA-MB-231 cells (a) Control cells; (b-d) Cells exposed to naked MNPs (62 µg/mL, 125 µg/mL and 500 µg/mL respectively) (e) positive control: H₂O₂ treatment; (f-h) Cells exposed to silica coated MNPs (62 µg/mL, 125 µg/mL and 500 µg/mL respectively) for 24h showing increase in fluorescence 76

Figure 29. Detection of lipid peroxidation (nmol MDA /mg protein) in MCF-10A, MCF-7 and MDA-MB-231 cells treated with different concentrations of naked and silica coated MNPs for 4 h and 24 h. 78

Figure 30. The histograms of the apoptotic effects of naked and silica coated MNPs at concentrations of 62 µg/mL, 125 µg/mL and 500 µg/mL, on MCF-10A, MCF-

7 and MDA-MB-231 cells. Bar graphs show percent apoptotic cells. Untreated (UT) cells are used as control. Four subpopulations and their percent distributions in different areas: Area A1 and A2 shows viable and dead cell (necrotic), A3 and A4 correspond to cells undergoing early and late apoptosis, respectively..... 81

Figure 31. The expression levels of apoptotic (PUMA and BAX) and anti-apoptotic (BCL-2, SURVIVIN) genes in MCF-10A, MCF-7, MDA-MB-231 cells after treatment with naked and silica coated MNPs for 24 h. 84

Figure 32. The expression levels of CYP1A1, CYP1B1, GSTZ1 and GSTM3 genes in MCF-10A, MCF-7, MDA-MB-231 cells after treatment with naked and silica coated MNPs for 24 h. 87

Figure 33. A schematic drawing, showing possible mechanisms of naked MNPs on the induction of cellular toxicity in the breast cancer cells. 89

Figure 34. (A) FT-IR spectra of -COOH modified CoFe MNPs. Particle size distribution of (B) -COOH modified CoFe MNPs and (C) 2DG modified CoFe MNPs. 91

Figure 35. Transmission electron micrographs (TEM) of MDA-MB-231 cells treated with 2DG-MNPs. MNPs are internalized and accumulated in cytoplasm. 92

Figure 36. ICP-OES measurements of iron concentration per cell (pg/cell) in MCF-10A, MCF-7 and MDA-MB-231 cells after treatment with COOH-MNPs and 2DG-MNPs at final concentrations of 125 µg/mL and 500 µg/mL after 24 h incubations. 93

Figure 37. ICP-OES measurements of iron concentration per cell (pg/cell) in MCF-10A, MCF-7 and MDA-MB-231 cells after treatment with 2DG-MNPs at final concentrations of 125 µg/mL after 2, 4, 8, 12 and 24 h incubations. 94

Figure 38. Light microscopy images of MCF-10A, MCF-7 and MDA-MB-231 cells that are stained with Prussian blue and following counterstained with nuclear fast red. Light pink coloring of cytoplasm, dark pink coloring of nucleus and blue

coloring of iron core of the molecules were seen. The cells were treated with COOH-MNPs and 2DG-MNPs at the concentrations of 125 µg/mL for 24 h. . 95

Figure 39. Cell viability of MDA-MB-231, MCF-7 and MCF-10A cells after treatment at different concentrations (62–500 µg/mL) of 2DG-MNPs for 24 and 72 h. 96

Figure 40. The apoptotic effects of untreated cells and the etoposide on MDA-MB-231, MCF-7 and MCF-10A. 98

Figure 41. The apoptotic effects of 2DG-MNP (125, 250 and 500 µg/mL) on MDA-MB-231, MCF-7 and MCF-10A cells for 24 h..... 99

Figure 42. Apoptotic cell populations in MDA-MB-231, MCF-7 and MCF-10A cells after treatment with 2DG-MNPs for 24 h..... 100

Figure 43. The expression levels of apoptotic (PUMA and BAX) and anti-apoptotic (Bcl-2, SURVIVIN) genes in MDA-MB-231, MCF-7 and MCF-10A cells after treatment with 2DG-MNP for 24 and 72 h..... 101

Figure 44. The expression levels of CYP1A1 and CYP1B1 genes in MCF-10A, MCF-7 and MDA-MB-231 cells after treatment with 2DG-MNP and 24 and 72 h growth. 102

Figure 45. The expression levels of GSTZ1 and GSTM3 genes in MDA-MB-231, MCF-7 and MCF-10A cells after treatment with 2DG-MNPs for 24 and 72 h. 104

Figure 46. A schematic drawing, showing possible mechanisms of cellular metabolism of 2DG-MNPs in the breast cancer cells..... 105

Figure 47. EF2K are highly expressed in triple negative and BRCA1 mutated cells. Western blot analysis of cell lysates of several cell lines were indicated..... 106

Figure 48. The uptake of Cy3 MNP-EF2K siRNA against MDA-MB-436 cells in vitro. Fluorescent microscopy images of cells treated with MNP- Cy3-siRNA, free Cy3 siRNA, Cy3 siRNA with hiPerFect for 4 h in 37 °C. Nuclei (blue) were

stained with DAPI. In vitro Prussian blue staining results, Prussian blue staining of MDA-MB-436 cells incubated with Free Cy3 siRNA, EF2K siRNA loaded MNP, EF2K siRNA with hiPerFect, respectively 108

Figure 49. The uptake of Cy3 MNP-EF2K siRNA against and HCC-1937 cells in vitro. Fluorescent microscopy images of cells treated with MNP- Cy3-siRNA, free Cy3 siRNA, Cy3 siRNA with hiPerFect for 4 h in 37 °C. Nuclei (blue) were stained with DAPI. In vitro Prussian blue staining results, Prussian blue staining of HCC-1937 cells incubated with Free Cy3 siRNA, EF2K siRNA loaded MNP, EF2K siRNA with hiPerFect, respectively 109

Figure 50. The uptake of Cy3 MNP-EF2K siRNA against MDA-MB-231 cells in vitro. Fluorescent microscopy images of cells treated with MNP- Cy3-siRNA, free Cy3 siRNA, Cy3 siRNA with hiPerFect for 4 h in 37 °C. Nuclei (blue) were stained with DAPI. In vitro Prussian blue staining results, Prussian blue staining of MDA-MB-231 cells incubated with Free Cy3 siRNA, EF2K siRNA loaded MNP, EF2K siRNA with hiPerFect, respectively. 110

Figure 51. Western blot analysis of EF2K levels 72 h post transfection with EF2K siRNA, control siRNA, MNP, MNP-EF2K siRNA in A) MDA-MB-436 B) in HCC-1937 cells 111

Figure 52. A. In vitro knockdown of EF2K by siRNA treatment inhibit colony formation of MDA-MB-436 and B. MDA-MB-231 cells. Representative colony formation assay of MDA-MB-436 and MDA-MB-231 cells treated with different formulation. 1) untreated 2) control siRNA 3) MNP 4) eEF2K siRNA 5) MNP-EF2K siRNA and colonies detected after two weeks later. All colonies were stained with crystal violet. Histogram showing the quantification of colony formation efficiency..... 113

Figure 53. Representative photographs show the effect of silencing of EF2K siRNA on MDA-MB-436 cells invasion by Matrigel Transwell invasion assay after 24 h treatment. The cells treated with different formulation 1) untreated 2) MNP 3) control siRNA 4) eEF2K siRNA 5) MNP-EF2K siRNA. Histogram showing the

quantification of % invasion of cells. All photographs were captured in a Leica light microscope under 20X magnification 115

Figure 54. Representative photographs show the effect of silencing of EF2K siRNA on HCC-1937 cells invasion by Matrigel Transwell invasion assay after 24 h treatment. The cells treated with different formulation 1) untreated 2) MNP 3) control siRNA 4) eEF2K siRNA 5) MNP-EF2K siRNA. Histogram showing the quantification of % invasion of cells. All photographs were captured in a Leica light microscope under 20X magnification 116

Figure 55. Representative photographs show the effect of silencing of EF2K siRNA on MDA-MB-231 cells invasion by Matrigel Transwell invasion assay after 24 h treatment. The cells treated with different formulation 1) untreated 2) MNP 3) control siRNA 4) eEF2K siRNA 5) MNP-EF2K siRNA. Histogram showing the quantification of % invasion of cells. All photographs were captured in a Leica light microscope under 20X magnification 117

Figure 56. Representative photographs show the silencing of eEF-2K in MDA-MB-436 and control cells motility by wound healing assay. The cells treated with different formulation 1) control siRNA 2) MNP 3) eEF2K siRNA 4) MNP-EF2K siRNA. Histogram showing the quantification of % migration of cells. After 48 h incubation, wound closure photographed under light microscope 118

Figure 57. Representative photographs show the silencing of eEF-2K in HCC-1937 and control cells motility by wound healing assay. The cells treated with different formulation 1) control siRNA 2) MNP 3) eEF2K siRNA 4) MNP-EF2K siRNA. Histogram showing the quantification of % migration of cells. After 48 h incubation, wound closure photographed under light microscope 120

Figure 58. Representative photographs show the silencing of eEF-2K in MDA-MB-231 and control cells motility by wound healing assay. The cells treated with different formulation 1) control siRNA 2) MNP 3) eEF2K siRNA 4) MNP-EF2K siRNA. Histogram showing the quantification of % migration of cells. After 48 h incubation, wound closure photographed under light microscope 121

Figure 59. Western blot analysis of eEF2K, p-eEF2, eEF2, p-Src, Src, FAK, p-FAK, p-Paxillin, Paxillin levels 72 h post transfection with EF2K siRNA, control siRNA, MNP, MNP-EF2K siRNA for MDA-MB-436 cells.....	123
Figure 60. Western blot analysis of eEF2K, p-eEF2, eEF2, p-Src, Src, FAK, p-FAK, p-Paxillin, Paxillin levels 72 h post transfection with EF2K siRNA, control siRNA, MNP, MNP-EF2K siRNA for HCC-1937 cells.	124
Figure 61. Treatments of tumor tissues with MNP-EF2K siRNA	126
Figure 62. Immunohistochemical analysis.....	128
Figure 63. <i>In vivo</i> tumor accumulations of MNP-EF2K siRNA.....	130
Figure 64. A. Control siRNA and MNP-EF2K siRNA were intravenously administered and tissues were removed 24 h after a single administration. Prussian blue staining of the spleen, liver, lung brain, heart and kidney. High levels of iron uptake were observed in the liver and spleens; Blue granule show that positive Prussian blue staining and counterstain with nuclear red staining B.H&E Histological analyses of tissue specimens after MNP-EF2K siRNA treatment. Liver, kidney, spleen, lung, heart and brain tissues of treated mice.....	131
Figure 65. Western blot analysis of tumor tissues 1.	132
Figure 66. Western blot analysis of tumor tissues 2	134
Figure 67. Western blot analysis of tumor tissues 3	135
Figure 68. Combination of AZD2281 and EF2K siRNA enhances growth inhibition of MDA-MB-436 cells	136
Figure 69. Schematic illustration of cancer therapy of BRCA1 mutated cancer	137
Figure 70. Detection of mycoplasma contaminations in MCF-10A, MCF-7 MDA-231 cells treated with MNPs.....	163

LIST OF TABLES

TABLES

Table 1. NM effects as the basis for pathophysiology and toxicity.....	14
Table 2 Zeta potential and average hydrodynamic sizes of aggregates of investigated CoFe-MNPs in different media.....	51
Table 3. IC ₅₀ values obtained on MDA-MB-231, MCF-7 and MCF-10A cells after exposure to naked and silica coated MNPs	65

LIST OF EQUATIONS

EQUATIONS

Equation 1. The formula for % Cell Viability.	35
Equation 2. Calculation of CBPI	38
Equation 3. Percentage ROS generation	39

ABBREVIATIONS

¹⁸ FDG	2-fluoro-2-deoxyglucose
2DG	2-amino-2-deoxy-glucose
4E-BP1	Eukaryotic translation initiation factor 4E-binding protein 1
Ago2	Argonaute 2
ALDH1A1	Aldehyde dehydrogenase 1 family, member A1
APTES	3-Aminopropyl trimethoxysilane
APTMS	3-Aminopropyl) trimethoxysilane
ATCC	American Type Culture Collection
BC	Breast cancer
BCL-2	B-cell lymphoma 2
BRCA1-2	BReast CAncer genes 1 and 2
CBMN	Cytokinesis-blocked micronucleus
CBPI	Cytokinesis block proliferation index
CCL2	The chemokine (C-C motif) ligand 2
CGH	Comparative genomic hybridization
CHEK1	Checkpoint kinase 1
CoFe MNP	Cobalt ferrite Magnetic Nanoparticle
CT	Comparative threshold
CYP1A1	Cytochrome P450, family 1, subfamily A, polypeptide 1
CYP1B1	Cytochrome P450, family 1, subfamily B, polypeptide 1
DAB	3,3'-Diaminobenzidine
DAPI	4,6-diamidino-2-phenylindole
DCFDA	2, 7-dichlorofluorescein diacetate

DF	Dilution factor
DLS	Dynamic light scattering
DMEM/Ham's F12	Dulbecco's Modified Eagle Medium/Ham's F-12
DMF	Dimethylformamide
DMSO	Dimethyl sulfoxide
DPBS	Dulbecco's Phosphate-Buffered Saline
dsRNA	Cytoplasmic long double-stranded RNA
DTT	Dithiothreitol
ECM	Extracellular matrix
EDC	(1-Ethyl-3-(3-dimethylaminopropyl) carbodiimide)
EDX	Energy Dispersive X-Ray analyser
eEF2	Elongation factor 2
eEF2K	Eukaryotic elongation factor 2 kinase
EGF	Epidermal Growth Factor
EGFR	Epidermal Growth Factor receptor
EMT	The epithelial-mesenchymal transition
ER	Estrogen receptor
EtOH	Ethanol
FAK	Focal adhesion kinase
FBS	Fetal bovine serum
FDA	Food and Drug Administration
FI	Flourescence Intensity
FITC	Fluorescein isothiocyanate
FSC	Forward-scattered
FT-IR	Fourier Transform Infrared Spectroscopy
GLUT-1	Glucose transporters
GSH	Glutathione
GSSG	Oxidized glutathione
GSTM3	Glutathione S-Transferase Mu 3

GSTZ1	Glutathione S-Transferase Zeta 1
GTP	Guanosine-5'-triphosphate
H&E	Hematoxylin eosin
H ₂ O ₂	Hydrogen peroxide
HCC1937	BRCA1 mutated lines
HER2	Human epidermal growth factor receptor 2
HMA	High melting-point agarose
HRP	Horseradish peroxidase
IC ₅₀	The concentration required inhibiting 50% of cell growth
ICP-OES	Inductively coupled plasma optical emission spectrometry
IgG	Immunoglobulin G
LMA	Low melting-point agarose
mAbs	Monoclonal antibodies
MAPK	Mitogen-activated protein kinase
MBTH	3-Methyl-2-benzothiazolinone hydrazone hydrochloride monohydrate
MCF-10A	Human mammary Epithelial Cell Line
MCF-7	Michigan Cancer Foundation-7
MDA	Malondialdehyde
MDA-MB-231	Human Breast Metastatic Adenocarcinoma
MDA-MB-436	BRCA1 mutated lines
MMC	Mitomycin C
MNPs	Magnetic nanoparticles
MRI	Magnetic resonance imaging
mTOR	Mammalian target of rapamycin
MTS	3-(4,5-dimethylthiazol-2-yl)-2,5-diphenyltetrazoliumbromide

NF-kB	Nuclear factor kB
NHS	N-Hydroxysuccinimide
NMs	Nanomaterials
NMR	Nuclear Magnetic Resonance
NP	Nanoparticle
Nrf-2	Nuclear factor erythroid 2-related factor
OECD	Organisation for Economic Co-operation and Development
PaCa	Pancreatic carcinoma cell lines
PARP1	Poly (ADP ribose) polymerase 1
PEG	Poly (ethyleneglycol)
PEI	Polyethilenimine
PET	Positron Emission Tomography
PI	Propidium iodide
PLA	Poly lactic acid
PLGA	Poly lactic co-glycolic acid
PMS	Phenazine methosulfate
PR	Progesterone receptor
PS	Phosphatidylserine
PTEN	Phosphatase and tensin homolog
PVA	Poly (vinyl alcohol)
PVP	Poly (vinylpyrrolidone)
RISC	RNA-induced Silencing Complex
ROS	Reactive oxygen species
RPMI-1640	Roswell Park Memorial Institute medium 1640
RT-qPCR	Real time quantitative polymerase chain reaction
SCGE	Single-Cell Gel Electrophoresis
siRNA	Small interfering RNA
SSC	Side-scatter
TBA	Thiobarbitutic acid

TBARS	Thiobarbituric acid reactive species
TEM	Transmission Electron Microscopy
TEOS	Tetraethyl orthosilicate
TNBC	The triple-negative breast cancer
TUNEL	Terminal deoxynucleotidyl transferase-mediated dUTP nick end labeling
VEGF	Vascular endothelial growth factor
VEGFA	Vascular endothelial growth factor A
XTT	2,3-bis-(2-methoxy-4-nitro-5-sulfophenyl)-2H- tetrazolium-5- carboxanilide

CHAPTER 1

INTRODUCTION

1.1 An Introduction to Nanomaterial

Nanoparticles (NPs) are an important class of nanomaterial defined as single particles with a diameter < 100 nm (nm = 1 billionth of a meter) [1]. When they compare to the biological systems according to their size, the nanoparticles are at least 1000 times small compared to the typical human cells. In this sense, researchers have been using the various kinds of nanoparticles in order to investigate biological processes involved in drug/gene delivery, bio imaging as well [2].

As seen in **Figure 1** there is huge differences between a 1 nm molecule, a 4 nm protein, and a 10 nm nanoparticle. Biological interactions between these molecules and various molecules such as ions in the cell will make the scheme very complex to clarify in a simple way.

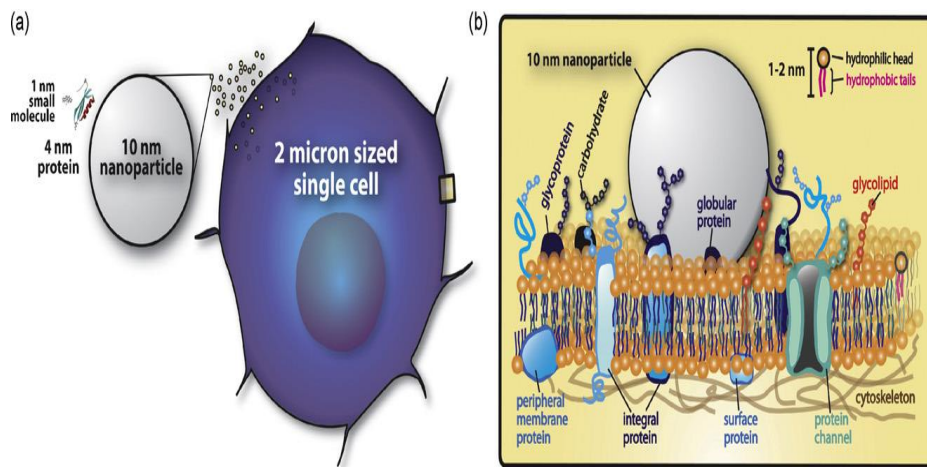


Figure 1. Size case. (a) The representative comparison of a 10 nm nanoparticle, proteins and small molecules in size and volume. A human cell, which is composed of biomolecules such as proteins, nucleic acids, is 1000 times larger in volume and size compared to a 10 nm nanoparticle. (b) The cell contains different proteins and a single 10 nm nanoparticle [3].

1.1.1 Physico-chemical and surface properties of nanoparticles

The unique physicochemical properties of NPs are the resultant to their unique morphology, chemical composition, structure, surface charge, chemical solubility and aggregation [4]. Especially, the particle size and surface area among nanomaterial characteristic have a great impact on biological studies. The sizes of NPs affect both their surface area and reactivity. When the sizes of the NPs decrease, their surface areas increase. Therefore, there is inverse relationship between NPs surface area and their size. When the surface area increase, the number of potential reactive groups on the NPs surface increase [5].

- **Size effects:** The properties like solubility, transparency, color, absorption or emission wavelength, conductivity, melting point and catalytic behavior are changed only by varying the particle size.

- **Composition effects:** The physicochemical behavior of nanomaterials is altered with the different nanoparticle compositions
- **Surface effects:** The surface characteristic of the nanoparticles leads to change their properties of dispersibility, conductivity, catalytic behavior and optical

1.1.2 Overview of different classes of nanoparticles

There are wide ranges of nanomaterials that can be tailored with chemically functional groups. They can be used in the varying application such as biosensors, imaging agents, targeted molecular delivery vehicles, and other biological tools. The fantastic freedom to design and modify nanomaterial to target cells is the fundamental ability suggested by nanotechnology, which contributes drug development, medical diagnostics, and clinical applications.

Liposomes are composed of lipid bilayer membranes surrounding an aqueous interior. They have similarities with biological membranes and have been used for improving the efficacy and safety of different drugs [6]. Polymer based nanoparticles are both biodegradable and biocompatible such as polysaccharide chitosan have been used for various biomedical applications [7]. Ceramic nanoparticles are composed of silica, titania and alumina that are inorganic materials with porous characteristics. They can be used for drug delivery [8]. The iron oxides are the class of magnetic and metallic nanoparticle which are used as targeting and imaging agents [9]. Gold shell nanoparticles are defined as metal-based agents, which are consisting of a dielectric core layered by gold metallic shell. Their unique optical and chemical properties make them suitable agents for biomedical imaging and therapeutic applications [10]. The fullerenes and nanotubes are members of carbon nanomaterials. Fullerenes are made of carbons that are unique shape with a polygonal structure. They can be functionalized for tissue binding [11].

1.2 Magnetic Nanoparticles

Nanoparticles are highly promising tools and have numerous potential use for a wide range of applications from diagnostics to the treatment of diseases [12-14]. Among them, magnetic nanoparticles (MNPs) have unique properties such as high magnetization value and passing cellular barriers and they have been used for many years as MRI agents, gene delivery agents, hyperthermia therapy, and tissue repair [15-17]. Cobalt is gaining increasing attentions as a highly effective magnetic resonance imaging (MRI) contrast agent, in combination with gold, iron and graphite, and platinum [18]. There are many reason that researcher chooses magnetic nanoparticles to use them in biomedicine. First, they have controllable sizes. They can be functionalized with different biological moieties. This makes them excellent platform for targeting and cancer therapy. Second, they are magnetic and can be manipulated by an external magnetic field gradient. This opens up many applications such as drug and gene delivery. The anticancer drug can be loaded to magnetic nanoparticles, which can be accumulated into tumor region directed by magnetic force. Third, the magnetic nanoparticles can be made to resonantly respond to a time-varying magnetic field, with advantageous results related to the transfer of energy from the exciting field to the nanoparticle. For example, the magnetic nanoparticle can be made to heat up, which leads to their use as hyperthermia agents, delivering toxic amounts of thermal energy to targeted bodies such as tumors; or as chemotherapy and radiotherapy enhancement agents, where a moderate degree of tissue warming results in more effective malignant cell destruction. Many other potential applications, are made available in biomedicine as a result of the special physical properties of magnetic nanoparticles [19].

1.2.1 Surface Modifications

Magnetic nanoparticles without any surface coating have hydrophobic surfaces and interact each other lead to agglomerate and increase in the their size [20].

NP coatings may be composed of several materials including polymeric and inorganic materials. Polymeric materials can be divided into natural and synthetic. Synthetic polymeric materials include poly (ethylene-co-vinyl acetate), poly (vinyl alcohol) (PVA), poly (vinylpyrrolidone) (PVP), poly (ethylene glycol) (PEG), poly (lactic-co-glycolic acid) (PLGA), etc. Gelatin, dextran, chitosan etc. are the examples for natural polymeric materials. Sodium oleate, dodecylamine, etc. are examples for various surfactants that are used in providing dispersibility in an aqueous medium.

1.2.2 Silica Coating

The researchers have investigated metallic core shell. These NPs have inner magnetic core with an outer layer of inorganic materials (**Figure 2**).

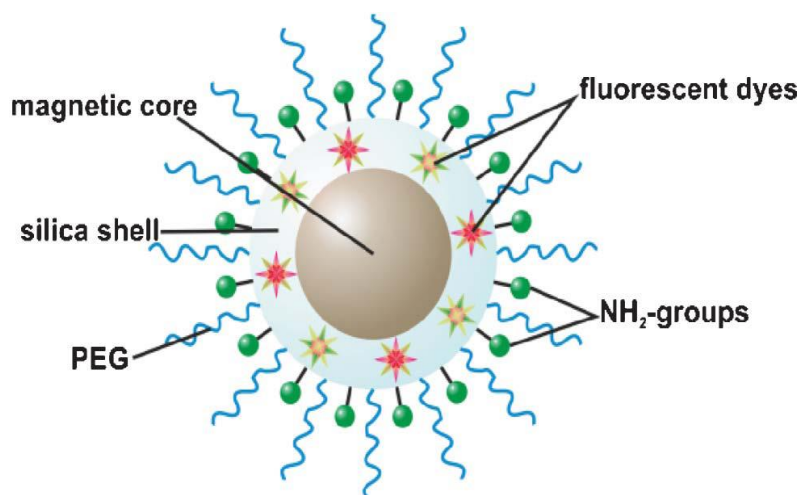


Figure 2. A schematic diagram of multifunctional silica coated magnetic nanoparticle indicating a core/shell structure with a layer of silica, SiO_2 , and functional groups attached to the shell [21].

The magnetic nanoparticles have been layered with silica, gold or gadolinium, etc. These coatings enhance not only the stability to the nanoparticles in solution but also provide a platform for binding helps in the various biological ligands surface for biomedical applications [22].

Some researcher indicate that silanol groups in silica coating facilitate the reaction with alcohols and silane coupling agents to not only provide dispersions that are stable in non-aqueous solvents but also give platform for covalent binding of specific ligands. The strong binding makes dissociation of these ligands a difficult task. In addition, the silica surface provide high stability to suspensions of the particles at high volume fractions, changes in pH or electrolyte concentration [19].

1.3 Applications of Magnetic Nanoparticles

1.3.1 Cancer Theranostics

Nanomaterial provides an excellent platform for different functional ligands. Magnetic nanoparticles (MNPs) have been used for drug delivery over the past 10 years. MNPs can be used as a dual diagnostic tool (in magnetic resonance imaging, MRI) and targetable drug carrier for therapy, a so-called “theranostic”[23].

1.3.2 Drug/Gene Delivery

The therapeutic drugs are injected intravenously to general systemic distribution, resulting in side effects for both tumor and normal cells. For example, there are many side effects of anti-inflammatory drugs on patients who have chronic arthritis. However, if such treatments could be localized into the site of a joint, it would be possible to reduce these side effects. The main goals are: (i) to reduce side effect of the cytotoxic drug, and (ii) to reduce the concentration required by more efficient, accumulation targeting of the drug. In magnetically targeted therapy, a cytotoxic drug is conjugated to the surface of a biocompatible magnetic nanoparticle vehicle. These drug/vehicle complexes are injected into the patient via the circulatory system. When the this complex circulate the bloodstream, external, high-gradient magnetic fields

are applied to accumulate the complex at a specific target site within the body (**Figure 3**) [24].

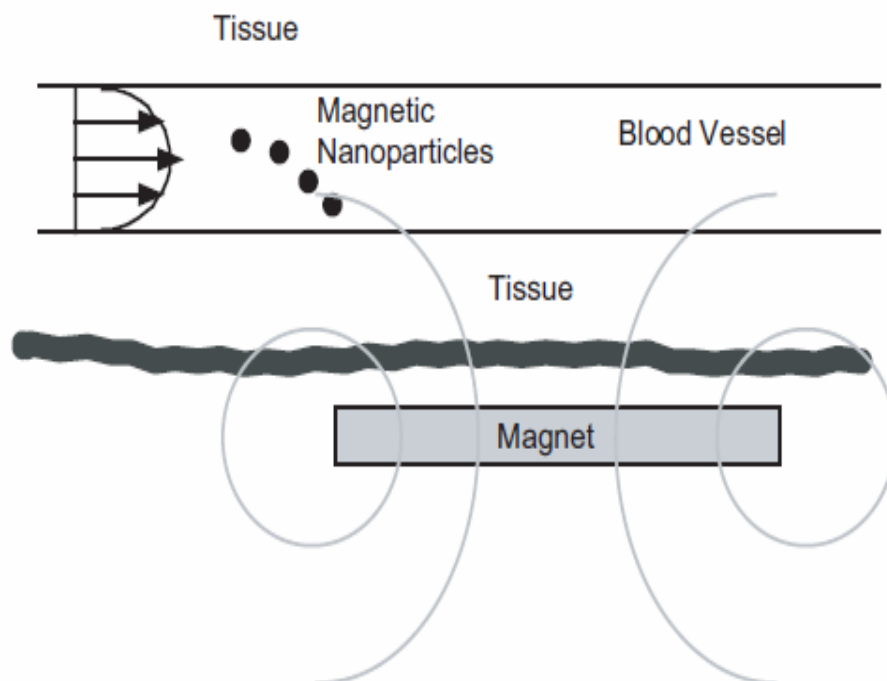


Figure 3. A Schematic diagram of magnetic drug delivery system: a magnet which is put outside of the body leads to capture magnetic carrier [24].

Gene delivery techniques can be used to insert a gene of interest into the host cell. Viral vectors, electroporation and transfection are commonly used the techniques for gene delivery. They have advantages and disadvantages in their efficacy. Viral gene techniques show high efficiency (80–90%), which introduce its genetic material into the host genome. The major disadvantage is unwanted side effect such as expression of viral genes. Another popular technique is electroporation, which show efficiency around 50–70%. The major disadvantage is that the electrical stimulation cause dying the most of host cells. The other technique is used for the delivery of genes, which is a transfection reagent. It shows efficiency around 20–30% that has disadvantage such as decreasing viability of the host cells. To use MNPs for gene delivery provide great advantages such as high efficiency and low cytotoxicity [25].

1.3.3 Active Targeting

Molecular targeting provides accumulation of MNPs in the tumor region based on the use of tumor-selective ligands. The main concept in active targeting is that cancer cells have different properties than normal cells such as overexpression of various receptors (**Figure 4**).

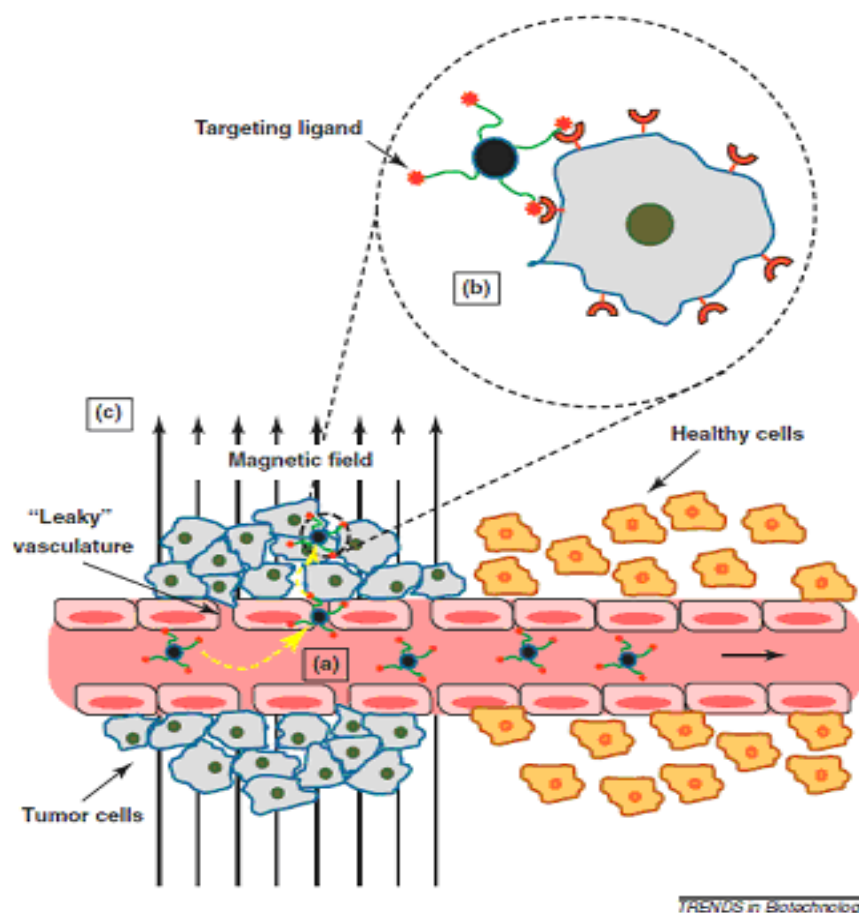


Figure 4. Representations of MNPs tumor-targeting modalities [23].

Therefore, the ligands are attached the surface of NPs which will specifically bind to the relevant receptors will target in cancerous tissue and, finally, will be uptake by the cancerous tissues [23]. There are various ligands, such as proteins, peptides, aptamers and small molecules, have been studied for

targeting studies in cancer therapy [23]. The first targeting agents that were studied for the specific targeting of MNPs composed of monoclonal antibodies (mAbs). The Food and Drug Administration (FDA)-approved Herceptin (trastuzumab) binds to the HER2/*neu* receptor that overexpressed on the surface of certain cancer cells (particularly in breast cancer). This has led to various applications of magnetic NPs for selective targeting of cancer cells [26]. However, due to the mAb with large dimensions and increasing immunogenicity, these modified nanoparticles pass poorly through biological barriers, which generate disadvantages for these targeting agents.

Cancer cells typically show high levels of glycolysis, even under aerobic conditions [27, 28]. The augmented demand for glucose to increase energy production in tumors and relatively rapid proliferation, give rise to high levels of expression and activity of cell surface glucose transport proteins, which can be used for tumor imaging using glucose analogs. Among all the glucose transporters, the GLUT-1 subtype is expressed in almost all tumor cell lines and tumor tissues [29].

Previous studies using [^{14}C] deoxy glucose showed cellular uptake by glucose transporters (GLUTs) and further phosphorylation for glycolytic processing [30, 31]. However, due to its structure, isomerization in the next step was prevented, the following metabolism was hindered, causing partially processed and labeled analogue to be accumulated in the cell. These findings have been applied extensively in clinical imaging by positron emission tomography (PET) in which ^{18}F FDG (2-fluoro-2-deoxyglucose) uptake is used to visualize tumor activity and location [32]. Also, recently 2DG is used for targeting nanoparticles into tumor cells [33-35].

The short peptides and small molecules have been used specifically for the delivery of MNPs to cancerous cells. The advantage of use these molecules are that hundreds or even thousands of molecules can be attached on the surface of nanoparticles. This provides nanoparticles, which contain hundreds of targeting molecules selectively binding and accumulation on cell containing

receptors, so an increased efficiency and affinity. Folic acid is the one of the commonly used ligand. All cancer types such as breast and lung overexpress the folate receptor on their cell surface. Their high bonding strength makes short peptides and other small molecules very advantageous. They have a reduced risk of bond breaking and loss of functionality after administration of the NPs into the body.

1.3.4 Cancer Diagnostics

During past decade, MNPs have been used as contrast agents in MRI. MNP cores have properties such as strong enhancement of transverse (T2 and T2*) relaxivity in tissue regions where MNPs have localized. Strong relaxivity is given on T2-weighted MR images as pronounced negative contrast (hypointensity) [36].

1.4 Nanoparticle/cell Interaction

Due to wide spread application of NPs, it is also imperative to evaluate their potential risks to biological systems [37]. The understanding of how magnetic nanoparticles (MNPs) interact with living system is one of the prerequisite pieces of information needed to be obtained before any further development for desired biomedical applications.

The aim of nanotoxicity research is to understand the mechanisms underlying NPs interactions with the cells. NPs uptake is first step for toxicity studies and follow cellular and morphological changes including metabolic pathways after internalization of NPs. Nanotoxicology studies tried to understand these events resulting from nanoparticle mediated cytotoxic effects on cells [37].

1.4.1 Transport of Nanoparticles

The internalization of nanoparticles are so called “the Trojan horse”, have been described already by former nanoparticles internalization studies that defined the process of phagocytosis to investigate the toxic effect of nickel and zinc

compounds [38]. Trojan horse mean nanoparticles are considered as vehicle and carry drug or material into the interior of the cell. For nanoparticles, there are many different routes to enter into the cells. Phagocytosis is not the only known route. There are also other possible routes for the internalization of metals, magnetic, or other nanomaterials systems by the cells, and for the different biological reactions that may undergo (**Figure 5**).

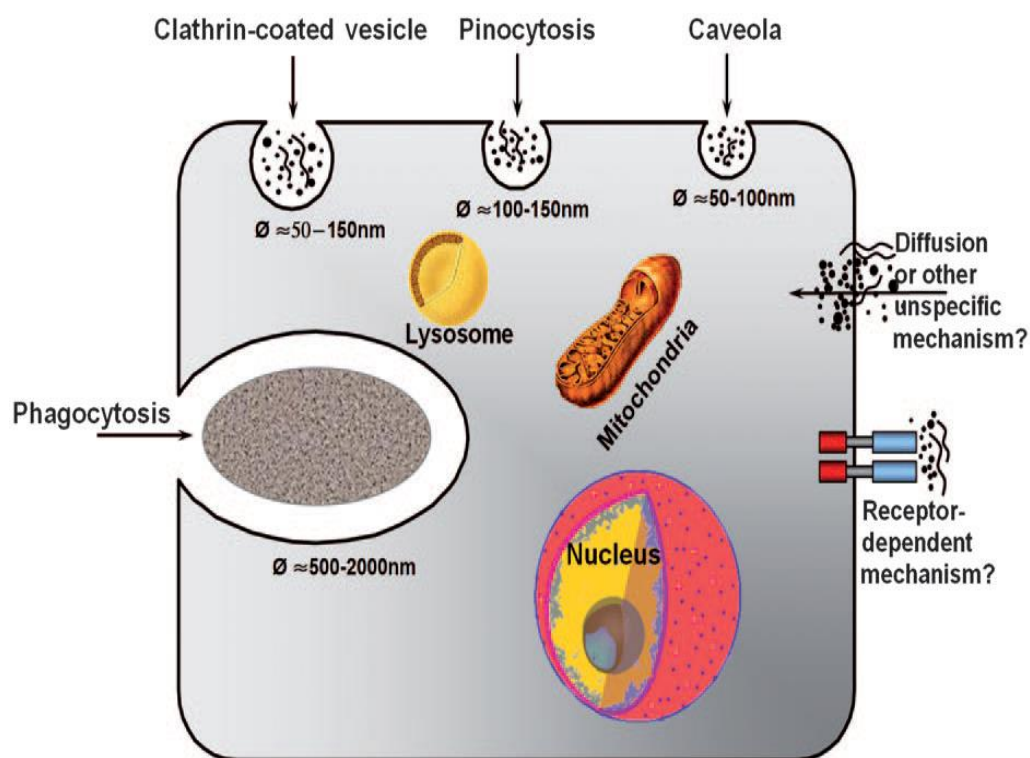


Figure 5. Possible cellular uptake mechanisms for nanomaterials. Nanomaterials may use different uptake routes into the cells [39].

Nanoparticles are smaller than 100 nm can pass into the cell “diffusion” through the plasma membranes, which is referred to as an adhesive interaction. Also, they use different vesicle transport pathway, for example transport of nanoparticles into cells bound to receptors [40]. Free transport through the membrane, however, can be consider to be more critical, as it allows particles to provide direct contact with the plasma proteins and with other molecules of the cell [39].

1.4.2 The Biology of Particle-Induced Oxidative Stress

The surface areas of NPs are very reactive therefore when they interact with the cells; they can cause reactive oxygen species (ROS)-production, and proinflammatory effects in the cell. ROS formation and oxidative stress are the best-developed paradigm to explain the toxic effects of nanoparticles [41]. ROS are produced at low amount in the mitochondrion under normal conditions, and there is a balance driven by antioxidant enzymes such as glutathione (GSH). On the other hand, when excessive amount of ROS generation during nanoparticle exposures, the antioxidant defenses may not be sufficient to neutralize them [42].

Oxidative stress is defined as a balance in which GSH is decreased while oxidized glutathione (GSSG) increased [42]. The cells modulate to this decrease in the GSH/GSSG ratio by responses [43].

According to the oxidative stress hypothesis, the lowest level of oxidative stress contain the trigger of antioxidant and detoxification enzymes [43]. Transcription factor nuclear factor erythroid 2-related factor (Nrf-2) triggers the promoters of phase II genes. At higher levels of oxidative stress, the inflammation and cytotoxicity play a role in protective response (**Figure 6**). Inflammation is result from the activation of pro-inflammatory signaling cascades [e.g., mitogen-activated protein kinase (MAPK) and nuclear factor kB (NF-kB) cascades], on the other hand mitochondrial perturbation cause the release of pro apoptotic factors (**Figure 6**) [4].

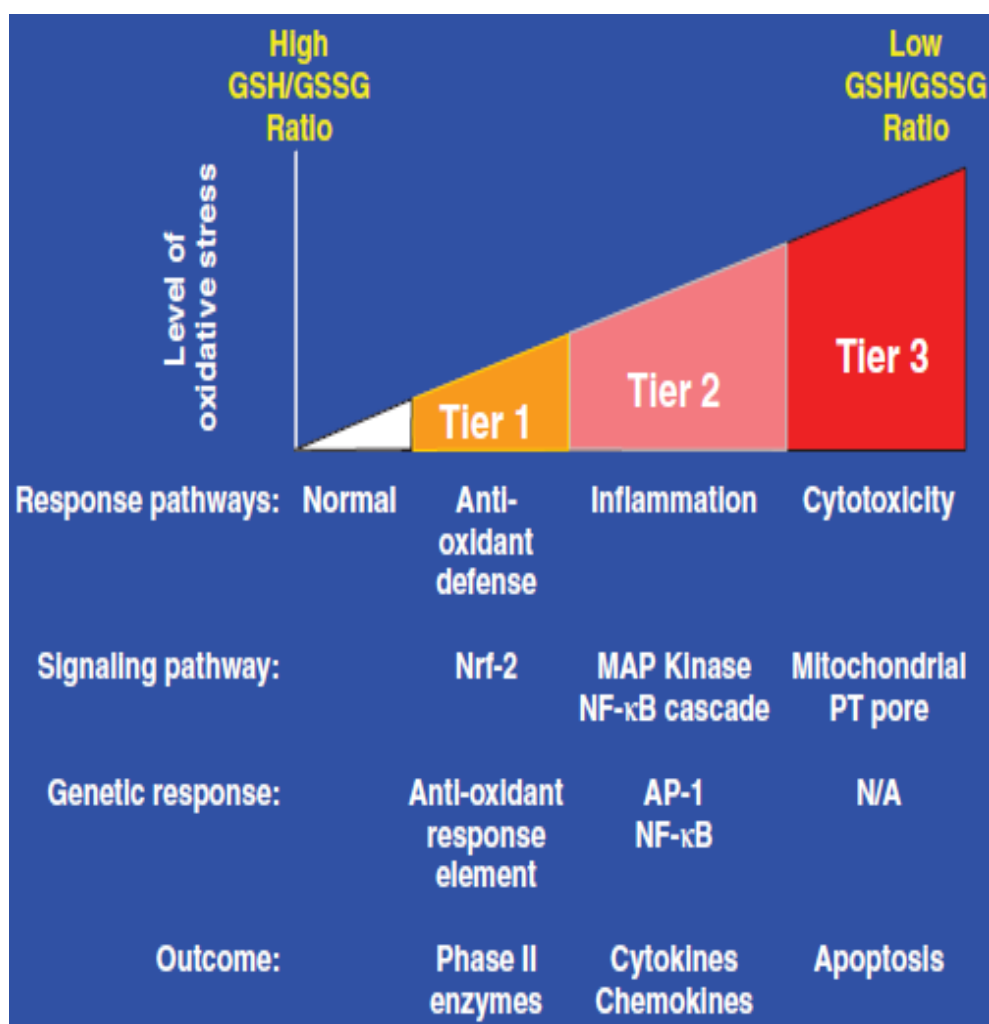


Figure 6. The oxidative stress model. At tier 1, phase II antioxidant enzymes are triggered by Nrf-2 to rebuild cellular redox homeostasis. At tier 2, activation of the MAPK and NF-κB pathways trigger pro-inflammatory responses. At tier 3, disruption of the mitochondrial permeability and electron transfer lead to cellular apoptosis or necrosis [42].

In addition to the hypothesis of oxidative stress, it should consider that new nanomaterials and their unique properties lead to different or novel mechanisms of toxicity [4].

Biological systems can interact with multiple pathways of injury, such as inflammation, apoptosis, necrosis, fibrosis, hypertrophy, metaplasia, and carcinogenesis (**Table 1**).

Table 1. NM effects as the basis for pathophysiology and toxicity [42].

Experimental NM effects	Possible pathophysiological outcomes
ROS generation*	Protein DNA and membrane injury* Oxiditive stress*
Oxidative stress*	Phase II enzyme induction, Inflammation* Mitochondrial perturbation*
Mitochondrial perturbation*	Inner membrane damage,* Permeabilty transition(PT) Pore opening* Energy failure* Apoptosis* Cytotoxicity
Infammation*	Tissue infiltration with inflammatory cells Fibrosis Granulomas

1.5 Cancer

Cancer is the general name given to a collection to related diseases in which normal cells are changed to cells capable of uncontrolled growth and invasion. The cancer cells grow abnormally and cover into surrounding tissues. Cancer is made up of trillions of cells which is originated from anywhere of the body.

Normally, the cells grow and divide to form new cells to constitute organs and tissues, which need cell turnover [44]. There is a balance between cell proliferation and apoptosis; a programmed cell death to control cell multiplicity. The genetic alterations such as mutations lead to disrupt this balance. Cellular multiplicity would be clinically detectable as a tumor. Tumor cells differ from normal cells in many ways. One important difference is that normal cells are more specialized than cancer cells. That is, normal cells can be functionalized for specific functions, cancer cells do not. They are able to ignore signals such as apoptosis and evade the immune system [45]. Some cancerous cells have characteristic such as malignant, and invasiveness. They can spread all over the body through distant places in the body through the blood or the lymph system and form new tumors far from the original tumor. They can cause the formation of new blood vessels (angiogenesis) and then penetrate into lymphatic or blood vessels [46]. On the other hand, benign tumors do not share same properties with malignant tumors; benign tumors can be quite large however cannot travel, or invade, nearby tissues. After surgery, they usually do not reappear unlike malignant tumors. Types of cancer are named according to the where they are originated from. Therefore more than hundred types of cancers have been known [46].

1.5.1 Breast Cancer

Breast cancer (BC) is the most common cancer in women worldwide, with nearly 1.7 million new cases diagnosed in 2012 (second most common cancer overall). This represents about 12% of all new cancer cases and 25% of all cancers in women [47]. Breast cancer is a heterogeneous disease. This mean each patients give different responses to therapy and their disease show variability in their molecular profiles [48] .

Breast cancer is originated from the malignant proliferation of epithelial cells lining the ducts or lobules of the breast. Both environmental and genetic risk factors lead to breast cancer such as alcohol, stress [49]. Some breast cancers

are not inherited, but others the mutations in the genes *BRCA1* and *BRCA2* are inherited. *BRCA1* and *BRCA2* are human genes that produce tumor suppressor proteins. These proteins are responsible for repair damaged DNA and, therefore, play a role in ensuring the stability of the cell's genetic material. When either of these genes is mutated, or altered, such that its protein product either is not made or does not function correctly, DNA damage may not be repaired properly. As a result, cells are more likely to develop additional genetic alterations that can lead to cancer. Together, *BRCA1* and *BRCA2* mutations account for about 20 to 25 percent of *hereditary* breast cancers [50] and about 5 to 10 percent of *all* breast cancers [51]. By contrast, according to the most recent estimates, 55 to 65 percent of women who inherit a harmful *BRCA1* mutation and around 45 percent of women who inherit a harmful *BRCA2* mutation will develop breast cancer by age 70 years [52, 53]. Angelia Jolie became a real phenomenon who carries mutation in her *BRCA1* gene and her decision led to increase awareness of breast cancer treatment (**Figure 7**). *BRCA1* mutant breast cancers are predominantly triple-negative (ER-, PR-, Her2-) and share multiple clinic pathologic features with TNBC (triple negative breast cancers) and thus generally have poorer prognosis than other breast cancers [54, 55]. *BRCA1* and *BRCA2* have roles in homologous recombination (HR) for DNA repair [56, 57]. When the remaining wild-type allele is lost in a cell, this repair mechanism does not work, resulting in genomic instability that is sufficient to promote tumor development [58, 59].

TNBC are high aggressive compared to HER2-positive breast cancers [60]. Although tamoxifen and Herceptin are used as good targeted therapy in ER +, HER2 + breast cancer [61], there is little targeted therapy for TNBC until the date [62]. The only known targeted therapy possible for TNBC is combination therapy such as chemotherapy with platinum [63] offering limited therapy with unwanted side effects [64].

Although there are many treatment and different therapy for breast cancer, it is still the most common cancer among women. Hence, much more research is needed to develop for treatment of breast cancer.

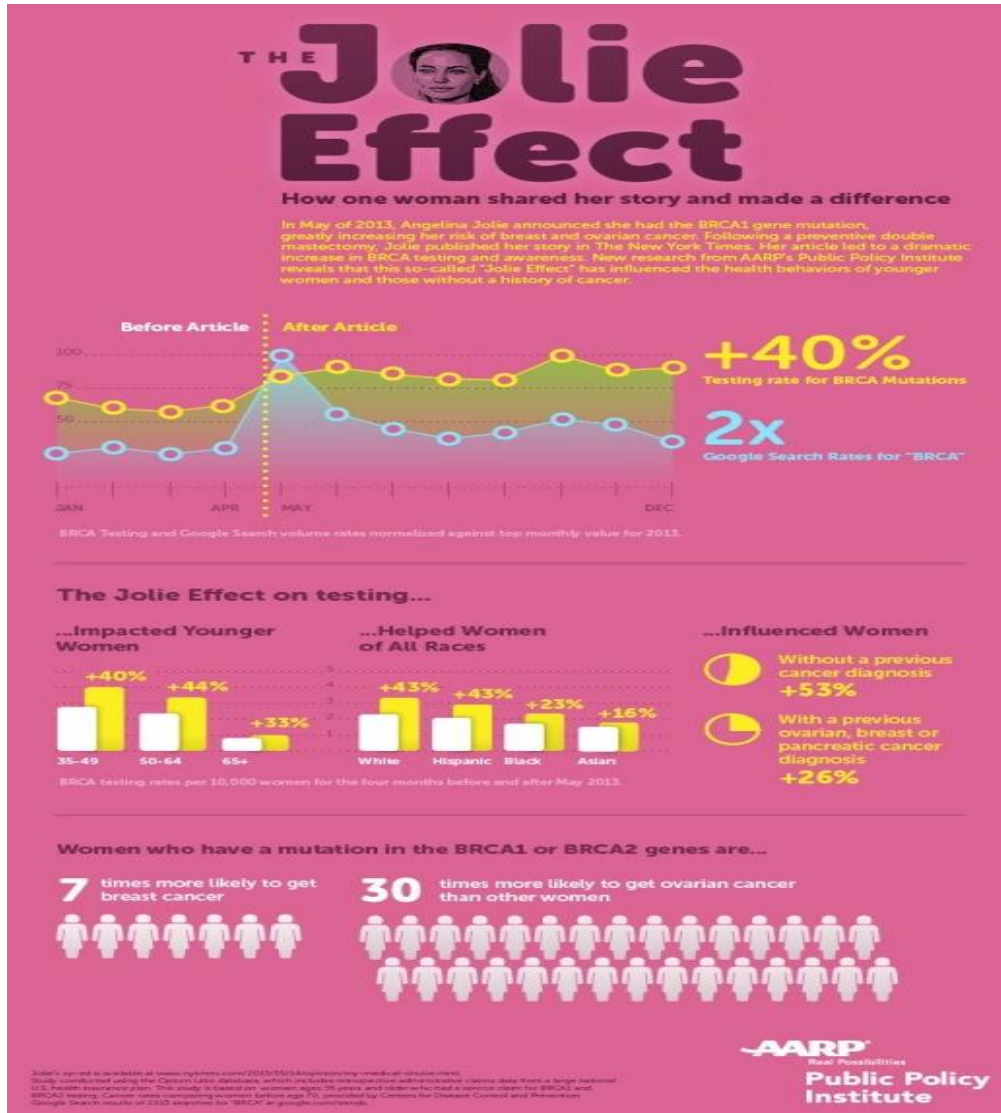


Figure 7. To better understand the so-called “Angelina Jolie effect”, AARP, in collaboration with Optum Labs, compared BRCA testing rates based on claims among commercially-insured women ages 35 and older in the US, before and after Ms. Jolie’s story was publicized in 2013. (<http://www.aarp.org>)

1.5.2 Treatment Strategies for BRCA1 mutated Breast Cancer

The surgery, radiotherapy and chemotherapy have been used for breast cancer treatments. If cancer is in the early stage, surgery can be good choice for treatment. Surgery contains the removal of the whole cancerous tissue together with adjacent tissues. For example, tumor and surrounding tissue are removed in lumpectomy while a whole breast is removed in mastectomy. The chemotherapy and radiation are applied to the patients after surgery to prevent reappearance of the cancer cells left. Both chemotherapy and radiotherapy have unwanted effects to healthy cells such as short disease-free intervals, rapidly progressive visceral disease, lymphangitic pulmonary disease, or intracranial disease. Combination therapies are needed to cure the breast cancer responds to multiple chemotherapeutic agents.

1.5.3 Possible Targeted Therapies

It is needed to improve novel therapeutic agents to prevent TNBC resistant to chemotherapy for patients. Novel targeted therapies (e.g. PARP, EGFR, c-kit and VEGF inhibitors alone or in combination with chemotherapy) are currently under investigation and have shown promising results in numerous phase II trials. TNBC originated from myoepithelial cells and therefore have similar surface biomarkers with these cells including CK5-6 and EGFR [65].

As seen in **Figure 8**, there are possible targeted therapies for breast cancer. For example, defect in p53 and the DNA repair pathway is involved in basal-like breast cancer causing genetic instability [66]. DNA repair defects usually are associated with lack of BRCA1 function [67]. Generally, majority of basal-like breast cancers have a defect in BRCA1 function [68]. Among the genes, checkpoint kinase 1 (CHEK1) and poly (ADP ribose) polymerase (PARP1) can be used as candidate targets. The dysregulation of kinases are also observed in TNBC. Phosphatase and tensin homolog (PTEN) defects have been reported in up to 30% of TNBCs which downregulate the AKT/mammalian target of

rapamycin (mTOR) pathway [69]. EGFR is present in 45–70% in which is another potential target for TNBC [70].

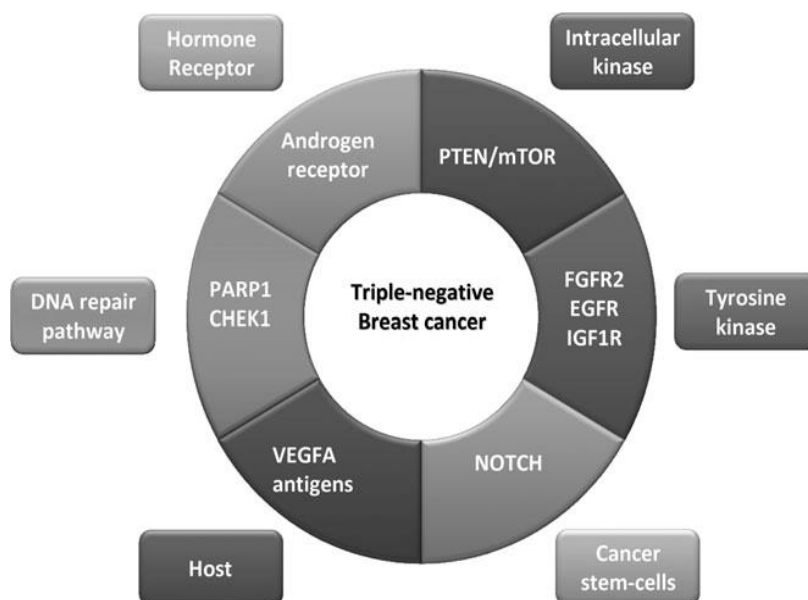


Figure 8. Candidate targets and pathways in triple-negative breast cancer [71].

In a comparative genomic hybridization (CGH) array study, vascular endothelial growth factor A (VEGFA) was observed to be increased in 34% of TNBCs [69]. There is correlation VEGF expression with high rate of TNBCs. TNBC was also reported as chemokine release, together with immune activation [72]. Also it is observed that there is strong correlation between immune activation and good prognosis [73]. It is shown that the androgen receptor is highly expressed in TNBC. It is found that the level of breast cancer stem cells (CD44⁺/CD24⁻/low) is very high in basal-like breast [74]. NOTCH pathway is another candidate targets have been reported in recent years.

1.5.4 PARP Inhibitors

Poly-ADP-ribose-polymerase (PARP)-1 is one of the central components, which is responsible for removing single-strand DNA breaks. Single-strand breaks may lead to double-strand breaks, Unless PARP work properly in BRCA1-mutated cells. Clinical studies show that BRCA1-null cells are

sensitive to PARP1 inhibitors [75]. Furthermore, in combination a PARP inhibitor with platinum-based chemotherapy can provide good results in preclinical models. Consequently, a number of clinical trials indicate that PARP inhibitors alone or in combination with platinum-based chemotherapy give promising results [76]. Results of two very important clinical trials implementing PARP inhibitors in patients with metastatic BC have recently been reported. These phase II results are promising but will need to be validated in larger possibly phase III trials.

1.5.5 Mechanism of siRNA-Mediated Gene Silencing

Small interfering RNA (siRNA) technology has great attention as a therapeutic intervention for targeted gene silencing in cancer. RNA interference is mechanism that short double-stranded RNAs are recognized by the endonuclease cleaved into two fragments called siRNA.

When siRNA gets into the cell, it merges with RNA-induced Silencing Complex (RISC), so a RISC-associated, ATP-dependent helicase activity unwinds the siRNA duplex, thus providing either of the two strands to independently guide target mRNA recognition. Next, Argonaute 2 (Ago2), cut the target mRNA and leads to its degradation, stopping protein expression. The mRNA silencing is accomplished via site-specific cleavage of the message in the region of the siRNA-mRNA duplex depend on the degree of complementarity between the guide strand and target mRNA. The cleavage products of the reaction are released and degraded leaving the siRNA-programmed RISC to survey and further deplete the available pool of target mRNA (**Figure 9**) [77].

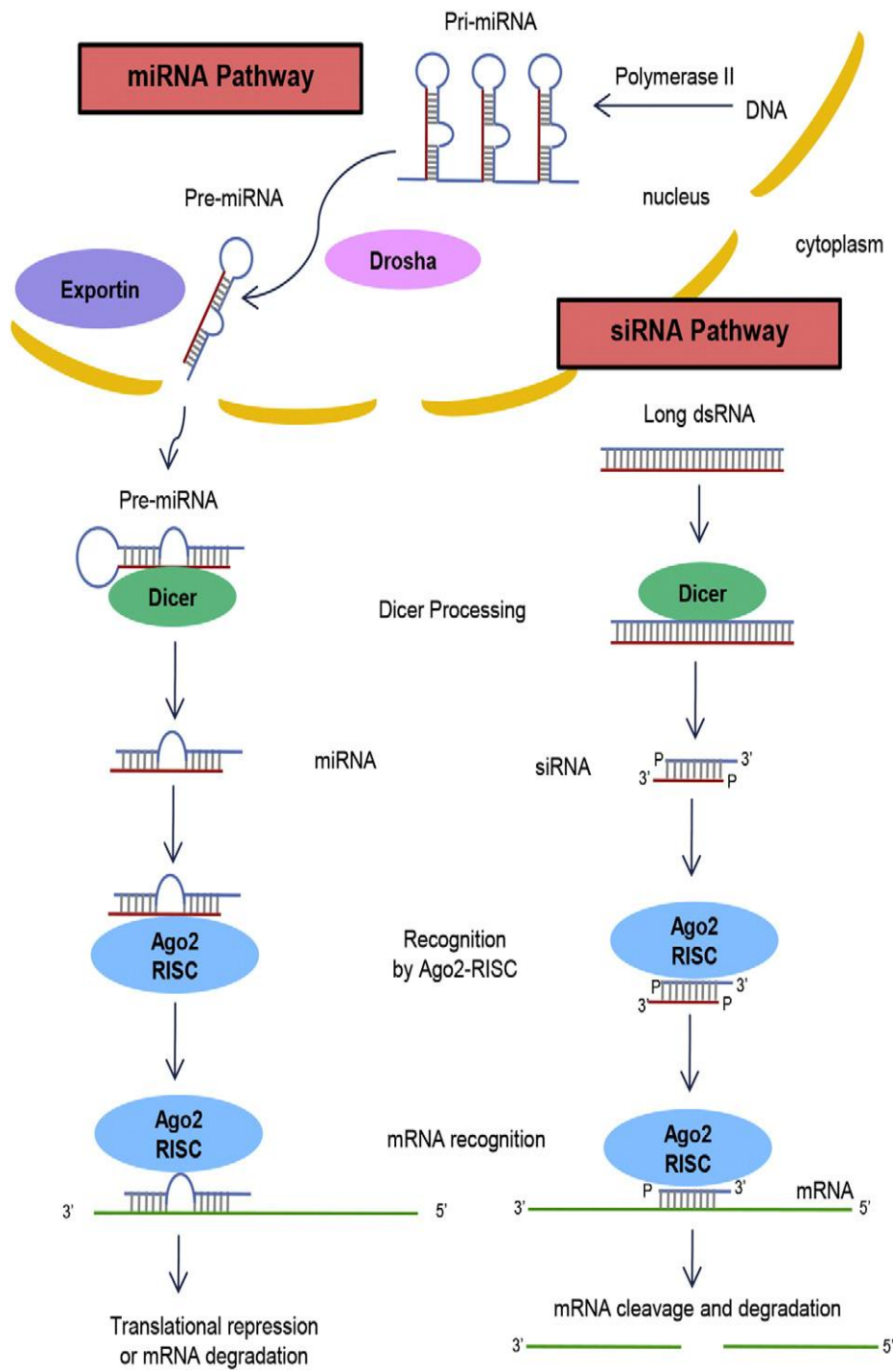


Figure 9. The RNA-interference process in mammalian cells. Cytoplasmic long double-stranded RNA (dsRNA) is cut by Dicer into small interfering RNA (siRNA) resulting in the cleavage and degradation of specific target mRNA [78].

To carry siRNA efficiently into tumor region, the carrier should be biocompatible, nonimmunogenic, and biodegradable as well as ability to escape rapid hepatic and renal clearance. Moreover, carrier should directly accumulate into tumor region.

There are many alternative agents to carry siRNA. Among them, nanoparticles hold promising agents and meet these requirements for delivery of siRNA. Nanoparticles can be divided into polymeric or metallic core. To use nanoparticle for delivery of siRNA, the physicochemical characterizations such as surface charge, size are important parameter whether determine uptake of particles, bio distribution, and safety by cells.

Nanoparticle is smaller than 200 nm, which is suitable for biomedical application. Negatively charged nanoparticles are removed faster than positively charged ones. In addition, hydrophilic coating such as polyethylene glycol (PEG) or a nonionic surfactant prolongs circulation time of the nanoparticles. Taken together, nanoparticles offer many advantages: (1) to prevent fast degradation of siRNA, (2) provide high local concentration of siRNA into tumor tissues, (3) enable as controlled release and (4) provide safe and effective platforms for siRNA delivery [77].

1.5.6 Eukaryotic Elongation Factor 2 Kinase

Eukaryotic elongation factor 2 kinase (eEF2K) is a member of the small group of atypical 'α-kinases' that phosphorylates and inhibits eukaryotic elongation factor 2 and decrease the elongation stage of protein synthesis, which normally use a great deal of energy and amino acids [79]. The only known substrate for eEF2K is elongation factor eEF2. Since phosphorylation of eEF2 at Thr56 disrupt its binding to the ribosome and thus slow down the rate of elongation [79].

Eukaryotic elongation factor 2 (eEF2) is a member of the GTP-binding translation EF family, which is vital for protein synthesis and can be completely inactivated by EF2 kinase phosphorylation [79, 80]. The eEF2 gene is found in chromosome 19 in humans and has a size of 9407 bases [80].

1.5.7 eEF2K in Cancer Therapeutics

In recent years eEF-2K has gained interest as therapeutic target [81, 82]. It was found to be highly expressed in cancer cells, whereas no detectable expression were found in normal cells [80].

The mitogen, hypoxia, metabolic stress and nutrients deprivation induce the up regulation of eEF-2K expression. Moreover, the autophagy is mechanism to conserve or direct energy for other cell function which is associated with activity of eEF-2K [82, 83]. The eEF-2K play roles as pro-survival kinase in cell growth, survival and drug resistance [83, 84].

Meric-Bernstam et al. collected primary tumors from 190 patients with stages I to III hormone receptor-positive breast cancer and the data showed that the eEF2K activity was increased and related with poor prognosis in hormone receptor-positive breast cancer. These data suggest that eEF2K can be as a prognostic marker and therapeutic target to treat breast cancer [85].

Ozpolat and his lab also showed that the therapeutic potential role of eEF-2K in pancreatic carcinoma cell lines. It was shown that targeting of eEF-2K induced the invasive phenotype of PaCa cells, through signaling pathways involving TG2/b1 integrin/Src/uPAR/MMP-2 and induction of (the epithelial-mesenchymal transition) EMT biomarkers which led migration of the cells and metastatic potential. Hence, eEF-2K could be also therapeutic target in pancreatic cancer [86].

The disruption of eEF-2K expression results in the knockdown of signaling pathways including growth, survival and resistance for the treatment of breast cancer [87]. An in vivo orthotopic model showed that the down regulation of the EF2K led to inhibition the growth of tumors and sensitizes the tumors to

doxorubicin. The data suggested that eEF-2K led tumorigenesis through the up regulation of pro-tumorigenic proteins and pathways including cyclin D1, c-Myc, c-Src/FAK and Akt (**Figure 10**) [87].

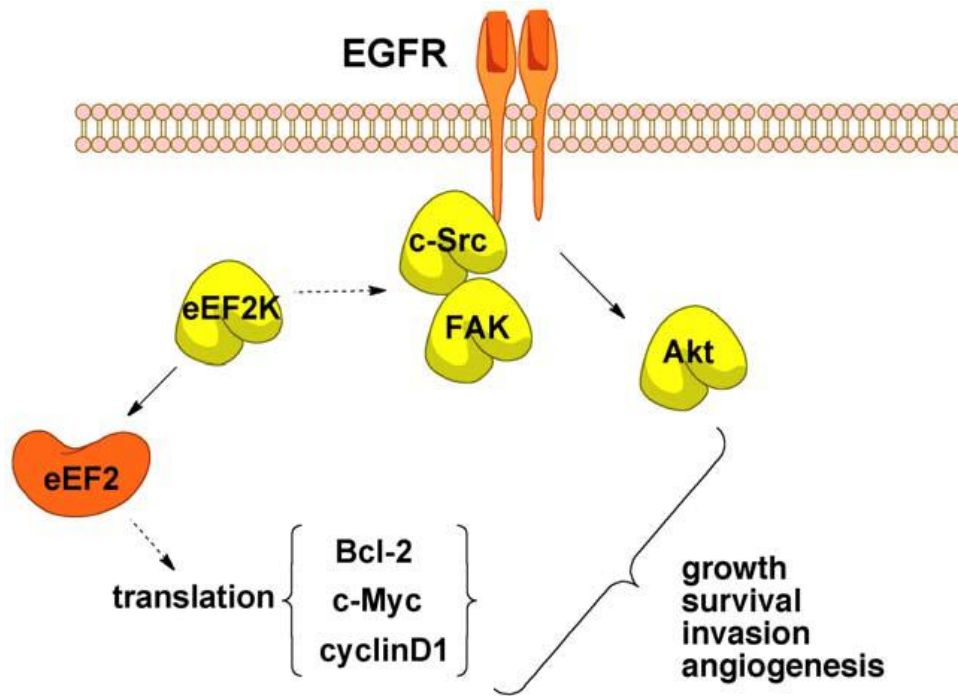


Figure 10. Targeting eEF-2K leads tumorigenesis in breast cancer cells. Pathways aided by eEF-2K are involved in cell growth, motility, angiogenesis, and survival. Solid arrows show known pathway while dashed arrows shows potential pathway [87].

1.6 Aim of This Study

In this study, the main goal is to design safe and effective functional magnetic nanoparticles for theranostic purposes.

For this reason, we will prepare cobalt ferrite magnetic nanoparticles (CoFe-MNPs) and use some surface modifiers in order to make them to internalize better into breast cancer cells.

We will then carry out *in vitro* characterization of these MNPs and further use them for *in vivo* animal studies.

CHAPTER 2

MATERIALS AND METHODS

2.1. Materials

All chemicals were analytical grade and were obtained from commercial sources having the highest purity available. In all the experimental studies, Millipore water purification system (Molsheim, France) was used to obtain deionized water of 18 MΩ cm. For cell culture assays, Roswell Park Memorial Institute (RPMI-1640) medium with phenol red and without phenol red (Lonza BE12-115F, Belgium), Dulbecco's Modified Eagle Medium/Ham's F-12 (DMEM/Ham's F12) (Lonza-BE12-719F) fetal bovine serum (FBS) (Sigma), gentamycin (Biological Industries), Hank's Balanced Salt Solution (BSS) (Biochrom AG), Dulbecco's Phosphate Buffered Saline (PBS) (Lonza), Trypsin/EDTA (Lonza BE02-007E), Trypan Blue (Biological Industries), Dimethyl sulfoxide (DMSO) (Applichem). Epidermal Growth Factor (EGF) was from Peprotech (New Jersey, USA). Hydrocortisone, insulin was purchased from Sigma-Aldrich (Saint Louis, Missouri, USA). 0.5 % (w/v) trypan blue, gentamycin sulfate XTT Cell Proliferation Kit were purchased from Biological Industries (Haemek, Israel). MTS and TUNEL colorimetric assay kit was purchased from Promega (Madison, WI). Annexin-V Apoptosis detection kits were obtained from Biolegend, (USA). Ethidium bromide, Chlorpromazine, Mitomycin C (MMC), Cytochalasin B and DCFDA were obtained from Sigma (USA). All RNA isolation, cDNA synthesis, q-RT-PCR experiments kits were obtained from 5 Prime (USA). For 2DG and siRNA

conjugation reactions; EDC and sulfo NHS were purchased from Pierce Chemical Co and 2DG were purchased from Sigma (USA). The siRNA, targeting EF2K (Sigma-Aldrich) was designed using siRNA-designing software (Qiagen, Valencia, CA, USA). HiPerFect Transfection Reagent was from Qiagen. AZD2281 (Olaparib) was obtained from Selleck Chemicals, USA. Antibodies; eEF-2K, p-EF2 (Thr-56), EF2, cyclin D1, p-Akt (Ser-473), Akt, p-Src (Tyr-416), Src, p-paxillin (Tyr-31), paxillin, 4E-BP1, p-4e-bp1, CD44, ALDH1A1, Claudin1, VEGF, (Cell Signaling Technology, Danvers, MA); p-FAK (Tyr-397), FAK (BD Transfection); c-Myc, (Santa Cruz Biotechnology, Santa Cruz, CA), CCL2 (Sigma Chemical, St. Louis, MO) Horseradish peroxidase-conjugated anti-rabbit or anti-mouse secondary antibody (Amersham Life Science, Cleveland, OH). Mouse anti-b-actin (primary) and donkey anti-mouse (secondary) antibodies were purchased from Sigma Chemical, St. Louis, MO. DAKO antigen retrieval solution (DAKO, North America Inc., Carpinteria, CA). IgG blocking from a Vector M.O.M. kit (Vector Laboratories, Inc., Burlingame, CA). Ki67 was from Thermo/Lab Vision, anti-CD31 (PharMingen, San Diego, CA), goat anti-rat HRP-conjugated secondary antibody (Jackson Immuno Research Laboratories Inc., West Grove, PA), DAB substrate (Vector Labs); Chemi-glow detection reagents were from Alpha Innotech, San Leandro, CA.

For nanoparticle synthesis, Iron (III) chloride ($\text{FeCl}_3 \cdot 9\text{H}_2\text{O}$, Riedel-de Haën), Cobalt (II) chloride 6-hydrate ($\text{CoCl}_2 \cdot 6\text{H}_2\text{O}$, Surechem), Sodium hydroxide pellets (NaOH, Sigma-Aldrich), Sodium Chloride (NaCl, Fisher Scientific Company), and Oleic acid ((9Z)-Octadec-9-enoic acid, Fluka) were used for the preparation of CoFe_2O_4 magnetic nanoparticles. In order to prepare silica coating on CoFe_2O_4 nanoparticles, Tetraethyl orthosilicate (TEOS, 98%, Aldrich), (3-Aminopropyl) trimethoxysilane (APTMS, $\geq 98.0\%$, Aldrich), and Ethanol (EtOH, $\geq 99.9\%$, Merck) were used. For the functionalization of CoFe_2O_4 nanoparticles with $-\text{NH}_2$ groups, (3-Aminopropyl triethoxysilane (APTES, $\geq 98.0\%$, Fluka), toluene ($\text{C}_6\text{H}_5\text{CH}_3$, $\geq 99.0\%$, Merck), and N, N-dimethylformamide (DMF, $\text{C}_3\text{H}_7\text{NO}$, $\geq 99.8\%$, Sigma-Aldrich) were used. The

attachment of –COOH group on the nanoparticles were done by using toluene ($C_6H_5CH_3$, $\geq 99.0\%$, Merck), N, N-dimethylformamide and succinic (glutaric) anhydride ($C_4H_4O_3$, $\geq 99\%$, Sigma- Aldrich).

2.2. Methods

2.2.1. Preparation, and Silica Coating of Cobalt Ferrite Nanoparticles (CoFe MNPs)

Cobalt ferrite (CoFe) MNPs were synthesized according to literature by co-precipitation method [88]. A salt solution containing 0.54 g $FeCl_3 \cdot 6H_2O$ and 0.238 g $CoCl_2 \cdot 6H_2O$ was prepared in 10 mL deionized water and then, 10 mL of 3M NaOH and 5mL of 1.5M NaCl were added to the salt solution drop wise simultaneously under magnetic stirring. After the addition of NaOH and NaCl, a black suspension was obtained. The reaction was performed at 80°C for an additional 1 h with vigorous stirring. After cooling to room temperature, CoFe MNPs were washed three times with deionized water and ethanol solutions by using a magnet. 20 mL CoFe MNPs colloidal suspension was used for silica coating using sol-gel method [89]. According to the method, 80 mL ethanol, and 170 μ L TEOS (Sigma–Aldrich) and 15 μ L APTMS (Sigma–Aldrich) were mixed and added to the CoFe MNPs colloidal suspension and stirred for 3 h at room temperature. Then, silica coated CoFe MNPs were washed three times with deionized water by using a magnet. Accordingly, the Zeta potential and average hydrodynamic sizes have been measured by dynamic light scattering (DLS) (Malvern Nano ZS90) in water, RPMI-1640 medium and complete medium at 25 °C. In order to mimic in vitro cell culture conditions, we chose to incubate CoFe-MNPs with cell culture medium supplemented with 10% FBS, containing plentiful protein. Fourier Transform Infrared Spectroscopy (FT-IR) (Alpha, Bruker) analysis was performed in order to investigate the bonds concerning the silica layer formed on the CoFe-MNPs. The Energy Dispersive X-Ray analyser (EDX) was used for elemental analysis of cobalt ferrite and silica coated cobalt ferrite nanoparticles.

2.2.2 Cell Culture

2.2.2.1 Cell Culturing and Treatments

Human breast cancer cell line MDA-MB-231 (invasive, metastatic, triple negative), MCF-7 (noninvasive) and non-cancer human breast cell line MCF-10A was obtained from ATCC (American Type Culture Collection, USA). MDA-MB-231 and MCF-7 cells were grown in RPMI supplemented with 10 % FBS and MCF 10A cells were grown in DMEM/Ham's F: 12 medium with phenol red containing 5% horse serum, 100 mg/mL Epidermal Growth Factor (EGF), 1 mg/mL hydrocortisone and 10 mg/mL insulin. Both the media contained penicillin and (100 units/mL) streptomycin. Cells were maintained at 37°C in a humidified atmosphere containing 5% CO₂/95% air, and were used between passages 4 and 15 in the experiments.

CoFe-MNPs dispersions were prepared by diluting the concentrated stock solutions in the cell culture complete medium at room temperature for all assays prior to the treatment of cells. Sonication in ultrasonic bath for 5 minutes at room temperature was used immediately before the cell treatment in each assay. Stock suspensions of (1 mg/mL) naked and silica coated CoFe-MNPs in complete medium were serially diluted to the concentration range of 15-500 µg/mL for cellular uptake, cytotoxicity genotoxicity, oxidative stress, and apoptosis assays.

2.2.2.2 Cell Thawing

The cells should be defrosted gradually. For this reason, the cryotubes were received from the liquid nitrogen and kept waiting for minutes at 37°C water bath. After defrosting of the cells, they were seeded in T75 cell culture flask that contain growth medium. The cells were attached the surface of flask and incubated in CO₂ incubator at 37°C. After twenty-four hours, the medium

containing dimethylsulfoxide (DMSO) medium was removed and replaced with fresh one.

2.2.2.3 Cell Passaging

The cells were grown in in the T75 flasks. When the cells reached confluence around 80 % of total surface of the flasks, the growth medium was discarded and the cells rinsed with phosphate buffered saline (PBS). Then, the cells were subject to trypsination with pre warmed trypsin/EDTA solution. After the cells were detached, the activity of trypsin was terminated with complete medium. The cell suspensions were centrifuged and the supernatant were removed. The cells were resuspended with the fresh complete medium and placed to new T75 flasks at 37°C, CO₂ incubator. This process was repeated depend on the cell types in every 3-4 times in a week.

2.2.2.4 Cell Freezing

The freezing medium was prepared to freeze the cells, which was containing the complete medium with ten percent DMSO. The cells were trypsinized; the detached cell suspensions were stained with trypan blue and counted. Approximately one mL of freezing medium was used for ten million cell suspensions. After calculating the cell number, the cell suspensions were centrifuged and supernatants were removed. The cells were resuspended with the freezing medium and placed into cryovials. The cryovials were gradually placed at -80°C. After one day, they were placed to liquid nitrogen tank.

2.2.2.5 Cell counting

5x10⁵cells /well were seeded in 6-well plates and incubated into the CO₂ incubator at 37°C. After twenty-four hours, the medium of the cells were discarded and washed with 1 mL of PBS. The cells were subjected to trypsination. Detached cell suspensions were transferred to separate eppendorfs and 0.25 % (w/v) trypan blue were applied for counting using hemocytometer

under light microscopy. 10 μ L of mixed cell suspension was put on two chambers of the hemocytometer. The calculations were done according to the averages of two chambers as follows;

Cell number / mL = the average cell number of the two chambers x DF x 10^4

DF= Dilution factor that was done with Trypan Blue

10^4 = Factor calculated from the dimensions of hemocytometer

The dimensions of each chamber on the hemocytometer were 1 cm length, 1 cm width and 0.1 cm height, having volume of 0.1 cm^3 or 10^{-4} mm^3 (10^{-4} mL).

2.2.3 Visualization of Intracellular MNP

2.2.3.1 Cellular Uptake by TEM

Qualitative analyses of internalized naked and silica coated MNPs were performed by TEM. The cells were seeded into six-well plates overnight and treated with MNPs for 24 h at 125 $\mu\text{g} / \text{mL}$ concentration. Cells were collected and fixed in 2.5% gluteraldehyde solution at $+4^\circ\text{C}$ and after phosphate buffer washing, fixed with 1% osmium tetroxide solution. The cells were dehydrated with graded alcohol series (50–60–70–80–90– 95–100%) and embedded in an Araldite mixture (Araldite CY 212 20 mL, DDSA 22 mL, BDMA 1.1 mL, Dibutylphthalate 0.5 mL). The cellblocks obtained were held at 60°C for 48 h to complete the polymerization procedure. After incubation, ultrathin sections were prepared using a diamond knife to a maximum thickness of 100 nm. The sections were stained with uranyl acetate & Reynold's lead citrate. The grids were examined under a transmission electron microscopy (TEM) (FEI Tecnai G2 Spirit TWIN).

2.2.3.2 Cellular Uptake of MNPs by ICP-OES

Quantitative analyses of internalized naked and silica coated MNPs were performed by inductively coupled plasma optical emission spectrometry (ICP-OES), measuring the iron content. Briefly, 2×10^6 cells were plated in 60x15mm culture dish and incubated for 2, 4, 8, 24 h with different concentrations of naked and silica coated MNPs (62-500 $\mu\text{g/mL}$). Then the cells were trypsinized and, collected in 15 mL falcon tubes. Cells were counted on hemacytometer and digested with concentrated HCl acid at least 24 h to obtain a clear solution. Samples were diluted with water. Standards were prepared as 0.1, 0.25, 0.5, 1, 2.5 and 5 ppm for iron element. Then the iron concentrations in digested samples were quantitated by ICP-OES (Direct Reading Echelle, Leeman Labs INC).

Some of the parameters used in ICP-OES measurements were as follows: Incident plasma power was 1.2 kW, plasma coolant and the auxiliary Ar gas flow rates were set at 18 L/min and 0.5 L/min respectively. The nebulizer Ar was used at a pressure of 50 psi. Peristaltic pump at 1.2mL/min flow rate was used for sample transportation.

To determine whether the uptake of MNPs into cells was energy-dependent or more generally, cell function dependent, the cells were incubated with MNPs under varying metabolic conditions. Energy dependence experiments were performed by pre-incubating the cells at 4°C for 30 min prior to exposure to MNPs. After this pre-incubation, cells were incubated with (250 $\mu\text{g/mL}$) naked and silica coated MNPs for 2 h at 4°C. The other cellular uptake study was performed at 37°C. For inhibition studies, eighty to ninety % confluent cells were pre-incubated with (0.1%) sodium azide, (0.45 M) sucrose and (6 $\mu\text{g/mL}$) chlorpromazine for 30 min in separate experiments and then incubated with naked and silica coated MNPs for 2 h at a final concentration of 250 $\mu\text{g/mL}$ (derived from IC_{50} experiments). After this incubation, the medium was removed and the samples were washed with DPBS, in order to ensure particle

removal from the outer cell membrane. Untreated cells and cells treated with only MNPs (no inhibitor) were used as negative and positive controls, respectively.

2.2.3.3 Cellular Uptake of MNPs by Prussian Blue Staining

For analysis of iron uptake with Prussian blue staining, three different human breast cell lines were incubated with naked or silica coated MNPs at 37 °C in 5 % CO₂ atmosphere for 24 h. After incubation, cells were washed two times with PBS and collected using 0.25 % trypsin. Subsequently, the cells were fixed with 4 % of formaldehyde and again washed with distilled water three times. The mixture of 5 % potassium ferrocyanide and 5 % hydrochloric acid solutions at a ratio of 1:1 was used as working solution and added to the fixed cells for 30 min incubation at room temperature. Cells were then washed by distilled water three times and counterstained with Nuclear Fast Red for 5 min and evaluated under Zeiss Axioscope Microscope, Goettingen, Germany [20].

2.2.3.4 Cellular Uptake of MNPs by Flow Cytometry

The uptake of MNPs using flow cytometry was carried out according to the method developed by Suzuki et al [90]. The principle of this assay is based on the differences in the intensity of the scattered light. The forward scattered (FSC) light stay constant during uptake of non-fluorescent MNPs, while side-scattered (SSC) light increases in proportion to the concentration of MNPs inside the cells. In our study, 10⁵ cells/mL were seeded in 6-well cell culture plates. After twenty-four hours incubations, the cells were treated with 50 and 100 µg/mL MNPs for 24 hours. The medium containing excessive MNPs were discarded and washed at least three times PBS. Then, the cells were detached using 0.25 % trypsin and centrifuged at 250 g for 5 min. The supernatant was removed and the pellet was resuspended in 4 % paraformaldehyde at 4 °C before measuring by flow cytometry. They were then centrifuged at 250 g for 5 min. The supernatant was again removed and the pellet was resuspended in

0.5 mL of PBS. The uptake of particles was determined by flow cytometer (Accuri II, BD BioSciences, San Jose, CA, USA) equipped with a 488 nm laser.

2.2.4 Cytotoxicity Assay

2.2.4.1 XTT assay

The cell proliferation 2,3-Bis-(2-Methoxy-4-Nitro-5-Sulfophenyl)-2H-Tetrazolium-5-Carboxanilide (XTT) kit was used for the cytotoxicity evaluation according to the manufacturer's instructions. Briefly the tetrazolium salt XTT was reduced to orange colored formazan compounds by the activity of mitochondrial enzymes of the metabolically active cells [22]. The formed product was water-soluble and can readily be observed with ELISA reader (Biotek, Epoch) at 415 nm. The results were given as percentage of viable cells relative to the control. Eight duplicates were prepared for each condition. The percentage of cell viability in the control group was shown as 100%. The concentration required inhibiting 50% of cell growth (IC₅₀), as the biomarker of cytotoxicity was determined from cytotoxicity curves.

The results were expressed in terms of percentage cellular viability with respect to concentrations and calculated with the formula given in Equation 1.

Equation 1. The formula for % Cell Viability.

$$\% \text{Cell Viability} = \frac{\text{Avg. OD}_{415} \text{ of treated well (with cell)} - \text{Avg. OD}_{415} \text{ of treated well (without cell)}}{\text{Avg. OD}_{415} \text{ of control well (with cell)} - \text{Avg. OD}_{415} \text{ of control well (without cell)}} \times 100$$

2.2.4.2 Trypan Blue Exclusion Method

250.000 cells/mL were seeded in 6 well plates and incubated for 24 h in CO₂ incubator at 37°C. After twenty hours incubations, the medium was removed

and the cells were exposed with varying concentrations of MNPs for 4 and 24 h. After twenty hours treatment, the medium was removed and washed with PBS and trypsin were applied. Suspended cells were collected in an eppendorf tube. Detached cell suspensions were transferred to separate eppendorfs and 0.25 % (w/v) trypan blue were applied for counting using hemocytometer under light microscopy. 10 μ L of mixed cell suspension was put on two chambers of the hemocytometer. Percent cell viability was calculated according to the equation that was given in the section 2.2.2.5.

2.2.5 Genotoxicity Assay

2.2.5.1 Single-Cell Gel Electrophoresis (SCGE, Comet)

The alkaline comet assay was performed according to Singh et al. [91] with slight modifications. Cells were seeded in 24 well plates. After 24 h incubation cells were treated with naked and silica coated MNPs ranging from 15 to 500 μ g/mL concentrations for 4 and 24 h treatments. Untreated complete medium and hydrogen peroxide (20 and 40 μ M H₂O₂) served as negative and positive controls, respectively. At the end of treatments the cells were washed three times with PBS and then trypsinized. Cells at a concentration of 2×10^4 cell/mL were suspended in 0.65 % low melting-point agarose (LMA) and layered onto a microscope slide precoated with 0.65 % high melting-point agarose (HMA) and covered with a coverslip. After solidification of agarose, the coverslips were removed and the slides were immersed in light-protected freshly prepared cold lysing solution (89% lysing buffer 2.5 M NaCl, 0.1 M Na₂EDTA, 10 mM Tris-HCl, 1% Triton X-100, 10% dimethyl sulfoxide; pH 10) overnight at 4 °C. Slides were pretreated 20 min in freshly prepared electrophoresis buffer (0.3 M NaOH, 1 mM Na₂EDTA; pH 13) to allow unwinding of DNA and then electrophoresis was carried out at 25 V and 300 mA for 20 min at 4 °C (Thermo EC250-90). The slides were neutralized three times for five min in neutralizing buffer (0.4 M Tris-HCl; pH 7.5). The gels were then stained with 20 μ g/mL ethidium bromide (Sigma, USA), and 50 cells per slide were scored using

Comet Assay III image-analysis software system (Perceptive Instruments, UK) attached to fluorescence microscope (Zeiss Axioscope, Germany). All the steps of the Comet assay were conducted under yellow lamp in the dark to prevent additional DNA damage. Tail moment (percent DNA in the tail) was chosen as the measure of DNA damage. Experiments were repeated three times and we used duplicate samples were used. Two slides were prepared for each sample. The cell viability was assessed using trypan blue dye exclusion assay.

2.2.5.2 Cytokinesis-Blocked Micronucleus (CBMN) assay

In vitro CBMN assay was carried out according to the Organisation for Economic Co-operation and Development (OECD) Guideline 487 (OECD, 2007) and Fenech [92]. Cells were seeded at a concentration of 2.5×10^5 cells/mL and incubated at 37°/5% CO₂ for 24 h in T25 flasks (Greiner Bio-one) and were treated at a concentration range of 15- 500 µg/mL of naked and silica coated MNPs for 4 and 24 h medium growth and (0,6µg/mL) Mitomycin C (MMC) were used as negative and positive controls, respectively. At the end of treatments, cells were washed with complete medium and (final concentration of 6 µg/mL) cytochalasin B was added for the last 24 h of the culture. The cells were harvested with (0.25%) trypsin and the cell suspension was centrifuged at 250 g for 10 min. Samples centrifuged and re-suspended in 0.075 M KCl at 4°C for 3 min as hypotonic treatment. Cells were then fixed with methanol–acetic acid (3:1; v/v) at least three times, dropped onto cold slides, air-dried and stained with Giemsa–May Grunwald. Micronucleus frequency was evaluated by scoring a total of 2000 binucleated (1000 binucleate cells from each replicate) cells per treatment at 400x magnification (Zeiss Axioscope Microscope, Goettingen, Germany). The cytokinesis block proliferation index (CBPI) was also calculated from 500 cells/concentration as recommended in the OECD Guideline No. 487 (OECD, 2007) as follows:

Equation 2. Calculation of CBPI

CBPI = (No of mononucleate cells + 2 x No of binucleate cells + 3 x No of multinucleate cells)/Total No of cells.

2.2.6 Measurement of Intracellular ROS

2.2.6.1 Assay of Reactive Oxygen Species (ROS)

The level of intracellular ROS production was investigated by the method of Wan et al [93] and with modifications by Wilson et al [94] using 2, 7-dichlorofluorescein diacetate (DCFDA) dye. 1×10^4 cells/well were seeded in a 96-well black –clear bottom plate. After 24 h incubation, the cells were exposed to both types of MNPs (62 to 500 $\mu\text{g/mL}$) for 4 and 24 h. The MNPs containing medium was aspirated and cells were washed twice with PBS. After, culture medium containing (20 μM) DCFDA dye was added to each well. The plate was incubated for 30 min at 37 °C and the medium containing DCFDA was removed. Two hundred μL of PBS was then added to each well and fluorescence intensity was measured in a Fluorescence BMG optima (Germany) multiwell plate reader, software at excitation and emission wavelengths of 485 and 530 nm, respectively. To assess if the auto fluorescence of MNPs interfere with the DCFDA dye, a set of experiment without cells were also conducted in parallel. The qualitative analysis of ROS generation was done using a FLoid cell imaging station (Thermo Fisher Scientific). For visualization, the adherent cells (MCF-7, MDA-MB-231, and MCF-10A) were seeded on coverslips before incubating with varying concentrations of both MNPs. The cells were incubated for 24 h with MNPs that were added to the culture medium. Control cells were grown without MNPs. The cells were then washed three times with PBS and incubated for 20 min with 10 mM DCFDA in serum free medium at 37 °C. The cells were subsequently washed three times with ice cold PBS, fixed with 2% paraformaldehyde for 15 min at room

temperature and the cell coated cover slip were finally mounted on microscope slides by using mounting medium with DAPI. All samples were observed on Fluid cell imaging station (Thermo Fisher Scientific).

Percentage ROS generation was calculated as follows, after correcting for background fluorescence:

Equation 3. Percentage ROS generation

$$= [(F485/530_{\text{sample}} - F485/530_{\text{sample blank}}) / (F485/530_{\text{control}} - F485/530_{\text{control blank}})] \times 100$$

2.2.6.2 Lipid Peroxidation Assay

The thiobarbituric acid reactive species (TBARS) assay was used to evaluate malondialdehyde (MDA) which is the product of lipid peroxidation formed [95]. The basis of assay is depending on the fact that the quantification of colored complex product between thiobarbituric acid (TBA) and MDA resulting from hydrolysis of acid. Briefly, the cells exposed with both MNPs were collected by scraping into water and 1% Triton-X100 was added to each sample. Five hundred μL of cell extract were mixed with 500 μL of hydrolysis solution (0.25 M HCl containing 3.75 % (v/v) TBA and 15 % (v/v) trichloroacetic acid) and incubated at 90 °C for 60 min. After cooling in ice to stop hydrolysis, the complex formed was extracted with 1 mL of n-butanol. The mixture was vigorously shaken and centrifuged at 3000 \times g for 10 min. The absorbance in butanolic phase was measured using a spectrophotometer (Multiskan Go, Thermo Fischer) at 530 nm. Hydrogen peroxide that induces lipid peroxidation of the cells was used as positive control. The results were calculated as nmole of MDA/ mg of protein and data were expressed as a ratio compared to the control. Bradford method was used to determine protein [96].

2.2.7 Apoptosis Assay

2.2.7.1 Annexin-V-FITC / PI Staining

FITC Annexin-V Apoptosis detection kit with PI were used in order to investigate the apoptotic effects of MNPs in MDA-MB-231, MCF-7 and MCF-10A cells described by the manufacturer. All cells (1×10^6) were treated with naked and silica coated MNPs for 24 h and stained with propidium iodide (PI) and fluorescein isothiocyanate (FITC)-conjugated Annexin-V. The stained cells were incubated on ice and a minimum of 10,000 events were acquired by using BD Accuri C6 flow cytometer (Becton-Dickinson, Franklin Lakes, NJ) and the percentage of cells for each event (early apoptotic, necrotic phase or late apoptotic) was obtained by using the Cell Quest Pro software (Becton-Dickinson).

2.2.7.2 Gene Expression Analysis

For real time quantitative polymerase chain reaction (RT-qPCR), the RealMasterMix Fast SYBR Kit (5 PRIME, USA) was used with the Rotor Gene 6000 (Corbett, Qiagen) cycler. The cells were cultured in six well plates as 10^4 cells per 2 mL for each well. Then, the cells were treated with 2DG-MNP at final concentrations of 125 and 500 $\mu\text{g/mL}$ for 24 and 72 hours. Total RNA was isolated using PerfectPure RNA Isolation Kit (5 PRIME, USA) according to the manufacturer's instructions. In order to generate first strand cDNA, RealMasterScript SuperMix Kit (5PRIME) was used. The mRNA levels of BAX, BCL-2, PUMA, SURVIVIN, CYP1A1, CY1B1, GSTM3 and GSTZ1 as well as β -actin, were assayed using gene-specific SYBR Green-based The RealMasterMix Fast (5PRIME) according to the manufacturer's instructions. All samples and controls were run in triplicate. Quantification was done by $2^{-\Delta\Delta\text{Ct}}$ method [97]. The data were normalized according to the reference gene, β -actin, and the level of candidate gene expression of 2DG-MNP treated and untreated samples were compared in order to investigate

relative gene expression. The primer sequences and amplification, melting and standard curves are displayed in Appendices B.

2.2.8 The Preparation of 2-amino-2-deoxy-glucose Labeled Cobalt Ferrite Magnetic Nanoparticles (2DG-MNPs)

2.2.8.1 Functionalization of Silica Coated Cobalt Ferrite Nanoparticles (CoFe MNPs)

After silica coating process, the nanoparticle surface was further modified with amine groups using APTES [98]. Two hundred μL APTES was added drop wise into the solution containing 12 mL DMF and 8 mL toluene under magnetic stirring for 24 h. The modified nanoparticles were washed with toluene by using a magnet and collected to re-disperse in 10 mL DMF. Then amine modified silica coated nanoparticles were functionalized with -COOH by using glutaric anhydride. The nanoparticle suspension in DMF was added drop wise to 10 mL DMF solution containing 0.1 g glutaric anhydride and was stirred for 24 h at room temperature. The -COOH modified CoFe MNPs (COOH-MNPs) were washed with DMF and the deionized water by using magnet. For the characterization of prepared COOH-MNPs, dynamic light scattering (DLS) (Malvern Nano ZS90) and, Fourier transform–infrared spectroscopy (FT–IR) (Alpha, Bruker) methods were utilized.

2.2.8.2 Modification of COOH-MNPs with 2-amino-2-deoxy-glucose (2DG)

For the immobilization of 2-amino-2-deoxy-glucose (2DG) on COOH-MNPs surface, surface activation was achieved via esterification reaction by EDC and NHS crosslinkers according to Xiong et al [33]. EDC (1-Ethyl-3-(3-dimethylaminopropyl) carbodiimide) (0.5 mM) and NHS (N-Hydroxysuccinimide) (2.5 mM) were added to the 10 mL of (1 mM) CoFe MNP solution and allowed to react for 30 min at room temperature. Then 2DG.HCl solution was added with a final concentration of 2 mg/mL to the

CoFe MNP solution and mixed for 2 h at room temperature. The 2DG conjugated CoFe MNPs (2DG-MNPs) were then washed three times with deionized water.

2.2.8.3 Spectrophotometric Determination of 2DG on COOH-MNPs

In the standard procedure [99], 2DG-MNPs samples in 100 μL of water was mixed with 100 μL , 0.5 N NaOH. Then, 100 μL of 3-methyl-2-benzothiazolinone hydrazone hydrochloride hydrate (MBTH) (Sigma-Aldrich, USA) reagent was added to this sample (the reagent was prepared by mixing 3 mg/ml MBTH and 1 mg/ml dithiothreitol (DTT) (Sigma-Aldrich, USA)). The prepared standard sugar solutions (0.1 - 1.0 mM) and the samples were heated for 15 min at 80 $^{\circ}\text{C}$ in an aluminum heat block. After heating, 200 μL of a solution containing 0.5 % ($\text{FeNH}_4(\text{SO}_4)_2 \cdot 12 \text{H}_2\text{O}$), 0.5% sulfamic acid (Sigma-Aldrich, USA), and 0.25 N HCl were added to each, then all the standard solutions and the samples were allowed to cool to room temperature and their absorbances were measured at 620 nm with Multiskan GO microplate reader (Thermo Scientific, USA). The similar procedure was also applied to the non-modified COOH-MNPs; called as control experiment. The amount of 2DG attached to the nanoparticle surface was then calculated and the results were given as mM glucose/mg nanoparticle.

2.2.9 Visualization of Intracellular 2DG-MNP

2.2.9.1 Cellular Uptake of 2DG-MNPs by TEM

Cellular internalization of 2DG-MNPs were studied by TEM as given previously in the section 2.2.3.1.

2.2.9.2 Cellular Uptake of 2DG-MNPs by ICP-OES

ICP-OES studies for cellular uptake of 2DG-MNPs were given by previously in the section 2.2.3.2.

2.2.9.3 Cellular Uptake of 2DG-MNPs by Prussian Blue Staining

Prussian blue staining studies for cellular uptake of 2DG-MNPs was given by previously in the section 2.2.3.3.

2.2.10 The cytotoxicity of 2DG-MNPs

2.2.10.1 Cell viability (XTT) assay

The potential cytotoxic effects of 2DG-MNPs were studied as given previously in the section 2.2.4.1.

2.2.11 Apoptosis Assay

2.2.11.1 Annexin-V-FITC/PI staining

Cells were seeded at a density of 1×10^6 in 6 well plates and were treated with 2DG-MNPs (125, 250 and 500 $\mu\text{g}/\text{mL}$) for 24 h. The details of experiments were given previously in the section 2.2.7.1.

2.2.11.2 Gene expression analysis

All types of cells were treated with 2DG-MNP at final concentrations of 125 and 500 $\mu\text{g}/\text{mL}$ for 24 and 72 h. The experimental details of gene expression analysis were given previously in section 2.2.7.2.

2.2.12 The Conjugation of EF2K siRNA to Cobalt Ferrite Magnetic Nanoparticle (MNP-EF2K siRNA)

2.2.12.1 Cell Lines and Culture

The human breast cancer MDA-MB-231 cells (Triple negative; ER-, PR-, HER-), MDA-MB-436 (BRCA1 mutated) were maintained in cultured in DMEM/F12 supplemented with 10 % FBS. HCC-1937 (BRCA1 mutated) cell were cultured in RPMI supplemented with 10 % FBS. All media contain (100 units/mL) penicillin and streptomycin. Cells were maintained at 37°C in a

humidified atmosphere containing 5% CO₂/95% air, and were used between passages 4 and 15.

2.2.12.2 Transfections with siRNA

The siRNA, targeting EF2K (Sigma-Aldrich) was designed using siRNA-designing software (Qiagen, Valencia, CA, USA):

EF2K siRNA#1,

5-3' sense strand GCCAACCCAGUACUACCAAA [dT]*[dT][AMC7F],

5-3' anti sense UUUGGUAGUACUGGUUGGC [dT]*[dT].

Control non-silencing siRNA

5-3' sense strand UUCUCCGAACGUGUCACGUUU [dT]*[dT]

5-3'anti sense ACGUGACACGUUCGGAGAAUU [dT]*[dT].

Cells were transfected with either siRNA, at a final concentration of 50 nM for 72 h using HiPerFect Transfection Reagent (Qiagen) according to the manufacturer's protocol. Non-silencing control siRNA-transfected cells were used as negative controls. After treatment, the cells were harvested/processed for further analysis and assays.

2.2.12.3 EDC/s-NHS Coupling Reactions

3' Amine modified eEF2k siRNA was immobilized on COOH modified Cobalt Ferrite MNP surface, the surface activation was achieved via esterification reaction by EDC and sulfo-NHS crosslinkers [33]. The aqueous solutions of coupling reagents EDC (0.5 mM) and sulfo-NHS (2.5 mM) were added to MNPs solution and allowed to react for 30 min at room temperature. The 3' Amine modified eEF2k siRNA were added to the MNP solution and then incubated for 3 h at room temperature. The complex was purified away with ultrafiltration filters.

2.2.12.4 *In vitro* Cellular Uptake

The cells were seeded at a density of 1×10^5 cells per well in Lab-tekII® chamber slide system in DMEM supplemented with 10% fetal bovine serum (FBS), 1% of a penicillin/streptomycin mixture. Cells were incubated for 24 h. Then, MNP-EF2K siRNA labeled with Cy3 was added to the medium for 4 h. After incubation, cells were fixed at room temperature for 15 min with 4% paraformaldehyde. Following cell fixation, cells were incubated with 4,6-diamidino-2-phenylindole (DAPI) at a concentration of 0.2 µg/mL in phosphate buffer saline (PBS) for 15 min protected from light, washed twice with PBS and once with water to avoid salt crystals formation.

2.2.12.5 Prussian Blue Staining

Approximately 1×10^5 cells were seeded in each cell culture chamber for growth overnight. After incubation with 100 µg/ml MNP-EF2K siRNA for 4 h, the cells were washed three times with PBS buffer. The details of experiments were given previously in the section 2.2.3.3.

2.2.12.6 Clonogenic Survival Assay

The basis of assay is depending on the fact that all the cells that generate the colony are the progeny of a single cell. The formed colonies can be seen with the naked eye and this is the of the maintenance of the capacity to reproduce [100]. Briefly, 300 cells were counted and mixed gently and seeded on a 24-well plate. After being incubated for 24 h, the cells were transfected with control and EF-2K siRNA, MNP, MNP-EF2K siRNA about 2 weeks later. Fixation and staining of clones was done with a mixture of 0.5% crystal violet in 50/50 for 30 min. The plates were washed with water and left for drying at room temperature. Colonies with a diameter of more than 50 cells were counted. Each experiment was performed in duplicate.

2.2.12.7 Matrigel Invasion Assay

The Boyden chamber invasion assay was carried out which mimics the *in vivo* metastasis process [101]. Invasive capacities of cancer cells can be determined by establishing a barrier of extracellular matrix (ECM) through which the cells are expected to invade. All cells were transfected with control or eEF2K siRNA, MNP, MNP-EF2K siRNA and 24 h later, cells were seeded onto Matrigel-coated Transwell filters (8-mm pore size) in Matrigel invasion chambers (BD Biosciences, San Jose, CA). Cells that invaded through the Matrigel onto the lower side of the filter were fixed, stained with the Hema-3 Stain System (Fisher Scientific), and photographed. The number of cells that invaded the lower side of the membrane was determined at 72 h by counting cells in a minimum of four randomly selected areas.

2.2.12.8 Migration Assay

The *in vitro* scratch wound healing assay was used to measure for cellular motility [86, 102]. The control, EF-2K siRNA, MNP and MNP-EF2K siRNA treated cells were seeded in 6-well plates (5×10^5 cells/well), and incubated until they were 90% confluent. The monolayer of cells was scratched carefully using a 10 μ L sterile pipette tip. The cellular debris was removed by washing twice with PBS and the cells were then incubated in complete medium. Immediately after wounding, images were captured with a phase-contrast microscope (Nikon Instruments Inc., Melville, NY, USA), in order to determine the wound width at time 0, and wound sizes were verified with an ocular ruler to ensure that all wounds were the same width at the beginning of the experiment. The wound healing was visualized by comparing photographs taken at 0 h with those taken at 24 and 48 h later, and analyzed for the distance migrated by the leading edge of the wound at each time-point. The distances between the wound edges were measured from images of the wound using the Image J 1.42 program. Three experiments were done in triplicate.

2.2.12.9 Western Blot Analysis

All three types of cells were plated in 25-cm² culture flasks (0.5x10⁶ cells/flask). After the treatments, the cells were collected, centrifuged, washed twice in ice cold PBS and whole-cell lysates were obtained by suspending the cells in a lysis buffer at 4°C. Lysates were centrifuged at 13,000 g for 10 min at 4°C, and the supernatant fractions were collected. Protein concentration for each sample was determined by Bradford assay (Bio-Rad, Hercules, CA), and Western blotting was performed as described Tekedereli et al [87]. The membranes were blocked with 5% dry milk or BSA and probed with the following primary antibodies: eEF-2K, p-EF2 (Thr-56), EF2, cyclin D1, p-Akt (Ser-473), Akt, p-Src (Tyr-416), Src, p-paxillin (Tyr-31), paxillin, 4E-BP1, p-4e-bp1, CD44, ALDH1A1, Claudin1, VEGF, p-FAK (Tyr-397), FAK, c-Myc, CCL2, Horseradish peroxidase-conjugated anti-rabbit or anti-mouse secondary antibody were used for detection. Chemi-glow detection reagents were used for chemiluminescent detection. The blots were visualized with a FluorChem 8900 imager and quantified by a densitometer using the Alpha Imager application program. Mouse anti-β-actin (primary) and donkey anti-mouse (secondary) antibodies were used to monitor β-actin expression as a internal control.

2.2.12.10 Orthotopic Xenograft Tumor Model of Breast Cancer

Athymic female nu/nu mice (4-5 week old) were obtained from the Department of Experimental Radiation Oncology at M. D. Anderson Cancer Center, Houston, TX. All studies were conducted according to an experimental protocol approved by the M. D. Anderson Institutional Animal Care and Use Committee. MDA-MB-436 cells (2×10⁶) were injected into the right middle mammary fat pad of each mouse. Two weeks after injection, when tumor size reached about 3–5 mm, EF2K or control siRNA loaded MNP treatments were initiated. Each mouse received 0.3mg/kg (equivalent of ~8 μg/mouse) non-silencing control siRNA or MNP-EF2K siRNA once a week (*i.v.* injection into the tail vein in 100 μL saline) for four weeks. Tumor growth was monitored

using the tumor calipers. The estimated volume was calculated based on the following equation: tumor volume = $1/2 \times \text{width}^2 \times \text{length}$. After 4 weeks of treatments, mice were euthanized with CO₂. And tumor tissues were removed for Western blot, Immunohistochemistry and TUNEL and Ki-67 analysis.

2.2.12.11 *In vivo* Tissue Distribution of MNP-siRNA nanoparticles

Control untreated mice and MNP-EF2K siRNA injected mice post injection was sacrificed after 24 h. Major organs including liver, spleen, kidney, heart, lung and tumor were collected, fixed in 4% formalin, conducted with paraffin embedded sections, stained with hematoxylin eosin (H&E) and Prussian blue, and then examined under a digital microscope (Leica QWin).

2.2.12.12 Immunohistochemical Analysis

Ki67 and terminal deoxynucleotidyl transferase-mediated dUTP nick end labeling (TUNEL) staining were done using formalin-fixed, paraffin-embedded tumor sections (8 mm thickness). Apoptotic events after treatment with siRNA were determined by the TdT-mediated dUTP nick end labeling (TUNEL) colorimetric assay in tumor sections, according to the manufacturer's protocol. Briefly, after deparaffinization, slides were treated with proteinase K (1:500). Endogenous peroxidase activity was blocked with 3% H₂O₂ in methanol. After being equilibrate with equilibration buffer at room temperature for 10 min. slides were incubated and labeled with TdT reaction mix for 60 minutes at 37°C in a humidified chamber and stop reaction in 2X SSC for 15 minutes. Samples were fixed and incubated with an equilibration buffer followed by a reaction buffer containing nucleotide mix and terminal deoxynucleotidyl transferase enzyme. Finally, samples were counterstained with DAPI and mounted. DNA fragmentation was detected by localized green fluorescence within the nucleus of apoptotic cells. For each tumor section, five randomly selected fields were used to visualize cells at 400× magnification.

2.2.12.13 Immunohistochemical Analysis Proliferation and Microvessel density CD31

The assay was performed accordingly to Gonzalez-Villasana [103]. Briefly, unstained sections of mouse tissues were deparaffinized and rehydrated. Antigen retrieval was performed with DAKO antigen retrieval solution. Endogenous peroxidase was blocked by hydrogen peroxide (3%). For protein blocking, IgG blocking from a Vector M.O.M. kit was applied for 1h (5% normal horse serum and 1% normal goat serum in PBS were used (for Ki67 and CD31). Primary antibodies against Ki67 and anti-CD31 were incubated overnight at 4° for Ki67, goat anti-rabbit HRP secondary antibody and for CD31, goat anti-rat HRP-conjugated secondary antibody diluted in blocking solution were added and incubated for 1h at room temperature. Slides were developed with DAB substrate and counterstained with Gill's no. 3 hematoxylin solution. To quantify Ki67 and CD31 expression, the number of positive (DAB-stained) cells was counted in five random fields per slide (one slide per mouse, 5 slides per group) a 200× magnification, and the percentage of cells that were Ki67 and CD31 positive was calculated for each group.

2.2.12.14 MTS assay for combination Olaparib (AZD2281) and MNP-EF2K siRNA

Cell viability was investigated with MTS assay kit according to manufacture instructions. Briefly, viable cells were seeded in 96 well plates (4×10^3 cells/wells). Cells were treated with control siRNA, AZD2281 with 10-25-50 μ M concentrations and MNP-EF2K siRNA and combinations for 72 h. After treatment, a solution containing MTS (3-(4,5-dimethylthiazol-2-yl)-5-(3-carboxymethoxyphenyl)-2-(4-sulfophenyl)-2H tetrazolium) and PMS (phenazine methosulfate) (20:1 v/v) was added to the cells for 2–3 h at 37 °C and the viable growing cells were estimated by monitoring the absorption of the product at 490 nm. All experiments were performed in triplicate and the results were reported as mean absorption \pm standard deviation.

2.2.12.15 Statistical analysis

Graphpad Prism VI statistical software (GraphPad Inc. CA, USA) was used to evaluate the statistical significance between groups by using one-way analysis of variance (ANOVA) for multiple comparisons and the Student's t-test p value of less than 0.05 ($p < 0.05$) was regarded as statistically significant. Data were presented as mean \pm standard error of the mean.

CHAPTER 3

RESULTS AND DISCUSSION

3.1 Characterization of Naked and Silica Coated CoFe MNPs

The hydrodynamic sizes and zeta potential of naked and silica coated CoFe-MNPs were summarized in **Table 2**. The Dynamic Light Scattering (DLS) results showed that there was no difference between naked and silica coated CoFe-MNPs. The average sizes of naked and silica coated CoFe-MNPs were found as 189.75 ± 4.20 nm and 160.03 ± 10.15 nm, respectively in complete medium and the zeta potentials of naked MNPs and silica coated CoFe-MNPs were obtained in complete medium and found as -9.76 mV and - 11.3 mV, respectively.

Table 2. Zeta potential and average hydrodynamic sizes of aggregates of investigated CoFe-MNPs in different media.

Particle (CoFe-MNP)	Media	Zeta Potential (mV)	DLS Mean size (nm)
SiO ₂ coated	Water	-39,5	175.73 ± 4.63
	RPMI-1640	-20,6	708.40 ± 14.28
	RPMI-1640 10%FBS	-9,76	160.03 ± 10.15
Naked	Water	-33.5	192.70 ± 15.13
	RPMI-1640	-15.4	869.00 ± 12.0
	RPMI-1640 10%FBS	-11.3	189.75 ± 4.20

The Energy Dispersive X-Ray (EDX) analysis for the naked and silica coated cobalt ferrite nanoparticles are shown in **Figure 11**. The C signal was coming from the carbon tape used for sampling. The presence of silica peak on the spectrum was considered as the indication of silica layer formation on the surface of cobalt ferrite nanoparticles.

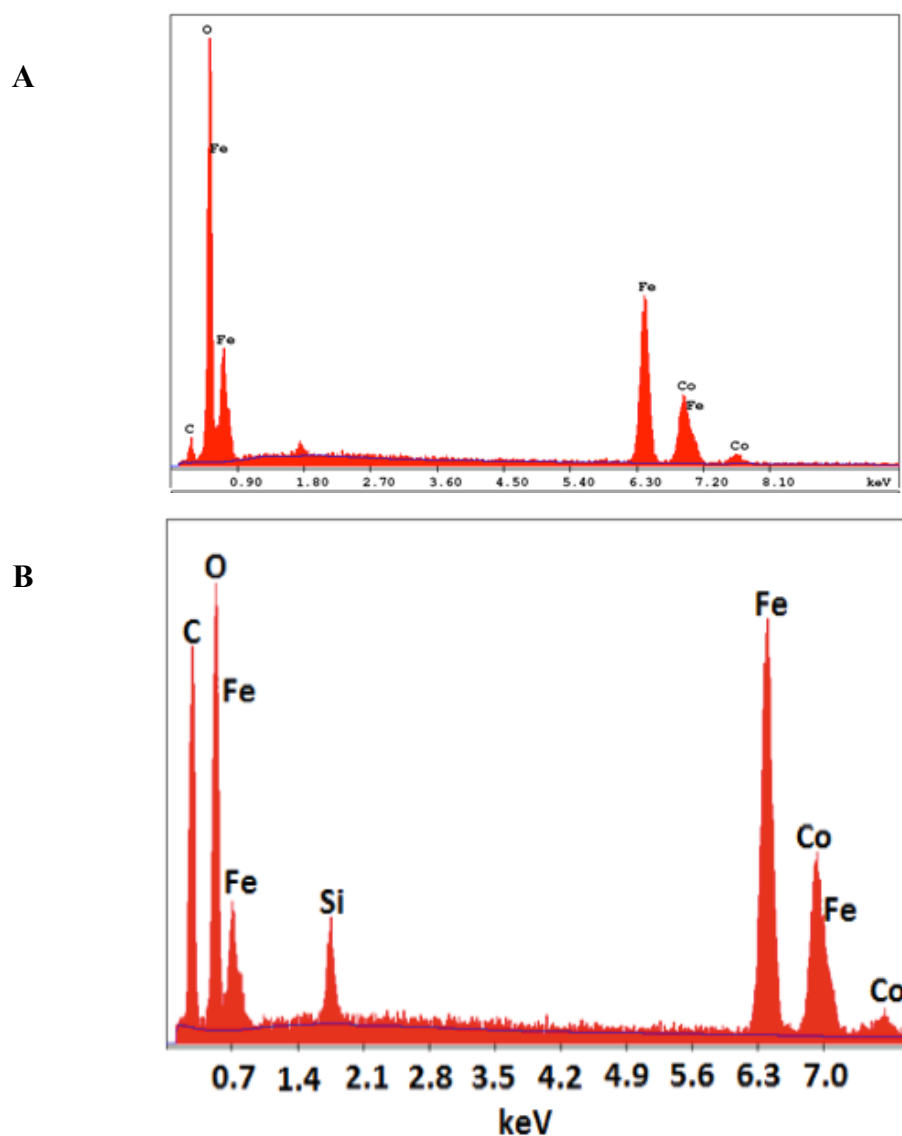


Figure 11. The EDX results of A) naked CoFe-MNPs and B) silica coated CoFe-MNPs.

FT-IR spectrum of the MNPs is given in **Figure 12**. Asymmetric and symmetric stretching of Si-O-Si vibrations was observed at 1080 cm^{-1} . Its appearance was correlated with the coating of silica layer on the cobalt ferrite particles. The bands around 1197 , 1085 cm^{-1} and 800 cm^{-1} represent the characteristic peaks of Si-O-Si stretching and Si-O bending.

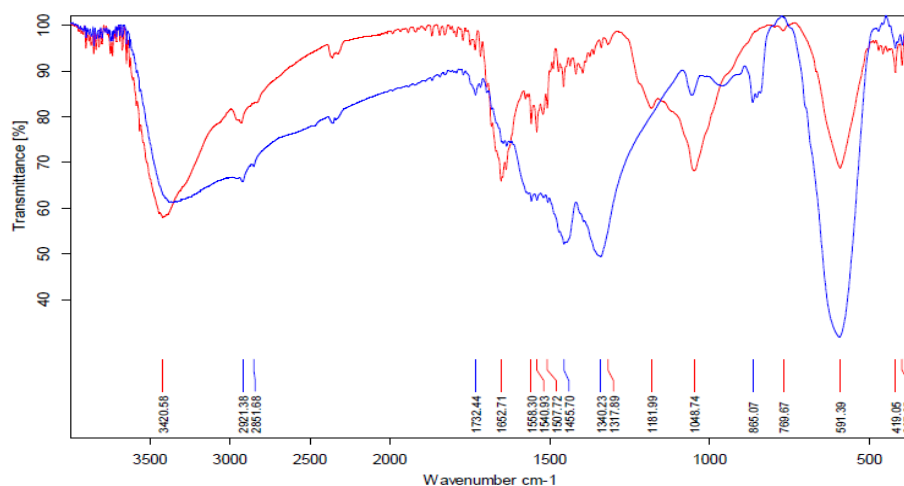


Figure 12. FTIR results of (a)(blue line) naked cobalt ferrite (CoFe-MNPs) and (b) (red line) silica coated cobalt ferrite magnetic nanoparticles (CoFe-MNPs).

The characterization of nanoparticles is essential for the toxicity studies, as it has been shown that the size, surface reactivity, and degree of aggregation impart for their differential response in biological systems [104, 105]. Accordingly, the size range of the CoFe-MNPs was smaller than 200 nm , which can be assumed as quite consistent for biomedical applications [104, 106]. All the CoFe-MNPs acquired a negatively charged surface. The absolute value of the zeta potentials were decreased to some extent when they were dispersed in the complete medium, revealing the adsorption of serum proteins which were less negatively charged at physiological conditions. In the culture media CoFe-MNPs were more stable and serum protein stabilized the particles by preventing strong aggregation.

3.2 Visualization of Intracellular MNP

3.2.1 Cellular Uptake by TEM

According to the TEM microphotographs, a significant increase in cellular uptake has been found with both naked and silica coated MNPs in MDA-MB-231 and MCF-10A cells as shown in **Figure 13-15**.

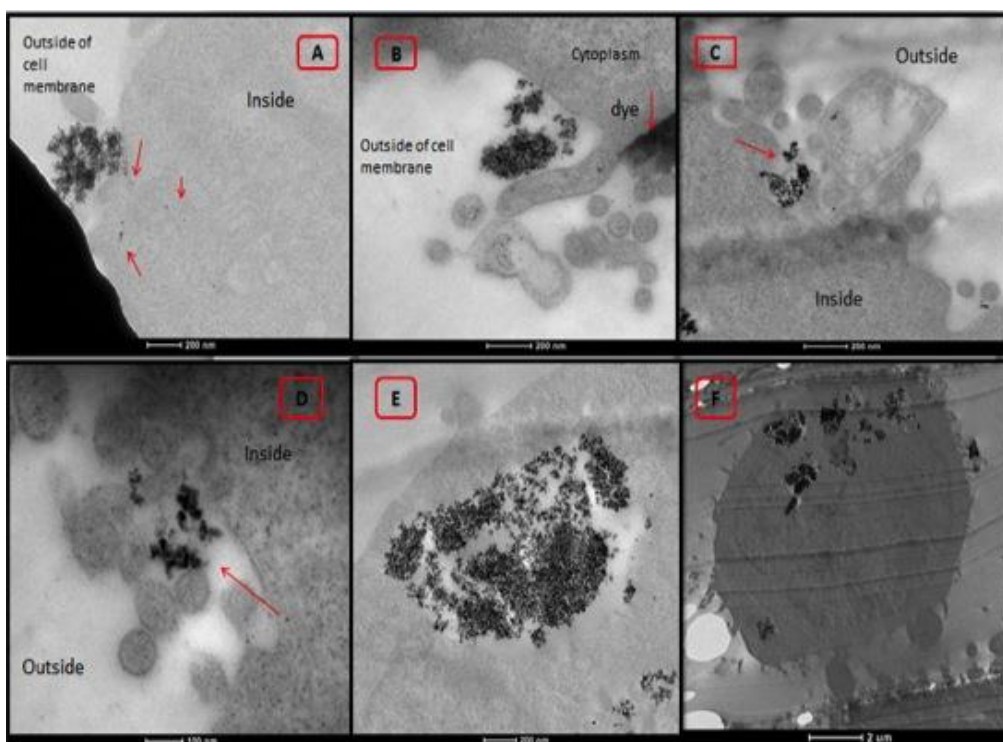


Figure 13. Representative TEM microphotographs of MDA-MB-231 cells treated with MNPs. The sections (a, c, d, e) were not stained with any reagent for detecting of cellular uptake of nanoparticles. Uptake of naked (a-b) and silica coated (c, d) MNPs were initiated upon the invagination of the plasma membrane (arrows shows MNPs). Some cells (b, c) still in the process of uptake at the plasma membrane. Some naked nanoparticles had already been internalized into the cells (e). Silica coated MNPs were trapped inside the endosome (f). The scale bar is 200 nm for (a, b, c, e), 2 μ m for (f) and 100 nm for (d). Images were collected using TEM and a digital camera.

These observations were also confirmed by a TEM micrograph of cells incubated with MNPs for 24 h (**Figure 14**), which showed large MNP aggregates inside the cytoplasm.

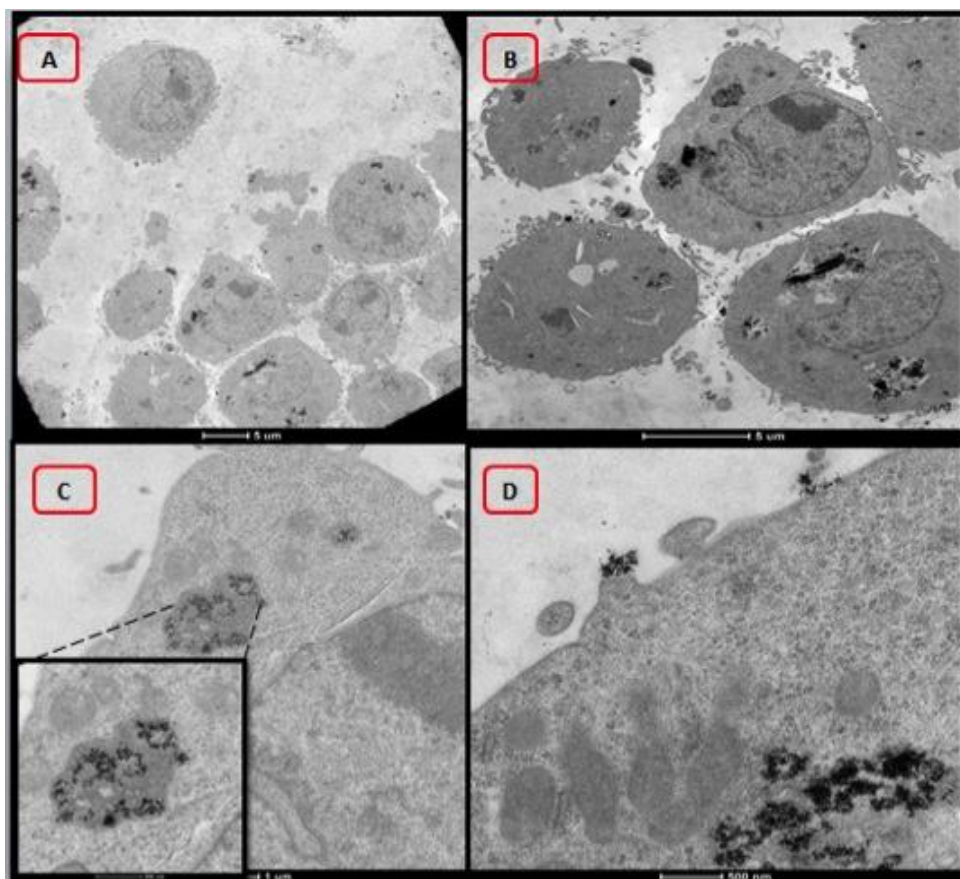


Figure 14. Internalization of MNPs in MDA-MB-231 cells observed with TEM. Naked MNPs are found in larger aggregates in bigger membrane bound vesicles (A-C), and already internalized silica coated MNPs aggregates in endosomes and in a multivesicular body (B-D) (The scale bar is 5 μm (a, b) and 1 μm (c), 500 nm (d)).

Most of the aggregates, independently of their size, were in vesicles. Certain MNPs aggregates could, as well, have escaped the vesicles and be present in the cytosol. No MNPs were found in the nucleus despite large quantities of internalized MNPs, internalization was still observed.

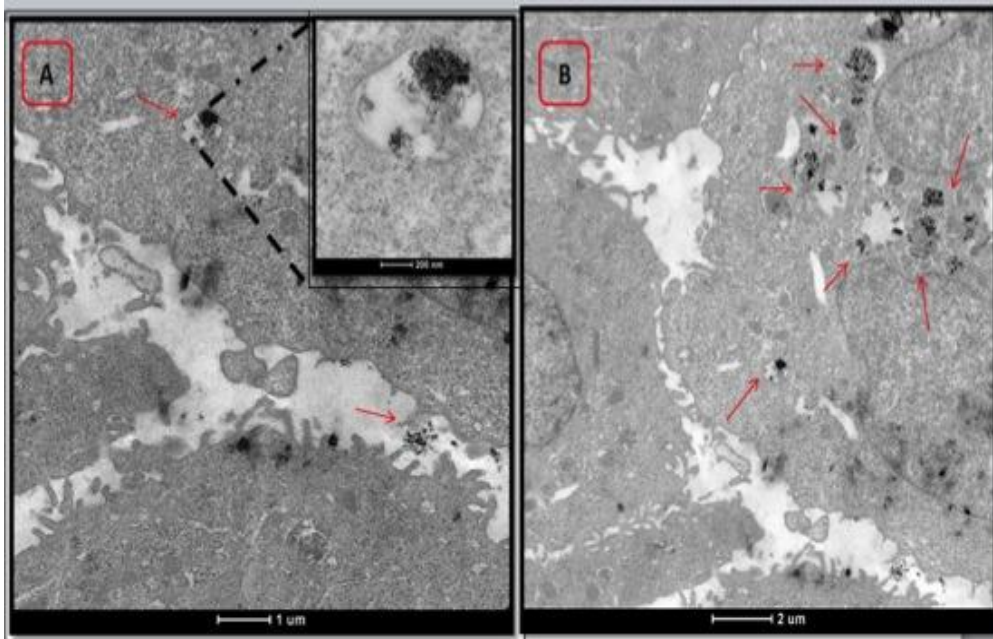


Figure 15. TEM images of ultrathin sections of MCF-10A cells. Magnified images of naked MNPs showed that the cluster is composed of individual nanoparticles inside of endosome (A). Image shows endosomes in cytosol that are loaded with silica coated MNPs (B). The scale bar is 1 μm (A) and 2 μm (B) and magnified image scale bar 200nm.

3.2.2 Cellular Uptake of MNPs by ICP-OES

According to cellular uptake results by inductively coupled plasma optical emission spectrometry (ICP-OES), iron concentrations per cell (pg/cell) for MDA-MB-231 and MCF-10A cells were given in **Figure 16**. It can be clearly seen that, the uptake of the silica coated and naked MNPs were concentration dependent and silica coated MNPs were significantly internalized more compared to naked one ($p < 0.001$) in both MDA-MB-231 and MCF-10A cells.

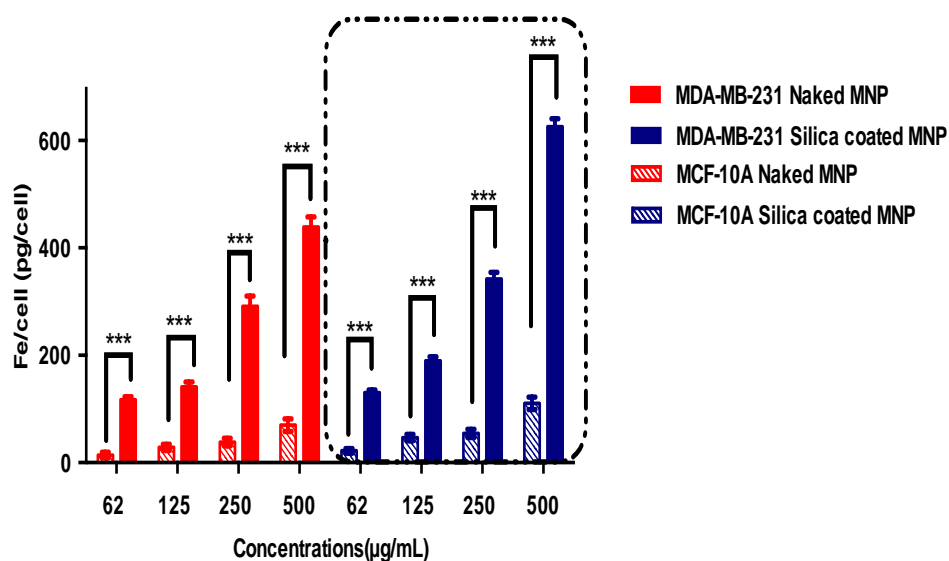


Figure 16. ICP-OES measurements and comparison of intracellular uptake of naked and silica coated CoFe-MNPs in MDA-MB-231 vs MCF-10A for 24 h. The iron concentrations of untreated cells were used as background. Error bars represent standard deviation (* $p < 0.05$, ** $p < 0.01$, *** $p < 0.001$)

As shown in **Figure 17**, the uptake of MNPs at 250 µg/mL concentration significantly increased in the first 4 h, but the uptake rate gradually slowed and reached a plateau at 8 h, The average uptake rates during the first 4 h were 24 and 42 pg/cell per hour for naked and silica coated MNPs in MCF-10A, respectively, 165 and 191 pg/cell per hour for naked and silica coated MNPs in MDA-MB-231 respectively. Moreover, compared to naked MNPs, silica coated ones exhibited higher uptake rate and internalized MNPs were significantly higher for MDA-MB-231 cells than that of MCF-10A cells.

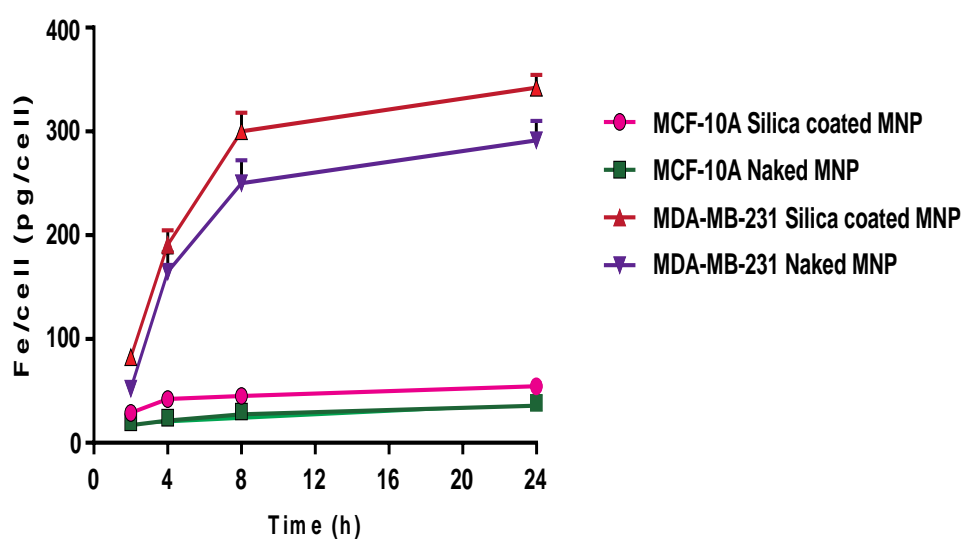


Figure 17. ICP-OES measurements of intracellular uptake of naked and silica coated in MDA-MB-231 and MCF-10A cells after 2 h, 4 h, 8 h and 24 h of CoFe-MNPs (250 $\mu\text{g/mL}$) incubation. The iron concentrations of untreated cells were used as background. Error bars represents standard deviation.

It is crucial to assess nanoparticles' uptake and correlate it with the cellular response, which could be linked to the toxicity as well. In our study the uptake studies revealed a good relationship between the uptake level and the incubation time. Also, the cellular uptake and potential saturated accumulation of CoFe-MNPs was cell and time dependent. According to our results, the highest iron content, representing internalized CoFe-MNPs, was measured in cancer MDA-MB-231 cells. Also, other studies confirmed that cancer cells were more prone to the internalization of the MNPs than normal cells [107]. The reason is that cancer cells possess higher endocytosis potential than normal cells due to the enhanced requirement for nutrients by virtue of their high metabolic activity and proliferation rate [108]. Typical TEM images demonstrated that MNPs were localized in the cytoplasm both for naked and silica coated ones while the nuclear membranes of the cells were intact.

As it can be seen from **Figure 18** and **Figure 19** the uptake of the naked and silica coated MNPs were significantly reduced as 27.5% and 45.32% in MDA-MB-231 cell line and 23.35 % and 31.38 % in MCF-10A cell line at 4°C when compared to 37°C, respectively ($p < 0.001$).

Similarly, metabolic inhibitors in terms of sucrose (0.45 M), sodium azide (0.1%), chlorpromazine (6 $\mu\text{g/mL}$) significantly prevented the delivery of the naked and coated CoFe MNPs into the both the cell lines when compared to control ($p < 0.001$).

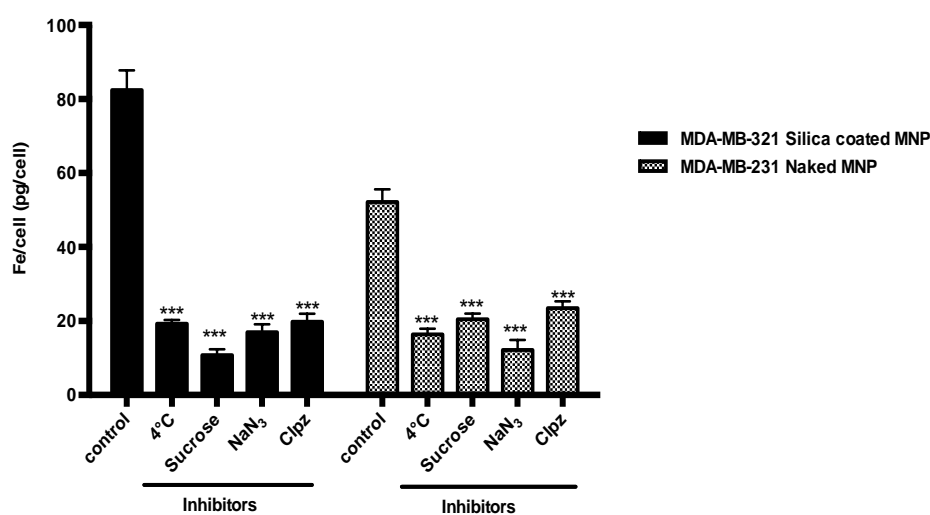


Figure 18. Uptake of CoFe-MNPs (compared to the controls at 37°C) in the presence of different endocytic inhibitors in MDA-MB-231 4°C, sucrose (0.45 M), NaN₃ (0.1%), and chlorpromazine (CLPZ) (6 $\mu\text{g/mL}$). The iron concentrations of untreated cells were used as background. Error bars represent standard deviation. (* $p < 0.05$, ** $p < 0.01$, *** $p < 0.001$)

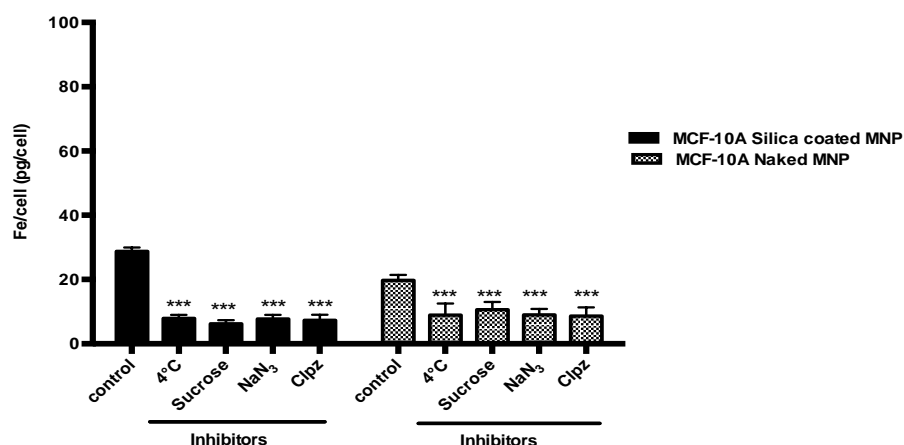


Figure 19. Uptake of CoFe-MNPs (compared to the controls at 37°C) in the presence of different endocytic inhibitors in MCF-10A 4°C, sucrose (0.45 M), NaN₃ (0.1%), and chlorpromazine (CLPZ) (6 µg/mL). The iron concentrations of untreated cells were used as background. Error bars represent standard deviation. (*p < 0.05, **p < 0.01, ***p < 0.001)

Cellular uptake of nanoparticles has been shown to be mediated by endocytosis, beginning with the invagination of the plasma membrane at either clathrin-coated pits or caveolae [109]. Consistently, we also observed the uptake of CoFe-MNPs into different cells was mediated by endocytosis.

Our results demonstrated that uptake of CoFe-MNPs into the cells required an appropriate temperature. It was shown that several proteins and enzymes were sensitive to the temperature, inhibited by lowered temperatures [110, 111]. Exposure to MNPs at 4°C and other metabolic inhibitors in terms of sucrose, NaN₃, chlorpromazine, resulted, as expected, to a very strong inhibition of endocytosis and halted internalization of CoFe-MNPs in both the cell lines. The results clearly demonstrated that CoFe-MNPs entered the cells in an energy-dependent manner. Taken together, the broader classes of endocytic pathways including macro pinocytosis and clathrin-mediated endocytosis are possible in the predominant uptake mechanisms for naked and silica coated CoFe-MNP in both cancer and non-cancer human breast cells.

3.2.3 Cellular Uptake of MNPs by Prussian Blue Staining

In order to visualize the cells exposed to both naked and silica coated MNPs, Prussian blue staining method was used and the microscopy images of the cells were evaluated by comparing the untreated cells as well as the particle type (Figure 20).

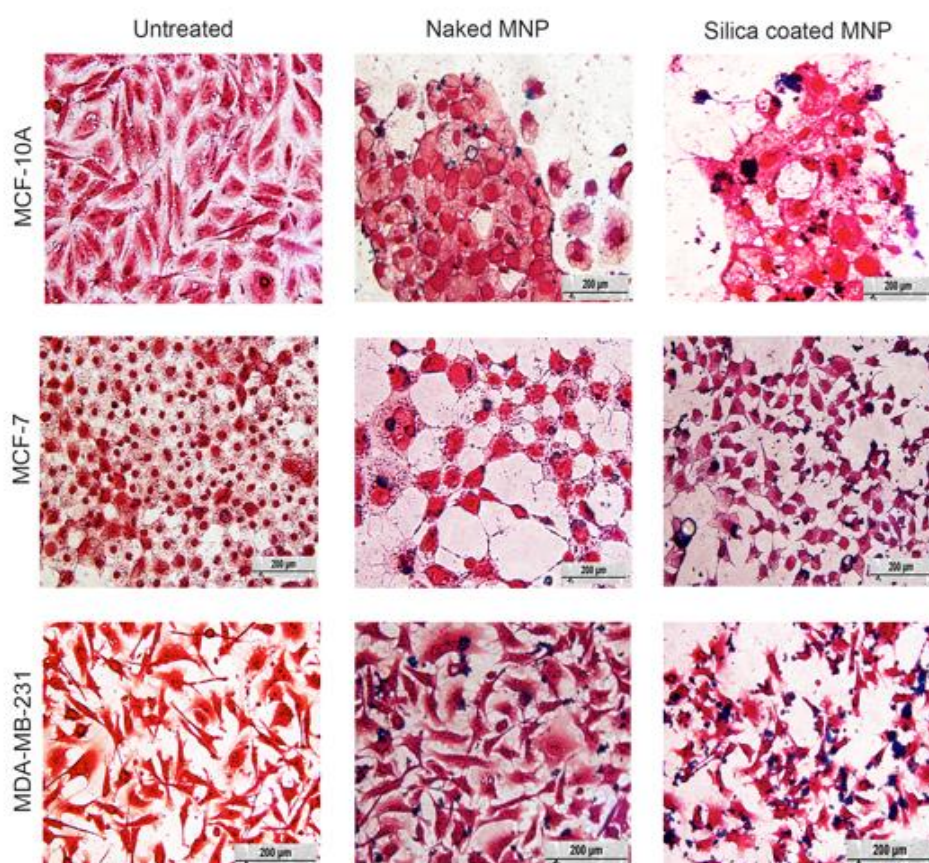


Figure 20. Light microscopy images of MDA-MB-231, MCF-7 and MCF-10A cells that are stained with Prussian blue, followed by counterstain nuclear fast red. Light pink coloring of cytoplasm, dark pink coloring of nucleus and blue coloring of iron core of the molecules were seen. The cells were treated with naked and silica coated MNPs at concentrations of 125 µg/mL for 24 h. The scale bar in the images is 200 µm.

When we compare the blue granules, which are MNPs, it is seen that though silica coated MNPs was internalized by all cell types, the nanoparticle uptake was much more in cancer cells than the normal cells. It is also obvious that the uptake of silica coated MNPs was higher than that of naked MNPs. MDA-MB-231 and MCF-7 cells have higher uptake capacity of compared to healthy cells, because of their higher nutrition requirement for proliferation and growth. Thus, they are likely to internalize more material with respect to healthy cells [112].

3.2.4 Cellular Uptake of MNPs by Flow cytometry

The uptakes of MNPs were evaluated in the breast cancer cells MDA-MB-231 and non-cancer breast epithelium cells MCF-10A using a flow cytometry. The side scatter (SSC) intensity, which represents granularity of a cell, and forward scatter (FSC) representing the size of cell [90] were analyzed as shown in **Figure 21**. Cells treated with MNPs showed a significant increase in the SSC-A mean indicating a marked uptake. After 24 h exposure, MDA-MB-231 cells showed an SSC-A population of 71% and 91.7 % at 50 and 100 $\mu\text{g/mL}$ concentrations, respectively as compared to the control cells (2.5 %). On the other hand, MCF-10A cells showed SSC-A population of 5.1 % and 16.8 % at 50 and 100 $\mu\text{g/mL}$, respectively as compared to the control cells (2.5%).

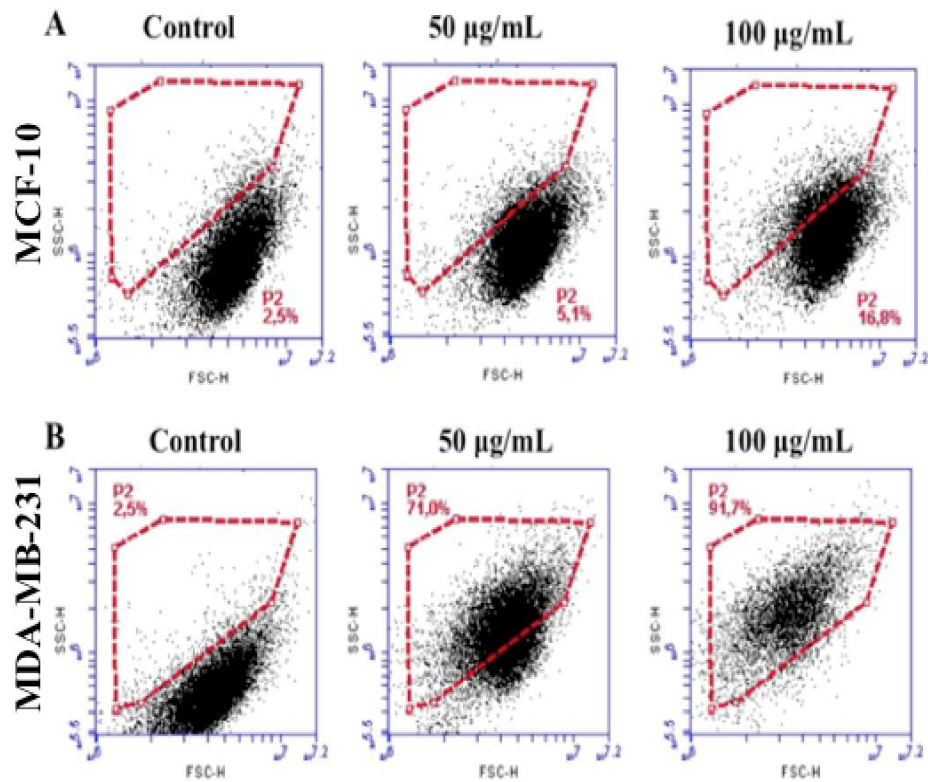


Figure 21. Uptake of MNPs into (A) normal epithelium (MCF10A) and (B) breast cancer cells (MDA-MB-231). Real images after treatments with different sized MNPs (50 and 100 $\mu\text{g/mL}$) are shown for 24 h and given in the flow cytometry histograms.

3.3 XTT Assay

The cytotoxic effects of naked and silica coated MNPs on MDA-MB-231; MCF-7 and MCF-10A cells were studied by using XTT assay (**Table 3**).

The lowest IC₅₀ value was obtained for MDA-MB-231 cells treated with naked MNP for 48 h that were followed by treatment with naked MNP for 24 h. Treatment with naked MNPs showed a strong viability reduction in MDA-MB-231, MCF-7 and MCF-10A cells. On the other hand, silica coated MNPs showed a slight toxicity, regardless of the surface charge (**Table 3**). In general, we observed that MCF-10A cells were more resistant to MNP treatment. Furthermore, MDA-MB-231 and MCF-7 cells were more susceptible to cytotoxic effects induced by MNPs as compared to MCF-10A

At first, MCF-10A did not exhibit cytotoxic effects after treatment with both naked and silica coated MNPs, however at high concentration as 1500 µg/mL, the viability decreased with naked MNPs at all three time points (**Table 3**). Naked and silica coated MNPs caused dose dependent decrease in cell viability for both cell lines and for all treatment durations (4, 24, 48 h) according to XTT assay.

Table 3. IC₅₀ values obtained on MDA-MB-231, MCF-7 and MCF-10A cells after exposure to naked and silica coated MNPs

	IC ₅₀ (µg/ml) 4h	95% CI	IC ₅₀ (µg/ml) 24 h	95% CI	IC ₅₀ (µg/ml) 48 h	95% CI
Naked MNPs MCF-10A	1532	1164 to 2015	973	783 to 1210	1289	951 to 1749
Naked MNPs MCF-7	1168	894 to 1526	845	753 to 948	1807	1442 to 2264
Naked MNPs MDA-MB-231	876	733 to 1046	444	368 to 535	322	261 to 397
Silica coated MNPs MCF-10A	2356	1719 to 3227	2076	1525 to 2826	2256	1581 to 3218
Silica coated MNPs MCF-7	1683	1222 to 2049	1081	924 to 1387	1841	1426 to 2377
Silica coated MNPs MDA-MB-231	1184	977 to 1436	488	375 to 635	633	518 to 775

The highlighting results due to the CoFe-MNPs cytotoxicity revealed that; cancer cells vs. non-cancer ones, naked particles vs. silica coated ones were more vulnerable to the toxicity. Similarly, Emanet et al. observed that the cytotoxicity of nanomaterial showed higher survival in slower proliferating human dermal fibroblasts (HDFs) when compared to the fast-growing human lung cancer cells (A549) [112]. The cytotoxicity has been found to be concentration dependent, which was in concordance with the scientific literature, based on the MNP studies. They showed that bare NPs had higher toxicity than to surface passivated NPs whereas silica coating improved the particles stability reducing both cytotoxic and genotoxic effects [113]. Polyacrylic acid (PAA) coated MNPs exhibited no cytotoxicity for short term exposure [114].

3.4 Genotoxicity Assay

3.4.1 Evaluation of Genotoxicity By the Alkaline Comet Assay

Naked MNPs showed concentration dependent increase in tail moment as the measure of the DNA damage, which was statistically significant starting at 62 $\mu\text{g}/\text{mL}$ ($p < 0.001$) at 4 h and at 15 $\mu\text{g}/\text{mL}$ ($p < 0.05$) at 24 h, as given in **Figure 22**. Silica coated MNP also showed concentration-dependent increase in tail moment but significant increase was only found at a concentration of 500 $\mu\text{g}/\text{mL}$ ($p < 0.001$) for 4 h and at 250 $\mu\text{g}/\text{mL}$ ($p < 0.05$) for 24 h in MDA-MB-231 cells. The cell viability measured by trypan blue assay during the treatments for DNA damage exceeded 70 % for all concentrations and time points used for MDA-MB-231 cells except for 500 $\mu\text{g}/\text{mL}$ of naked MNPs at 24 h in which the viability decreased below 70 %.

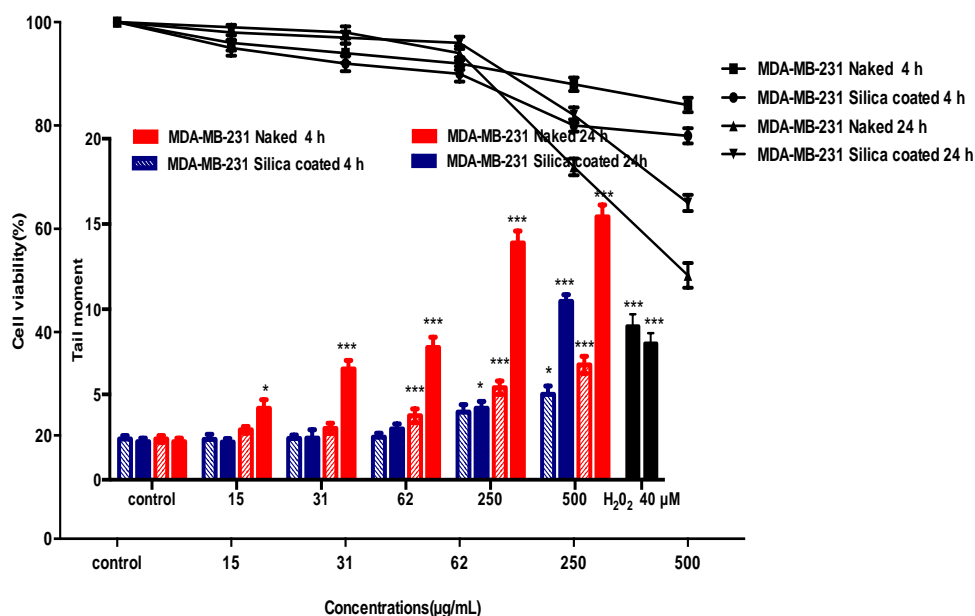


Figure 22. DNA damage in MDA-MB-231 cells after 4 and 24 hours of exposure to different concentrations of naked and silica coated CoFe-MNP; olive tail moment (arbitrary unit); cell viability. (* $p < 0.05$, ** $p < 0.01$, *** $p < 0.001$)

DNA damage was also concentration dependent for the treatment of MCF-10A cells with both naked and silica coated MNPs for 4 and 24 h treatments (**Figure 23**). Statistically significant increase in the tail moment was found between the concentration range of 125-500 $\mu\text{g/mL}$ for both 4 and 24 h treatment of naked MNPs while the increase was observed only at a concentration of 500 $\mu\text{g/mL}$ for 24 h treatment for silica coated ones ($p < 0.001$). Also, in MCF-10A cells DNA damage was found to be lower compared to MDA-MB-231 cells. The cell viability exceeded 70% for all concentrations and time points used for MCF-10A cells.

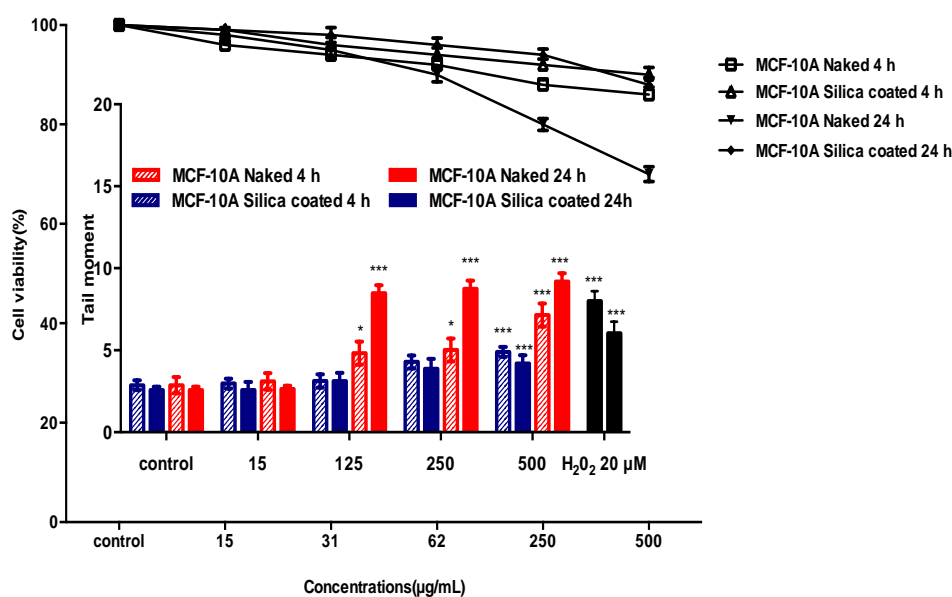


Figure 23. DNA damage in MCF-10A cells after 4 and 24 h of exposure to different concentrations of CoFe-MNPs; olive tail moment (arbitrary unit); cell viability. (* $p < 0.05$, ** $p < 0.01$, *** $p < 0.001$). Some of the concentration (31-62 $\mu\text{g/mL}$) are not given in the figure as effects are not significant.

3.4.2 Evaluation of the Genotoxicity by Cytokinesis Blocked Micronucleus (CBMN) assay

MDA-MB-231 cells treated with naked and silica coated MNPs showed concentration-dependent increase in MN frequency (%) as the measure of genotoxicity which was statistically significant starting at 31 $\mu\text{g/mL}$ ($p < 0.01$) as seen in **Figure 24**, for 4 and 24 h treatments of naked MNPs and at 500 $\mu\text{g/mL}$ ($p < 0.001$) for 4 h and at concentrations of 250 $\mu\text{g/mL}$ and 500 $\mu\text{g/mL}$ ($p < 0.001$) for 24 h incubation for silica coated ones. There was no statistically significant difference due to CBPI among the treatments.

Mitomycin C (MMC) is isolated from *Streptomyces caespitosus*, which is antibiotic containing a quinone. MMC produces free radicals as it metabolized. The formed ROS damages biological macromolecules such as nucleic acids,

proteins, and lipids. Therefore, Mitomycin C (MMC) is used as positive control in the following experiments.

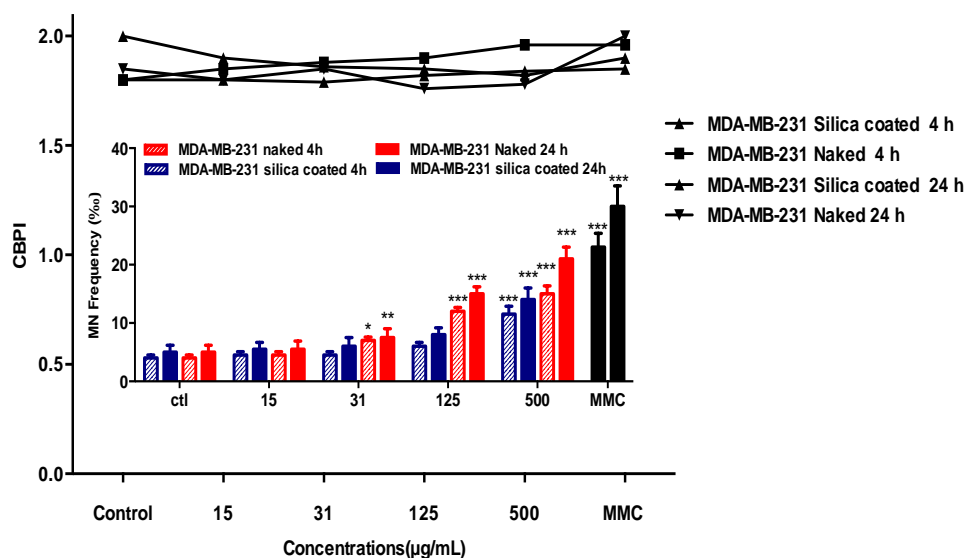


Figure 24. Micronucleus frequency (%) of MDA-MB-231 treated with CoFe-MNPs showing binucleated cell and CBPI (cytokinesis block proliferation index). The data represent 2000 binucleated cells for MDA-MB-231 binucleated cells. (* $p < 0.05$, ** $p < 0.01$, *** $p < 0.001$)

MCF-10A cells treated with naked and silica coated MNPs showed concentration dependent increase in MN frequency (%) as a measure of genotoxicity which was statistically significant starting at a concentration of 125 µg/mL ($p < 0.01$) for 4 h treatment and at 62 µg/mL ($p < 0.01$) for 24 h treatment with naked MNPs as given in **Figure 25**. Whereas there was no statistical significance of MN induction below the concentration of 250 µg/mL for silica coated MNP in MCF-10A cells ($p < 0.001$) for 4 and 24 h. The MN frequency (%) in naked MNPs treated MCF-10A cells was relatively higher than the coated ones. Also, MN formation in MDA-MB-231 cells was higher than MCF-10A for 4 and 24 h.

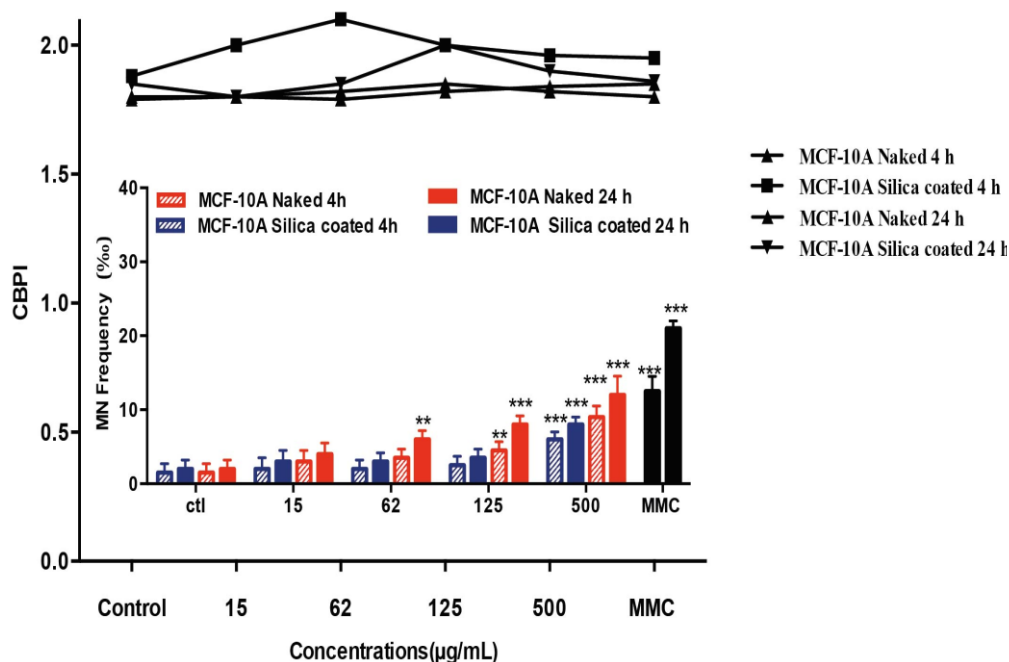


Figure 25. Micronucleus frequency (%) of MCF-10A treated with CoFe-MNPs showing binucleated cell and CBPI (cytokinesis block proliferation index). The data represent 2000 binucleated cells for MCF-10A binucleated cells. * $p < 0.05$, ** $p < 0.01$, *** $p < 0.001$

Genotoxicity as the intermediate step of the carcinogenesis has the aspect of hazard identification via genotoxicity testing methods. It is a requisite to use validated and standardized genotoxicity assays for newly developed or synthesized diverse array of nanoparticles in order to determine the toxicity profiles [115]. For nanoparticles primary (direct contact with DNA and indirect contact with the genetic material i.e. via ROS generation) and secondary (inflammation mediated) genotoxicity mechanisms are prevailing [116, 117]. The use of genotoxicity tests was found to be very rare for the MNPs while most of the studies were focused on the cytotoxicity and characterization of the particles [33, 118]. Thus, in this study, as a valuable contribution to the MNP research, in vitro genotoxicity of naked and silica coated CoFe-MNPs was evaluated for the first time by the in vitro cytokinesis blocked micronucleus assay (CBMN) and comet assay in cancer

and non-cancer breast cell lines. In the mechanistic toxicity assessment of nanoparticles in vitro micronucleus assay and comet assay are found to be valuable tools. In vitro micronucleus assay has been validated and appeared among the OECD guidelines with the capability of reflecting clastogenic and aneugenic chromosomal anomalies [119].

Comet assay, we used parallel to the in vitro CBMN assay, is a sensitive method for detecting DNA strand breaks, at the level of individual cells detecting many types of DNA damage, i.e. strand breaks, alkali labile sites, and incomplete excision repair sites [120]. Since nanoparticles have a large surface area to mass ratio, they are highly reactive to adsorb or release free radicals those could cause DNA damage [116].

Both the genotoxicity assays revealed similar results with regards to the CoFe-MNPs even they have different mechanisms to put forward the genotoxicity. The micronucleus frequency and DNA damage have been increased by the treatment of both naked and coated CoFe-MNPs in a concentration-dependent manner in the non-cytotoxic concentrations. Parallel to the cytotoxicity outcome naked CoFe-MNPs vs. silica coated ones and cancer cells vs. non-cancer cells were more vulnerable to the genotoxicity. One of the reasons is that normal and cancer cells have different tolerances to the same nanoparticles depending on time and concentration. Cancer cells display an enhanced state of oxidative stress due to oncogenic stimulation, increased metabolic activity and mitochondrial dysfunction, leads to DNA damage that cannot be repaired in time, leading to gene instability that may evoked by the nanoparticles [121]. Even though the cellular uptake of the silica coated CoFe MNPs were higher than the naked ones, the higher genotoxicity with naked CoFe MNPs could be explained by the reactive surface effect of the naked MNPs. The modification of MNPs surface through the silica layer creates an additional protective coating, which reduces toxicity and improves their

biocompatibility. This enhances MNPs resistance to the acidic conditions of lysosomal environment, reducing the degradation process of the cobalt/iron core and slowing down the ions release. This study suggests that silica coated CoFe-MNPs can be safely and effectively used as nanocarrier for biomedical applications such as gene or drug delivery agents with effectively uptake by cells. Our study could support the surface reactivity generated OH radicals' of nanoparticles is the key element in the NPs toxicity mechanism.

When considering the many variables such as different MNPs, cell types, culture conditions, and surface modifications used, it could be speculative to compare the results of our study on CoFe-MNPs with other MNP studies. For assessing the potential toxicity of them there are many international activities those suggesting to consider each of the NPs as a different entity [116] and to use a case by case approach for the hazard identification. Though, our results could serve as new data on CoFe-MNPs toxicity, while there was no study conducted in the same manner.

3.5 Measurement of Intracellular ROS

3.5.1 Assay for Reactive Oxygen Species (ROS)

Nanoparticles are very reactive without any surface coating because of having a large surface area to mass ratio. Therefore, it is possible that NPs may adsorb or release free radicals on to their surface [43]. There are many research that is associated with ROS generation by NPs [122]. Reactive oxygen species generated by MNPs cause damage in various cellular components, leading to DNA breaks, lipid membrane peroxidation, and protein carbonylation. Free radicals are not easily detected due to their short-lived properties. Therefore, ROS production is usually evaluated by indirect methods such as measurement of the various end products of reactions with lipids, proteins and DNA [123].

The ability of naked and silica coated MNPs to induce the intracellular ROS generations in MCF-10A, MCF-7; and MDA-MB-231 cells were studied with

DCF fluorescence technique. An interesting result obtained from this study is that, the effects of the two types of MNPs were quite different. Treatment with the naked MNP caused all the cells to generate an elevated amount of total intracellular ROS in concentration and time-dependent manner. The results are given in **Figures 26-28**.

Percent DCF formation significantly increased in MCF-10A cells treated with naked MNPs up to 151 % and 202 %, while silica coated MNPs caused an increase of 104 % and 140 % fluorescence intensity (compared to control) in MCF-10A cells at 4 and 24 h respectively.

Percent DCF formation was observed in MCF-7 cells with an increase of 245 % and 280 % for naked, 180 % and 210 % for silica coated for 4 and 24 h, respectively.

In MDA-MB-231 cells treated with naked and silica coated MNPs, ROS production was increased by 270 %, 305 % and 200 %, 240 % at 4 and 24 h, respectively.

In agreement with our fluorometry results (percent DCF formation), visualization of ROS generation with the Fluorescence Microscope showed that, the DCF fluorescence intensity was increased in a concentration dependent manner in all cells treated with the naked MNPs, while fluorescence intensity was insignificant in the controls, meaning that, ROS generation occurred in response to naked MNPs (**Figures 26-28**). The core metals induced notably high levels of ROS generation and resulting cell death at each concentration used. These data provide sufficient evidence that, the generation of intracellular ROS is a result of the accumulated- aggregated naked MNPs in the cells. These results are also consistent with the articles stating that, the silica-coated MNPs protect the cells from oxidative stress by preventing soluble iron mobilization or acidic erosion [113].

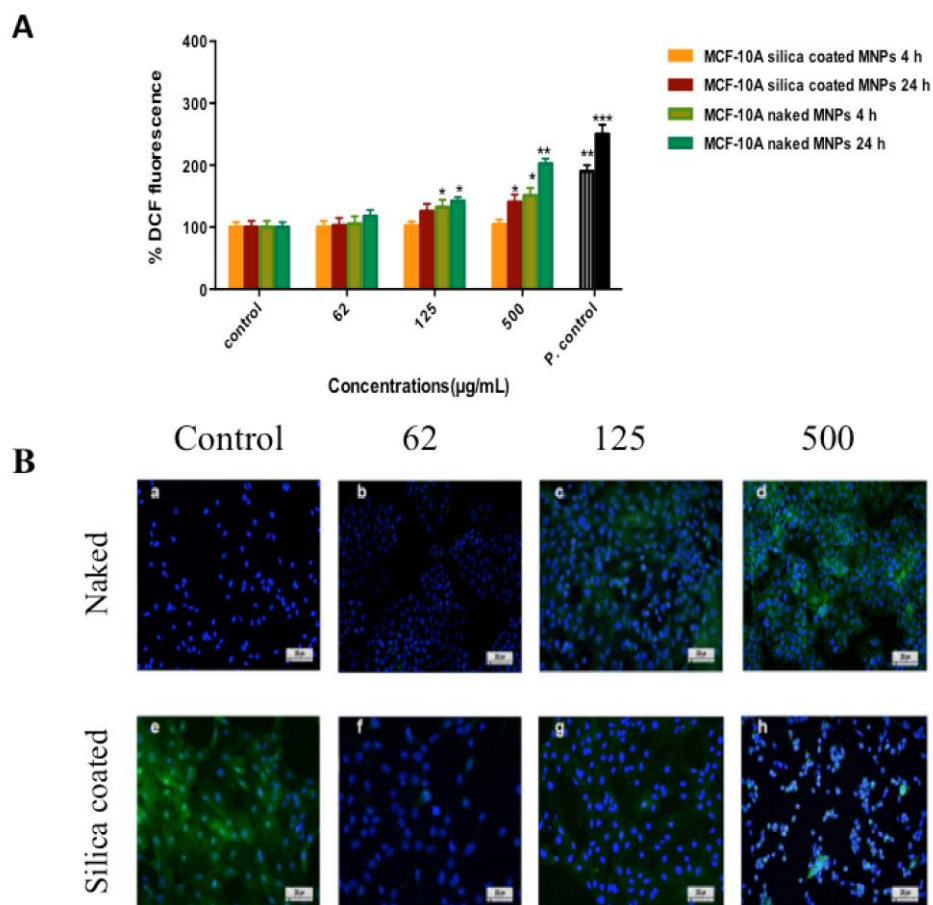


Figure 26. Effects of naked and silica coated MNPs on the generation of reactive oxygen species (ROS) in (A) MCF-10A cells for 4 and 24 h. The % DCF fluorescence of the control cells was considered 100 %. (B) Representative images of production of ROS using DCFDA dye in MCF-10A cells (a) Control cells, (b-d) Cells exposed to naked MNPs (62 µg/mL, 125 µg/mL and 500 µg/mL, respectively) (e) positive control: H₂O₂ treatment, (f-h) Cells exposed to silica coated MNPs (62 µg/mL, 125 µg/mL and 500 µg/mL respectively) for 24 h showing increase in fluorescence (the scale bar in the images 200 µm). *p < 0.05, **p < 0.01, ***p < 0.001

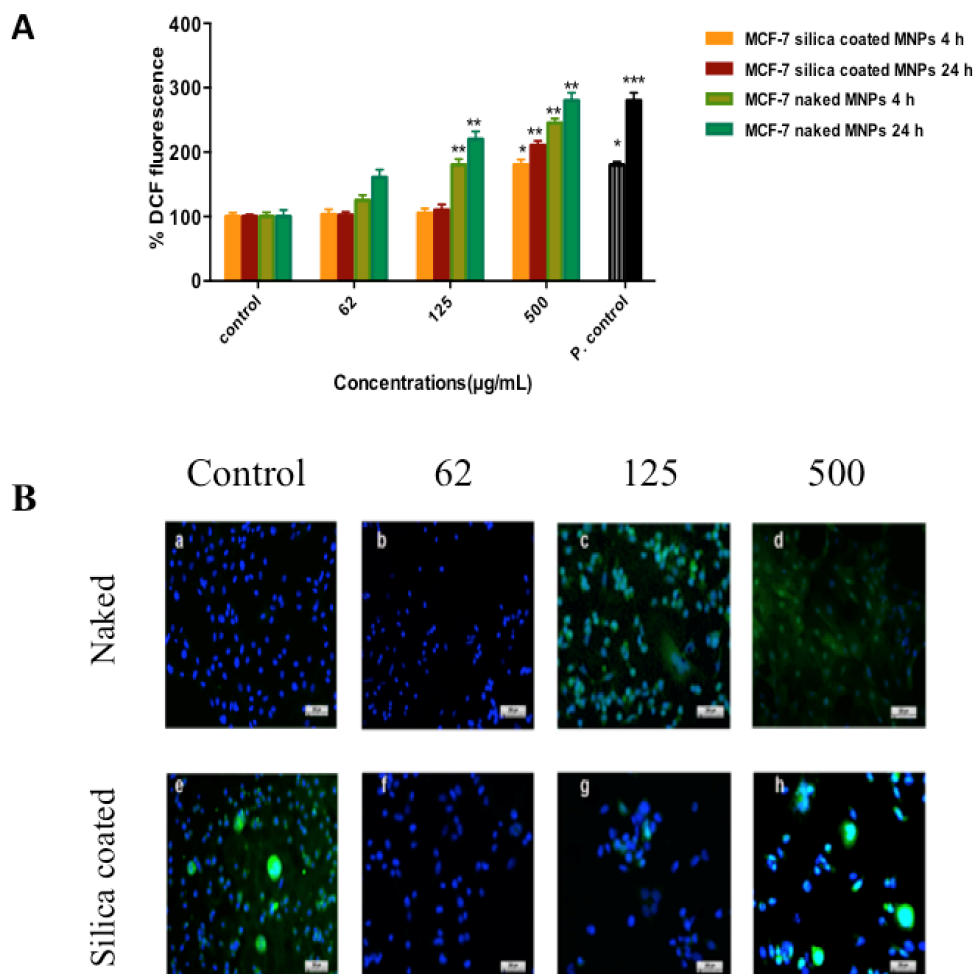


Figure 27. Effects of naked and silica coated MNPs on the generation of reactive oxygen species (ROS) in (A) MCF-7 cells for 4 and 24 h. The % DCF fluorescence of the control cells was considered 100 %. (B) Representative images of production of ROS using DCFDA dye in MCF-7 cells (a) Control cells; (b-d) Cells exposed to naked MNPs (62 µg/mL, 125 µg/mL and 500 µg/mL respectively) (e) positive control; H₂O₂ treatment; (f-h) Cells exposed to silica coated MNPs (62 µg/mL, 125 µg/mL and 500 µg/mL respectively) for 24 h showing increase in fluorescence (The scale bar in the images 200 µm). *p < 0.05, **p < 0.01, ***p < 0.001

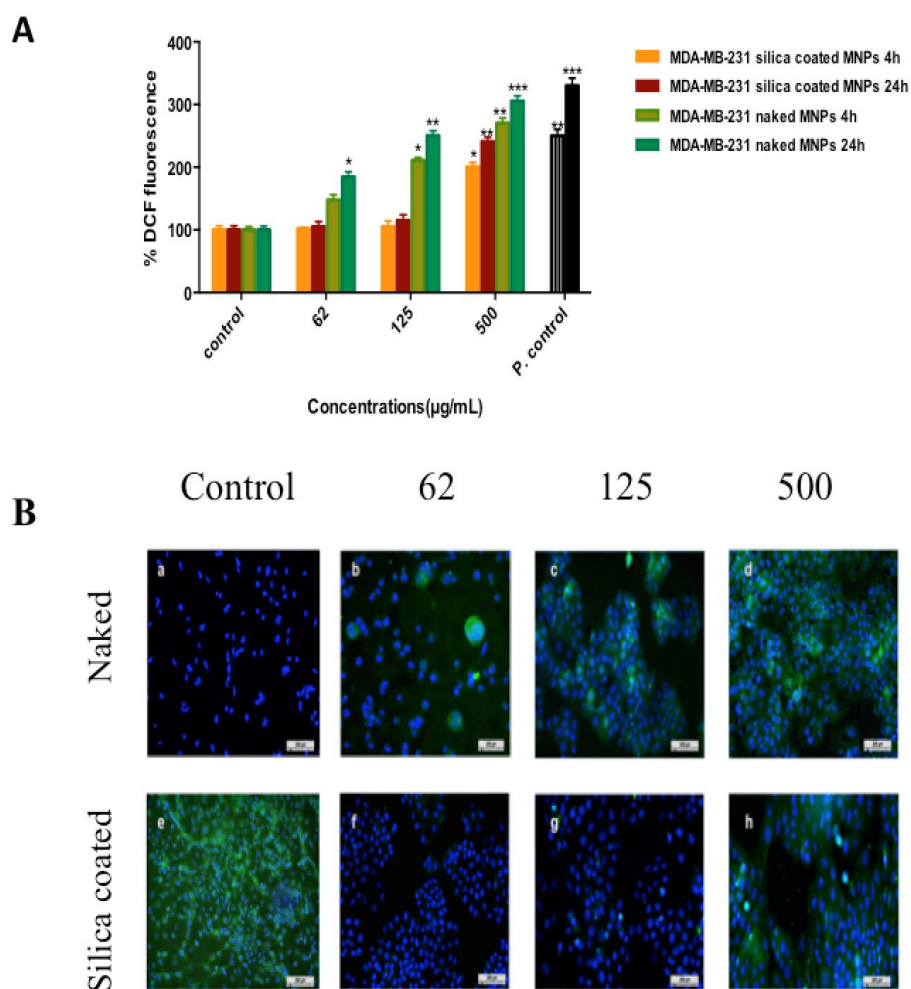


Figure 28. Effects of naked and silica coated MNPs on the generation of reactive oxygen species (ROS) in (A) MDA-MB-231 cells for 4 and 24 h. The % DCF fluorescence of the control cells was considered 100%. Representative images of production of ROS using DCFDA dye in MDA-MB-231 cells (a) Control cells; (b-d) Cells exposed to naked MNPs (62 µg/mL, 125 µg/mL and 500 µg/mL respectively) (e) positive control: H₂O₂ treatment; (f-h) Cells exposed to silica coated MNPs (62 µg/mL, 125 µg/mL and 500 µg/mL respectively) for 24 h showing increase in fluorescence (The scale bar in the images 200 µm). *p < 0.05, **p < 0.01, ***p < 0.001

3.5.2 Lipid Peroxidation (TBARS) Assay

We examined the amount of MDA formed using TBARS assay as ROS can damage cell membranes and formation of MDA is a major indicator of lipid peroxidation. As seen in **Figure 29**, MDA levels statistically increased in time and concentration dependent manner after 4 and 24 h exposure to both MNPs in all cells. However, naked MNPs caused lipid peroxidation significantly higher than the silica coated ones.

MCF-7 and MDA-MB-231 cells treated with naked and silica coated MNPs showed time and concentration dependent increase in MDA levels which were statistically significant starting at 62 $\mu\text{g/mL}$ ($p < 0.05$) for naked MNPs and at 500 $\mu\text{g/mL}$ ($p < 0.05$) for silica coated ones for 4 and 24 h treatments.

Statistically significant increase in MDA levels were found for the concentration range of 125-500 $\mu\text{g/mL}$ at both 4 and 24 h treatments for naked MNPs while only concentration of 500 $\mu\text{g/mL}$ for 24 h resulted in an increase in MDA levels for silica coated ones ($p < 0.001$). Also, MDA levels in MCF-10A cells found to be lower compared to MDA-MB-231 and MCF-7 cells.

Lipid peroxidation and oxidative stress has been cited to be one of the most important mechanisms of cellular toxicity related to NP exposure. Furthermore, NP-induced lipid peroxidation and oxidative stress leads to DNA damage and apoptosis. So we further study the effect of both types of MNPs on apoptotic rates of MDA-MB-231, MCF-7 and MCF-10A cells.

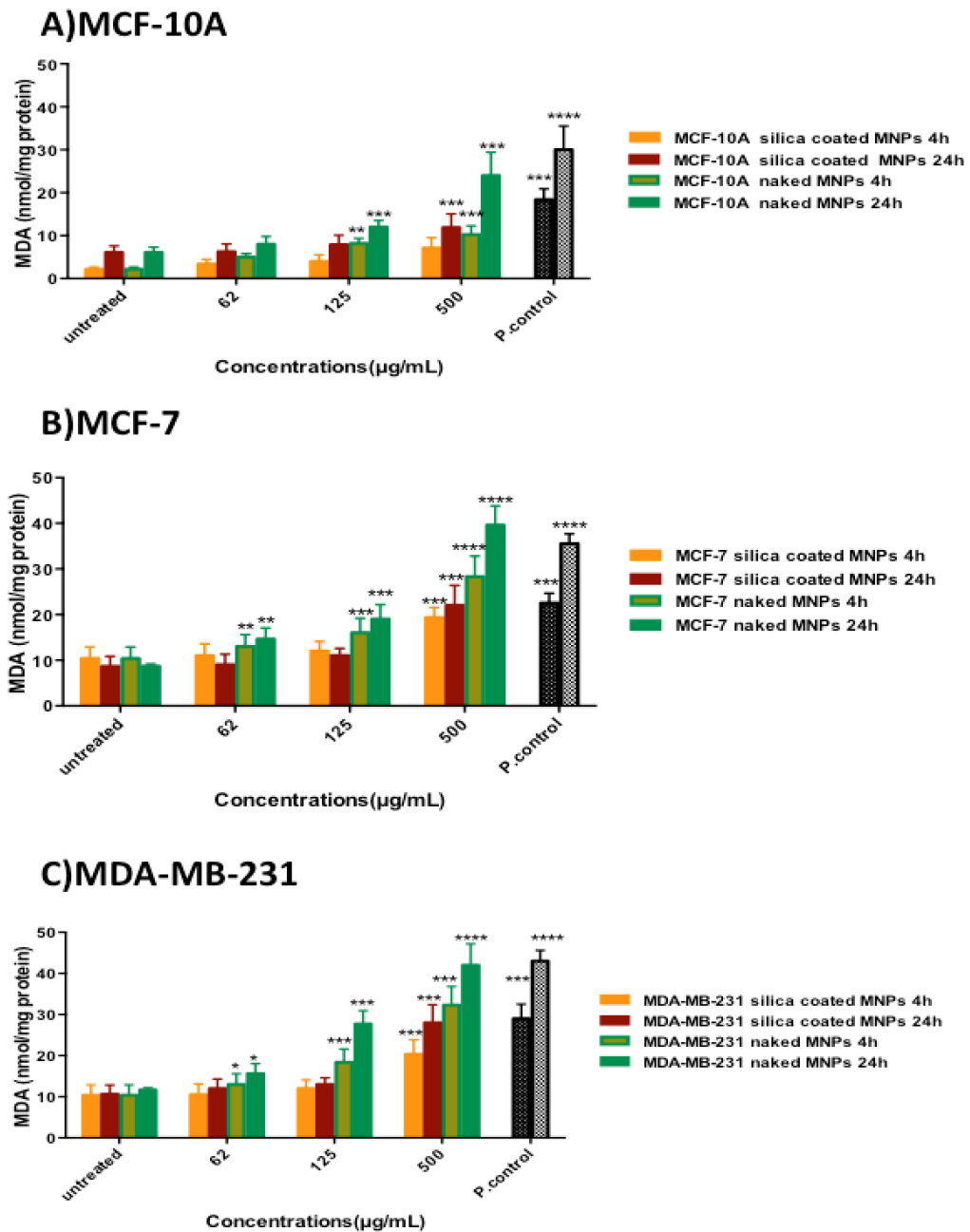


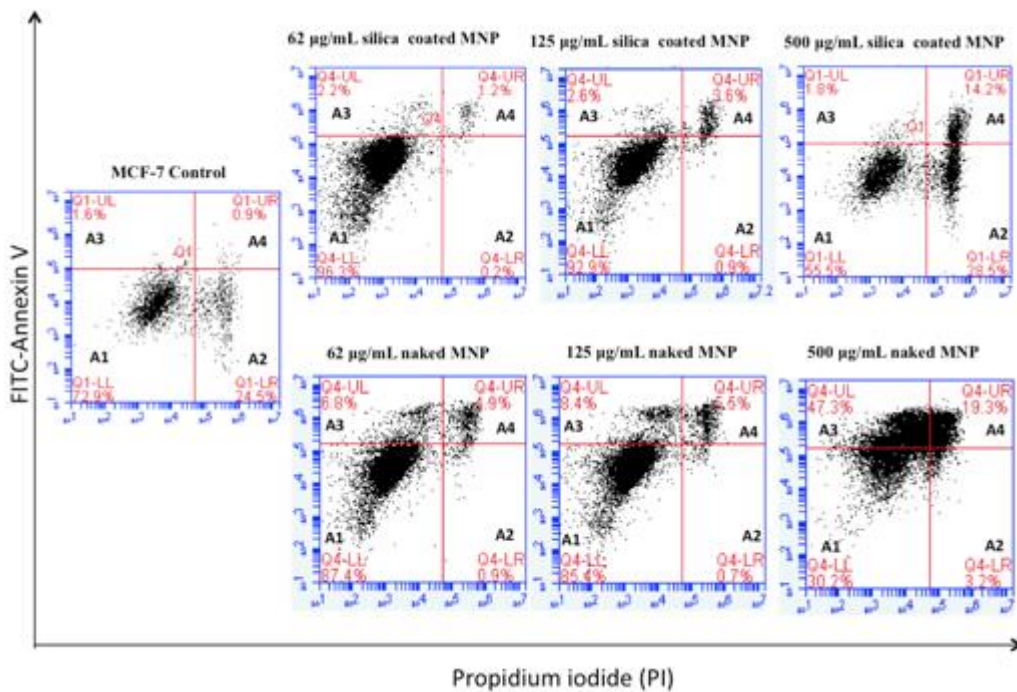
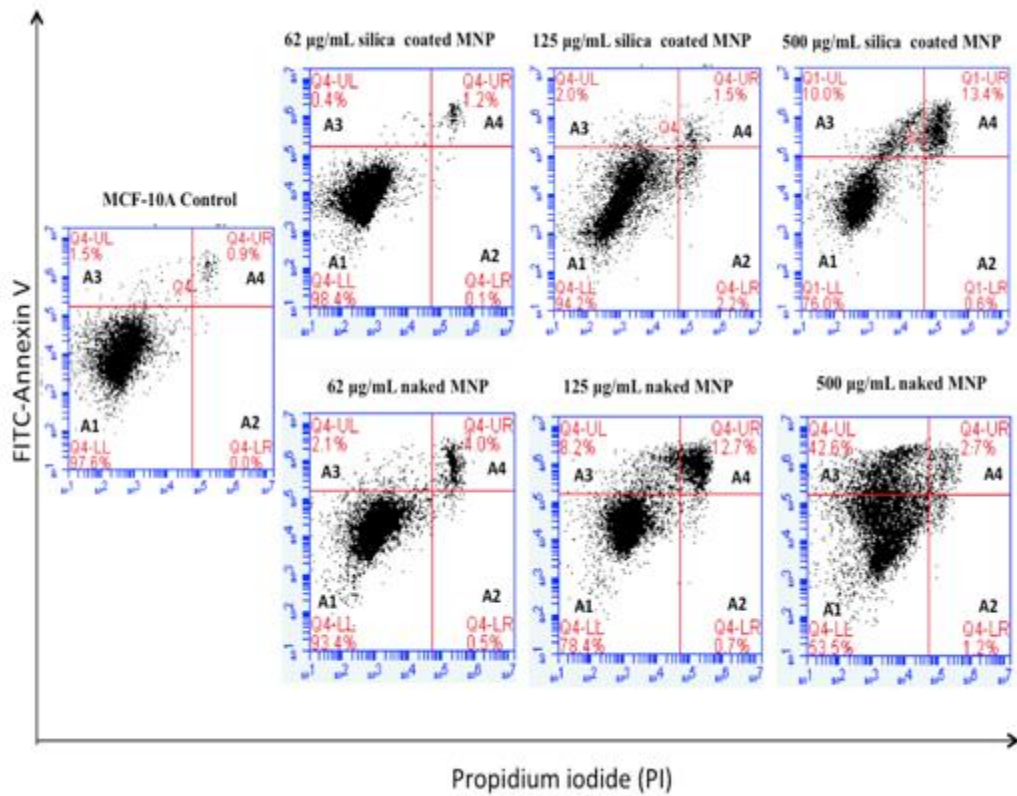
Figure 29. Detection of lipid peroxidation (nmol MDA /mg protein) in MCF-10A, MCF-7 and MDA-MB-231 cells treated with different concentrations of naked and silica coated MNPs for 4 and 24 h. * $p < 0.05$, ** $p < 0.01$, *** $p < 0.001$

3.6 Apoptosis Assay

3.6.1 Annexin-V-FITC / PI Assay

Apoptosis was determined by using Annexin-V-FIT/PI assay in order to understand the nature of cell death in all cell types upon exposure to naked and silica coated MNPs at three different concentrations of 62, 125 and 500 $\mu\text{g}/\text{mL}$ for 24 h. Flow cytometry analysis of MDA-MB-231, MCF-7 and MCF-10A cells carried out by double labeling with Annexin V-fluorescein isothiocyanate and propidium iodide.

The results are given in **Figure 30**. MDA-MB-231 cells without any treatment showed 2.6 % apoptosis at 24 h whereas, in cells treated with 3 concentrations of naked MNP, the apoptosis was calculated as 13.9, 29.3 and 62.2 % ($p < 0.05$). The percentage of apoptosis in silica coated MNP treatment group increased from 6.4% to 23.7% at 24 h ($p < 0.01$). The percentage of both early and late apoptosis of MDA-MB-231 cells treated with naked MNP significantly increased compared to silica coated MNPs. Similar trend was observed for MCF-7 cells treated with either naked or silica coated MNPs. The percentage of apoptosis in silica coated MNP treated cells increased from 2.4% to 23.4% at 24 h ($p < 0.01$), whereas for naked MNP treated cells, the apoptosis increased from 20.9 to 45.3%. These results indicated that, naked MNP alone-induced apoptotic pathway, while silica coating decreased apoptotic effects. So, silica coating can serve as an excellent carrier agent for MNPs.



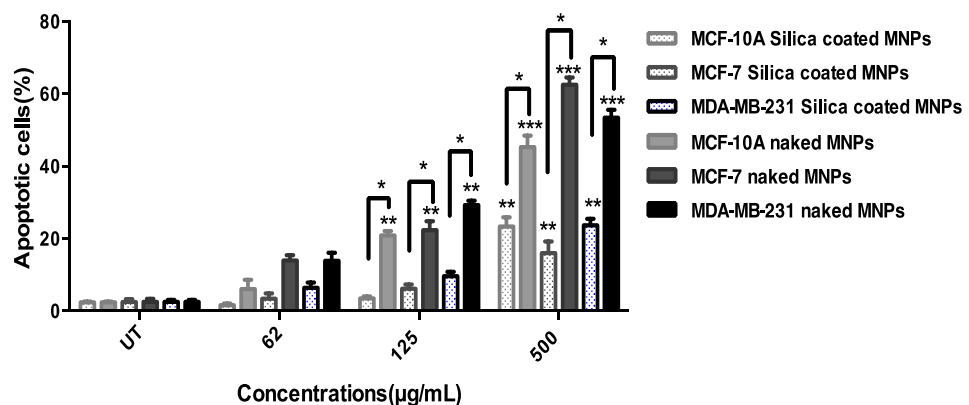
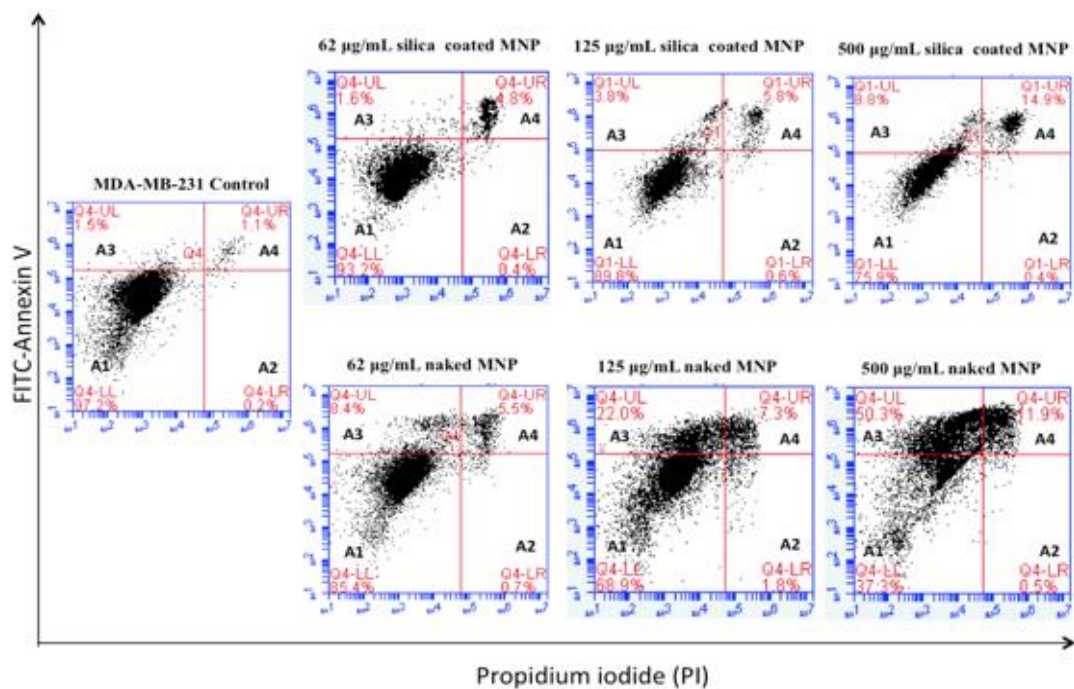


Figure 30. The histograms of the apoptotic effects of naked and silica coated MNPs at concentrations of 62 µg/mL, 125 µg/mL and 500 µg/mL, on MCF-10A, MCF-7 and MDA-MB-231 cells. Four subpopulations and their percent distributions in different areas: Area A1 and A2 shows viable and dead cell (necrotic), A3 and A4 correspond to cells undergoing early and late apoptosis, respectively. Bar graphs show percent apoptotic cells. Untreated (UT) cells are used as control. (* $p < 0.05$, ** $p < 0.01$, *** $p < 0.001$).

3.6.2 Effect of Naked and Silica Coated MNPs on Apoptotic Gene Expressions

Further analysis of apoptotic pathway is carried out by looking at the gene expression levels of apoptotic and anti-apoptotic proteins after treatment of cells with both types of MNPs. Gene expressions were determined by using quantitative PCR in all MDA-MB-231, MCF-7 and MCF-10A cells after treatment with naked and silica coated MNPs at three different concentrations of 62, 125 and 500 $\mu\text{g}/\text{mL}$, for 24 h. The results are given in **Figure 31**. Gene expression analysis results revealed that, the apoptotic PUMA and BAX genes were up regulated and the gene expressions were increased from 2.7 to 8.38 fold and 2.5 to 10.9 fold, respectively, in metastatic cancer MDA-MB-231 cells when treated with naked MNP at a concentration range of 62 to 500 $\mu\text{g}/\text{mL}$, for 24 h. On the other hand, the down regulation of anti-apoptotic SURVIVIN gene was observed by a decrease in gene expression from 2.5 to 7.1-fold ($p < 0.05$). Similar trends were observed for both MCF-10A and MCF-7 cells treated with naked MNPs.

All MCF-7, MDA-MB-231 and MCF-10A cells treated with naked and silica coated MNPs showed time and concentration dependent increase in apoptotic gene (BAX, PUMA) expressions and a decrease in anti-apoptotic genes (SURVIVIN and BCL-2) which were statistically significant at concentration of 125 $\mu\text{g}/\text{mL}$ ($p < 0.05$) for naked MNPs and at 500 $\mu\text{g}/\text{mL}$ ($p < 0.05$) for silica coated MNPs for 24 h treatments.

Apoptosis is the main way to maintain the cellular homeostasis between cell division and the cell death that can be initiated via two principal signaling pathways: the death receptor-mediated extrinsic apoptotic pathway and the mitochondrion-mediated intrinsic apoptotic pathway. Previous studies have revealed that, the majority of the NPs trigger apoptosis through the mitochondrion-mediated pathway [124, 125]. Thus, most probably the effect

of the cell deaths observed by the naked MNPs is related with the mitochondrion-mediated apoptotic pathway.

Consistent with our previous experiment, naked MNPs caused significantly more ROS production and lipid peroxidation than the silica coated ones. In order to test the impact of this finding on apoptosis, we performed the ANNEXIN V-FITC assay and also checked the expression levels of apoptotic (BAX, PUMA) and anti-apoptotic genes (SURVIVIN, BCL-2). The results were in good agreement with the ROS and lipid peroxidation data, namely naked MNPs strongly increased the levels of apoptosis and the expression level of apoptotic genes and decreased the expression level of anti-apoptotic genes unlike the silica coated MNPs. As we discussed the oxidative stress data, all the results are consistent with each other; we further interpret our results and concluded that, the increased cellular stress in the cells caused by the MNPs, is responsible for apoptosis.

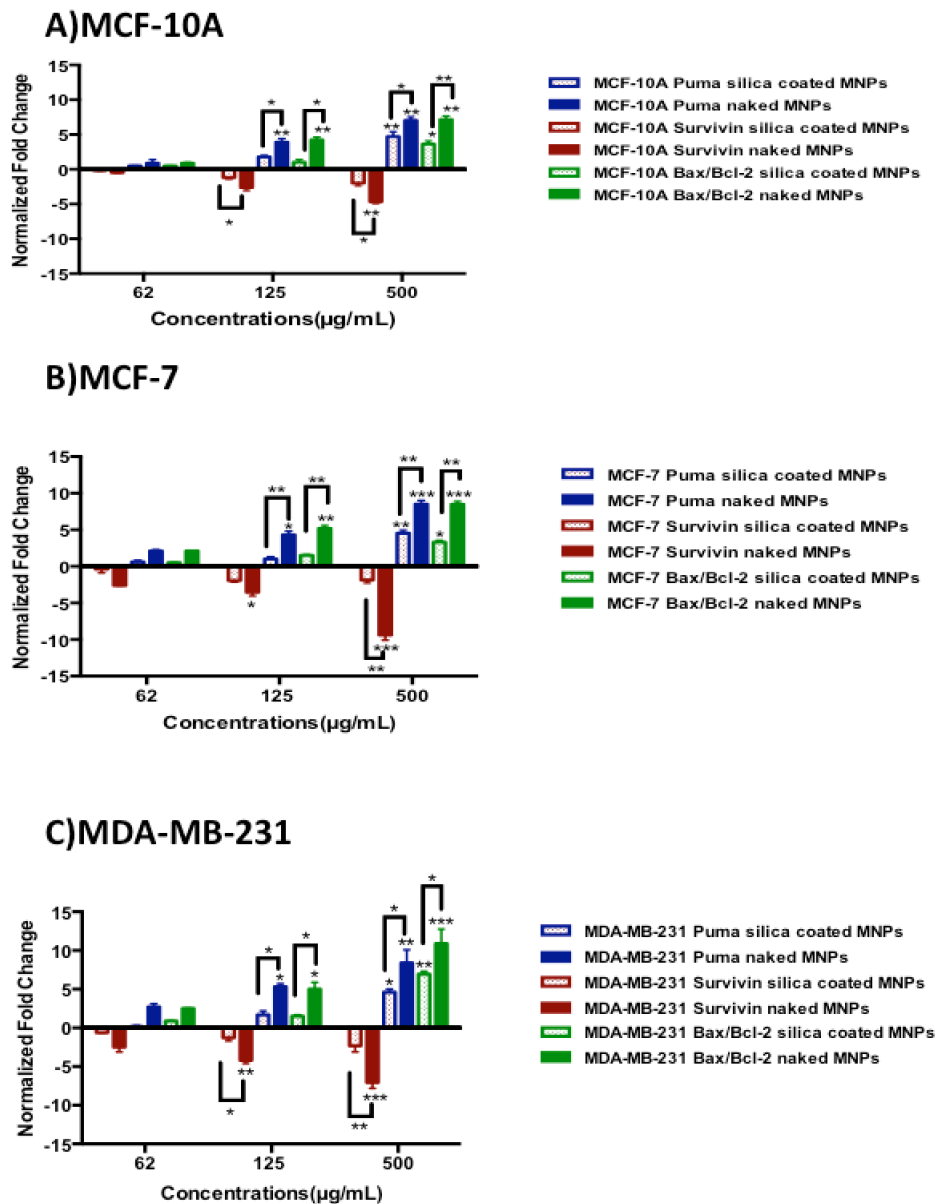


Figure 31. The expression levels of apoptotic (PUMA and BAX) and anti-apoptotic (BCL-2, SURVIVIN) genes in MCF-10A, MCF-7, MDA-MB-231 cells after treatment with naked and silica coated MNPs for 24 h. Fold changes of the genes in the cells were normalized with respect to the internal control gene β -actin. * $p < 0.05$, ** $p < 0.01$, *** $p < 0.001$.

3.7 mRNA Expression Analysis of Phase I and Phase II Enzymes.

3.7.1 Effect of Naked and Silica Coated MNPs on CYP1A1 and CYP1B1 Gene Expressions

Cells appear to modulate the expression of several antioxidant enzymes and stress-related genes in response to oxidative stress. The effect of naked and silica coated MNPs on gene expressions of four drug-metabolizing enzymes were also investigated. Drug metabolism, which is also known as xenobiotic metabolism, is the biochemical modification of pharmaceutical compounds or xenobiotics through specialized enzymes, known as Phase I and Phase II reactions. CYP1B1 and CYP1A1 genes, are coding for enzymes, which catalyze many reactions involved in drug metabolism [126]. Cytochromes P450 are a superfamily of drug metabolizing phase I enzymes responsible for metabolism of most xenobiotics and are required for the efficient elimination of foreign chemicals from the body. They also play role in carcinogenesis and cancer progression [127].

All cells treated with naked and silica coated MNPs showed concentration dependent increase in the expression levels of these genes which were statistically significant starting at 125 $\mu\text{g}/\text{mL}$ ($p < 0.05$) for naked MNPs and at a concentration of 500 $\mu\text{g}/\text{mL}$ ($p < 0.05$) for silica coated ones for 24 h treatments (**Figure 32**).

Both CYP1A1 and CYP1B1 showed an expression ratio greater than 2-fold in non cancer MCF-10A cells treated with naked MNP at concentration of 125 and 500 $\mu\text{g}/\text{mL}$ whereas no significant change was observed at concentration of 125 $\mu\text{g}/\text{mL}$ for silica coated MNPs. Overall, the highest gene expressions were observed in metastatic MDA-MB-231 cells.

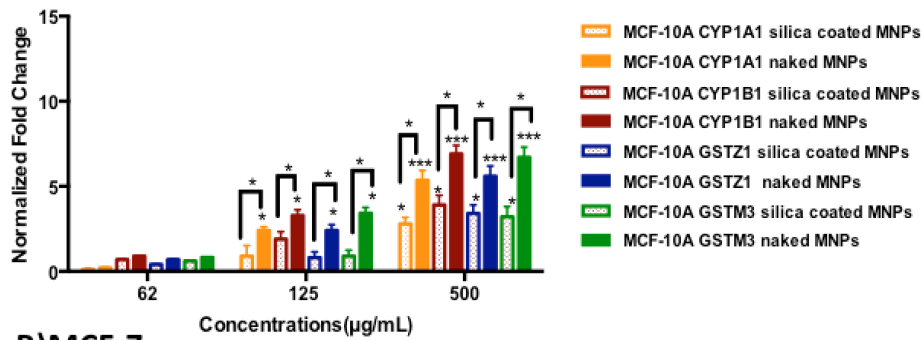
3.7.2 Effect of Naked and Silica coated MNPs on GSTZ1 and GSTM3 Gene Expressions.

Glutathione S-transferases (GSTs) are a multigene family of drug metabolizing enzymes, which are important in phase II metabolism functioning in cellular detoxification of electrophilic compounds, including carcinogens, therapeutic drugs, environmental toxins and products of oxidative stress, by conjugation with glutathione [128]. Genetic variations can change an individual's susceptibility to carcinogens and toxins as well as affect the toxicity and efficacy of certain drugs. Unfortunately, little is known about the effects of NPs on both CYPs and GSTs [129].

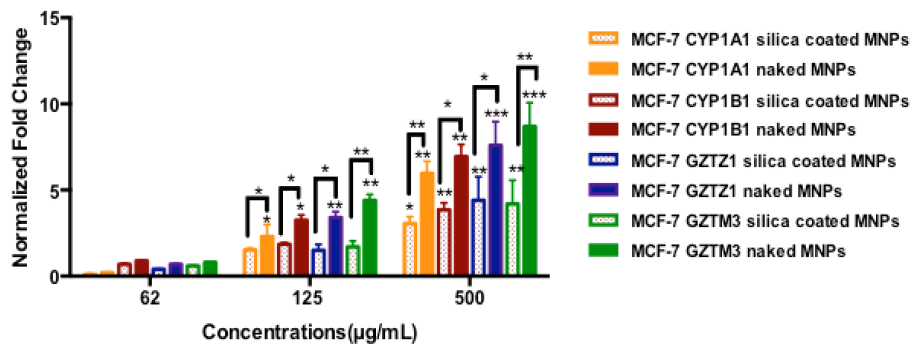
In our study, the expression of GSTZ1 and GSTM3 genes increased 3.4 and 5.2 fold in MDA-MB-231 cells treated with silica coated MNPs, whereas the expression of these genes increased 8.6 and 9.7 fold for naked ones, respectively, at a concentration range from 62 to 500 $\mu\text{g}/\text{mL}$ for 24 h. Naked MNP treatment increased the expressions of both GSTZ1 and GSTM3 genes in MCF-7 cells by 7.6 and 8.7 fold, respectively whereas silica coated MNP treatment increased the expression of these genes by 4.4 and 4.2 fold, respectively (**Figure 32**).

The results also indicated that, both CYP1A1 and CYP1B1 showed an expression ratio greater than 2-fold in non-cancer MCF-10A cells treated with naked MNP at concentration of 125 and 500 $\mu\text{g}/\text{mL}$ whereas no significant change was observed at concentration of 125 $\mu\text{g}/\text{mL}$ for silica coated MNPs (**Figure 32**).

A) MCF-10A



B) MCF-7



C) MDA-MB-231

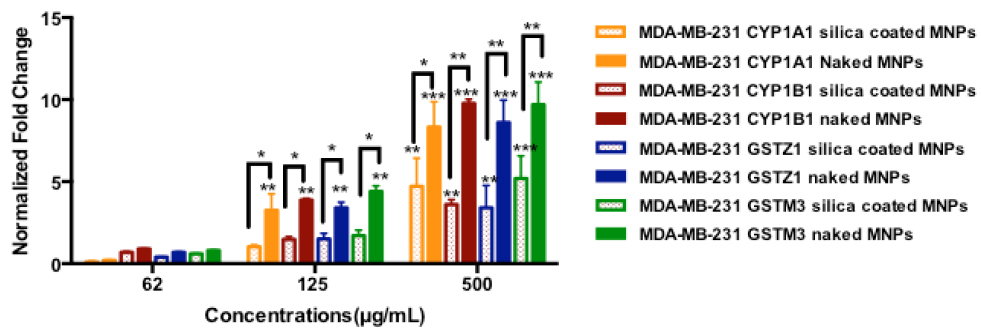


Figure 32. The expression levels of CYP1A1, CYP1B1, GSTZ1 and GSTM3 genes in MCF-10A, MCF-7, MDA-MB-231 cells after treatment with naked and silica coated MNPs for 24 h. Fold changes of the genes in the cells were normalized with respect to the internal control gene β -actin. * $p < 0.05$, ** $p < 0.01$, *** $p < 0.001$.

These findings are consistent with the observation that naked MNP uptake might increase the rate of CYP1A1 and CYP1B1 mRNA transcription by inducing metabolic stress. MNP-induced oxidative stress and mitochondrial dependent apoptosis are evident in several pathophysiological states and could be a specific defense mechanism maintaining homeostasis in response to the accumulation of O⁻ and other reactive oxygen species at later time points.

Our preliminary data has suggested that exposure of MNPs lead to an oxidative stress indicated by an increase in GSTM3 and GSTZ1 gene expression, in addition CYP1A and CYP1B1 gene expression were also increased, which might triggered the morphological modifications, like mitochondrial damage in a dose dependent manner.

Our results also showed that, although silica coated MNPs internalized better than the naked ones, they caused less oxidative stress and reduced possible effects of MNP-induced cellular toxicity in the breast cells.

Also naked NPs induced higher expressions of GSTM3 and GSTZ1 genes compared to silica coated MNPs. Because silica forms protective hydrophilic shell around NP this might hinder the cell defense response and ended up in low response to internalized MNP.

We then investigated how the surface of NPs affected their interactions with cells *in vitro*. The aim of our study was to evaluate the surface properties of MNPs for their potential use. The results clearly showed the importance of careful analysis and individual interpretation for each cell-NP system and additional work must be undertaken in order to be able to fully investigate NP cell interaction and to use MNPs safely for nanomedicine applications. In this part of the study, we compared the effect of silica coating on cobalt ferrite magnetic-core nanoparticles focusing on the potential of apoptosis, lipid peroxidation, ROS generation and resulting oxidative stress.

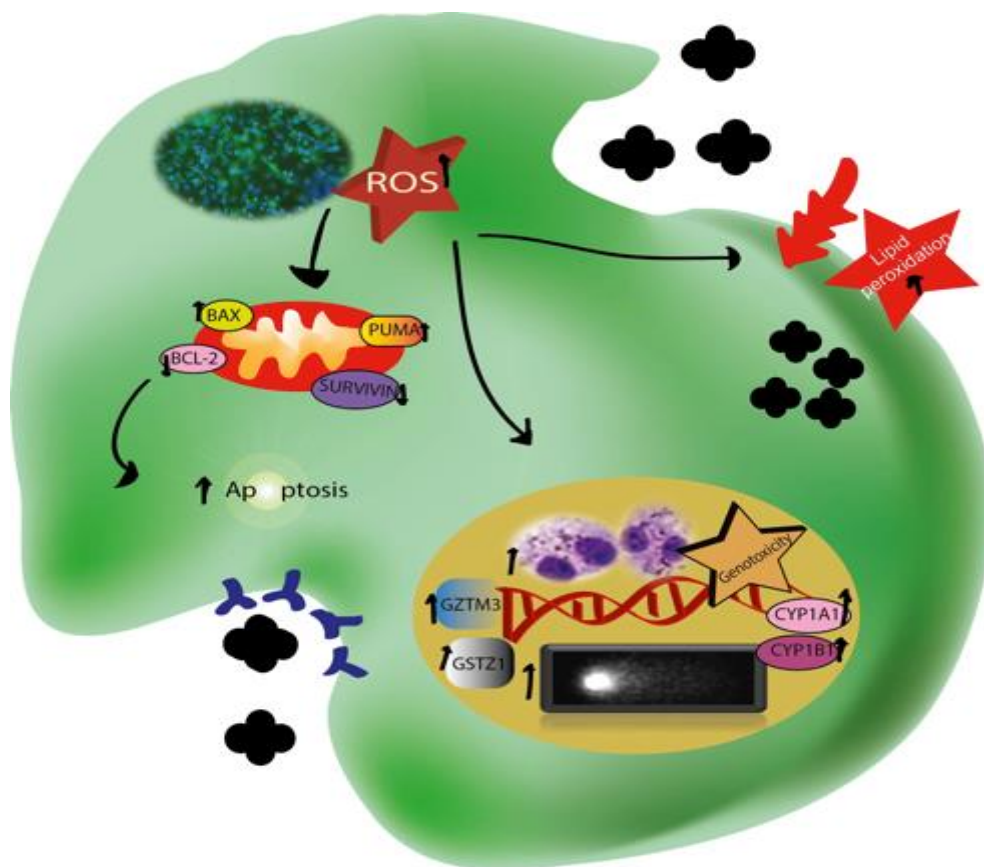


Figure 33. A schematic drawing, showing possible mechanisms of naked MNPs on the induction of cellular toxicity in the breast cancer cells. Naked CoFe-MNPs can lead to mitochondrial disruption and, to ROS production after internalization. Oxidative stress (excess ROS generation) might induce damage in breast cell, such as lipid peroxidation, DNA damage (directly or indirectly) and expression levels of some Phase I and Phase II genes expression levels. All these events can results in cellular apoptosis.

In following part of the study we further modified the silica coated MNPs with 2-deoxy glucose in order to achieve a selective uptake of MNPs into cancer cells.

3.8 The Conjugation of 2-amino-2-deoxy-glucose to Cobalt Ferrite Magnetic Nanoparticle (2DG-MNPs)

3.8.1. Characterization of Modified CoFe MNPs

FT-IR spectroscopy measurement was used for the characterization of the silica coating and carboxyl groups on the surface of cobalt ferrite (CoFe) MNPs. FT-IR spectrum of this nanoparticle is given in **Figure 34**. The bands around 1197, 1085 cm^{-1} and 800 cm^{-1} represent the characteristic peaks of Si-O-Si stretching and Si-O bending. Thus, it is clear that silica layer was successfully coated on to the surface of nanoparticles [130]. Additionally, the bands between around 1400 cm^{-1} together with the band at 1718 cm^{-1} indicate the characteristic peaks of carboxylic acid and support the presence of carboxylic acid and the 2DG on the surface of the NP [98, 131].

The hydrodynamic sizes of -COOH modified and 2DG attached MNPs were determined with DLS measurements in water at 25 °C. The average sizes of COOH-MNPs and 2DG-MNPs were found as 175.7 ± 4.7 nm and 211 ± 3.5 nm, respectively (**Figure 34**) and the zeta potentials of COOH-MNPs and 2DG-MNPs were obtained in water and calculated as -39.5 mV and -10.5 mV, respectively. The decrease in surface negative charge for 2DG-MNPs was due to the conjugation of 2-amino-2-deoxy-glucose molecules to the carboxyl groups.

After attaching the 2DG to the MNP, the amount of 2DG on the CoFe MNPs surface was calculated as 37.02 ± 2.4 mM glucose/mg NP, by using spectrophotometric determination of 2DG. Both the non-modified COOH-MNPs and the blank do not contain any 2DG, as expected.

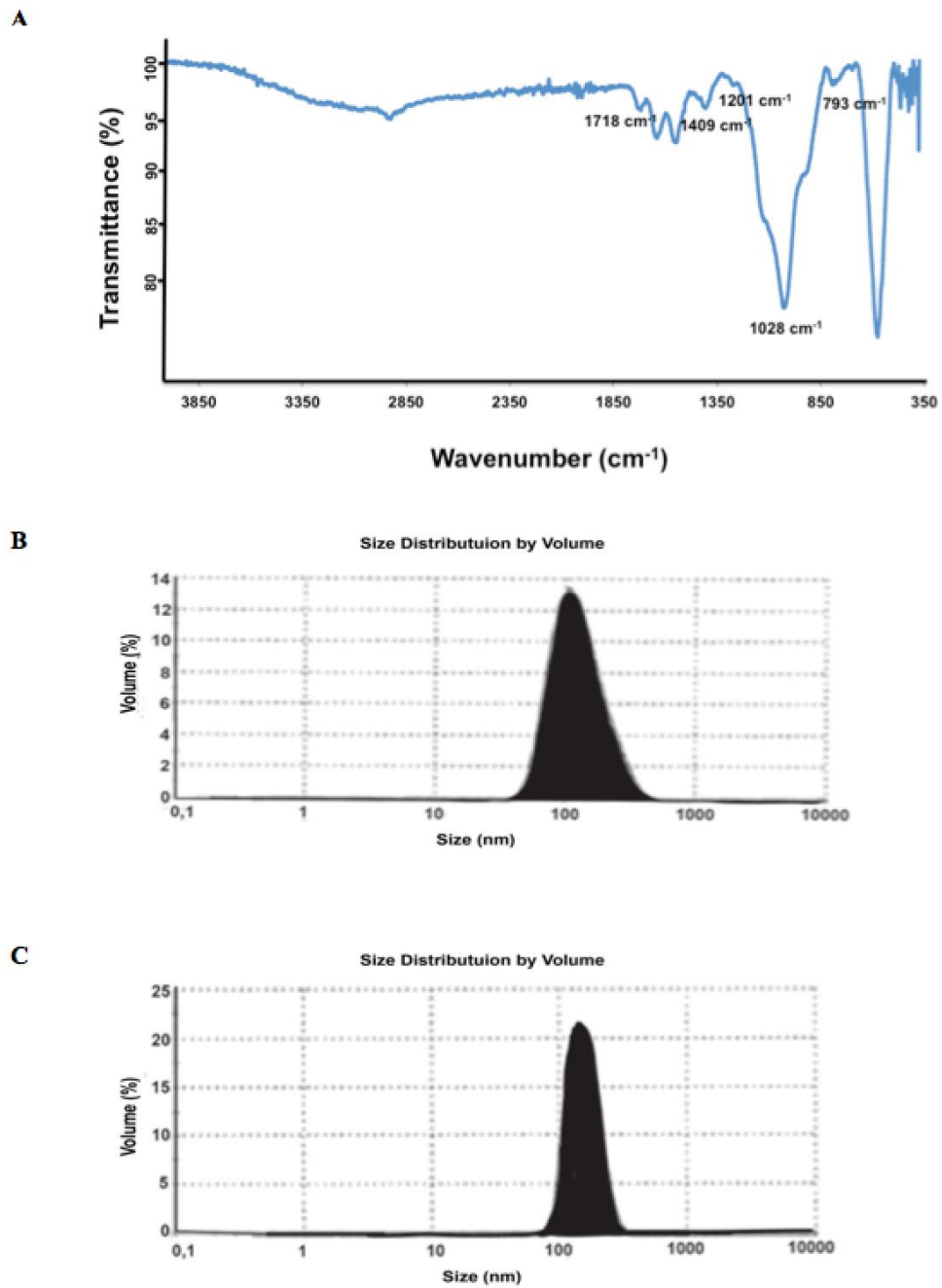


Figure 34. (A) FT–IR spectra of -COOH modified CoFe MNPs. Particle size distribution of (B) -COOH modified CoFe MNPs and (C) 2DG modified CoFe MNPs.

3.8.2. Cellular Uptake of 2DG-MNPs

3.8.2.1 Cellular Uptake of 2DG-MNPs by TEM

Qualitative analyses of internalized 2DG-MNPs were performed by TEM. MDA-MB-231 cells were incubated with 2DG-MNPs (125 $\mu\text{g/mL}$) for 24 h. As seen from **Figure 38**, TEM images demonstrated that 2DG-MNPs were localized in the cytoplasm and a successful increase in cellular uptake was observed with 2DG-MNPs especially in MDA-MB-231.

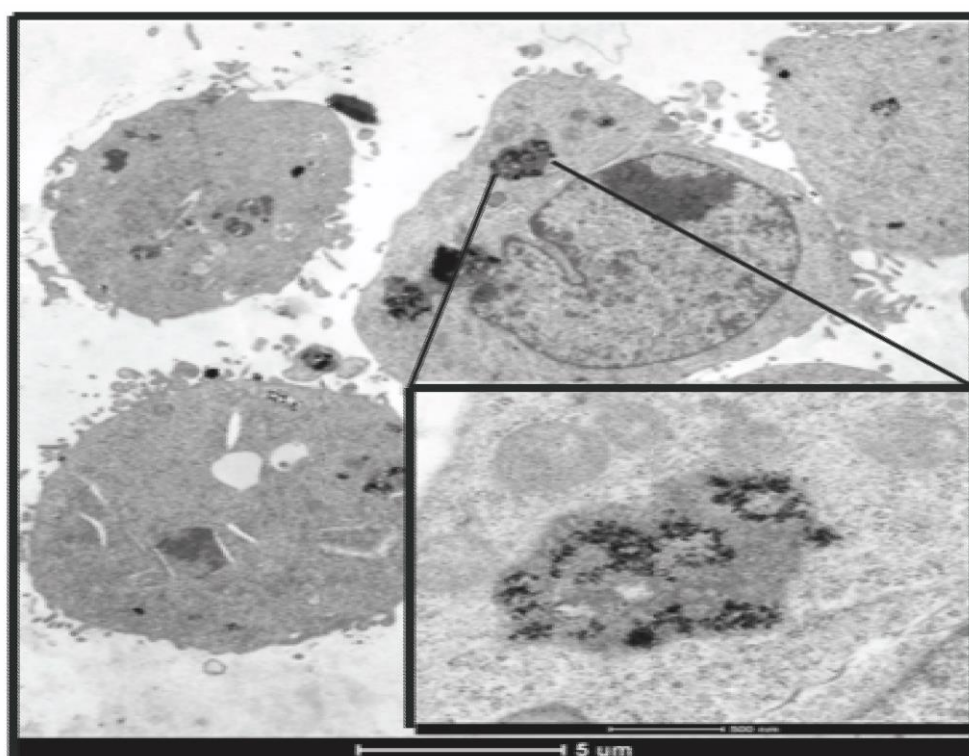


Figure 35. Transmission electron micrographs (TEM) of MDA-MB-231 cells treated with 2DG-MNPs. MNPs are internalized and accumulated in cytoplasm. The scale bar is 500 nm and 5 μm .

3.8.2.2 Cellular Uptake of 2DG-MNPs by (ICP-OES)

The breast cancer cells, MDA-MB-231, MCF-7 and non-cancer MCF-10A cells were incubated with both COOH-MNPs and 2DG-MNPs at the concentrations of 125 and 500 $\mu\text{g/mL}$ for 24 h in separate experiments. Iron concentration per cell (pg/cell) in three types of cells and the comparisons between different MNP samples are given in **Figure 36**.

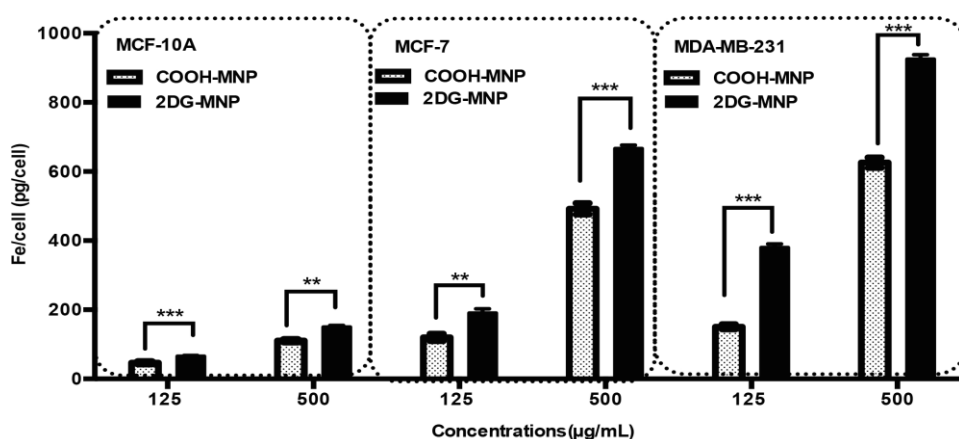


Figure 36. ICP-OES measurements of iron concentration per cell (pg/cell) in MCF-10A, MCF-7 and MDA-MB-231 cells after treatment with COOH-MNPs and 2DG-MNPs at final concentrations of 125 $\mu\text{g/mL}$ and 500 $\mu\text{g/mL}$ after 24 h incubations. (***) $p < 0.001$, ** $p < 0.01$)

It was clearly seen from the figure that, 2DG-MNPs were significantly internalized more than modified COOH-MNPs ($p < 0.01$ and $p < 0.001$) into all cell types. Both type of MNPs showed a concentration dependent feature for internalization, however the rate of uptake was lowest in non-cancer human breast epithelial cells, MCF-10A, which is again a very important characteristic for the selective targeting. Enhanced nutrient requirement mainly glucose, in cancer cells due to their high metabolic activity and proliferation rate is most probably the reason for this increased uptake in cancer cells compared to normal cells. The uptake trend of 2DG-MNPs (125 $\mu\text{g/mL}$) over varying times is also given in **Figure 37**.

As seen in **Figure 37**, the uptake of 2DG-MNPs increased in the first 4 h, but the uptake rate gradually slowed and reached a plateau after 12 h in all cell types. The iron concentration per cell (pg/cell) in MDA-MB-231, MCF-7 and MCF-10A cells are calculated as 210, 130 and 45 pg /cell at the end of first 4 h, respectively.

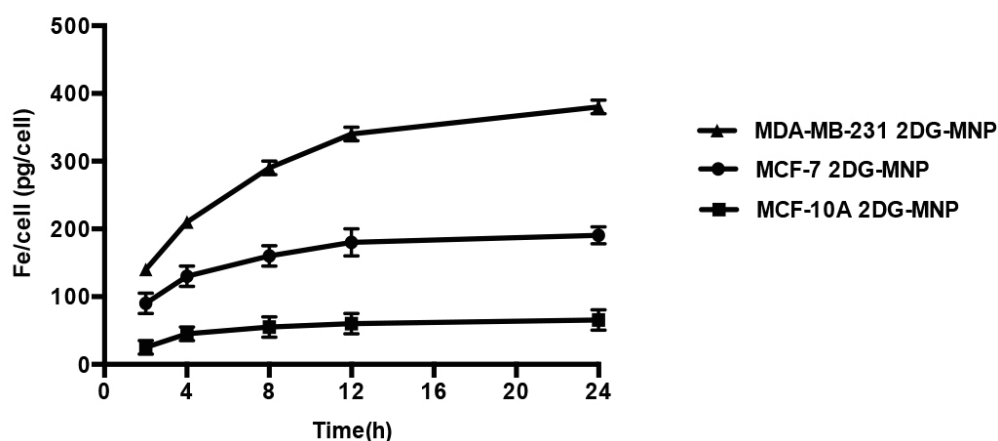


Figure 37. ICP-OES measurements of iron concentration per cell (pg/cell) in MCF-10A, MCF-7 and MDA-MB-231 cells after treatment with 2DG-MNPs at final concentrations of 125 $\mu\text{g/mL}$ after 2, 4, 8, 12 and 24 h incubations.

3.8.2.2 Cellular Uptake of 2DG-MNPs by Prussian Blue Staining

In order to visualize the cells exposed to both COOH-MNPs and 2DG MNPs, Prussian blue staining method was used and the microscopy images of the cells were evaluated by comparing the untreated cells as well as the particle types (**Figure 38**).

When we compare the blue granules, which are MNPs, it is seen that though 2DG-MNPs were internalized by all cell types; the nanoparticle uptake was much more in cancer cells than the non-cancerous cells as confirmed by our previous ICP-OES results. It is also obvious that the uptake of 2DG-MNPs was higher than that of COOH-MNPs.

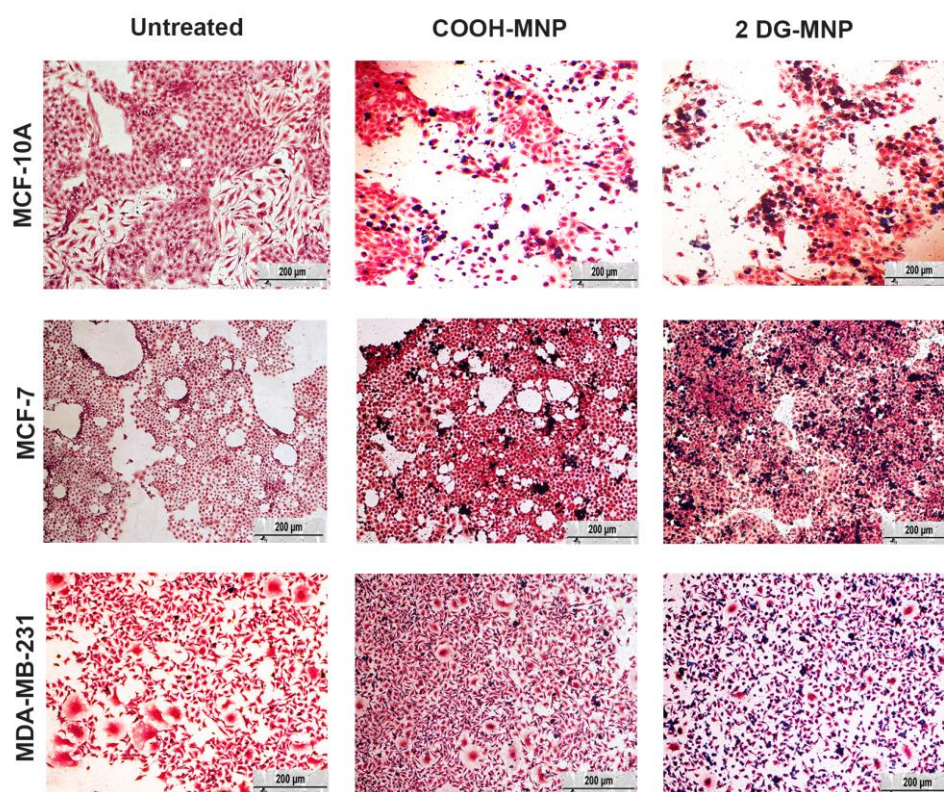


Figure 38. Light microscopy images of MCF-10A, MCF-7 and MDA-MB-231 cells that are stained with Prussian blue and following counterstained with nuclear fast red. Light pink coloring of cytoplasm, dark pink coloring of nucleus and blue coloring of iron core of the molecules were seen. The cells were treated with COOH-MNPs and 2DG-MNPs at the concentrations of 125 $\mu\text{g}/\text{mL}$ for 24 h. The scale bar in the images is 200 μm .

3.8.3. Cell viability (XTT) Assay

The dose response and time dependent cell viability profiles were obtained for 2DG-MNPs treated MDA-MB-231, MCF-7 and MCF-10A cells in order to compare the cytotoxic effects of MNPs on these cell lines (**Figure 39**).

IC₅₀ values were calculated as 282.3 ± 3.4 and 202.9 ± 6.2 $\mu\text{g}/\text{mL}$ for metastatic cancer MDA-MB-231, and 305.1 ± 4.8 and 258.8 ± 5.2 $\mu\text{g}/\text{mL}$ for MCF-7 cells incubated for 24 h and 72 h, respectively. In normal MCF-10A cells, these

values were calculated as 512.9 ± 3.8 for 24 h and 341.2 ± 6.3 $\mu\text{g}/\text{mL}$ for 72 h at 37 °C.

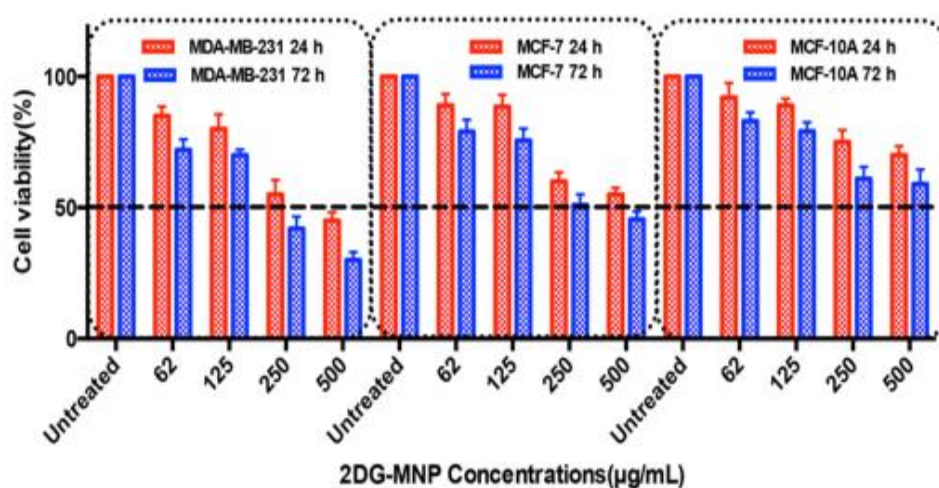


Figure 39. Cell viability of MDA-MB-231, MCF-7 and MCF-10A cells after treatment at different concentrations (62–500 $\mu\text{g}/\text{mL}$) of 2DG-MNPs for 24 and 72 h.

When we compare the IC_{50} values, non-cancer MCF-10A cells were affected less by the treatment with 2DG-MNPs than the breast cancer cells. Interestingly, MDA-MB-231 cells also have lower IC_{50} values compared to MCF-7 cells, which could be further used for selective targeting of these MNPs into breast cancer cells. The concentration of 500 μg 2DG-MNPs /mL showed high cytotoxic effects on both MDA-MB-231 and MCF-7 for both 24 and 72 h of growth. The cell viability decreased below 50 % when the concentration is reached to 500 $\mu\text{g}/\text{mL}$, whereas non-cancer MCF-10A cells treated with 2DG-MNPs showed only slight toxicity compared to cancer cells. From this data, we chose 125 $\mu\text{g}/\text{mL}$ concentration of 2DG-MNP as low concentration, and 500 $\mu\text{g}/\text{mL}$ as high concentration to be used in cell lines for the subsequent experiments.

3.8.4 Apoptosis Assay

3.8.4.1 Annexin-V-FITC / PI Assay

Apoptosis was determined by using Annexin-V-FIT/PI assay in order to understand the nature of cell death in all cell types upon exposure to 2DG-MNPs with three distinct concentrations, 125, 250 and 500 $\mu\text{g}/\text{mL}$ for 24 h. Original data is given in **Figure 40** and **Figure 41** for all experiments performed and the results obtained from the histograms are summarized in **Figure 42**. Apoptotic cell death, which is induced by 2DG-MNPs, was confirmed and quantified by flow cytometry analysis. As seen from the figure 39, apoptosis increases in a dose dependent manner in all cell types. The increase is statistically significant at 500 $\mu\text{g}/\text{mL}$ concentration ($p < 0.05$). Both cancerous MDA-MB-231 and normal MCF-10A cells showed the highest apoptotic cell deaths. At a lower concentration of 125 $\mu\text{g}/\text{mL}$ 2DG MNP, though not statistically significant, both cancerous cell lines undergo apoptosis more, compared to non-cancer cells.

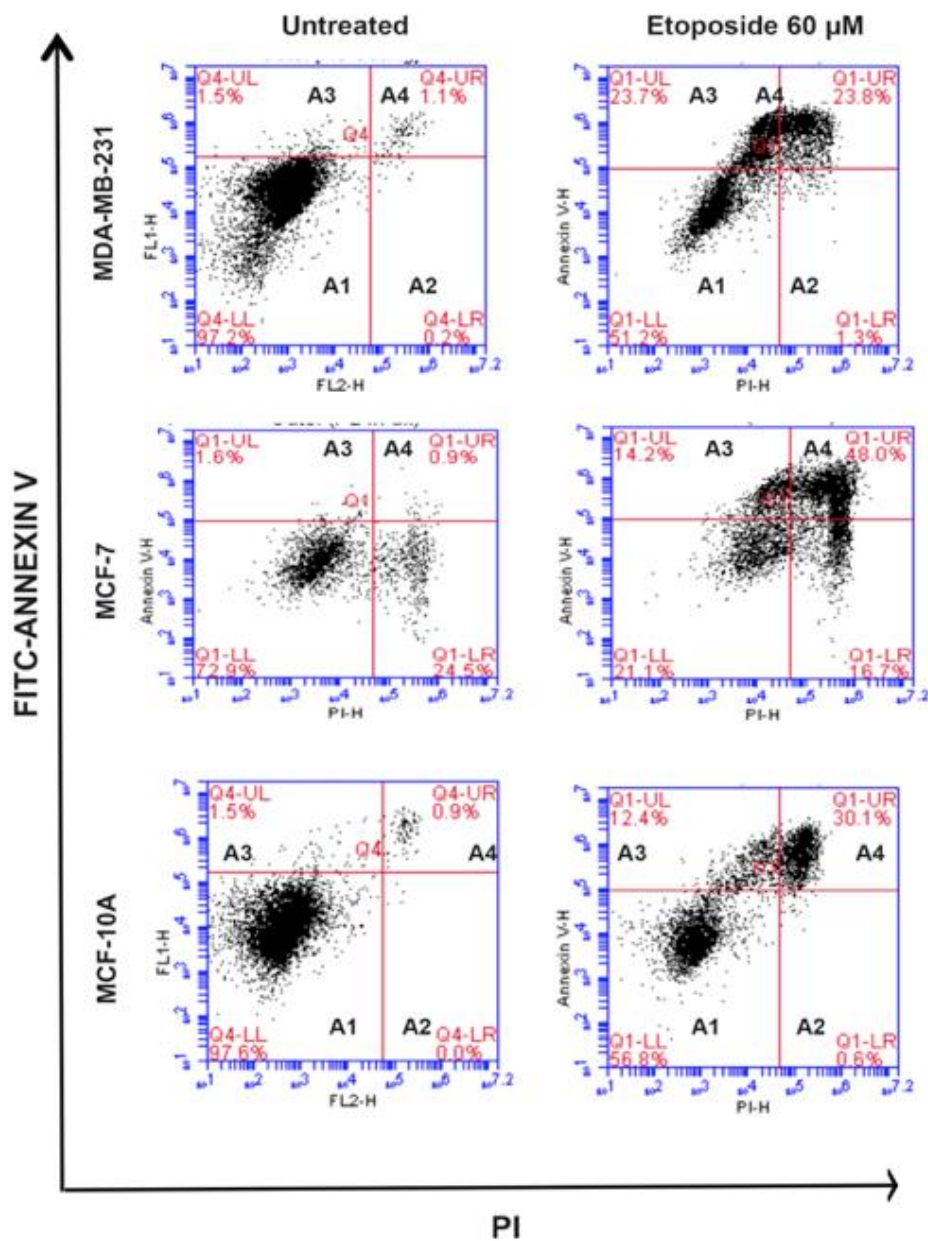


Figure 40. The apoptotic effects of untreated cells and the etoposide on MDA-MB-231, MCF-7 and MCF-10A. Four subpopulations and their percent distributions in different areas: Area A1 and A2 shows viable and dead cell (necrotic), A3 and A4 correspond to cells undergoing early and late apoptosis, respectively.

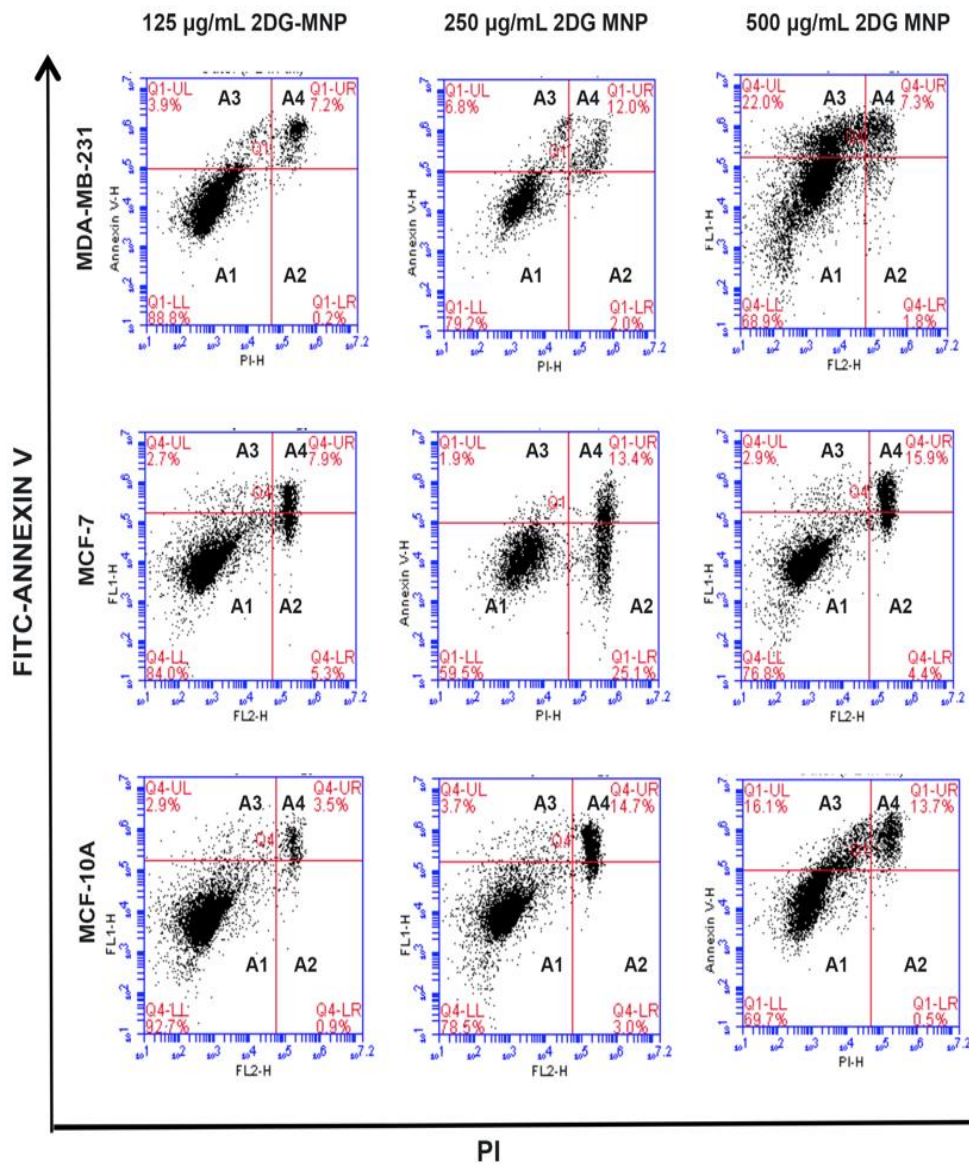


Figure 41. The apoptotic effects of 2DG-MNP (125, 250 and 500 µg/mL) on MDA-MB-231, MCF-7 and MCF-10A cells for 24 h. Four subpopulations and their percent distributions in different areas: Area A1 and A2 shows viable and dead cell (necrotic), A3 and A4 correspond to cells undergoing early and late apoptosis, respectively.

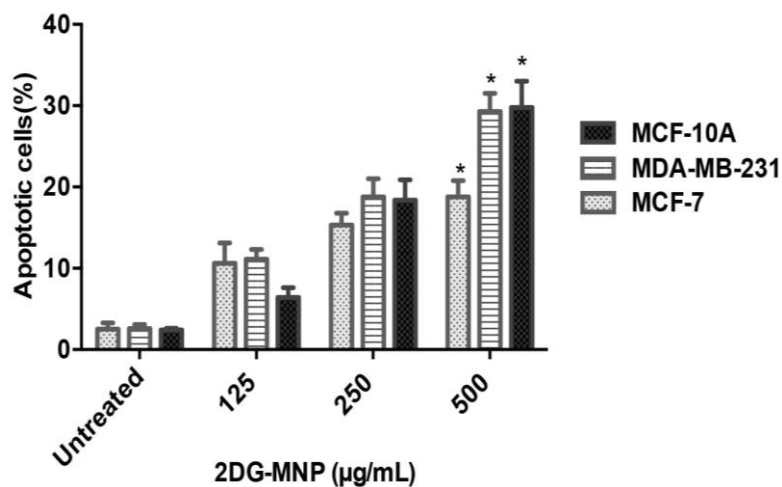


Figure 42. (A) Apoptotic cell populations in MDA-MB-231, MCF-7 and MCF-10A cells after treatment with 2DG-MNPs for 24 h (* $p < 0.05$). Untreated (UT) cells are used as control.

3.8.4.2 Effect of 2DG-MNPs on Apoptotic Gene Expressions

Further analysis of gene expression levels of apoptotic and anti-apoptotic proteins was determined by using quantitative PCR in all cells treated with 2DG-MNPs (125 and 500 µg/mL) at 24 and 72 h (**Figure 43**). The apoptotic PUMA and BAX/BCL-2 genes were up regulated by 4.5 and 5-fold, respectively, in metastatic cancer MDA-MB-231 cells treated with 2DG-MNPs (500 µg/mL) for 24 h, while anti-apoptotic SURVIVIN gene was down regulated by 3.3-fold ($p < 0.05$). Similar trend was observed for MCF-7 and MCF-10A cells. All these fold changes further increased with time of treatment.

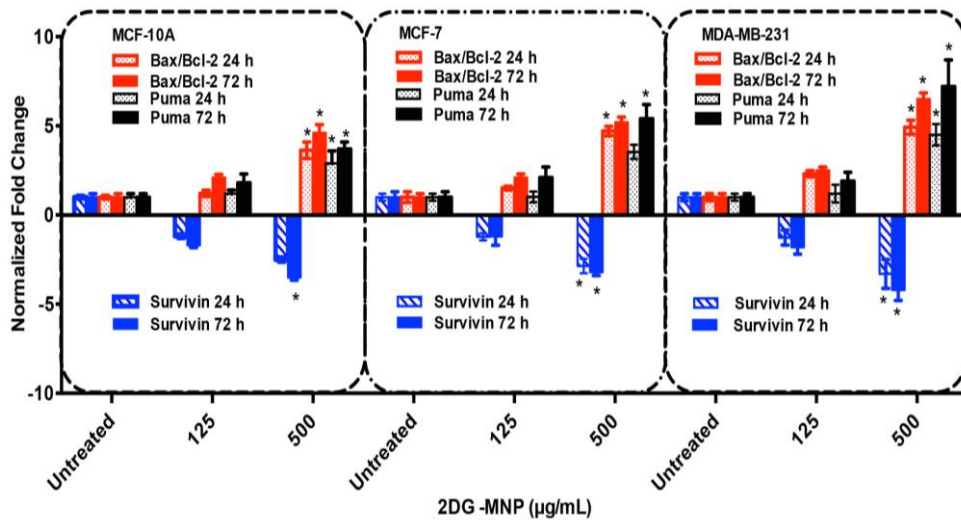


Figure 43. (B) The expression levels of apoptotic (PUMA and BAX) and anti-apoptotic (Bcl-2, SURVIVIN) genes in MDA-MB-231, MCF-7 and MCF-10A cells after treatment with 2DG-MNP for 24 and 72 h. Fold changes of the genes in the cells were normalized with respect to the internal control gene β -actin, (* $p < 0.05$).

In agreement with our flow cytometry results there was no significant up regulation of PUMA and BAX/BCL-2 and down regulation of SURVIVIN for all cells treated with 2DG-MNP at low concentration whereas there was significant change in gene expression levels for cells treated with 2DG-MNP at high concentration for 24 and 72 h. Thus, most probably the effect of the cell deaths observed at high concentrations of 2DG-MNPs is related with the mitochondrion-mediated apoptotic pathway.

3.8.5 mRNA Expression Analysis of Phase I and Phase II enzymes

3.8.5.1 Effect of 2DG-MNPs on CYP1A1 and CYP1B1 Gene Expression

The mRNA levels of four drug-metabolizing enzymes, namely, CYP1A1 and CYP1B1 and GSTZ1 and GSTM3 were studied in order to investigate the cellular response after the internalization of 2DG-MNPs into the breast cells.

In our data, both CYP1A1 and CYP1B1 showed an expression ratio greater than 2-fold in non-cancer MCF-10A cells treated with 2DG-MNPs (500 $\mu\text{g}/\text{mL}$) whereas no significant change was observed for 2DG-MNPs (125 $\mu\text{g}/\text{mL}$) at 24 and 72 h. (**Figure 44**).

The expression ratio of CYP1A1 and CYP1B1 was 7.2-fold and 7.8-fold in MDA-MB-231 cells treated with 2DG-MNPs (500 $\mu\text{g}/\text{mL}$) for 72 h, respectively, whereas the change was around 2-fold for 2DG-MNPs (125 $\mu\text{g}/\text{mL}$) even at 72 h (**Figure 44**). Similar results were observed in MCF-7 cells as well.

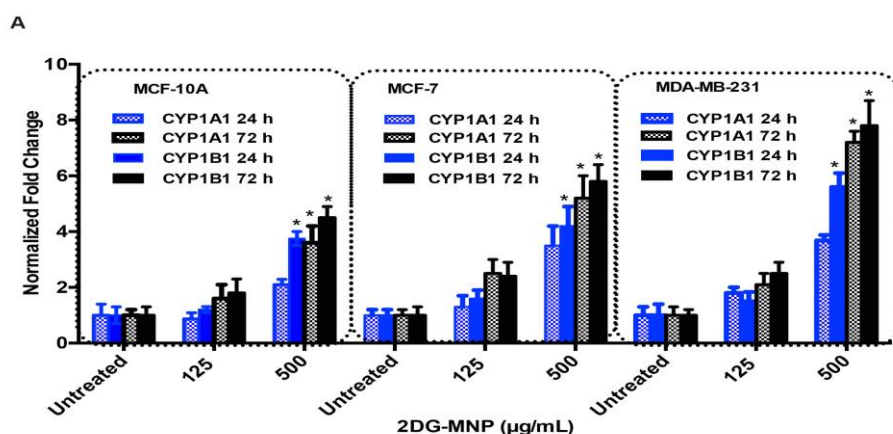


Figure 44. The expression levels of CYP1A1 and CYP1B1 genes in MCF-10A, MCF-7 and MDA-MB-231 cells after treatment with 2DG-MNP and 24 and 72 h growth. Fold changes of the genes in the cells were normalized with respect to the internal control gene β -actin. (* $p < 0.05$)

In summary, at high concentration of 2DG-MNPs, cancer cells seemed to up regulate the expression of both genes more than normal MCF-10A cells. Overall, the highest gene expressions were observed in metastatic MDA-MB-231 cells. Besides, the over expression of CYP1B1 and CYP1A1 genes can be interpreted as the increased uptake of MNPs. Though at low concentration no induction was observed in both CYP1B1 and CYP1A1 expressions, at increased concentration of 2DG-MNP, both CYP1B1 and CYP1A1 expressions are up regulated.

3.8.5.2 Effect of 2DG-MNPs on GSTZ1 and GSTM3 Gene Expressions

Glutathione S-transferases (GSTs) are important in Phase II metabolism functioning in cellular detoxification of electrophilic compounds, including carcinogens, therapeutic drugs, environmental toxins and products of oxidative stress, by conjugation with glutathione [128]. Previous studies showed that the predominantly expressed GSTs in MCF-7 breast cancer cells are mainly GSTM3 and GSTZ1 isoforms [132]. Expressions of these genes should increase in response to internalization of 2DG-MNP into the cells. Both GSTM3 and GSTZ1 gene expressions were found to be higher in MDA-MB-231 and MCF-7 breast cancer cells compared to non-cancer epithelial MCF-10A cells, which might be the result of the lower uptake of MNPs into normal cells. It is known that, GSTs are more intensively expressed in tumor cells [133, 134]. Further studies are required in order to investigate the role of GSTs in 2DG-MNP treatments.

In this study, the expression of GSTZ1 and GSTM3 genes increased in MDA-MB-231 cells treated with 2DG-MNPs (125 $\mu\text{g}/\text{mL}$) by 1.9 and 2.1-fold, respectively, at 24 h. 2DG-MNP treatments increased the expressions of both GSTZ1 and GSTM3 genes in MCF-7 cell by 1.0 and 1.7 fold, respectively. Their expression on the other hand, appeared to be unchanged in MCF-10A. Thus, 2DG-MNP treatments slightly up regulated the expression of GSTZ1 and GSTM3 genes in cancer cells (**Figure 45**). The treatment of MDA-MB-231

cells with 2DG-MNPs (500 $\mu\text{g}/\text{mL}$) also increased the expression by 4.5 and 5.9 fold in GSTZ1 and GSTM3 genes, respectively. Treatment of MCF-7 cells with 2DG-MNPs resulted in 4.2 fold increase for GSTZ1 and 4.9 fold increase for GSTM3, in addition to this, the treatment of MCF-10A cells with 2DG-MNPs resulted in 2.2 fold increase for GSTZ1 and 3.8 fold increase for GSTM3 for 72 hours (**Figure 45**).

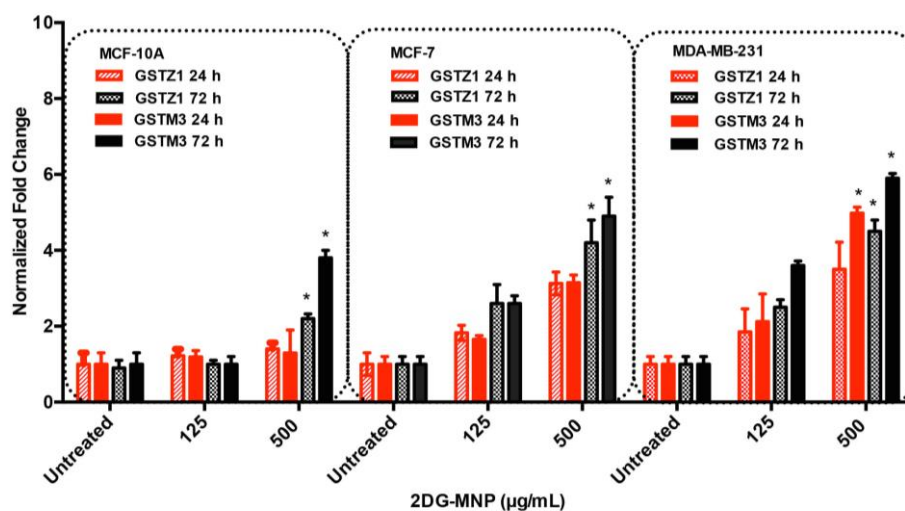


Figure 45. The expression levels of GSTZ1 and GSTM3 genes in MDA-MB-231, MCF-7 and MCF-10A cells after treatment with 2DG-MNPs for 24 and 72 h. Fold changes of the genes in the cells were normalized with respect to the internal control gene β -actin. (* $p < 0.05$)

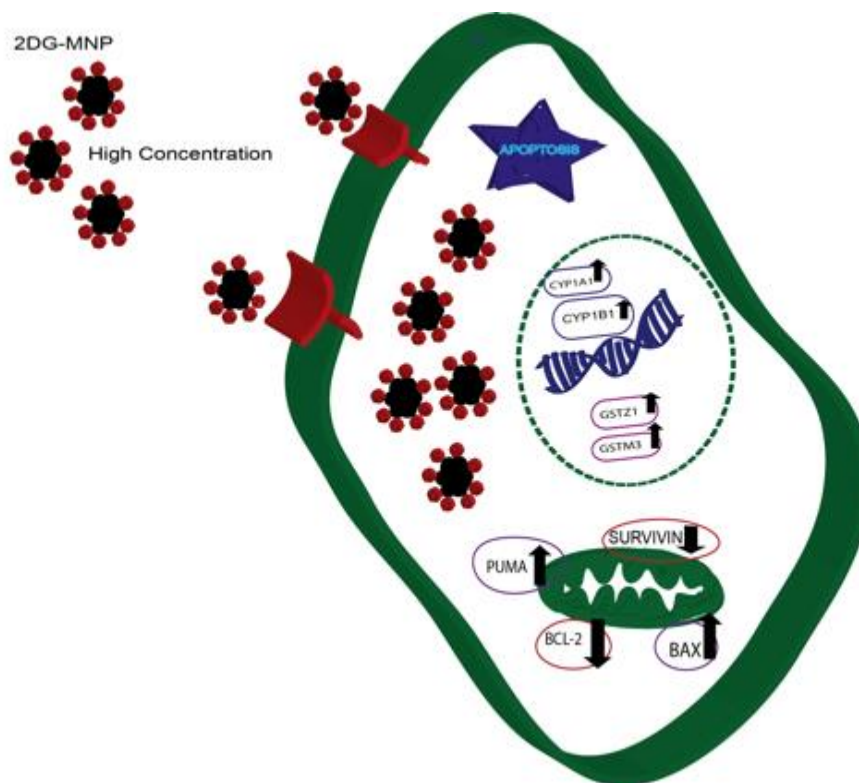


Figure 46 A schematic drawing, showing possible mechanisms of cellular metabolism of 2DG-MNPs in the breast cancer cells. 2DG labeling lead to an increase in selective targeting of MNPs in human breast cells. The cellular uptake of 2DG-MNPs can be associated with cellular and morphological changes, such as, the exposure of cells to high concentration 2DG-MNPs induced cytotoxicity, apoptosis and the expression levels of some Phase I and Phase II genes.

In the following and last part of the study, for therapeutical use of MNPs, EF2K siRNA is attached and after further characterization studies, in vivo use of the NP was carried out.

3.9 The Conjugation of EF2K siRNA to Cobalt Ferrite Magnetic Nanoparticle (MNP-EF2K siRNA)

3.9.1 EF2K is overexpressed in BRCA1 mutated and triple negative breast cancer

We first investigated the relative expression of eEF2K protein in BRCA1 mutated breast cancer cells (MDA-MB-436 and HCC-1937) compared to normal untransformed breast cells (MCF10A). Because BRCA1 mutated tumors are considered as triple negative breast cancer (TNBC) we also looked at eEF2K expression in TNBC cell lines, including MDA-MB231 and BT20. We found that eEF2-K is highly unregulated BRCA1 mutated cells and TNBC compared with MCF10A, which do not have detectable eEF2K expression (Figure 47).

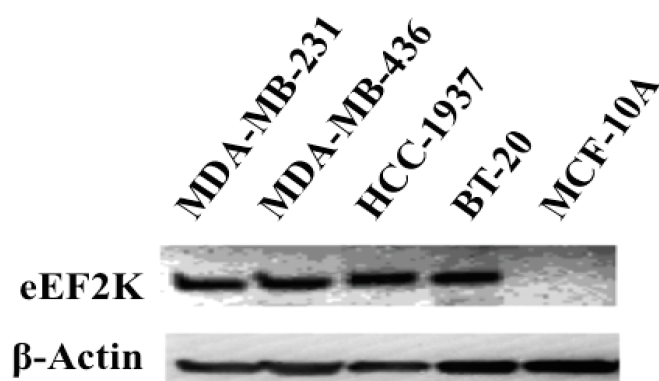


Figure 47. EF2K are highly expressed in triple negative and BRCA1 mutated cells. Western blot analysis of cell lysates of several cell lines were indicated. β-actin was used as a control.

3.9.2 Knockdown of EF2K by MNP- siRNA in BRCA1 mutated breast cells

To visualize the uptake of MNP-EF2K siRNA and down regulation of eEF2K protein in BRCA1 mutated cells, we first labeled eEF2K siRNA with fluorescent tag (Cy3) and conjugated it to the MNPs by using EDC chemistry and administered the fluorescence labeled siRNA MNPs to MDA-MB-436, MDA-MB-231 and HCC-1937 cells for 4 h. Fluorescent labeled siRNA (50 nM) transfected by commercially available transfection reagent (hiPerFect) and free Cy3-siRNA were used as controls. Cells were fixed in a chamber slide using 4% paraformaldehyde and then nuclei (blue) were stained with DAPI for 10 minutes, and siRNA uptake was analyzed by fluorescence microscopy. The slides were also stained with Prussian blue to show uptake iron containing MNPs and indicated successful internalization of siRNA and MNPs by the cells (**Figure 48-50**). We observed blue staining indicating the iron core of MNP-EF2K-siRNA in the cells but not in free Cy3 siRNA treated cells (**Figure 48-50**). Moreover, Cy3 labeled eEF-2K siRNA loaded MNP led to higher siRNA uptake compared with to commercially available transfection reagent hiPerFect, which was used as a positive control for siRNA transfection. Free Cy3-EF2K siRNA showed little or no uptake and accumulation observed for all three cells (**Figure 48-50**). Fluorescent microscopy further showed a strong fluorescence signal in the cells treated with Cy3 labeled siRNA-MNPs while incubation of cells with free Cy3-siRNA resulted in weak fluorescence, indicating that MNPs can promote the uptake of siRNA into BRCA1 mutated cells.

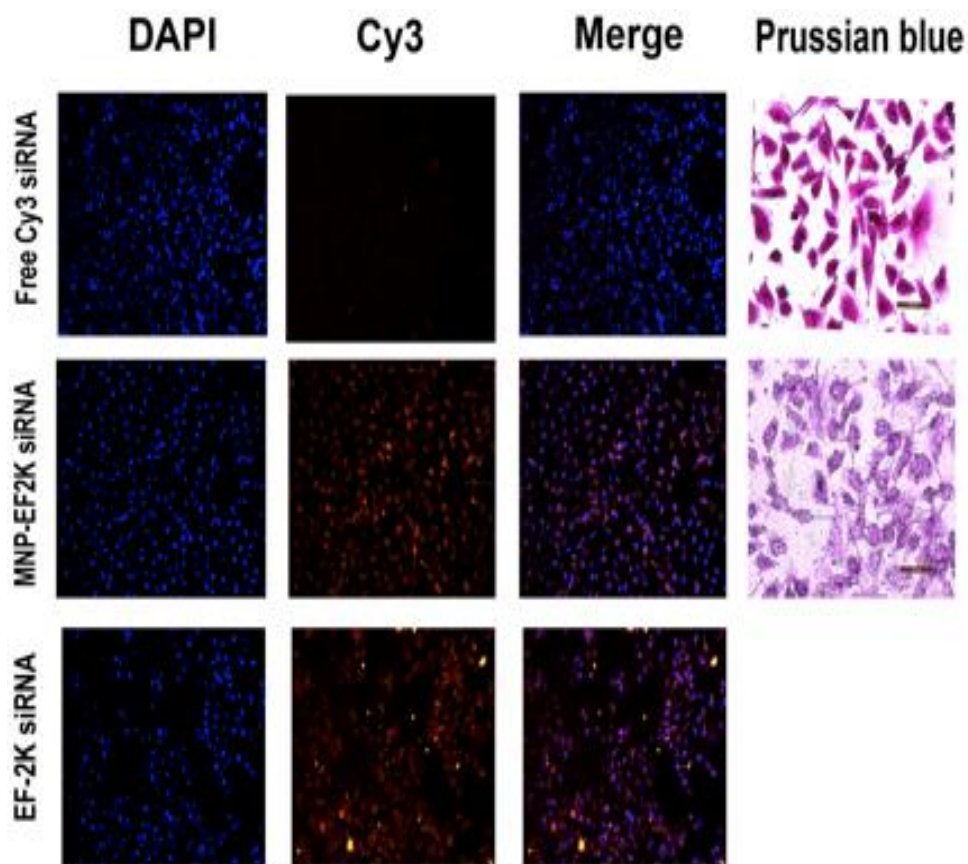


Figure 48. The uptake of Cy3 MNP-EF2K siRNA against MDA-MB-436 cells in vitro. Fluorescent microscopy images of cells treated with MNP-Cy3-siRNA, free Cy3 siRNA, Cy3 siRNA with hiPerFect for 4 h in 37 °C. Nuclei (blue) were stained with DAPI. In vitro Prussian blue staining results, Prussian blue staining of MDA-MB-436 cells incubated with Free Cy3 siRNA, EF2K siRNA loaded MNP, EF2K siRNA with hiPerFect, respectively.

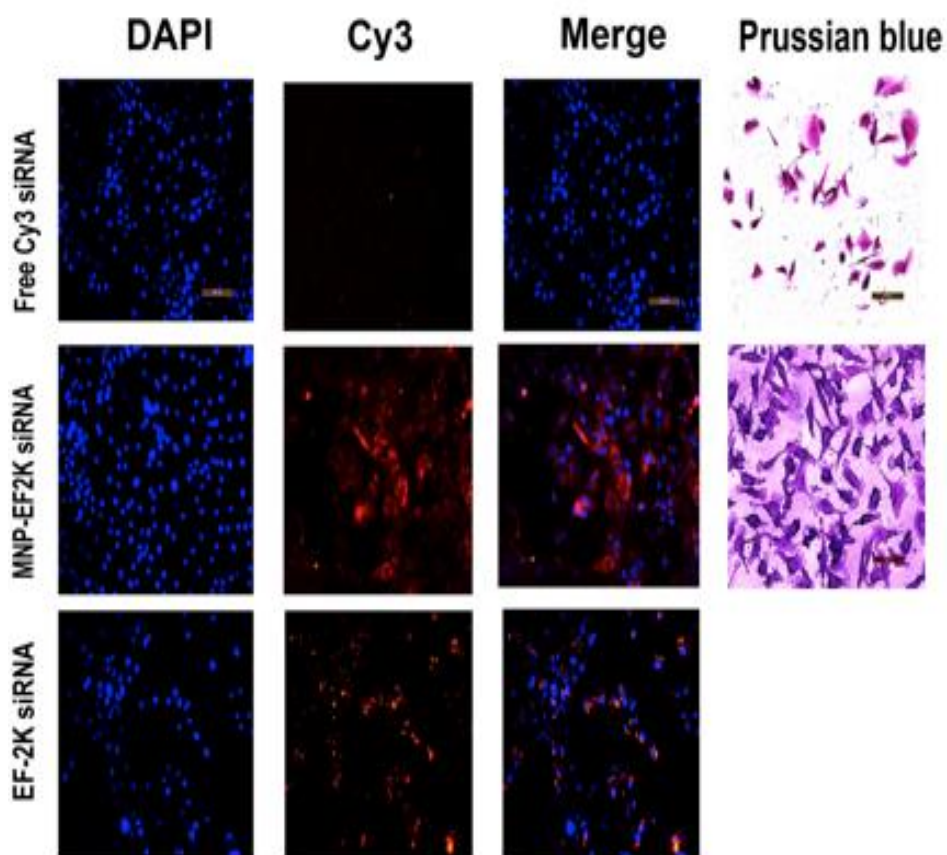


Figure 49. The uptake of Cy3 MNP-EF2K siRNA against and HCC-1937 cells in vitro. Fluorescent microscopy images of cells treated with MNP-Cy3-siRNA, free Cy3 siRNA, Cy3 siRNA with hiPerFect for 4 h in 37 °C. Nuclei (blue) were stained with DAPI. In vitro Prussian blue staining results, Prussian blue staining of HCC-1937 cells incubated with Free Cy3 siRNA, EF2K siRNA loaded MNP, EF2K siRNA with hiPerFect, respectively.

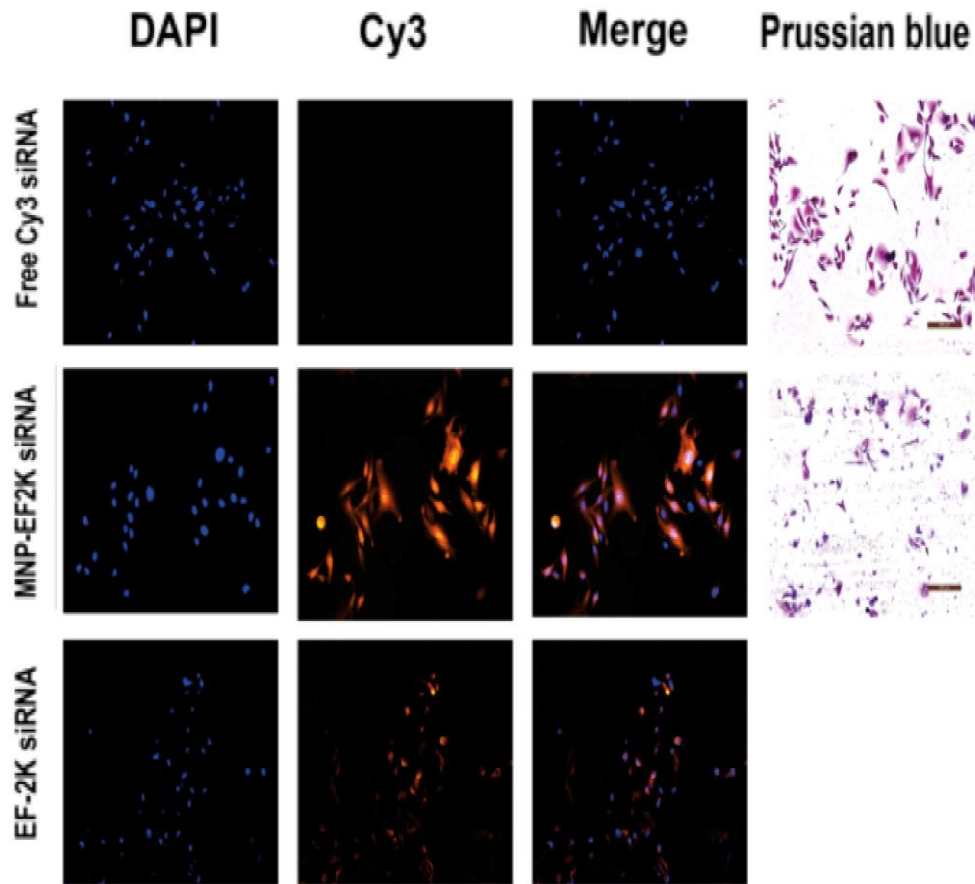


Figure 50. The uptake of Cy3 MNP-EF2K siRNA against MDA-MB-231 cells in vitro. Fluorescent microscopy images of cells treated with MNP-Cy3-siRNA, free Cy3 siRNA, Cy3 siRNA with hiPerFect for 4 h in 37 °C. Nuclei (blue) were stained with DAPI. In vitro Prussian blue staining results, Prussian blue staining of MDA-MB-231 cells incubated with Free Cy3 siRNA, EF2K siRNA loaded MNP, EF2K siRNA with hiPerFect, respectively.

The biological activity of siRNA delivered by MNPs was further investigated with eEF2K siRNA. As shown in **Figure 51**, eEF2K protein levels analyzed by Western blot 72 h post transfection showed that control siRNA and empty MNPs had no effect to down regulate eEF2K expression while eEF2K siRNA (with HiPerFect), and MNP-EF2K siRNA almost down regulated eEF2K expression in MDA-MB-436 and HCC-1937 cells. Moreover it seems that and MNP-EF2K siRNA inhibited eEF2K expression better than eEF2K siRNA with HiPerFect (**Figure 51**).

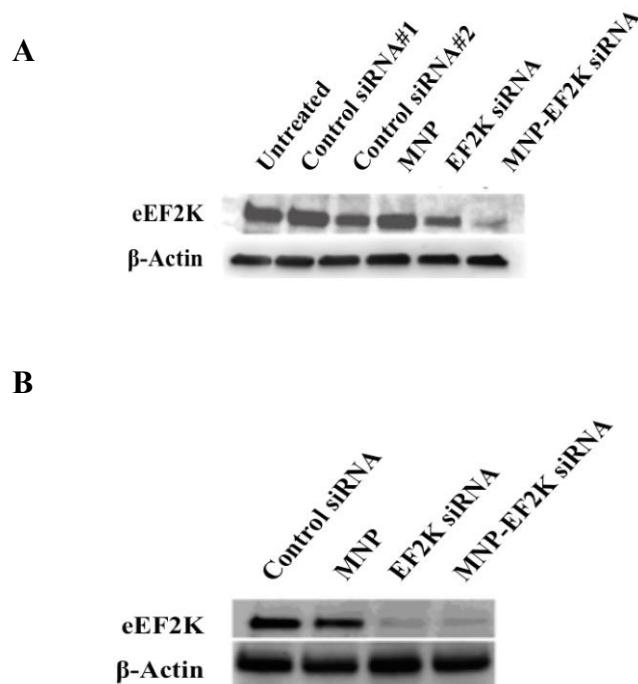


Figure 51. Western blot analysis of EF2K levels 72 h post transfection with EF2K siRNA with HiPerFect, control siRNA, MNP, MNP-EF2K siRNA in A) MDA-MB-436 B) in HCC-1937 cells. Transfection was carried out for 72 h, which was optimized in previous experiments (data not shown).

3.9.3 Knockdown of EF2K inhibits migration and invasion of BRCA1 mutated breast cancer cells

To understand the role and significance of up regulated EF2K expression in BRCA1 mutated cells we first determined the effects of inhibiting EF2K by siRNA-based knockdown on cell proliferation and colony formation (clonogenicity) in MDA-MB-436 and MDA-MB-231 cells. When MDA-MB-436 cells were treated with control siRNA, EF2K siRNA, MNP, MNP-EF2K siRNA (50 nM), significantly reduction in proliferation and colony formation of MDA-MB-436 (**Figure 52**) cells was observed in EF2K-targeted cells compared to control cells. Figure 52 shows that in MDA-MB-436 cells, MNP has similar effective with control siRNA in inducing growth inhibition (80.09% and 85%, respectively) whereas EF2K siRNA also showed significant inhibition of the tumor cell colony formation ($p < 0.05$), but the degree of inhibition was less than MNP-EF2K siRNA showed the most significant inhibitory effect, resulting in 34% of growth inhibition of MDA-MB-436 cells.

Similar phenomenon was observed in MDA-MB-231 cells, which showed decreased clonogenicity in following treatment with EF2K siRNA, MNP-EF2K siRNA. MNP-EF2K siRNA was more effective than EF2K siRNA (**Figure 52**) (43.6%, vs. 26.6% $p < 0.05$).

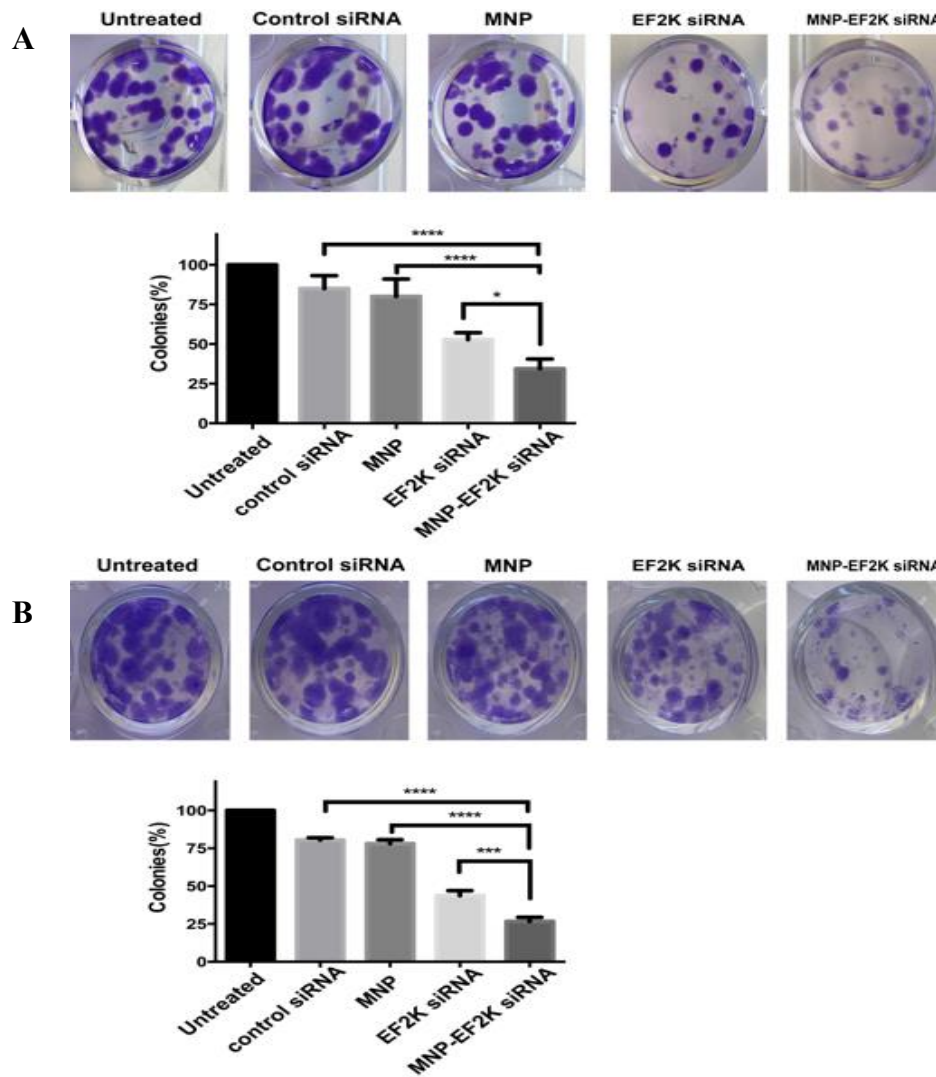


Figure 52. In vitro knockdown of EF2K by siRNA treatment inhibits colony formation of A. MDA-MB-436 and B. MDA-MB-231 cells. Representative colony formation assay of MDA-MB-436 and MDA-MB-231 cells treated with different formulation. 1) untreated 2) control siRNA with HiPerFect 3) MNP 4) eEF2K siRNA with HiPerFect 5) MNP-EF2K siRNA and colonies detected after two weeks later. All colonies were stained with crystal violet. Histogram showing the quantification of colony formation efficiency * $P < 0.05$ vs. control siRNA

3.9.4 Targeting eEF2K impairs BRCA1 mutated cell invasion and migration through inhibition of SRC/FAK/Paxillin

To determine if eEF2K promotes the invasive phenotype of MDA-MB-436 and HCC1937 breast cancer cells, we carried out *in vitro* invasion assays using Matrigel-coated Boyden chambers where the Matrigel served as a reconstituted basement membrane. After 72 h eEF2K siRNA or control siRNA treatment, cells were placed in the Boyden chamber and the number of cells migrated and invaded through the matrigel and passing the pores of membranes were stained and counted under a Leica light microscope (10X objective) and a representative image was captured using the 20X objective.

The depletion of eEF2K by eEF2K siRNA-hiPerFect and MNP-EF2K siRNA led to a significant decrease in the number of MDA-MB-436 cells that were able to invade across matrigel-coated membranes compared to control siRNA reduced the invasion of 42.4% and 22.4%, respectively compared to controls (MNP and control siRNA) (* $p < 0.05$) (**Figure 53**). HCC-1937 cells treated with MNP EF2k siRNA (31.08%) significantly inhibited the invasion better than eEF-2K siRNA-hiPerfect (45.46%) and compared to control siRNA (* $P < 0.05$) (**Figure 54**).

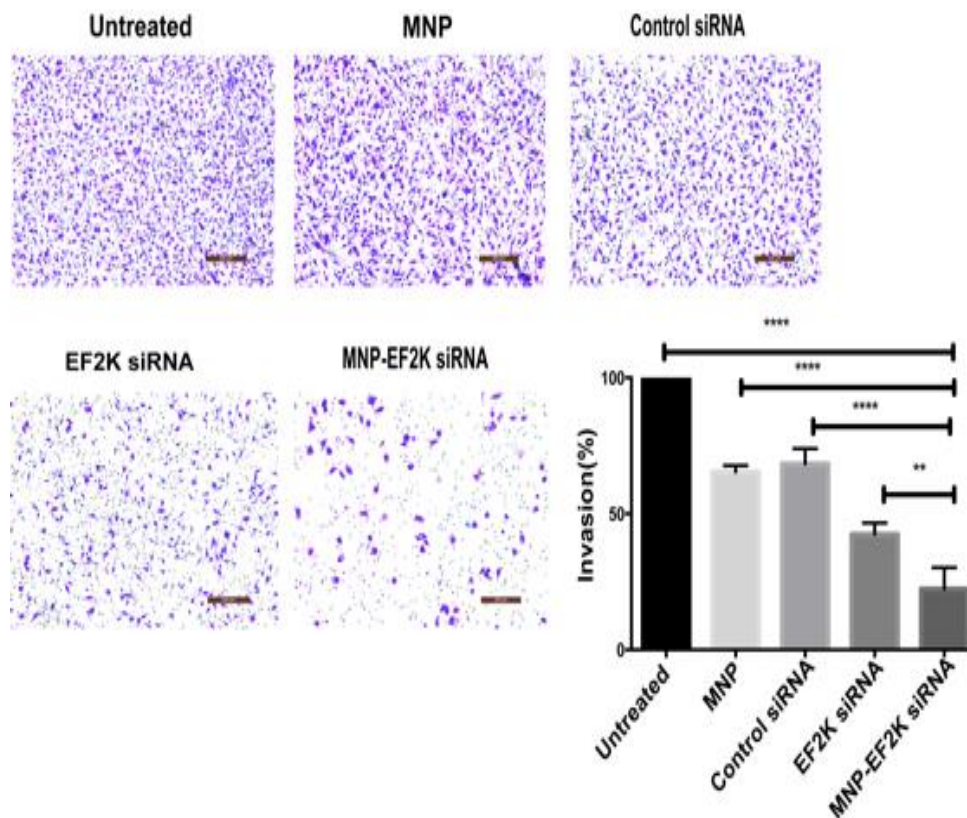


Figure 53. Representative photographs show the effect of silencing of EF2K siRNA on MDA-MB-436 cells invasion by Matrigel Transwell invasion assay after 24 h treatment. The cells treated with different formulation 1) untreated 2) MNP 3) control siRNA with HiPerFect 4) eEF2K siRNA with HiPerFect 5) MNP-EF2K siRNA. Histogram showing the quantification of % invasion of cells. All photographs were captured in a Leica light microscope under 20X magnification.

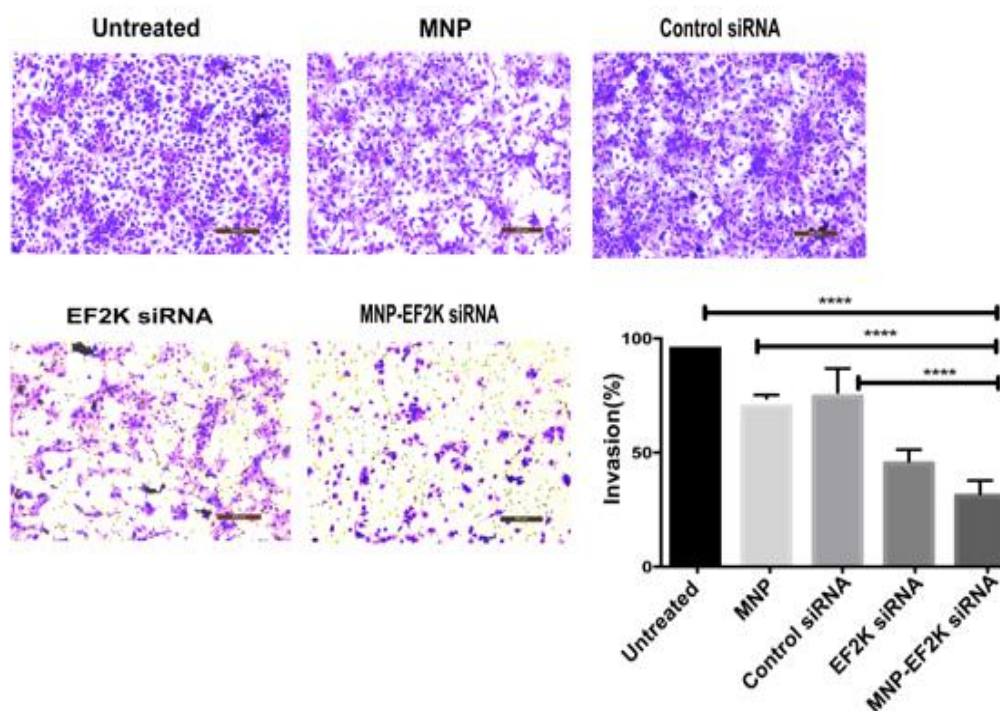


Figure 54. Representative photographs show the effect of silencing of EF2K siRNA on HCC-1937 cells invasion by Matrigel Transwell invasion assay after 24 h treatment. All. The cells treated with different formulation 1) untreated 2) MNP 3) control siRNA with HiPerFect 4) eEF2K siRNA with HiPerFect 5) MNP-EF2K siRNA. Histogram showing the quantification of % invasion of cells. All photographs were captured in a Leica light microscope under 20X magnification.

The other finding was observed by the knockdown of MNP-EF2K siRNA, which significantly reduced the invasion of MDA-MB-231, cells by about 42.74% and 29.86%, respectively (**Figure 55**) and also there is differences between cells treated with control siRNA and MNP about 82.81% and 60.97 %, respectively. These results showed that MNP alone less effective on invasiveness of MDA-MB-231 compared to control siRNA.

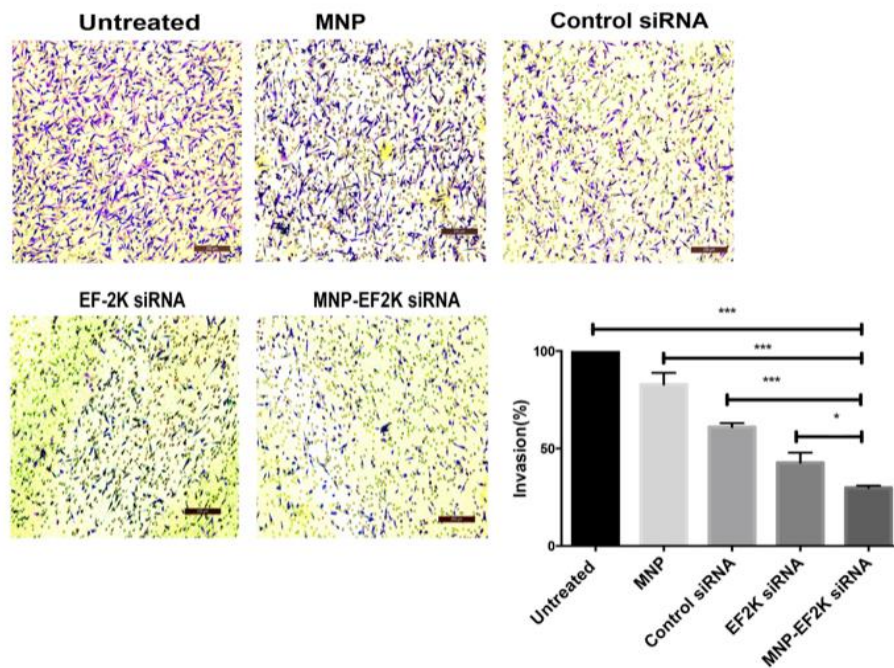


Figure 55. Representative photographs show the effect of silencing of EF2K siRNA on MDA-MB-231 cells invasion by Matrigel Transwell invasion assay after 24 h treatment. The cells treated with different formulation 1) untreated 2) MNP 3) control siRNA with HiPerFect 4) eEF2K siRNA with HiPerFect 5) MNP-EF2K siRNA. Histogram showing the quantification of % invasion of cells. All photographs were captured in a Leica light microscope under 20X magnification.

In order to determine the role of eEF2K siRNA in the cell motility of BRCA1 mutated cells in *in vitro* scratch assay was carried out MDA-MB-436 cells. The results indicate that the knockdown of eEF2K by eEF2K siRNA showed reduced motility compared to the control cells. As can be seen in **Figure 56**, the cells with suppression of eEF2K by siRNA were not able to close the space in the culture when compared with control siRNA after 48 h. The knockdown of eEF2K siRNA by MNP-EF2K siRNA in MDA-MB-436 resulted in significantly less motility (28.9%) than eEF2K siRNA-hiPerFect (46.67%).

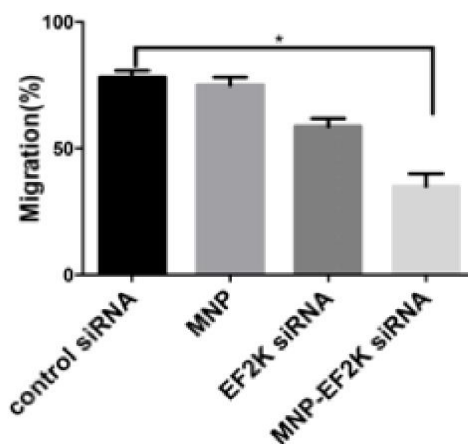
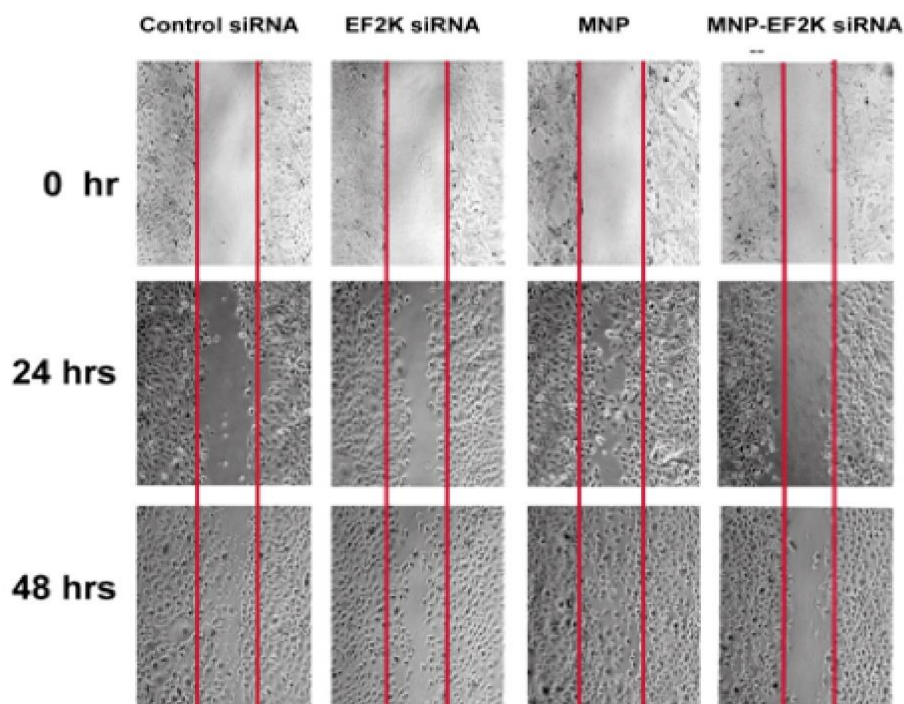


Figure 56. Representative photographs show the silencing of eEF-2K in MDA-MB-436 and control cells motility by wound healing assay. The cells treated with different formulation 1) control siRNA with HiPerFect 2) MNP 3) eEF2K siRNA with HiPerFect 4) MNP-EF2K siRNA. Histogram showing the quantification of % migration of cells. After 48 h incubation, wound closure photographed under light microscope.

We next examined the involvement of eEF2K in HCC-1937 cell motility using the scratch assay at earlier time-points (24 and 48 h). The analysis revealed that the distance covered by migrating cells (at 24 and 48 h) was significantly decreased when HCC-1937 cells were exposed to eEF2K siRNA, MNP, MNP-EF2K siRNA compared to cells non-silencing control siRNA, respectively (**Figure 57**). The eEF2K-knockdown (58.67%) cells exhibited less migratory capacity to the wounded areas in compared control siRNA treatments. Similar results were observed in MDA-MB-231 (**Figure 58**). Clearly, the knockdown of eEF2K by MNP-EF2K siRNA (35.07%) suppressed cell motility and migration, comparing with the control cells, further supporting the role of eEF2K in motility of BRCA1 mutated breast cancer cells.

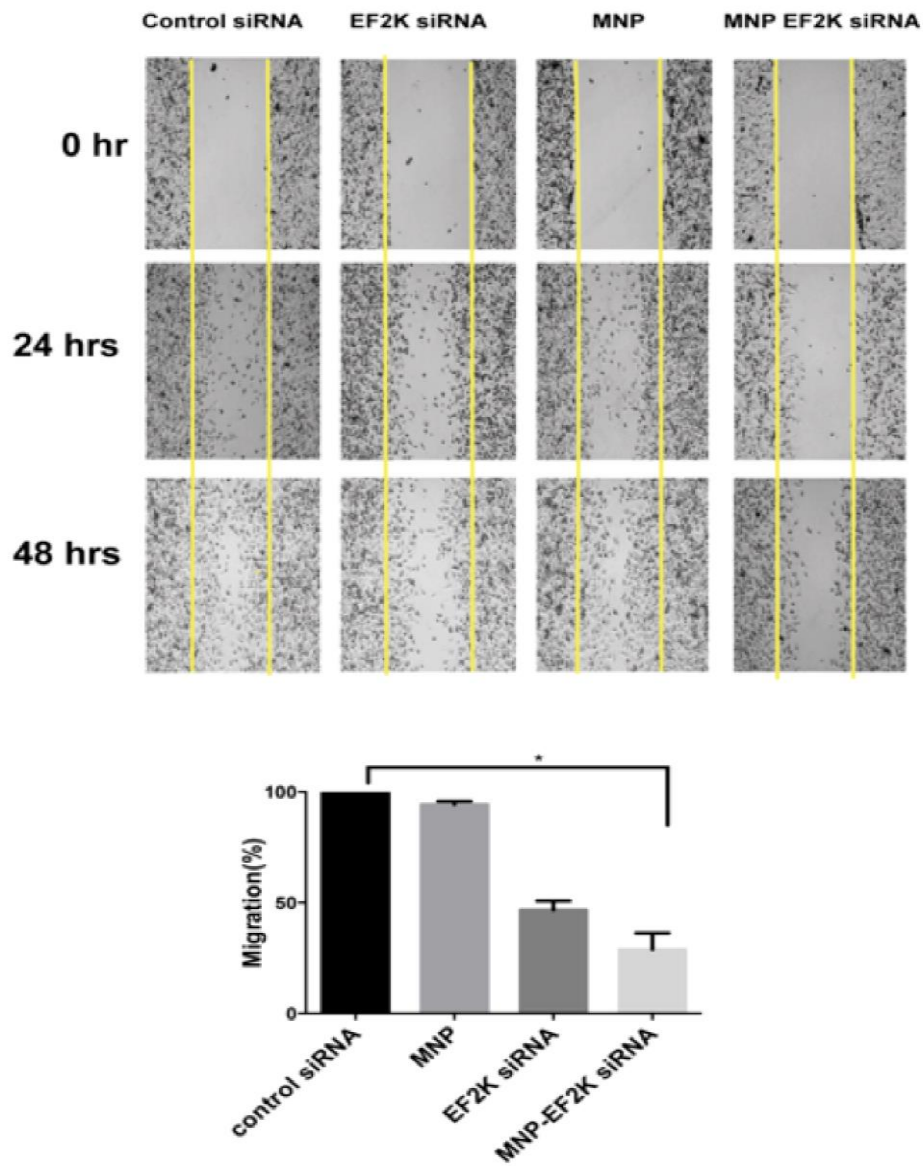


Figure 57. Representative photographs show the silencing of eEF-2K in HCC-1937 and control cells motility by wound healing assay. . The cells treated with different formulation 1) control siRNA with HiPerFect 2) MNP 3) eEF2K siRNA with HiPerFect 4) MNP-EF2K siRNA. Histogram showing the quantification of % migration of cells. After 48 h incubation, wound closure photographed under light microscope.

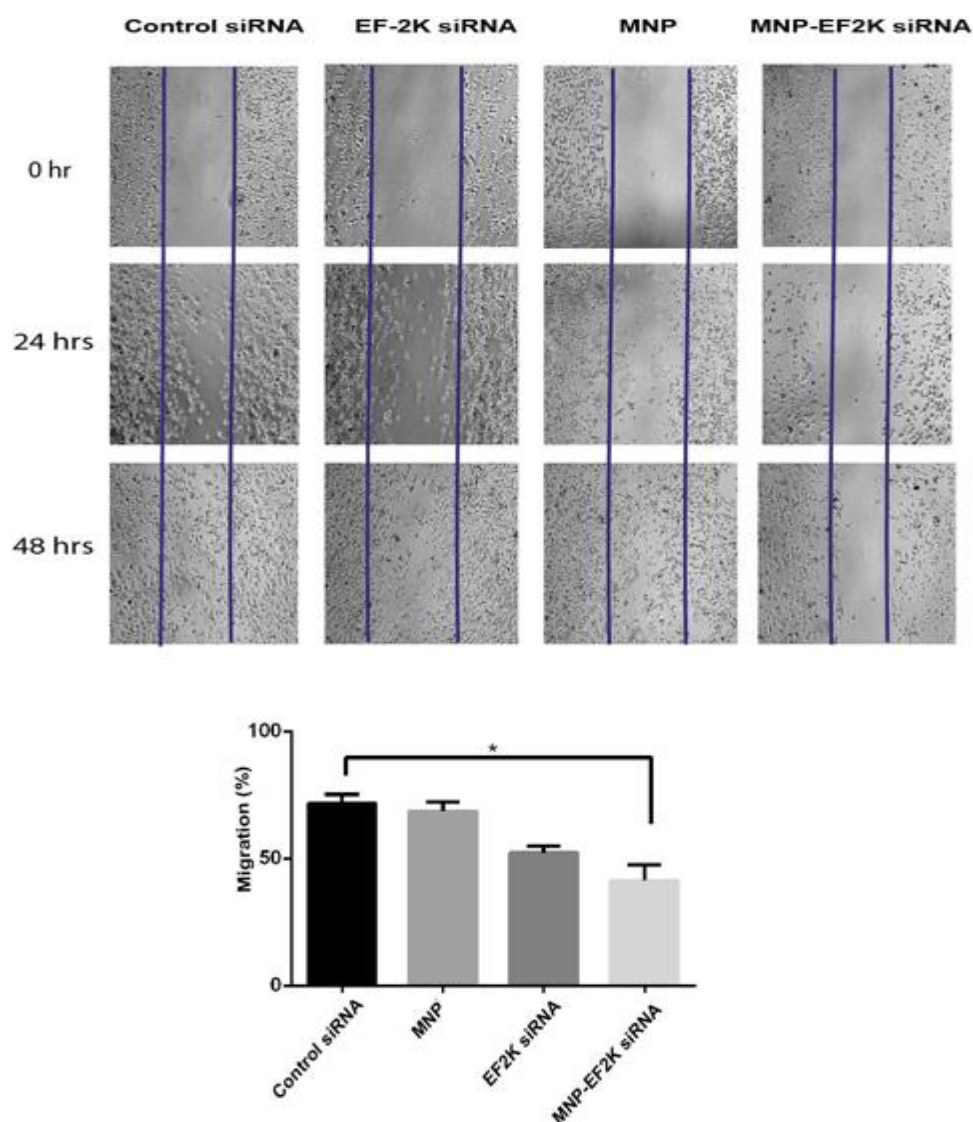


Figure 58. Representative photographs show the silencing of eEF-2K in MDA-MB-231 and control cells motility by wound healing assay. . The cells treated with different formulation 1) control siRNA with HiPerFect 2) MNP 3) eEF2K siRNA with HiPerFect 4) MNP-EF2K siRNA. Histogram showing the quantification of % migration of cells. After 48 h incubation, wound closure photographed under light microscope.

To further elucidate the potential molecular mechanisms by which eEF2K mediates BRCA1 mutated breast cancer cell migration and invasion we examined the possible involvement of the non-receptor protein tyrosine kinase c-Src, which is known to play critical roles in adhesion, migration and invasion as well as proliferation in breast cancer cells [135]. Because c-Src activity is associated with poor patient prognosis and survival its is considered one of the most important molecular target for treatment of breast and other cancers [136]. As shown in **Figure 59-60** that knockdown of eEF2K by siRNA led to a significant reduction in the activity of c-Src as evidenced by reduction of phosphorylated at Tyr-416 residue in MDA-MB-436 and HCC-1937 cells. Focal adhesion kinase (FAK) regulates cell adhesion and migration and is auto phosphorylated on Tyr-397, which results in increased kinase activity upon engagement with integrin [137]. We also found that a significant reduction in FAK phosphorylation (Tyr-397) (**Figure 59-60**) in BRCA1 mutated cancer cells. Similar effects were observed in inhibition paxillin activation, which is downstream of Src/FAK signaling in both cell lines (**Figure 59-60**). Overall our data suggest that eEF2K is involved in activation Src/Fak/Paxillin complex and inhibition of this engagement cascade may be the underlying mechanisms that mediate inhibition cell invasion and proliferation after targeting eEF2K in BRCA1 mutated cells.

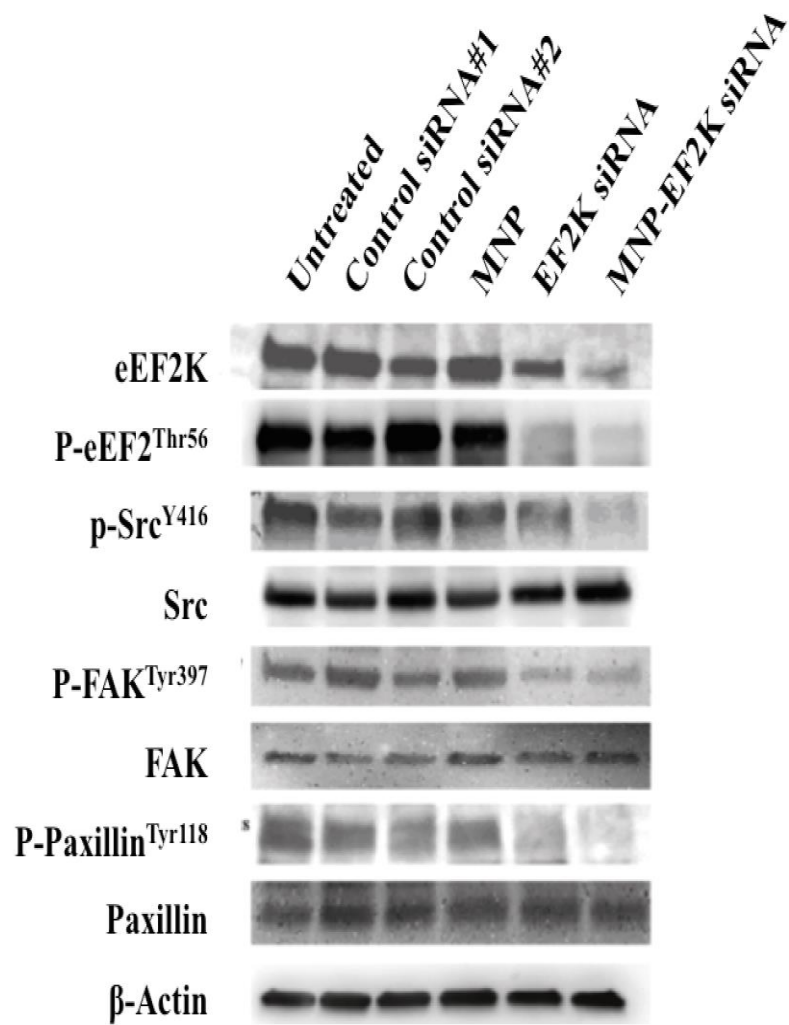


Figure 59. Western blot analysis of eEF2K, p-eEF2, eEF2, p-Src, Src, FAK, p-FAK, p-Paxillin, Paxillin levels 72 h post transfection with EF2K siRNA, control siRNA, MNP, MNP-EF2K siRNA for MDA-MB-436 cells. Transfection was carried out for 72 h, which was optimized in previous experiments (data not shown).

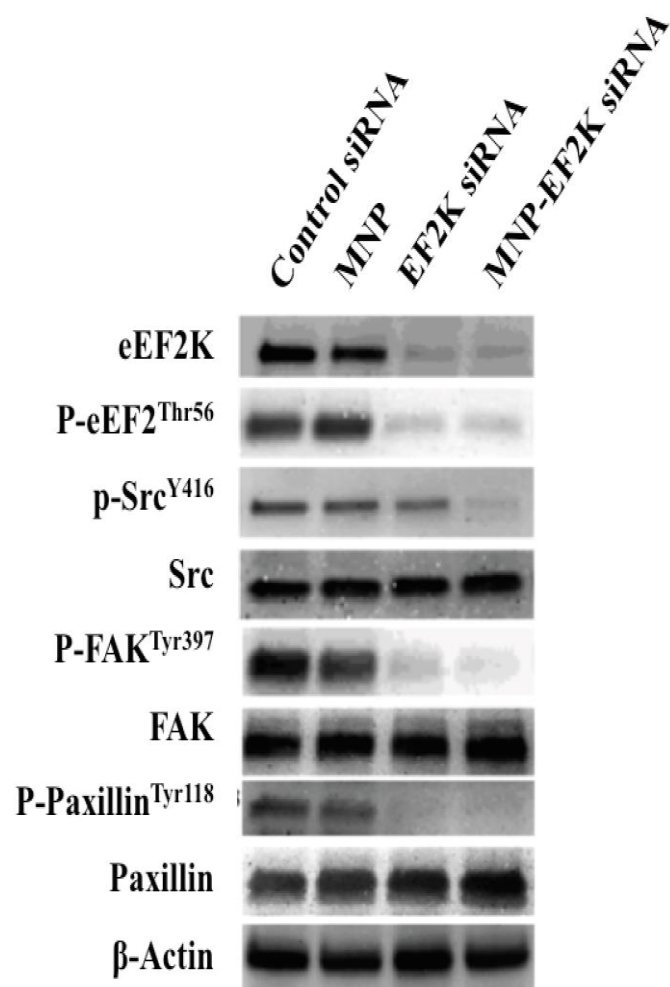
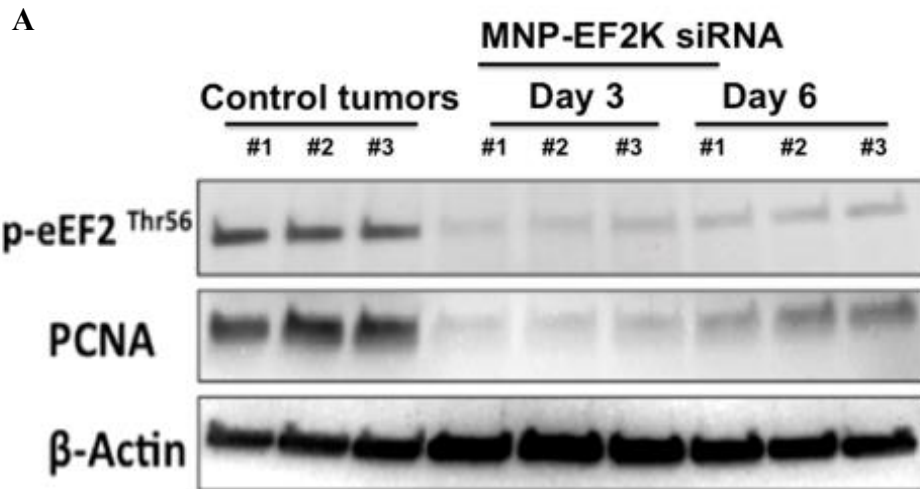


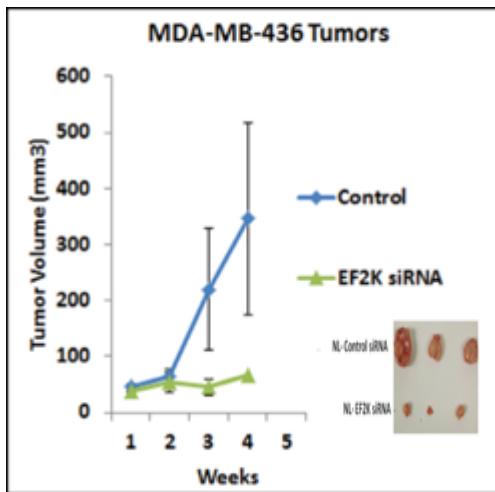
Figure 60. Western blot analysis of eEF2K, p-eEF2, eEF2, p-Src, Src, FAK, p-FAK, p-Paxillin, Paxillin levels 72 h post transfection with EF2K siRNA, control siRNA, MNP, MNP-EF2K siRNA for HCC-1937 cells. Transfection was carried out for 72 h, which was optimized in previous experiments (data not shown).

3.9.5 *In vivo* Targeting of EF2K leads to antitumor activity in BRCA1 xenograft models

We first investigated the *in vivo* target down modulation of eEF2K by systemically administered MNP-EF2K siRNA nanoparticles for effective therapeutic targeting eEF2K for evaluate potential of eEF2K in in an orthotropic model of BRCA1 mutated breast cancer in nude mice. About 12 days after BRCA1 mutated tumor cell (MDA-MB-436) injections into mammary fat pat of nude mice MNP-EF2K siRNA or control siRNA was systemically (i.v.) administered from the tail vein of once a week for 4 weeks (total of 4 injections). Treatment with MNP-EF2K siRNA resulted in a significant down-regulation of eEF2K activity as evidenced by a decrease of phosphorylation of its downstream target p-eEF2 in the tumors and PCNA expression (**Figure 61**) and significant inhibition of tumor growth (**Figure61**). No toxicity were observed during 4-week of treatment in the mice exposed to MNP-EF2K siRNA and the mice appeared healthy with normal eating drinking habits and did not lose weight during the treatment (**Figure 61**).



B



C

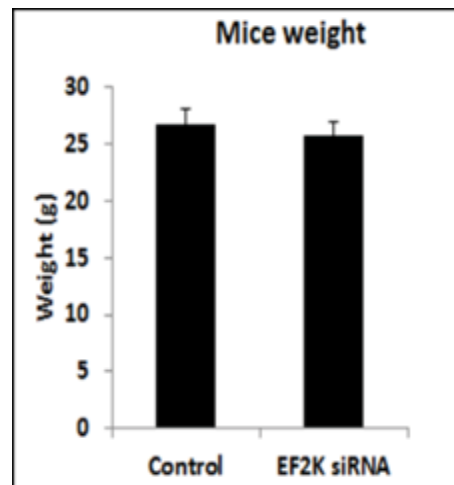


Figure 61. Treatments of tumor tissues with MNP-EF2K siRNA. Following treatment with MNP-EF2K siRNA, tumor tissues were removed from mice and subjected to Western blot analysis. Treatment of mice with MNP-EF2K siRNA results in the knockdown of EF2K in different tumors with the consequent reduction in p-eEF2 (Thr-56), PCNA **B**. Effect of MNP-EF2K siRNA treatment on tumor weight and **C**. mice weight.

3.9.6 *In vivo* inhibition of eEF2K inhibits tumor cell proliferation, microvessel density and induces apoptosis in BRCA1 mutated tumor xenografts

Given the significant growth inhibitory effects of down-regulating eEF2K in BRCA1 mutated tumors, the tumor samples collected after 4 weeks of treatment were evaluated for *in vivo* proliferation markers, evidence of the induction of apoptosis and microvessel density for angiogenesis. The tumors from MNP-EF2K siRNA -treated mice demonstrated a significant increase in TUNEL positive cells indicating induction of apoptosis (72.7%) compared with control siRNA treated tumors (17.4 %) (**Figure 62**).

Histologic examination of tumor tissue also showed a marked decrease in proliferation marker Ki-67 and angiogenesis as evidenced by reduced microvessel density by CD31 staining of tumor endothelial cells in the MNP-EF2K siRNA treated tumors (**Figure 62**). Ki67 was used as a marker of cellular proliferation. Ki67 labeling index was decreased by 39.07% in the MNP-EF2K siRNA treatment group ($p < 0.0001$) compared to the control group. The average mean vessel density was decreased by 36.4% in the MNP-EF2K siRNA treatment group compared to the control group ($p < 0.001$, $n = 3$) suggesting anti-angiogenic activity after MNP-EF2K siRNA treatment.

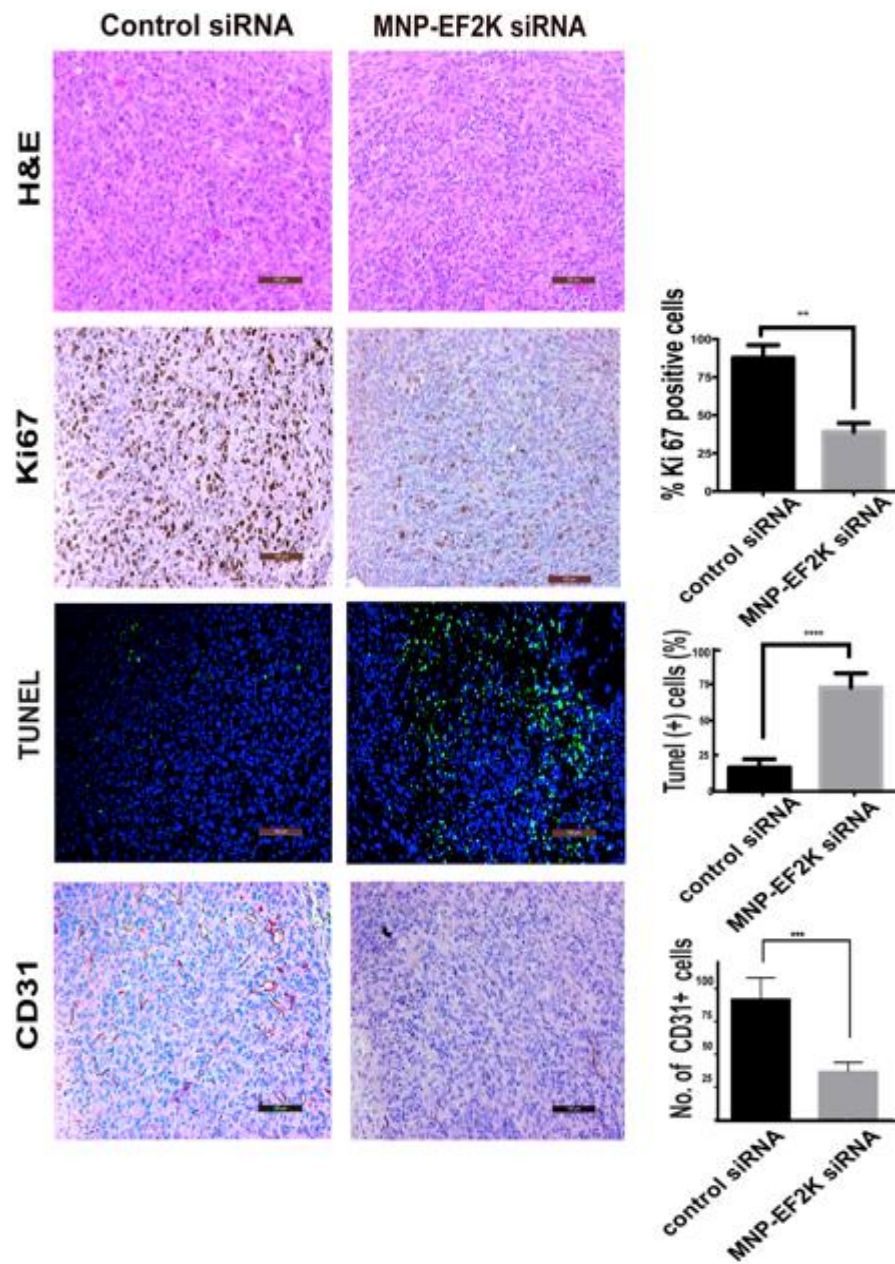


Figure 62. Immunohistochemical analysis. Knockdown of eEF-2K leads to decreased proliferation and increased apoptosis of breast tumor in vivo. H&E histological analysis, Immunohistochemical staining for Ki67 and CD31 and TUNEL was conducted to assess cell proliferation and apoptosis.

3.9.7 MNP-EF2K siRNA nanoparticles accumulate in BRCA1 mutated tumor tissues

We also evaluated the bio distribution of MNP-EF2K siRNA nanoparticles in normal and BRCA1 mutated breast tumor tissues. To this end Prussian blue and nuclear fast red staining was performed on tissue sections of organs and tumors obtained from the mice after MNP-EF2K siRNA (**Figure 63**). While Prussian blue which stains the iron core of MNPs were widely detected in the tumor sections but it was mostly negative in the tissue sections of the brains, lung, and heart from mice injected with MNP-EF2K siRNA and only a few scattered iron-positive cells were detected in some sections, suggesting that the MNPs could efficiently deliver siRNA to the BRCA1 mutated tumor. As expected iron uptake was strong in the spleen and liver due to reticuloendothelial system (RES) and filtering function of these organs (**Figure 64**). Histopathological examination of the liver and spleen tissues by hematoxylin and eosin yielded no signs of tissue damage (**Figure 64**).

MNP-EF2K siRNA Treated Tumor tissue

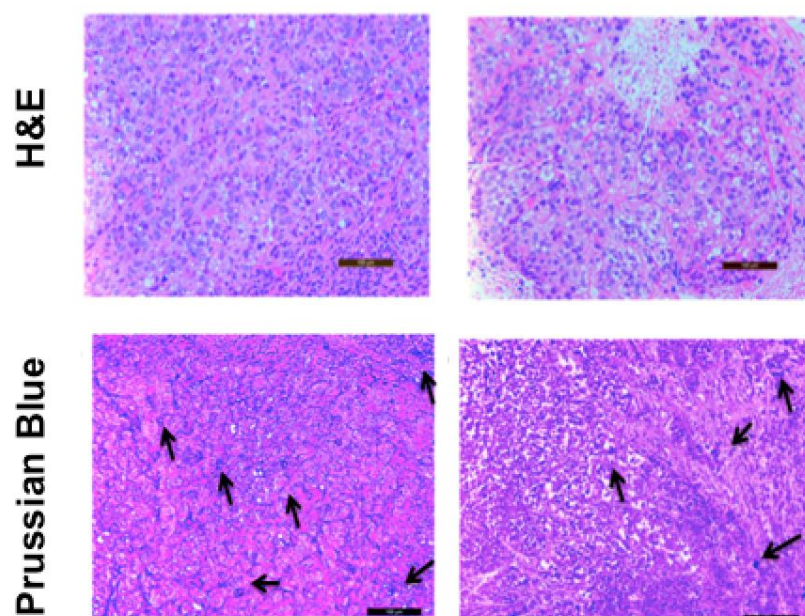


Figure 63. *In vivo* tumor accumulations of MNP-EF2K siRNA in mice. H&E and Prussian blues staining of tumor sections. Excess iron accumulated in the indicated tumors 24 h after intravenous injection MNPs. (High amount of blue granules were observed in the tumor section)

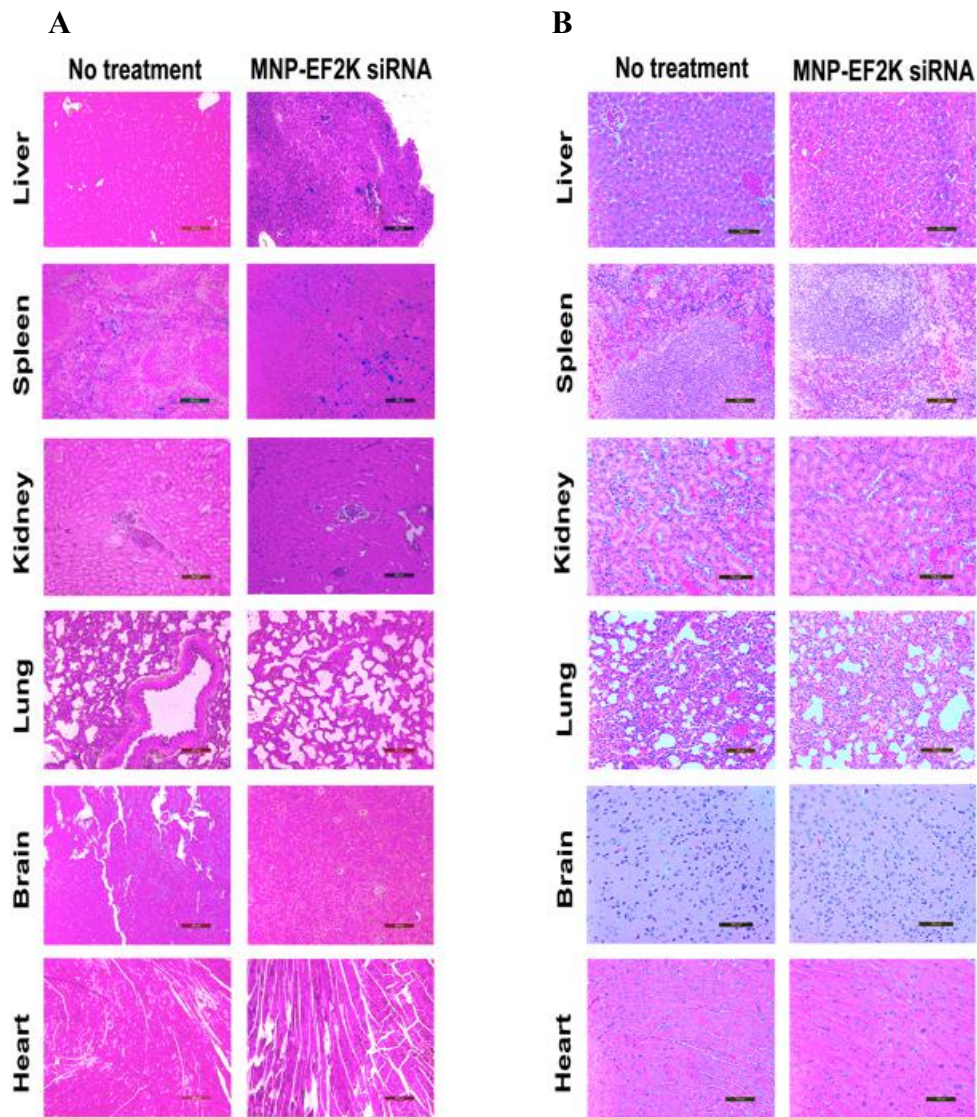


Figure 64. **A.** Control siRNA and MNP-EF2K siRNA were intravenously administered and tissues were removed 24 h after a single administration. Prussian blue staining of the spleen, liver, lung brain, heart and kidney. High levels of iron uptake were observed in the liver and spleens; Blue granule show that positive Prussian blue staining and counterstain with nuclear red staining **B.** H&E Histological analyses of tissue specimens after MNP-EF2K siRNA treatment. Liver, kidney, spleen, lung, heart and brain tissues of treated mice.

3.9.8 *In vivo* Targeting of EF2K inhibits cyclin D1, autophagy and impairs the activity of c-Src/ FAK/ Paxillin complex

To further investigate the *in vivo* anti-tumor mechanism and elucidate signaling pathways affected in response to targeting eEF2K we evaluated in cell cycle regulator CyclinD1 that mediates G₀ to G₁ transition and autophagy by western blotting in xenografted BRCA1 mutated tumors (**Figure 65**). Cyclin D1 promotes entry of cells into the S-phase of the cell cycle, induces proliferation and can cause malignant transformation. Our findings indicate that cyclin D1 and autophagy marker LC3- is inhibited in BRCA1 mutated tumors by targeting of eEF2K, suggesting that cell cycle inhibition and reduced autophagic activity which helps cells to survive in hypoxic and metabolically challenged tumor environment and contribute to inhibition of tumor growth in addition to induction of apoptosis.

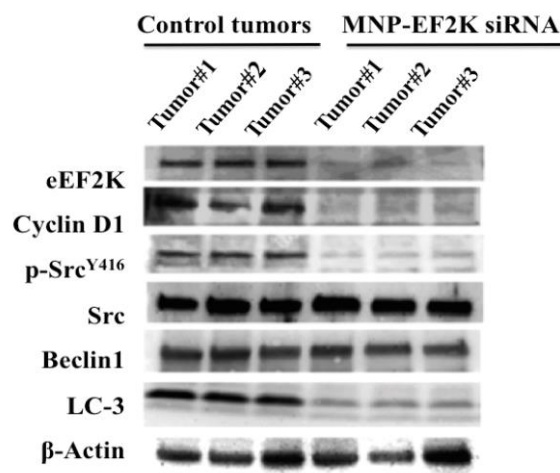


Figure 65. Western blot analysis of tumor tissues 1. Following treatment with MNP-EF2K, tumor tissues were removed from mice and subjected to Western blot analysis. Treatment of mice with MNP-EF2K siRNA results in the knockdown of EF2K in different tumors with the consequent reduction in EF2K, p-Src, Src, Cyclin D1, Beclin, and LC3.

3.9.9 Knockdown eEF2K leads to decrease the expression level of MCP-1 in BRCA1 mutated tumors

Monocyte chemo attractant protein-1 (MCP-1) is a chemokine that plays many roles in tumor development and progression [138]. MCP-1 is produced not only by tumor cells but also by stromal cells such as fibroblasts, endothelial cells, and monocytes [139]. MCP-1 expression was associated with macrophage accumulation and correlated with the concentration of various angiogenic regulators, and that MCP-1/VEGF was an independent prognostic indicator in breast cancer [140]. Thus we investigated if eEF2K inhibition reduces MCP1 expression *in vivo* in BRCA1 mutated tumors (**Figure 66**)- suggesting that eEF2K inhibition –induced MCP1 down regulation may play a role in reduction of macrophages and angiogenesis, which further contributes anti tumors effects of eEF2K inhibition.

3.9.10 Targeting eEF-2K inhibits PI3K/Akt/mTOR/ 4EBP1 in BRCA1 mutated tumors

We also found that the down-regulation of eEF2K inhibited the expression c-Myc, PI3K/AKT, both of which promotes cell survival and proliferation, in BRCA1 mutated tumors *in vivo* (**Figure 66**). Control of mRNA translation to protein is an important point of regulation for gene expression. Translation is deregulated in cancer through a variety of mechanisms. The most recognized alteration in translation is the overexpression of eukaryotic initiation factor 4E (eIF4E), the mRNA 5'cap-binding protein. High levels of phosphorylated eIF4E-binding protein 1 (p4E-BP1) have been associated with worse prognosis in several tumor types including breast cancer [85]. The knockdown of eEF2K inhibited the expression of p-4E-BP1 both *in vivo* and *in vitro* (**Figure 66**). Here we found that down-regulation of eEF-2K inhibited the expression p-4E-BP1, leading to inhibition of protein translation and indicating the role of eEF2K in regulation of translation.

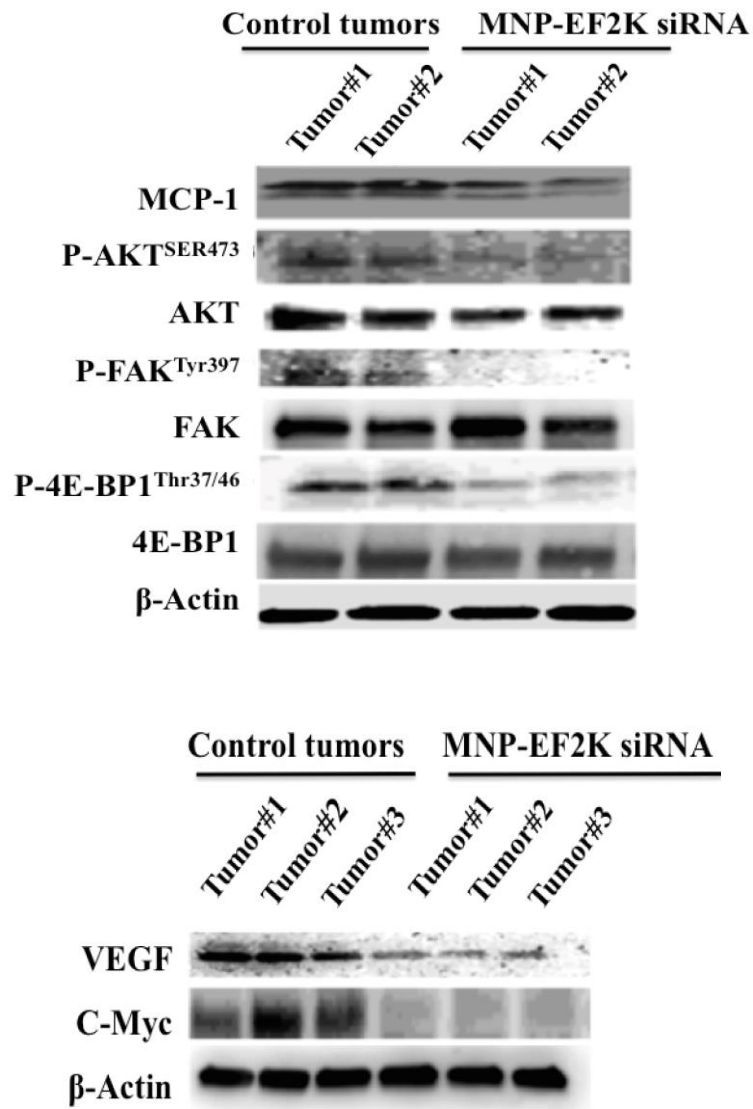


Figure 66. Western blot analysis of tumor tissues 2. Results in the knockdown of EF2K in different tumors with the consequent reduction in MCP-1, p-Akt, AKT, p-FAK, FAK, p-4EBP1, 4EBP1, VEGF, C-Myc levels. C-myc is involved in proliferation and downregulation was observed in MNP-EF2K treated tumors.

3.9.11 Targeting eEF-2K leads a decrease Stem Cell like markers in BRCA1 mutated tumors

Cancer stem cells (CSC) are subpopulation of undifferentiated tumorigenic cells within the tumors that show unique characteristics such as tumor-initiation, self-renewal, and the ability of proliferation, which are responsible for tumor progression, metastasis and also tumor heterogeneity resulting from differentiation [141] ALDH1A1, a putative CSC marker, belongs to the ALDH1 family and is expressed in normal and malignant human mammary stem cells over expression of this marker is associated with poor prognosis in breast [142]. CD44, a specific receptor for hyaluronic acid and adhesion/homing molecule is a multifunctional class I transmembrane glycoprotein expressed in almost all normal and cancer cells [143]. Our finding suggests that eEF2K inhibition caused ALDH1A1/CD44 down regulation in *vivo* in BRCA1 mutated tumors (**Figure 67**).

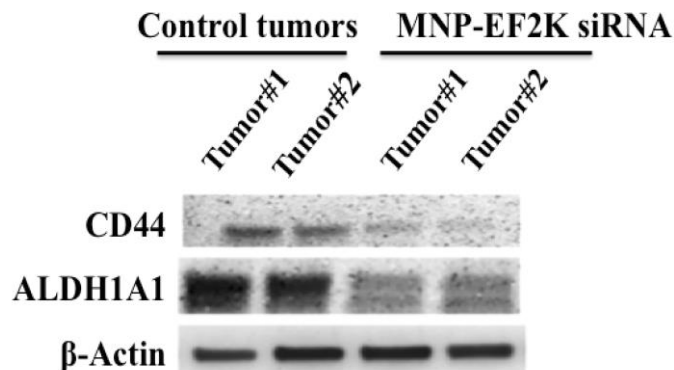


Figure 67. Western blot analysis of tumor tissues 3. Results in the knockdown of EF2K in different tumors with the consequent reduction in CD-44 and ALDH1A1 down-regulation.

3.9.12 Combination of PARP inhibitors with eEF2K siRNA enhance the BRCA1 mutated breast cancer proliferation

Recent clinical studies suggest that PARP (Poly ADP Ribose Polymerase) inhibitors are effective only in 26-50% of patients with BRCA1 mutated tumors. Also, patients who initially respond PARP inhibitors soon become resistant to these therapies [144]. We investigated if inhibition of eEF2K sensitizes BRCA1 mutated breast cancer cells to PARP inhibitor. As seen in **Figure 68**, we found that AZD2281 (PARP inhibitor) induced a dose dependent growth inhibition of MDA-MB-436 cells at ranging 10 to 50 μ M concentration. The growth inhibition effect of combination of AZD2281 and MNP-EF2K siRNA was significantly higher than AZD2281 treatment alone ($p < 0.05$) Control siRNA and DMSO used as negative control and didn't have any growth inhibition effect. The control siRNA and AZD2281 combinations also induced growth inhibition effects whereas the combinations AZD2281 with MNP-EF2K siRNA enhanced significantly superior growth inhibitions in MDA-MB-436 cells indicating eEF2K siRNA sensitize BRCA1 mutated breast cancer cells to PARP inhibitor.

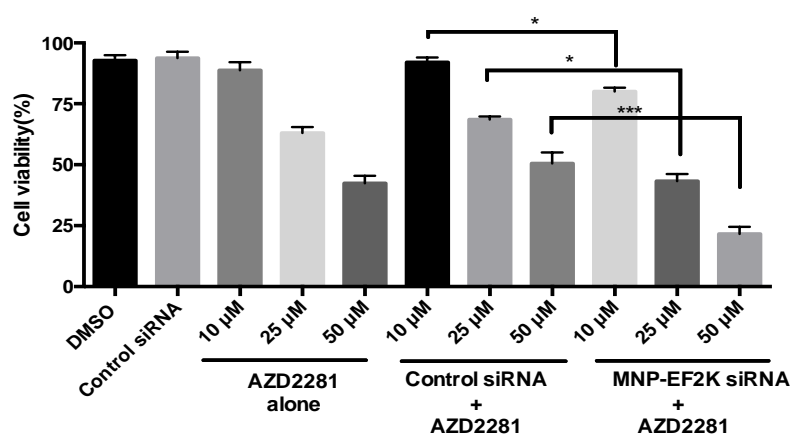


Figure 68. Combination of AZD2281 and EF2K siRNA enhances growth inhibition of MDA-MB-436 cells

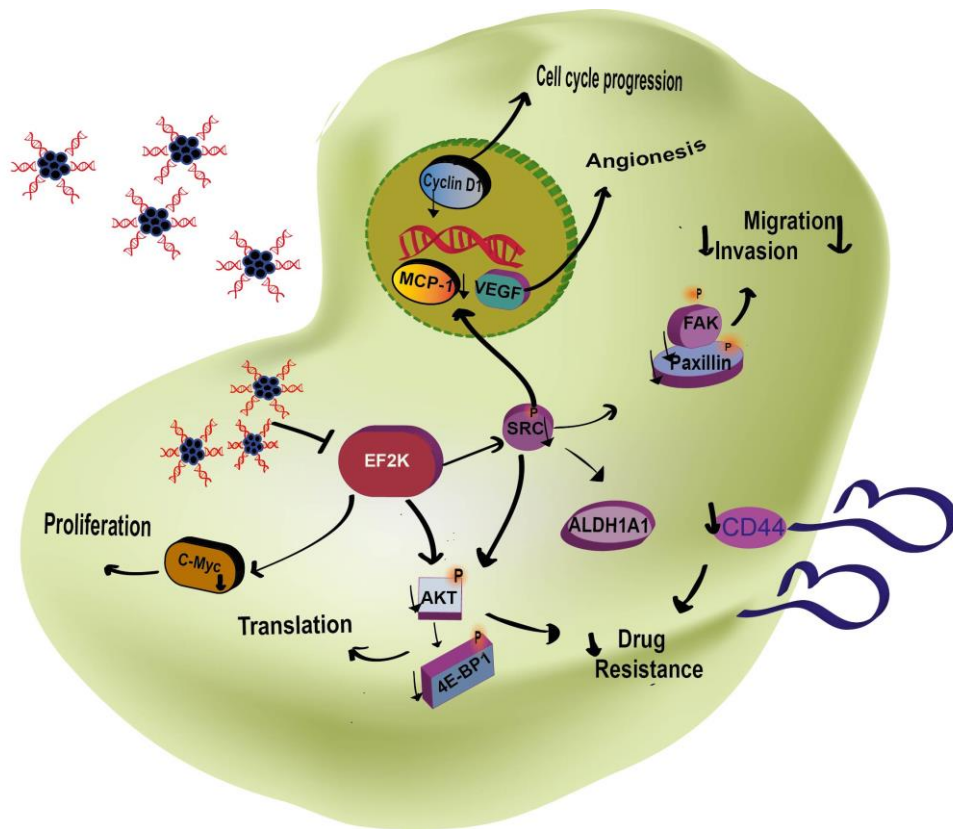


Figure 69 Schematic illustration of cancer therapy of BRCA1 mutated cancer. Targeting eEF2K can lead to signal transduction pathways that promote tumorigenesis in BRCA1 mutated cancer. The downregulation of eEF2K impairs BRCA1 mutated cell invasion and migration through inhibition of SRC/FAK/Paxillin. Furthermore, Targeting EF-2K inhibits PI3K/AkT/mTOR/ 4EBP1 and leads a decrease stem cell like markers in BRCA1 mutated tumors. EF2K may be a novel potential therapeutic target in this cancer.

Our studies demonstrated for the first time that eEF2K promotes BRCA1 mutated breast cancer proliferation; motility/ invasion and tumorigenesis, indicating that eEF2K plays an important role in growth and progression of BRCA1 mutated breast cancer. Moreover, our study also demonstrated that eEF2K might serve as a potential therapeutic target in these cancers. Furthermore, systemic delivery of siRNA by MNP can provide safe, sequence-specific inhibition of the gene eEF2K by with significant anti-tumor efficacy in orthotopic tumor models, providing an important tool for the in vivo systemic use of siRNA or siRNA-based therapies, which is considered as a novel class of therapeutics especially for those “undruggable” targets.

eEF2K is an atypical kinase calcium-calmoduline activated kinase that belongs to alpha family of kinases activated with serine /threonine kinase activity [79]. The eEF2K regulates many cellular processes, such as protein synthesis, cell cycle progression, and induction of autophagy and apoptosis in cancer cells. It also has a critical function during stressful conditions, such as nutrient-deprived condition, hypoxia, and DNA damage [82-84]. Especially energy or nutrient deprivation mediated induction of cAMP activated PKA and AMPK act as a positive regulators of eEF2K leading to increased phosphorylation of EF2 and inhibition/ slowing down of the protein synthesis [145, 146], allowing the cells to conserve energy or direct energy to other cellular functions.

We showed for the first time that eEF2K expression is highly significantly up regulated in BRCA1 mutated (also considered as TNBC) and TNBC cells compared with normal non tumorigenic breast epithelium, which led us to hypothesize that this kinase is highly needed in BRCA1 mutated cancer cells lines and could act as a pro-survival kinase. Our studies suggest that in fact eEF2K promotes important and clinically significant survival pathways and the signaling pathways related to cell growth, survival, migration and invasion, drug resistance, angiogenesis, stem-cell ness or stem cell maintenance, all of which contribute to tumorigenesis and progression of BRCA1 mutated breast cancer.

Src kinases are highly expressed in a variety of human tumors which often plays an integral part of cellular migration, proliferation, adhesion, and angiogenesis [135]. Moreover, Src directly interacts non-receptor focal adhesion kinase (FAK) and related with metastasis through its ability to induce the epithelial-to-mesenchymal transition [137]. Thus Src is one of the most important targets in solid tumors and there is a great deal of efforts to develop Src inhibitors, some of which are being tested in clinical trials. Our study identified that the activity of Src (p-Tyr-416) and FAK (p-Tyr-397) and Paxillin (p-Tyr-118) are inhibited after targeting eEF2K siRNA, lead to profound inhibition of in the invasive phenotype of BRCA1 mutated breast cancer.

Angiogenic growth factors bind to the receptor endothelial cell surface and induce cascades of downstream signaling pathways during tumor angiogenesis. It was reported that inhibition of Src/ FAK expression leads to a down regulation of VEGF expression and result to increase MCP-1 expression, showing that both VEGF and MCP-1 are modulated by Src tyrosine kinase. Consistent with these *in vivo* results, Src and VEGF expression in knockdown eEF2K-treated solid tumors was also inhibited. The downregulation of these angiogenic growth factor and kinase cause downregulation of the signaling pathways involved in tumor microenvironment. This may explain why EF2K exerted such potent inhibitory actions on tumor angiogenesis and tumor growth *in vivo*.

Another our interesting finding is that we detected the decreased expression of ALDH1A1 and CD44 was also observed in BRCA1 mutated tumor samples with overexpressed eEF2K. CD44 and ALDH1A1 are putative markers of CSC that were shown to be associated with drug resistance in cancer cells [147]. Therefore, this study is important for developing future personalized medicine eEF2K-targeted therapies, cancer stem cell markers and biomarkers associated with eEF2K inhibition and understanding mechanisms of drug resistance/sensitivity and developing novel combination therapy approaches.

Recent clinical studies suggest that PARP inhibitors are effective only in a portion of BRCA1 mutated patients who have low rate of response [148]. Further, it is currently unclear whether tumors that respond to combinations of PARP inhibitors. Thus novel targets are needed to identify effectively and an answer to this question will help define which cancers may benefit from this approach. In this study, the combination of eEF2K siRNA and AZD2281 significantly decreased BRCA1 mutated cancer cells viability compared with control siRNA cells and cells treated with each agent alone. The results showed that inhibition of eEF2K sensitized BRCA1 mutated tumors to PARP inhibitor AZD2281.

Magnetic nanoparticles (MNPs) have unique properties such as high magnetization value and pass cellular barrier that have been used for many years as MRI agents imaging and diagnostic purposes and for gene delivery applications [15-17]. Using MNPs to target eEF2K provide relatively low siRNA dose and no additional chemical modification for the siRNA. MNP-EF2K siRNA in combination with small-molecule drugs are likely to further increase the anti-tumor efficiency for future experiments. Taken together, MNP-EF2K siRNA has the potential to become a useful tool in BRCA1 mutated cancer therapy siRNA loaded MNP may efficiently escape the reticuloendothelial system and pass into the tumor.

CHAPTER 4

CONCLUSION

The understanding how MNPs interact with living systems are the prerequisite information one needs to obtain before any further development of these nanomaterial for desired biomedical applications. Therefore we firstly intended to address the need for improved understanding the cyto-and genotoxicity of the MNPs and explored uptake of MNPs in human breast cell models. Uptake of the highest amounts of MNPs was observed in metastatic cells and the uptake of the silica coated MNPs were higher than the naked ones in both cell lines. Naked MNPs represented higher level of cytotoxicity and genotoxicity than silica coated MNPs. Moreover, metastatic cells seemed to be more susceptible to MNPs toxicity than normal cells. There was concentration and time dependent increase in DNA damage and MN frequency (‰) even at the lowest concentration for naked MNPs while silica coated MNPs didn't show genotoxicity below the concentration of 250 µg/mL. Moreover, the extent of DNA damage and MN frequency (‰) was much higher in cancer cells as compared to the normal cells. According to our results, silica coating ameliorated both cytotoxicity and genotoxicity as well the internalization of MNPs.

Studies on the interface between the chemical parameters of nanostructures and cell biology are just beginning and a great deal is unknown about the interaction of nanostructures with cells and the potential toxicity, which may result. Cellular interactions of nanoparticles are one of the big interests and still

underway. One mechanism frequently discussed is the induction of oxidative damage of cellular constituents, either due to the generation of reactive oxygen species (ROS) or by inactivation of antioxidant defense system. Keeping in view the significant lack of toxicity data for CoFe-MNPs on human cancer breast cell lines, the our study was designed to investigate naked and silica coated MNPs induced the potential apoptosis, lipid peroxidation, ROS formation through ROS generation and oxidative related gene expression levels of some drug metabolizing enzymes in human cancer breast cell lines. ROS generation, lipid peroxidation and apoptosis were observed in the group treated with only a high concentration of silica MNPs while they were observed significantly even at low concentration in the group treated with naked MNPs. The core metals induced notably high levels of ROS generation and cell death at each concentration used. These data provide sufficient evidence to infer that the generation of intracellular ROS is caused by the accumulation of aggregated naked CoFe-MNPs. This is consistent with reports that silica-coated CoFe-MNPs protected cells from oxidative stress by preventing soluble iron mobilization or acidic erosion

Then 2-Amino-2-deoxy-glucose (2DG) were further conjugated with COOH modified CoFe MNPs in order to target over expressed GLUT1 in cancer cells (MDA-MB-231 and non-MCF-7) more than the normal breast cells (MCF-10A) and investigated for its effects on cellular uptake, cytotoxicity and apoptosis in two different breast cancer cell lines. The results were compared with that of the normal breast cells. Finally we studied the effect of 2DG-MNPs on gene expressions of two Phase I (CYP1A1, CYP1B1) and two phase II (GSTM3, GSTZ1) drug metabolizing enzymes in cells treated with 2DG-MNPs.

2-amino-2-deoxy-glucose (2DG) was successfully conjugated to -COOH modified cobalt ferrite magnetic nanoparticles (CoFe MNPs), which was designed to target tumor cells through glucose transporters as a potential targetable drug/gene delivery agent for cancer treatment. According to our

results, it is apparent that 2DG-MNPs were internalized more efficiently than COOH-MNPs under same conditions, in all cells ($p < 0.001$). Moreover, the highest amount of uptake was observed in MDA-MB-231 cells, which is followed by MCF-7 and normal MCF-10A for both MNPs. The apoptotic effects of 2DG-MNPs was further evaluated, and it was found that apoptosis was not induced at low concentration of 2DG-MNPs, in MDA-MB-231 cells, whereas dramatic cell death was observed at higher concentrations. Same trend was observed for both MCF-7 and normal MCF-10A cells. Apoptotic cell death was further confirmed by gene expression analysis. In addition, the gene expression levels of some drug metabolizing enzymes, two Phase I (CYP1A1, CYP1B1) and two Phase II (GSTM3, GSTZ1) were also studied in cells treated with 2DG-MNPs and the expression levels of these genes were seen to increase at high concentration of 2DG-MNPs, whereas at low concentration no induction was observed. In conclusion, Selective uptake of 2DG-MNPs was shown in breast cancer cells that provide an opportunity to design a nanocarrier with specific therapeutic action with reduced side effects in terms of cytotoxicity.

Finally, recent advancements in the understanding of genetic events in breast cancers with inherited mutations in *BRCA1* or *BRCA2* have allowed the development of poly (ADP-ribose) polymerase inhibitors (PARP) for the treatment of these patients. However, the reported response rates for these agents range from 26%-50% in clinical studies, indicating that upto 74% of patients may not have response to PARP inhibitors and those patients who initially respond eventually become resistant and have progressive disease. Thus, novel therapeutic interventions for the BRCA1 mutated patients who do not respond to PARP inhibitors or become resistant to them are critical to expanding the scope of therapy for these patients. To address this unmet need and for an improved understanding the molecular pathways and abnormalities - we investigated the expression and role of an atypical kinase, Eukaryotic elongation factor-2 kinase (EF-2K) in the BRCA1 mutated breast cancer. We

found that eEF-2K is markedly up regulated in BRCA1 mutated cell lines and knockdown of the gene by siRNA significantly inhibited colony formation, proliferation, migration and invasion of BRCA1 mutated cells. Furthermore, in vivo therapeutic targeting of eEF-2K by long-acting slow release magnetic nanoparticles incorporating eEF2K siRNA (i.v, 0.3mg/kg, once in a week) significantly inhibited growth of BRCA1 mutated tumor growth in orthotopic xenograft models in mice. In vivo inhibition of EF2K lead to inhibition of molecules and pathways that are involved in migration/invasion (Src/FAK/paxillin), angiogenesis (VEGF), proliferation, cell cycle, survival, translational regulation (c-myc, CyclinD1, Akt,/, 4E-BP1). Collectively, our results suggest, for the first time, that eEF-2K is involved in tumorigenesis and progression of BRCA1 mutated breast cancer and may be a novel a novel potential therapeutic target in this cancer.

Targeted MNP-EF2K siRNA are efficacious at a relatively low siRNA dose and do not require chemical modification of the siRNA for stabilization. Future experiments employing MNP-EF2K siRNA in combination with small-molecule drugs are likely to further enhance the anti-tumor potency of this system. We therefore conclude that MNP-EF2K siRNA formulated in targeted EF-2K has the potential to become a useful tool in BRCA1 mutated cancer therapy siRNA loaded MNP could efficiently evade the RES uptake, and target and penetrate the tumor after *i.v.* injection.

REFERENCES

- [1] P. Borm, F.C. Klaessig, T.D. Landry, B. Moudgil, J. Pauluhn, K. Thomas, R. Trottier, S. Wood, Research strategies for safety evaluation of nanomaterials, part V: role of dissolution in biological fate and effects of nanoscale particles, *Toxicol Sci*, 90 (2006) 23-32.
- [2] M.E. Akerman, W.C. Chan, P. Laakkonen, S.N. Bhatia, E. Ruoslahti, Nanocrystal targeting in vivo, *Proc Natl Acad Sci U S A*, 99 (2002) 12617-12621.
- [3] W.H. Suh, K.S. Suslick, G.D. Stucky, Y.H. Suh, Nanotechnology, nanotoxicology, and neuroscience, *Prog Neurobiol*, 87 (2009) 133-170.
- [4] A. Nel, Atmosphere. Air pollution-related illness: effects of particles, *Science*, 308 (2005) 804-806.
- [5] G. Oberdorster, A. Maynard, K. Donaldson, V. Castranova, J. Fitzpatrick, K. Ausman, J. Carter, B. Karn, W. Kreyling, D. Lai, S. Olin, N. Monteiro-Riviere, D. Warheit, H. Yang, Principles for characterizing the potential human health effects from exposure to nanomaterials: elements of a screening strategy, *Part Fibre Toxicol*, 2 (2005) 8.
- [6] W.T. Al-Jamal, K. Kostarelos, Liposomes: from a clinically established drug delivery system to a nanoparticle platform for theranostic nanomedicine, *Accounts of chemical research*, 44 (2011) 1094-1104.
- [7] R. Jayakumar, D. Menon, K. Manzoor, S.V. Nair, H. Tamura, Biomedical applications of chitin and chitosan based nanomaterials—A short review, *Carbohydrate Polymers*, 82 (2010) 227-232.
- [8] O.V. Salata, Applications of nanoparticles in biology and medicine, *Journal of nanobiotechnology*, 2 (2004) 3.
- [9] A. Figuerola, R. Di Corato, L. Manna, T. Pellegrino, From iron oxide nanoparticles towards advanced iron-based inorganic materials designed for biomedical applications, *Pharmacological Research*, 62 (2010) 126-143.
- [10] E. Boisselier, D. Astruc, Gold nanoparticles in nanomedicine: preparations, imaging, diagnostics, therapies and toxicity, *Chemical Society Reviews*, 38 (2009) 1759-1782.

- [11] R. Partha, J.L. Conyers, Biomedical applications of functionalized fullerene-based nanomaterials, *International journal of nanomedicine*, 4 (2009) 261.
- [12] L. Kong, C.S. Alves, W. Hou, J. Qiu, H. Möhwald, H. Tomás, X. Shi, RGD Peptide-Modified Dendrimer-Entrapped Gold Nanoparticles Enable Highly Efficient and Specific Gene Delivery to Stem Cells, *ACS applied materials & interfaces*, 7 (2015) 4833-4843.
- [13] L. Li, L. Zhang, T. Wang, X. Wu, H. Ren, C. Wang, Z. Su, Cancer Therapy: Facile and Scalable Synthesis of Novel Spherical Au Nanocluster Assemblies@ Polyacrylic Acid/Calcium Phosphate Nanoparticles for Dual-Modal Imaging- Guided Cancer Chemotherapy (*Small* 26/2015), *Small*, 11 (2015) 3082-3082.
- [14] K. Nelson, P. Winter, M. Shokeen, S. Wang, M.Y. Berezin, Nanoparticles for Bioimaging, *Nanotechnology for Biomedical Imaging and Diagnostics: From Nanoparticle Design to Clinical Applications*, 151-192.
- [15] S. Mornet, S. Vasseur, F. Grasset, E. Duguet, Magnetic nanoparticle design for medical diagnosis and therapy, *Journal of Materials Chemistry*, 14 (2004) 2161-2175.
- [16] H. Dähring, J. Grandke, U. Teichgräber, I. Hilger, Improved Hyperthermia Treatment of Tumors Under Consideration of Magnetic Nanoparticle Distribution Using Micro-CT Imaging, *Molecular Imaging and Biology*, (2015) 1-7.
- [17] S. Majidi, F. Zeinali Sehrig, M. Samiei, M. Milani, E. Abbasi, K. Dadashzadeh, A. Akbarzadeh, Magnetic nanoparticles: Applications in gene delivery and gene therapy, *Artificial cells, nanomedicine, and biotechnology*, (2015) 1-8.
- [18] S. Amiri, H. Shokrollahi, The role of cobalt ferrite magnetic nanoparticles in medical science, *Materials Science and Engineering: C*, 33 (2013) 1-8.
- [19] Q.A. Pankhurst, N.T.K. Thanh, S.K. Jones, J. Dobson, Progress in applications of magnetic nanoparticles in biomedicine, *Journal of Physics D: Applied Physics*, 42 (2009) 224001.
- [20] I.W. Hamley, Nanotechnology with soft materials, *Angew Chem Int Ed Engl*, 42 (2003) 1692-1712.

- [21] C. Sun, J.S. Lee, M. Zhang, Magnetic nanoparticles in MR imaging and drug delivery, *Adv Drug Deliv Rev*, 60 (2008) 1252-1265.
- [22] A.K. Gupta, R.R. Naregalkar, V.D. Vaidya, M. Gupta, Recent advances on surface engineering of magnetic iron oxide nanoparticles and their biomedical applications, *Nanomedicine (Lond)*, 2 (2007) 23-39.
- [23] J.T. Cole, N.B. Holland, Multifunctional nanoparticles for use in theranostic applications, *Drug delivery and translational research*, 5 (2015) 295-309.
- [24] Q.A. Pankhurst, J. Connolly, S.K. Jones, J.J. Dobson, Applications of magnetic nanoparticles in biomedicine, *Journal of physics D: Applied physics*, 36 (2003) R167.
- [25] D. Kami, S. Takeda, Y. Itakura, S. Gojo, M. Watanabe, M. Toyoda, Application of magnetic nanoparticles to gene delivery, *International journal of molecular sciences*, 12 (2011) 3705-3722.
- [26] D. Artemov, N. Mori, R. Ravi, Z.M. Bhujwala, Magnetic resonance molecular imaging of the HER-2/neu receptor, *Cancer Res*, 63 (2003) 2723-2727.
- [27] J.G. Rajendran, D.A. Mankoff, F. O'Sullivan, L.M. Peterson, D.L. Schwartz, E.U. Conrad, A.M. Spence, M. Muzi, D.G. Farwell, K.A. Krohn, Hypoxia and glucose metabolism in malignant tumors: evaluation by [18F]fluoromisonidazole and [18F]fluorodeoxyglucose positron emission tomography imaging, *Clin Cancer Res*, 10 (2004) 2245-2252.
- [28] S.S. Gambhir, J. Czernin, J. Schwimmer, D.H. Silverman, R.E. Coleman, M.E. Phelps, A tabulated summary of the FDG PET literature, *J Nucl Med*, 42 (2001) 1s-93s.
- [29] A. Luciani, J.C. Olivier, O. Clement, N. Siauve, P.Y. Brillet, B. Bessoud, F. Gazeau, I.F. Uchegbu, E. Kahn, G. Frija, C.A. Cuenod, Glucose-receptor MR imaging of tumors: study in mice with PEGylated paramagnetic niosomes, *Radiology*, 231 (2004) 135-142.
- [30] K.C. Schmidt, G. Lucignani, L. Sokoloff, Fluorine-18-fluorodeoxyglucose PET to determine regional cerebral glucose utilization: a re-examination, *J Nucl Med*, 37 (1996) 394-399.

- [31] L. Sokoloff, M. Reivich, C. Kennedy, M.H. Des Rosiers, C.S. Patlak, K.D. Pettigrew, O. Sakurada, M. Shinohara, The [14C]deoxyglucose method for the measurement of local cerebral glucose utilization: theory, procedure, and normal values in the conscious and anesthetized albino rat, *J Neurochem*, 28 (1977) 897-916.
- [32] D.J. Yang, C.G. Kim, N.R. Schechter, A. Azhdarinia, D.F. Yu, C.S. Oh, J.L. Bryant, J.J. Won, E.E. Kim, D.A. Podoloff, Imaging with 99mTc ECDG targeted at the multifunctional glucose transport system: feasibility study with rodents, *Radiology*, 226 (2003) 465-473.
- [33] F. Xiong, Z.-y. Zhu, C. Xiong, X.-q. Hua, X.-h. Shan, Y. Zhang, N. Gu, Preparation, characterization of 2-deoxy-D-glucose functionalized dimercaptosuccinic acid-coated maghemite nanoparticles for targeting tumor cells, *Pharmaceutical research*, 29 (2012) 1087-1097.
- [34] B. Aydogan, J. Li, T. Rajh, A. Chaudhary, S.J. Chmura, C. Pelizzari, C. Wietholt, M. Kurtoglu, P. Redmond, AuNP-DG: deoxyglucose-labeled gold nanoparticles as X-ray computed tomography contrast agents for cancer imaging, *Mol Imaging Biol*, 12 (2010) 463-467.
- [35] X.H. Shan, P. Wang, F. Xiong, N. Gu, H. Hu, W. Qian, H.Y. Lu, Y. Fan, MRI of High-Glucose Metabolism Tumors: a Study in Cells and Mice with 2-DG-Modified Superparamagnetic Iron Oxide Nanoparticles, *Mol Imaging Biol*, (2015).
- [36] A.K. Gupta, R.R. Naregalkar, V.D. Vaidya, M. Gupta, Recent advances on surface engineering of magnetic iron oxide nanoparticles and their biomedical applications, (2007).
- [37] T.D. Schladt, K. Schneider, H. Schild, W. Tremel, Synthesis and bio-functionalization of magnetic nanoparticles for medical diagnosis and treatment, *Dalton Transactions*, 40 (2011) 6315-6343.
- [38] D. Beyersmann, A. Hartwig, Carcinogenic metal compounds: recent insight into molecular and cellular mechanisms, *Archives of toxicology*, 82 (2008) 493-512.
- [39] H.F. Krug, K. Kern, J.M. Wörle-Knirsch, S. Diabate in *Nanomaterials—Toxicity, Health and Environmental Issues*, Vol. 5, Wiley-VCH, Weinheim, 2006.

- [40] M.A. Dobrovolskaia, S.E. McNeil, Immunological properties of engineered nanomaterials, *Nature nanotechnology*, 2 (2007) 469-478.
- [41] A.A. Shvedova, V.E. Kagan, B. Fadeel, Close encounters of the small kind: adverse effects of man-made materials interfacing with the nano-cosmos of biological systems, *Annual review of pharmacology and toxicology*, 50 (2010) 63-88.
- [42] B. Halliwell, J.M.C. Gutteridge, *Free radicals in biology and medicine*, Oxford university press Oxford 1999.
- [43] T. Xia, M. Kovochich, J. Brant, M. Hotze, J. Sempf, T. Oberley, C. Sioutas, J.I. Yeh, M.R. Wiesner, A.E. Nel, Comparison of the abilities of ambient and manufactured nanoparticles to induce cellular toxicity according to an oxidative stress paradigm, *Nano letters*, 6 (2006) 1794-1807.
- [44] J.S. Bertram, The molecular biology of cancer, *Mol Aspects Med*, 21 (2000) 167-223.
- [45] D. Hanahan, R.A. Weinberg, The hallmarks of cancer, *cell*, 100 (2000) 57-70.
- [46] P.A. Hall, *Introduction to the Cellular and Molecular Biology of Cancer*. 3rd edn. LM Franks and NM Teich. Oxford University Press, Oxford, 1997. No. of pages: 468. Price:£ 55.00 (Hardback). ISBN: 0 19 854854 0, Wiley Online Library, 1998.
- [47] J. Ferlay, I. Soerjomataram, R. Dikshit, S. Eser, C. Mathers, M. Rebelo, D.M. Parkin, D. Forman, F. Bray, Cancer incidence and mortality worldwide: sources, methods and major patterns in GLOBOCAN 2012, *International Journal of Cancer*, 136 (2015) E359-E386.
- [48] A. Bosch, P. Eroles, R. Zaragoza, J.R. Vina, A. Lluch, Triple-negative breast cancer: molecular features, pathogenesis, treatment and current lines of research, *Cancer Treat Rev*, 36 (2010) 206-215.
- [49] L. Balducci, W.B. Ershler, G.H. Lyman, M. Extermann, *Comprehensive geriatric oncology*, CRC Press 2004.
- [50] D.F. Easton, How many more breast cancer predisposition genes are there?, *Breast Cancer Res*, 1 (1999) 14-17.

- [51] P.M. Campeau, W.D. Foulkes, M.D. Tischkowitz, Hereditary breast cancer: new genetic developments, new therapeutic avenues, *Hum Genet*, 124 (2008) 31-42.
- [52] A. Antoniou, P.D. Pharoah, S. Narod, H.A. Risch, J.E. Eyfjord, J.L. Hopper, N. Loman, H. Olsson, O. Johannsson, A. Borg, B. Pasini, P. Radice, S. Manoukian, D.M. Eccles, N. Tang, E. Olah, H. Anton-Culver, E. Warner, J. Lubinski, J. Gronwald, B. Gorski, H. Tulinius, S. Thorlacius, H. Eerola, H. Nevanlinna, K. Syrjakoski, O.P. Kallioniemi, D. Thompson, C. Evans, J. Peto, F. Lalloo, D.G. Evans, D.F. Easton, Average risks of breast and ovarian cancer associated with BRCA1 or BRCA2 mutations detected in case Series unselected for family history: a combined analysis of 22 studies, *Am J Hum Genet*, 72 (2003) 1117-1130.
- [53] S. Chen, G. Parmigiani, Meta-analysis of BRCA1 and BRCA2 penetrance, *J Clin Oncol*, 25 (2007) 1329-1333.
- [54] S.R. Lakhani, M.J. Van De Vijver, J. Jacquemier, T.J. Anderson, P.P. Osin, L. McGuffog, D.F. Easton, The pathology of familial breast cancer: predictive value of immunohistochemical markers estrogen receptor, progesterone receptor, HER-2, and p53 in patients with mutations in BRCA1 and BRCA2, *J Clin Oncol*, 20 (2002) 2310-2318.
- [55] J. Palacios, E. Honrado, A. Osorio, A. Cazorla, D. Sarrió, A. Barroso, S. Rodríguez, J.C. Cigudosa, O. Diez, C. Alonso, Phenotypic characterization of BRCA1 and BRCA2 tumors based in a tissue microarray study with 37 immunohistochemical markers, *Breast cancer research and treatment*, 90 (2005) 5-14.
- [56] M.E. Moynahan, J.W. Chiu, B.H. Koller, M. Jasin, Brca1 controls homology-directed DNA repair, *Mol Cell*, 4 (1999) 511-518.
- [57] A. Tutt, D. Bertwistle, J. Valentine, A. Gabriel, S. Swift, G. Ross, C. Griffin, J. Thacker, A. Ashworth, Mutation in Brca2 stimulates error-prone homology-directed repair of DNA double-strand breaks occurring between repeated sequences, *Embo j*, 20 (2001) 4704-4716.
- [58] A. Tutt, A. Ashworth, The relationship between the roles of BRCA genes in DNA repair and cancer predisposition, *Trends Mol Med*, 8 (2002) 571-576.
- [59] M.S. Huen, S.M. Sy, J. Chen, BRCA1 and its toolbox for the maintenance of genome integrity, *Nat Rev Mol Cell Biol*, 11 (2010) 138-148.

- [60] J.S. Reis-Filho, A.N. Tutt, Triple negative tumours: a critical review, *Histopathology*, 52 (2008) 108-118.
- [61] Tamoxifen for early breast cancer: an overview of the randomised trials. Early Breast Cancer Trialists' Collaborative Group, *Lancet*, 351 (1998) 1451-1467.
- [62] N.E. Hynes, H.A. Lane, ERBB receptors and cancer: the complexity of targeted inhibitors, *Nat Rev Cancer*, 5 (2005) 341-354.
- [63] J.E. Uhm, Y.H. Park, S.Y. Yi, E.Y. Cho, Y.L. Choi, S.J. Lee, M.J. Park, S.H. Lee, H.J. Jun, J.S. Ahn, W.K. Kang, K. Park, Y.H. Im, Treatment outcomes and clinicopathologic characteristics of triple-negative breast cancer patients who received platinum-containing chemotherapy, *Int J Cancer*, 124 (2009) 1457-1462.
- [64] R. Torrisi, A. Balduzzi, R. Ghisini, A. Rocca, L. Bottiglieri, F. Giovanardi, P. Veronesi, A. Luini, L. Orlando, G. Viale, A. Goldhirsch, M. Colleoni, Tailored preoperative treatment of locally advanced triple negative (hormone receptor negative and HER2 negative) breast cancer with epirubicin, cisplatin, and infusional fluorouracil followed by weekly paclitaxel, *Cancer Chemother Pharmacol*, 62 (2008) 667-672.
- [65] C. Jones, A. Mackay, A. Grigoriadis, A. Cossu, J.S. Reis-Filho, L. Fulford, T. Dexter, S. Davies, K. Bulmer, E. Ford, S. Parry, M. Budroni, G. Palmieri, A.M. Neville, M.J. O'Hare, S.R. Lakhani, Expression profiling of purified normal human luminal and myoepithelial breast cells: identification of novel prognostic markers for breast cancer, *Cancer Res*, 64 (2004) 3037-3045.
- [66] T. Sorlie, C.M. Perou, R. Tibshirani, T. Aas, S. Geisler, H. Johnsen, T. Hastie, M.B. Eisen, M. van de Rijn, S.S. Jeffrey, T. Thorsen, H. Quist, J.C. Matese, P.O. Brown, D. Botstein, P.E. Lonning, A.L. Borresen-Dale, Gene expression patterns of breast carcinomas distinguish tumor subclasses with clinical implications, *Proc Natl Acad Sci U S A*, 98 (2001) 10869-10874.
- [67] E. Matros, Z.C. Wang, G. Lodeiro, A. Miron, J.D. Iglehart, A.L. Richardson, BRCA1 promoter methylation in sporadic breast tumors: relationship to gene expression profiles, *Breast Cancer Res Treat*, 91 (2005) 179-186.
- [68] N. Turner, M.B. Lambros, H.M. Horlings, A. Pearson, R. Sharpe, R. Natrajan, F.C. Geyer, M. van Kouwenhove, B. Kreike, A. Mackay, A. Ashworth, M.J. van de Vijver, J.S. Reis-Filho, Integrative molecular profiling

of triple negative breast cancers identifies amplicon drivers and potential therapeutic targets, *Oncogene*, 29 (2010) 2013-2023.

[69] F. Andre, B. Job, P. Dessen, A. Tordai, S. Michiels, C. Liedtke, C. Richon, K. Yan, B. Wang, G. Vassal, S. Delaloge, G.N. Hortobagyi, W.F. Symmans, V. Lazar, L. Pusztai, Molecular characterization of breast cancer with high-resolution oligonucleotide comparative genomic hybridization array, *Clin Cancer Res*, 15 (2009) 441-451.

[70] T.O. Nielsen, F.D. Hsu, K. Jensen, M. Cheang, G. Karaca, Z. Hu, T. Hernandez-Boussard, C. Livasy, D. Cowan, L. Dressler, L.A. Akslen, J. Ragaz, A.M. Gown, C.B. Gilks, M. van de Rijn, C.M. Perou, Immunohistochemical and clinical characterization of the basal-like subtype of invasive breast carcinoma, *Clin Cancer Res*, 10 (2004) 5367-5374.

[71] N. Berrada, S. Delaloge, F. Andre, Treatment of triple-negative metastatic breast cancer: toward individualized targeted treatments or chemosensitization?, *Ann Oncol*, 21 Suppl 7 (2010) vii30-35.

[72] C. Desmedt, B. Haibe-Kains, P. Wirapati, M. Buyse, D. Larsimont, G. Bontempi, M. Delorenzi, M. Piccart, C. Sotiriou, Biological processes associated with breast cancer clinical outcome depend on the molecular subtypes, *Clin Cancer Res*, 14 (2008) 5158-5165.

[73] A.E. Teschendorff, A. Miremadi, S.E. Pinder, I.O. Ellis, C. Caldas, An immune response gene expression module identifies a good prognosis subtype in estrogen receptor negative breast cancer, *Genome Biol*, 8 (2007) R157.

[74] S.Y. Park, H.E. Lee, H. Li, M. Shipitsin, R. Gelman, K. Polyak, Heterogeneity for stem cell-related markers according to tumor subtype and histologic stage in breast cancer, *Clin Cancer Res*, 16 (2010) 876-887.

[75] H. Farmer, N. McCabe, C.J. Lord, A.N. Tutt, D.A. Johnson, T.B. Richardson, M. Santarosa, K.J. Dillon, I. Hickson, C. Knights, N.M. Martin, S.P. Jackson, G.C. Smith, A. Ashworth, Targeting the DNA repair defect in BRCA mutant cells as a therapeutic strategy, *Nature*, 434 (2005) 917-921.

[76] S. Rottenberg, J.E. Jaspers, A. Kersbergen, E. van der Burg, A.O. Nygren, S.A. Zander, P.W. Derksen, M. de Bruin, J. Zevenhoven, A. Lau, R. Boulter, A. Cranston, M.J. O'Connor, N.M. Martin, P. Borst, J. Jonkers, High sensitivity of BRCA1-deficient mammary tumors to the PARP inhibitor AZD2281 alone and in combination with platinum drugs, *Proc Natl Acad Sci U S A*, 105 (2008) 17079-17084.

- [77] B. Ozpolat, A.K. Sood, G. Lopez-Berestein, Liposomal siRNA nanocarriers for cancer therapy, *Advanced drug delivery reviews*, 66 (2014) 110-116.
- [78] G. Ozcan, B. Ozpolat, R.L. Coleman, A.K. Sood, G. Lopez-Berestein, Preclinical and clinical development of siRNA-based therapeutics, *Advanced drug delivery reviews*, (2015).
- [79] J.W. Kenney, C.E. Moore, X. Wang, C.G. Proud, Eukaryotic elongation factor 2 kinase, an unusual enzyme with multiple roles, *Advances in biological regulation*, 55 (2014) 15-27.
- [80] H. Zhu, X. Yang, J. Liu, L. Zhou, C. Zhang, L. Xu, Q. Qin, L. Zhan, J. Lu, H. Cheng, Eukaryotic elongation factor 2 kinase confers tolerance to stress conditions in cancer cells, *Cell Stress and Chaperones*, 20 (2015) 217-220.
- [81] I. Tekedereli, S.N. Alpay, C.D.J. Tavares, Z.E. Cobanoglu, T.S. Kaoud, I. Sahin, A.K. Sood, G. Lopez-Berestein, K.N. Dalby, B. Ozpolat, Targeted silencing of elongation factor 2 kinase suppresses growth and sensitizes tumors to doxorubicin in an orthotopic model of breast cancer, (2012).
- [82] G.J. Browne, C.G. Proud, Regulation of peptide- chain elongation in mammalian cells, *European Journal of Biochemistry*, 269 (2002) 5360-5368.
- [83] X. Wang, W. Li, M. Williams, N. Terada, D.R. Alessi, C.G. Proud, Regulation of elongation factor 2 kinase by p90RSK1 and p70 S6 kinase, *The EMBO journal*, 20 (2001) 4370-4379.
- [84] E. Connolly, S. Braunstein, S. Formenti, R.J. Schneider, Hypoxia inhibits protein synthesis through a 4E-BP1 and elongation factor 2 kinase pathway controlled by mTOR and uncoupled in breast cancer cells, *Molecular and cellular biology*, 26 (2006) 3955-3965.
- [85] F. Meric-Bernstam, H. Chen, A. Akcakanat, K.A. Do, A. Lluch, B.T. Hennessy, G.N. Hortobagyi, G.B. Mills, A. Gonzalez-Angulo, Aberrations in translational regulation are associated with poor prognosis in hormone receptor-positive breast cancer, *Breast cancer research : BCR*, 14 (2012) R138.
- [86] A.A. Ashour, N. Gurbuz, S.N. Alpay, A.A. Abdel-Aziz, A.M. Mansour, L. Huo, B. Ozpolat, Elongation factor-2 kinase regulates TG2/beta1 integrin/Src/uPAR pathway and epithelial-mesenchymal transition mediating pancreatic cancer cells invasion, *Journal of cellular and molecular medicine*, 18 (2014) 2235-2251.

- [87] I. Tekedereli, S.N. Alpay, C.D. Tavares, Z.E. Cobanoglu, T.S. Kaoud, I. Sahin, A.K. Sood, G. Lopez-Berestein, K.N. Dalby, B. Ozpolat, Targeted silencing of elongation factor 2 kinase suppresses growth and sensitizes tumors to doxorubicin in an orthotopic model of breast cancer, *PloS one*, 7 (2012) e41171.
- [88] K. Maaz, A. Mumtaz, S.K. Hasanain, A. Ceylan, Synthesis and magnetic properties of cobalt ferrite (CoFe₂O₄) nanoparticles prepared by wet chemical route, *Journal of Magnetism and Magnetic Materials*, 308 (2007) 289-295.
- [89] Y. Kobayashi, M. Horie, M. Konno, B. Rodríguez-González, L.M. Liz-Marzán, Preparation and properties of silica-coated cobalt nanoparticles, *The Journal of Physical Chemistry B*, 107 (2003) 7420-7425.
- [90] H. Suzuki, T. Toyooka, Y. Ibuki, Simple and easy method to evaluate uptake potential of nanoparticles in mammalian cells using a flow cytometric light scatter analysis, *Environmental science & technology*, 41 (2007) 3018-3024.
- [91] N.P. Singh, R.E. Stephens, E.L. Schneider, Modifications of alkaline microgel electrophoresis for sensitive detection of DNA damage, *International journal of radiation biology*, 66 (1994) 23-28.
- [92] M. Fenech, The in vitro micronucleus technique, *Mutation Research/Fundamental and Molecular Mechanisms of Mutagenesis*, 455 (2000) 81-95.
- [93] C.P. Wan, E. Myung, B.H. Lau, An automated micro-fluorometric assay for monitoring oxidative burst activity of phagocytes, *J Immunol Methods*, 159 (1993) 131-138.
- [94] M.R. Wilson, J.H. Lightbody, K. Donaldson, J. Sales, V. Stone, Interactions between ultrafine particles and transition metals in vivo and in vitro, *Toxicol Appl Pharmacol*, 184 (2002) 172-179.
- [95] H. Ohkawa, N. Ohishi, K. Yagi, Assay for lipid peroxides in animal tissues by thiobarbituric acid reaction, *Anal Biochem*, 95 (1979) 351-358.
- [96] M.M. Bradford, A rapid and sensitive method for the quantitation of microgram quantities of protein utilizing the principle of protein-dye binding, *Anal Biochem*, 72 (1976) 248-254.

- [97] K.J. Livak, T.D. Schmittgen, Analysis of relative gene expression data using real-time quantitative PCR and the 2(-Delta Delta C(T)) Method, *Methods*, 25 (2001) 402-408.
- [98] Y.P. He, S.Q. Wang, C.R. Li, Y.M. Miao, Z.Y. Wu, B.S. Zou, Synthesis and characterization of functionalized silica-coated Fe₃O₄ superparamagnetic nanocrystals for biological applications, *Journal of Physics D: Applied Physics*, 38 (2005) 1342.
- [99] G.E. Anthon, D.M. Barrett, Determination of reducing sugars with 3-methyl-2-benzothiazolinonehydrazone, *Anal Biochem*, 305 (2002) 287-289.
- [100] J.A. Plumb, Cell sensitivity assays : clonogenic assay, *Methods in molecular medicine*, 28 (1999) 17-23.
- [101] L.M. Shaw, Tumor cell invasion assays, *Methods in molecular biology (Clifton, N.J.)*, 294 (2005) 97-105.
- [102] C.C. Liang, A.Y. Park, J.L. Guan, In vitro scratch assay: a convenient and inexpensive method for analysis of cell migration in vitro, *Nature protocols*, 2 (2007) 329-333.
- [103] V. Gonzalez-Villasana, E. Fuentes-Mattei, C. Ivan, H.J. Dalton, C. Rodriguez-Aguayo, R.J. Fernandez-de Thomas, B. Aslan, C.M.P. Del, G. Velazquez-Torres, R.A. Previs, S. Pradeep, N. Kahraman, H. Wang, P. Kanlikilicer, B. Ozpolat, G. Calin, A.K. Sood, G. Lopez-Berestein, Rac1/Pak1/p38/MMP-2 Axis Regulates Angiogenesis in Ovarian Cancer, *Clinical cancer research : an official journal of the American Association for Cancer Research*, 21 (2015) 2127-2137.
- [104] A. Albanese, P.S. Tang, W.C. Chan, The effect of nanoparticle size, shape, and surface chemistry on biological systems, *Annu Rev Biomed Eng*, 14 (2012) 1-16.
- [105] B. Fadeel, A.E. Garcia-Bennett, Better safe than sorry: Understanding the toxicological properties of inorganic nanoparticles manufactured for biomedical applications, *Adv Drug Deliv Rev*, 62 (2010) 362-374.
- [106] B. Ozpolat, A.K. Sood, G. Lopez-Berestein, Nanomedicine based approaches for the delivery of siRNA in cancer, *J Intern Med*, 267 (2010) 44-53.

- [107] C. Yu, J. Zhao, Y. Guo, C. Lu, X. Ma, Z. Gu, A novel method to prepare water-dispersible magnetic nanoparticles and their biomedical applications: magnetic capture probe and specific cellular uptake, *J Biomed Mater Res A*, 87 (2008) 364-372.
- [108] M. Sincai, D. Ganga, M. Ganga, D. Argherie, D. Bica, Antitumor effect of magnetite nanoparticles in cat mammary adenocarcinoma, *Journal of magnetism and magnetic materials*, 293 (2005) 438-441.
- [109] O. Harush-Frenkel, E. Rozentur, S. Benita, Y. Altschuler, Surface charge of nanoparticles determines their endocytic and transcytotic pathway in polarized MDCK cells, *Biomacromolecules*, 9 (2008) 435-443.
- [110] J.S. Kim, T.J. Yoon, K.N. Yu, M.S. Noh, M. Woo, B.G. Kim, K.H. Lee, B.H. Sohn, S.B. Park, J.K. Lee, M.H. Cho, Cellular uptake of magnetic nanoparticle is mediated through energy-dependent endocytosis in A549 cells, *J Vet Sci*, 7 (2006) 321-326.
- [111] J. Saraste, G.E. Palade, M.G. Farquhar, Temperature-sensitive steps in the transport of secretory proteins through the Golgi complex in exocrine pancreatic cells, *Proc Natl Acad Sci U S A*, 83 (1986) 6425-6429.
- [112] M. Emanet, Ö. Şen, Z. Çobandede, M. Çulha, Interaction of carbohydrate modified boron nitride nanotubes with living cells, *Colloids and Surfaces B: Biointerfaces*, 134 (2015) 440-446.
- [113] M.A. Malvindi, V. De Matteis, A. Galeone, V. Brunetti, G.C. Anyfantis, A. Athanassiou, R. Cingolani, P.P. Pompa, Toxicity assessment of silica coated iron oxide nanoparticles and biocompatibility improvement by surface engineering, (2014).
- [114] V.B. Bregar, J. Lojk, V. Šuštar, P. Veranič, M. Pavlin, Visualization of internalization of functionalized cobalt ferrite nanoparticles and their intracellular fate, *International journal of nanomedicine*, 8 (2013) 919.
- [115] P.J.A. Borm, D. Robbins, S. Haubold, T. Kuhlbusch, H. Fissan, K. Donaldson, R. Schins, V. Stone, W. Kreyling, J. Lademann, The potential risks of nanomaterials: a review carried out for ECETOC, *Particle and fibre toxicology*, 3 (2006) 11.
- [116] V. Stone, H. Johnston, R.P.F. Schins, Development of in vitro systems for nanotoxicology: methodological considerations, *Critical reviews in toxicology*, 39 (2009) 613-626.

- [117] N. Singh, B. Manshian, G.J.S. Jenkins, S.M. Griffiths, P.M. Williams, T.G.G. Maffei, C.J. Wright, S.H. Doak, NanoGenotoxicology: the DNA damaging potential of engineered nanomaterials, *Biomaterials*, 30 (2009) 3891-3914.
- [118] S.C. Hong, J.H. Lee, J. Lee, H.Y. Kim, J.Y. Park, J. Cho, J. Lee, D.-W. Han, Subtle cytotoxicity and genotoxicity differences in superparamagnetic iron oxide nanoparticles coated with various functional groups, *International journal of nanomedicine*, 6 (2011) 3219.
- [119] R.A. El-Zein, M.B. Schabath, C.J. Etzel, M.S. Lopez, J.D. Franklin, M.R. Spitz, Cytokinesis-blocked micronucleus assay as a novel biomarker for lung cancer risk, *Cancer research*, 66 (2006) 6449-6456.
- [120] A.R. Collins, Measuring oxidative damage to DNA and its repair with the comet assay, *Biochimica et Biophysica Acta (BBA)-General Subjects*, 1840 (2014) 794-800.
- [121] H. Pelicano, D. Carney, P. Huang, ROS stress in cancer cells and therapeutic implications, *Drug resistance updates : reviews and commentaries in antimicrobial and anticancer chemotherapy*, 7 (2004) 97-110.
- [122] N. Singh, G.J.S. Jenkins, R. Asadi, S.H. Doak, Potential toxicity of superparamagnetic iron oxide nanoparticles (SPION), *Nano reviews*, 1 (2010).
- [123] J. Ahmad, M. Ahamed, M.J. Akhtar, S.A. Alrokayan, M.A. Siddiqui, J. Musarrat, A.A. Al-Khedhairi, Apoptosis induction by silica nanoparticles mediated through reactive oxygen species in human liver cell line HepG2, *Toxicology and applied pharmacology*, 259 (2012) 160-168.
- [124] V. Sharma, D. Anderson, A. Dhawan, Zinc oxide nanoparticles induce oxidative DNA damage and ROS-triggered mitochondria mediated apoptosis in human liver cells (HepG2), *Apoptosis*, 17 (2012) 852-870.
- [125] M.M. Mkandawire, M. Lakatos, A. Springer, A. Clemens, D. Appelhans, U. Krause-Buchholz, W. Pompe, G. Rödel, M. Mkandawire, Induction of apoptosis in human cancer cells by targeting mitochondria with gold nanoparticles, *Nanoscale*, (2015).
- [126] R.M. Mroz, R.P.F. Schins, H. Li, L.A. Jimenez, E.M. Drost, A. Holownia, W. MacNee, K. Donaldson, Nanoparticle-driven DNA damage mimics irradiation-related carcinogenesis pathways, *European Respiratory Journal*, 31 (2008) 241-251.

- [127] D.W. Nebert, D.W. Russell, Clinical importance of the cytochromes P450, *The Lancet*, 360 (2002) 1155-1162.
- [128] C.C. McIlwain, D.M. Townsend, K.D. Tew, Glutathione S-transferase polymorphisms: cancer incidence and therapy, *Oncogene*, 25 (2006) 1639-1648.
- [129] A.C.M. Ramalhinho, J.A. Fonseca-Moutinho, L.A.T.G. Breitenfeld Granadeiro, Positive association of polymorphisms in estrogen biosynthesis gene, CYP19A1, and metabolism, GST, in breast cancer susceptibility, *DNA and cell biology*, 31 (2012) 1100-1106.
- [130] Y.-H. Lien, T.-M. Wu, Preparation and characterization of thermosensitive polymers grafted onto silica-coated iron oxide nanoparticles, *Journal of colloid and interface science*, 326 (2008) 517-521.
- [131] B.L. Frey, R.M. Corn, Covalent attachment and derivatization of poly (L-lysine) monolayers on gold surfaces as characterized by polarization-modulation FT-IR spectroscopy, *Analytical Chemistry*, 68 (1996) 3187-3193.
- [132] E. Scharmach, S. Hessel, B. Niemann, A. Lampen, Glutathione S-transferase expression and isoenzyme composition during cell differentiation of Caco-2 cells, *Toxicology*, 265 (2009) 122-126.
- [133] T.C. Shea, S.L. Kelley, W.D. Henner, Identification of an anionic form of glutathione transferase present in many human tumors and human tumor cell lines, *Cancer Res*, 48 (1988) 527-533.
- [134] N. Traverso, R. Ricciarelli, M. Nitti, B. Marengo, A.L. Furfaro, M.A. Pronzato, U.M. Marinari, C. Domenicotti, Role of glutathione in cancer progression and chemoresistance, *Oxidative medicine and cellular longevity*, 2013 (2013).
- [135] R.S. Finn, Targeting Src in breast cancer, *Annals of oncology : official journal of the European Society for Medical Oncology / ESMO*, 19 (2008) 1379-1386.
- [136] J.M. Summy, G.E. Gallick, Treatment for advanced tumors: SRC reclaims center stage, *Clinical cancer research : an official journal of the American Association for Cancer Research*, 12 (2006) 1398-1401.
- [137] S.K. Mitra, D.D. Schlaepfer, Integrin-regulated FAK-Src signaling in normal and cancer cells, *Current opinion in cell biology*, 18 (2006) 516-523.

- [138] R. Salcedo, M.L. Ponce, H.A. Young, K. Wasserman, J.M. Ward, H.K. Kleinman, J.J. Oppenheim, W.J. Murphy, Human endothelial cells express CCR2 and respond to MCP-1: direct role of MCP-1 in angiogenesis and tumor progression, *Blood*, 96 (2000) 34-40.
- [139] T. Kitamura, B.-Z. Qian, D. Soong, L. Cassetta, R. Noy, G. Sugano, Y. Kato, J. Li, J.W. Pollard, CCL2-induced chemokine cascade promotes breast cancer metastasis by enhancing retention of metastasis-associated macrophages, *The Journal of experimental medicine*, 212 (2015) 1043-1059.
- [140] T. Ueno, M. Toi, H. Saji, M. Muta, H. Bando, K. Kuroi, M. Koike, H. Inadera, K. Matsushima, Significance of macrophage chemoattractant protein-1 in macrophage recruitment, angiogenesis, and survival in human breast cancer, *Clinical Cancer Research*, 6 (2000) 3282-3289.
- [141] Z. Madjd, E. Gheytanchi, E. Erfani, M. Asadi-Lari, Application of stem cells in targeted therapy of breast cancer: a systematic review, *Asian Pac J Cancer Prev*, 14 (2013) 2789-2800.
- [142] C. Ginestier, M.H. Hur, E. Charafe-Jauffret, F. Monville, J. Dutcher, M. Brown, J. Jacquemier, P. Viens, C.G. Kleer, S. Liu, A. Schott, D. Hayes, D. Birnbaum, M.S. Wicha, G. Dontu, ALDH1 is a marker of normal and malignant human mammary stem cells and a predictor of poor clinical outcome, *Cell Stem Cell*, 1 (2007) 555-567.
- [143] A. Jaggupilli, E. Elkord, Significance of CD44 and CD24 as cancer stem cell markers: an enduring ambiguity, *Clin Dev Immunol*, 2012 (2012) 708036.
- [144] B. Arun, U. Akar, A.M. Gutierrez-Barrera, G.N. Hortobagyi, B. Ozpolat, The PARP inhibitor AZD2281 (Olaparib) induces autophagy/mitophagy in BRCA1 and BRCA2 mutant breast cancer cells, *Int J Oncol*, 47 (2015) 262-268.
- [145] J. Bain, L. Plater, M. Elliott, N. Shpiro, C. Hastie, H. McLauchlan, I. Klevernic, J. Arthur, D. Alessi, P. Cohen, The selectivity of protein kinase inhibitors: a further update, *Biochem. J*, 408 (2007) 297-315.
- [146] C.E.J. Moore, H. Mikolajek, S.R. da Mota, X. Wang, J.W. Kenney, J.M. Werner, C.G. Proud, Elongation factor 2 kinase is regulated by proline hydroxylation and protects cells during hypoxia, *Molecular and cellular biology*, 35 (2015) 1788-1804.

[147] L.Y. Bourguignon, K. Peyrolier, W. Xia, E. Gilad, Hyaluronan-CD44 interaction activates stem cell marker Nanog, Stat-3-mediated MDR1 gene expression, and ankyrin-regulated multidrug efflux in breast and ovarian tumor cells, *J Biol Chem*, 283 (2008) 17635-17651.

[148] J.F. Liu, D.P. Silver, PARP Inhibitors: Science and Current Clinical Development, *Current opinion in oncology*, 22 (2010).

APPENDICES

A. DETECTION OF MYCOPLASMA

Mycoplasma is a form of bacteria that lacks a nucleus and a cell wall, and are thus unaffected by many antibiotics. The types of nanoparticle formulations generally tested for mycoplasma contamination include those that incorporate a component derived from a bacterial culture, animal or hybridoma. All cell lines underwent regular passages and were routinely checked for mycoplasma contamination.

Cells were grown in 60x15 mm culture dish, Then nanoparticles were added to the cell culture media, After 24 h incubation, Transfer 0.5-1.0ml cell culture supernatant into a 2ml centrifuge tube. To pellet cellular debris, centrifuge the sample at 250 x g briefly. Transfer the supernatant into a fresh sterile tube and centrifuge at 15,000-20,000 x g for 10 minutes to sediment mycoplasma. Carefully decant the supernatant and keep the pellet (the pellet will not always be visible). Re-suspend the pellet with 50µl of the Buffer Solution and mix thoroughly with a micropipet. Heat to 95°C for 3 minutes. The test sample can be stored at this stage at -20°C for later use.

Reagents Volume H₂O 35µl

Reaction Mix 10µl

Test sample 5µl

2. Overlay mineral oil (approximately 40µl) to avoid the evaporation of the reaction mixture.

3. Place all tubes in DNA thermal cycler. Set the parameters for the following conditions and perform PCR.

94°C 30 secs.

94°C 30 secs.

60°C 120 secs. 35 cycles

72°C 60 secs.

94°C 30 secs.

60°C 120 secs.

72°C 5 min.

C. Analysis of amplified products by gel electrophoresis:

1. Apply 20µl of the PCR product to the gel electrophoresis.

Do not add loading buffer to the samples. Use 2% agarose gel.

2. Perform agarose gel electrophoresis with the PCR amplified samples to verify the amplified product and its size.

The size of DNA fragments amplified using the specific primers in this kit is 270bp.

D. Control Template:

By the use of 1µl of Positive Template Control as a test sample, PCR efficiency can be checked. The size of the PCR product obtained using the positive template with primer pairs is 270bp.

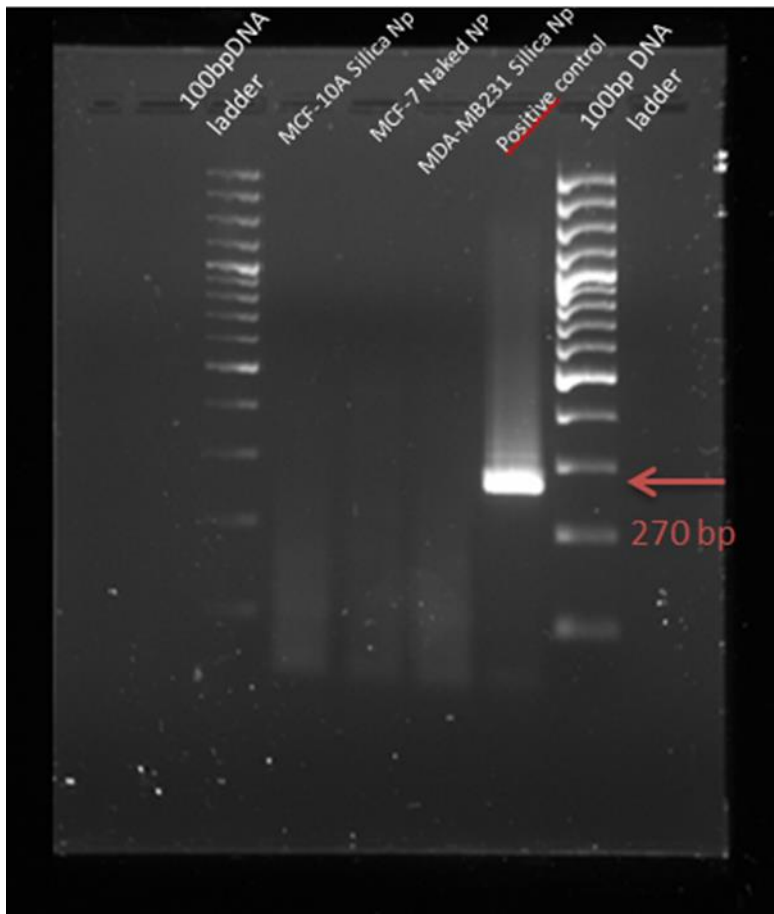


Figure 70. Detection of mycoplasma contaminations in MCF-10A, MCF-7 MDA-231 cells treated with NPs

APPENDICES

B. PRIMER SEQUENCES

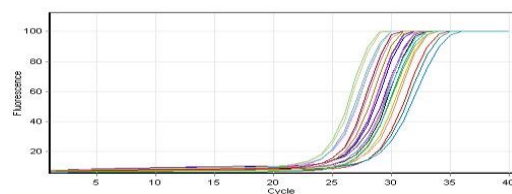
Primer sequences for BCL-2, BAX, PUMA, SURVIVIN, CYP1A1, CYP1B1, GSTM3, GSTZ1 and β -ACTIN genes.

Primer	Sequence 5' to 3'
BCL-2 Forward	GGATTGTGGCCTTCTTTGAG
BCL-2 Reverse	TCTTCAGAGACAGCCAGGAGA
BAX Forward	TCTGACGGCAACTTCAACTG
BAX Reverse	TTGAGGAGTCTCACCCAACC
PUMA Forward	GACCTCAACGCACAGTA
PUMA Reverse	CTAATTGGGCTCCATCT
SURVIVIN Forward	AGCCAGATGACGACCCCATAGAGG
SURVIVIN Reverse	AAAGGAAAGCGCAACCGGACGA
CYP1A1 Forward	TAGACACTGATCTGGCTGC
CYP1A1 Reverse	GGGAAGGCCCATCAGCATC
CYP1B1 Forward	AACGTCATGAGTGCCGTGTGT
CYP 1B1 Reverse	GGCCGGTACGTTCTCCAAATC
GSTM3 Forward	AGGGGTCAGCGCTCTTGCTT
GSTM3 Reverse	GGGAAATGCCACAGTATCGCAGC
GSTZ1 Forward	GCATCGACTACAAGACGGTGCCC
GSTZ1 Reverse	GAAGTCGCGGAGTGGGACGC
b-ACTIN Forward	CAGAGCAAGAGAGGCATCCT
b-ACTIN Reverse	TTGAAGGTCTCAAACATGA

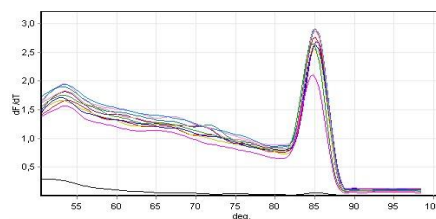
APPENDICES

C. AMPLIFICATION CURVES, MELT CURVES, STANDARD CURVES

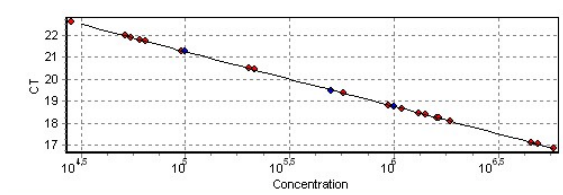
BCL-2



Amplification curve; the accumulation of fluorescence emission at each reaction cycle.

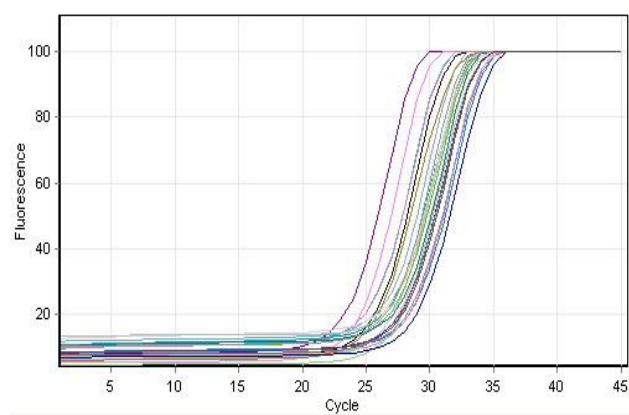


Melting curve; the fluorescence emission change vs. temperature.
Single peak means single PCR product.

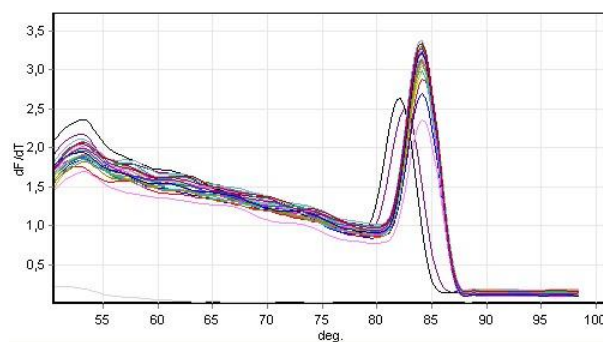


Standard curve generated from serial dilutions of chosen cDNA to calculate quantities of *BCL-2* mRNAs

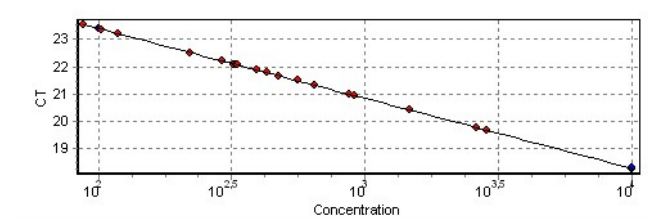
BAX



Amplification curve; the accumulation of fluorescence emission at each reaction cycle.

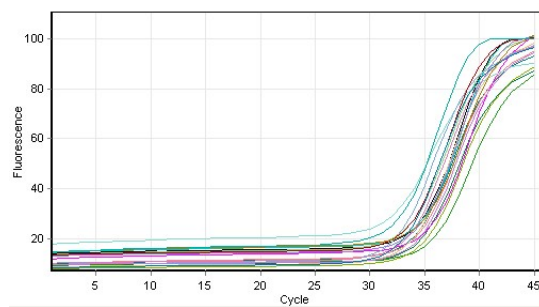


Melting curve; the fluorescence emission change versus temperature. Single peak means single PCR product.

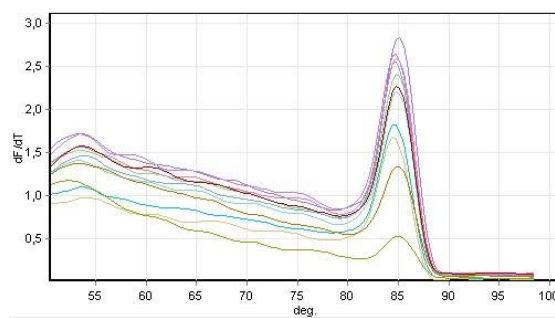


Standard curve generated from serial dilutions of chosen cDNA to calculate quantities of *BAX* mRNAs

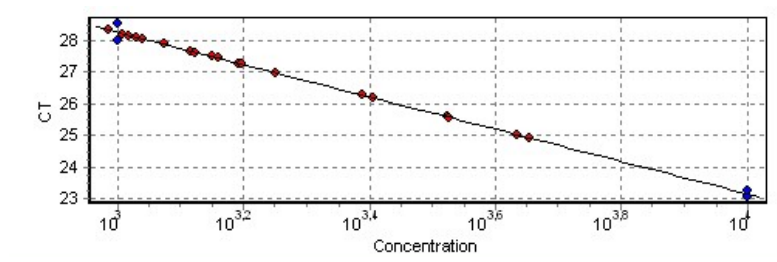
PUMA



Amplification curve; the accumulation of fluorescence emission at each reaction cycle.

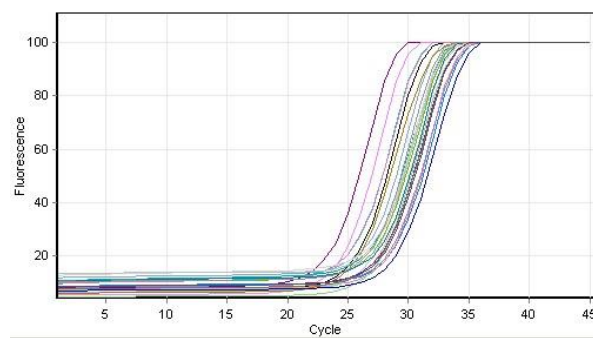


Melting curve; the fluorescence emission change versus temperature. Single peak means single PCR product.

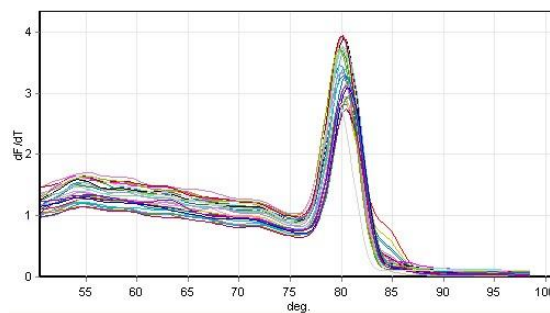


Standard curve generated from serial dilutions of chosen cDNA to calculate quantities of *PUMA* mRNAs

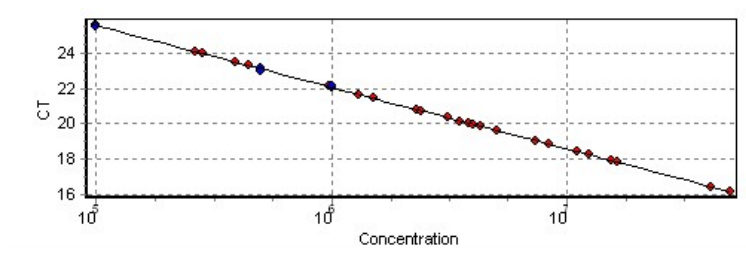
SURVIVIN



Amplification curve; the accumulation of fluorescence emission at each reaction cycle.

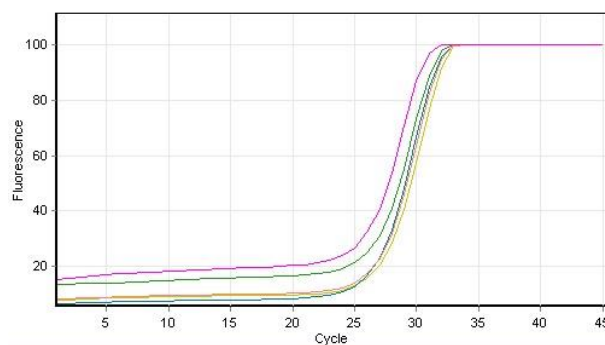


Melting curve; the fluorescence emission change vs. temperature. Single peak means single PCR product.

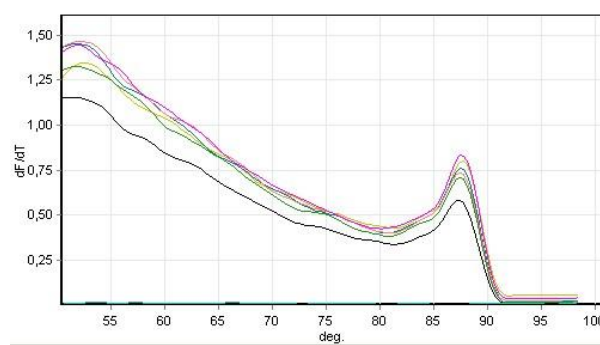


Standard curve generated from serial dilutions of chosen cDNA to calculate quantities of *SURVIVIN* mRNAs

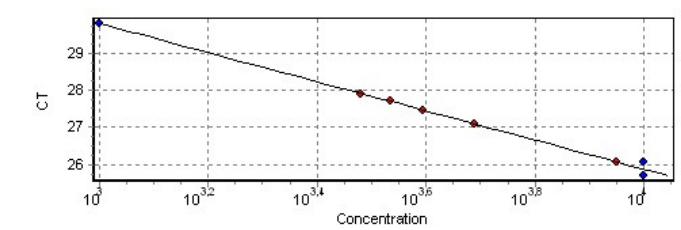
CYP1A1



Amplification curve; the accumulation of fluorescence emission at each reaction cycle.

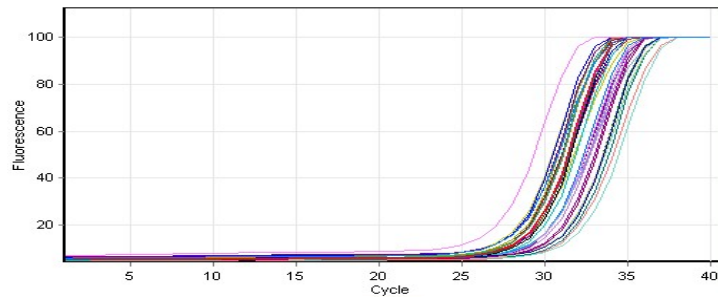


Melting curve; the fluorescence emission change versus temperature. Single peak means single PCR product.

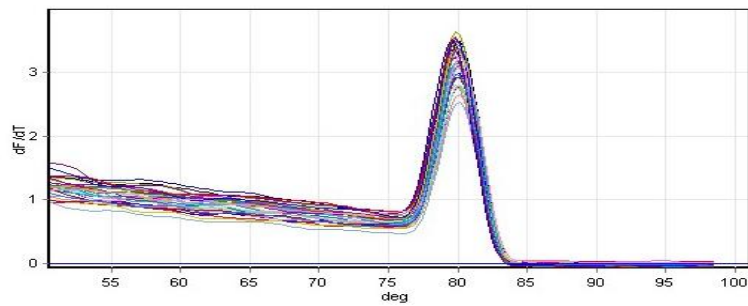


Standard curve generated from serial dilutions of chosen cDNA to calculate quantities of *CYP1A1* mRNAs

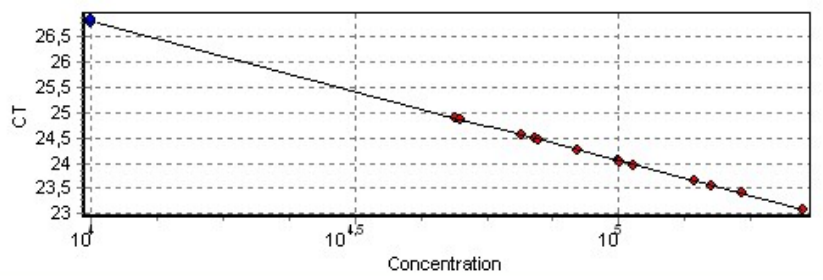
CYP1B1



Amplification curve; the accumulation of fluorescence emission at each reaction cycle.

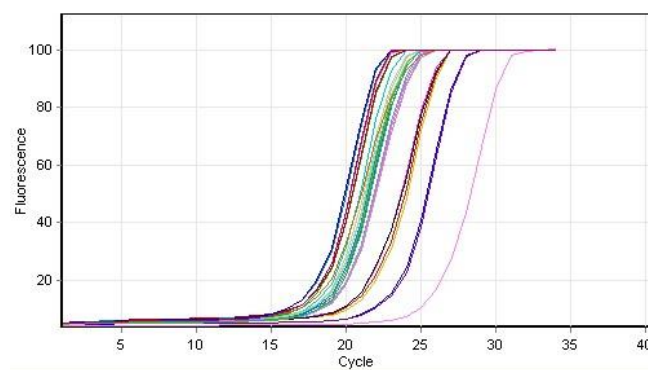


Melting curve; the fluorescence emission change versus temperature. Single peak means single PCR product.

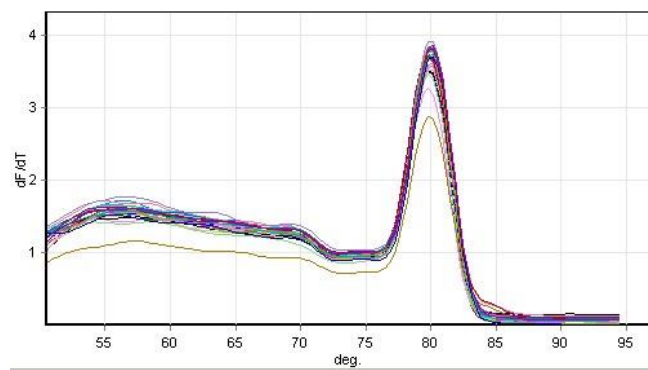


Standard curve generated from serial dilutions of chosen cDNA to calculate quantities of *CYP1B1* mRNAs

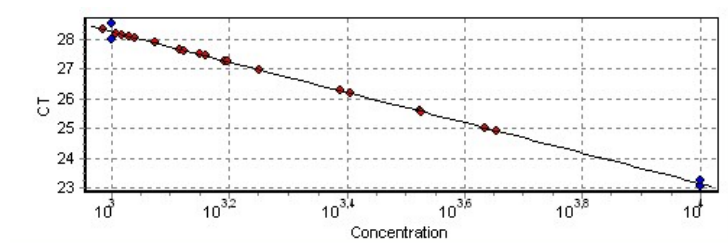
GSTM3



Amplification curve; the accumulation of fluorescence emission at each reaction cycle.

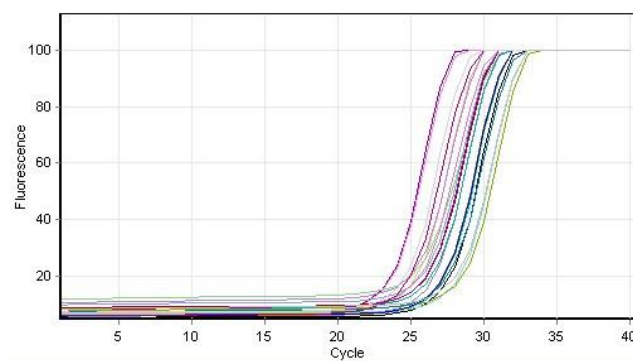


Melting curve; the fluorescence emission change versus temperature. Single peak means single PCR product.

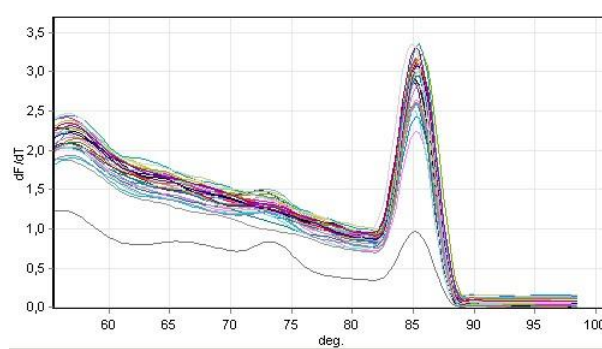


Standard curve generated from serial dilutions of chosen cDNA to calculate quantities of *GSTM3* mRNAs

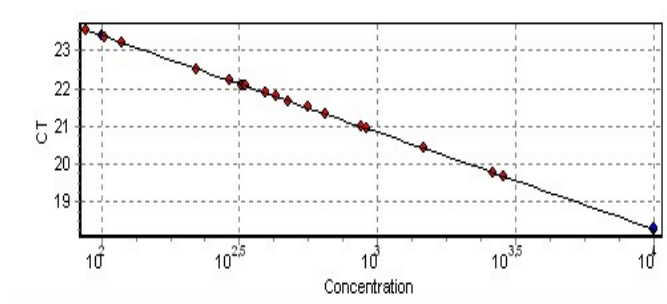
GSTZ1



Amplification curve; the accumulation of fluorescence emission at each reaction cycle.

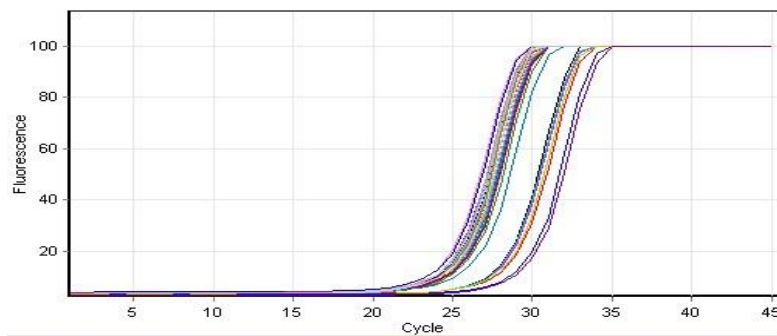


Melting curve; the fluorescence emission change versus temperature. Single peak means single PCR product.

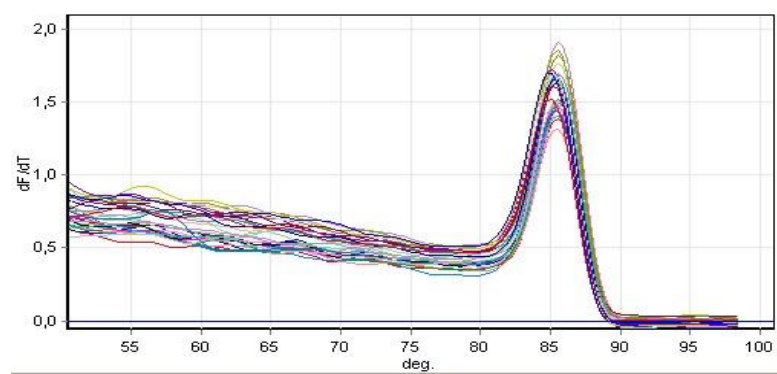


Standard curve generated from serial dilutions of chosen cDNA to calculate quantities of *GSTZ1* mRNAs

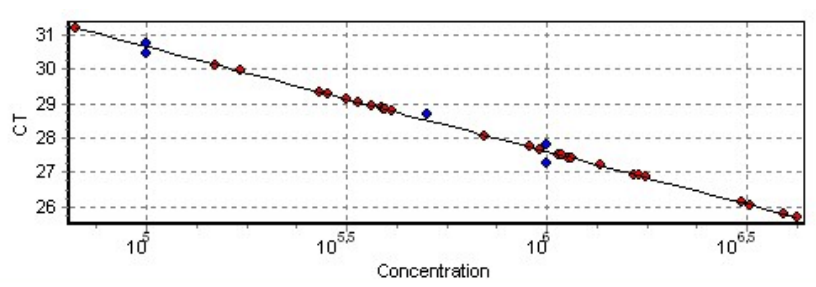
β -Actin



Amplification curve; the accumulation of fluorescence emission at each reaction cycle.



Melting curve; the fluorescence emission change versus temperature. Single peak means single PCR product.



Standard curve generated from serial dilutions of chosen cDNA to calculate quantities of β -ACTIN mRNAs

VITA

ELİF AŞIK

Paşakent Mah. 1059 sok. Gökkuşığı sit
No 10/9 Bandırma/Balıkesir TURKEY

Personal phone: 0553 109 8290

sensoy.elif@gmail.com

PERSONAL DETAILS

- Date of Birth: 07/12/1984
- Sex: Female
- Nationality: Turkish
- Marital Status: Single

EDUCATION

September 2007 – November 2015: B.Sc. on Ph.D. Degree. Graduate program in **Biotechnology**, Graduate School Natural and Applied Sciences, Middle East Technical University, Ankara, TURKEY

(Graduation CGPA: 3.32/4.0)

Thesis title; Applications of the multifunctional magnetic nanoparticles for development of molecular therapies for breast cancer

Supervisor: Prof.Dr.Tülin Güray

Co-supervisor: Prof.Dr. Mürvet Volkan

July 2014 – July 2015: PhD Fellowship in Department of Experimental Therapeutics, The University of Texas, MD Anderson Cancer Center, Houston, Texas, USA

2002- 2007: B.Sc. degree in Biology, Turkey

(Graduation CGPA: 3.30/4.0)

INTERSHIP

- İstanbul University-Institute of Experimental Medicine-Department of Immunology
- Hacettepe University-Department of Biochemistry

HONOR/AWARDS

- International Doctoral Research Fellowship from The Scientific and Technological Research Council of Turkey Research Project Fund (TUBITAK)
- 2012 EUROTOX Travel grants

WORK EXPERIENCES

- 2013-2014 2-deoxy-D-glucose (2-DG) Labeled Cobalt Ferrite (CoFe₂O₄) Magnetic Nanoparticles for Cancer targeting and therapy The Scientific and Technological Research Council of Turkey (TUBITAK) Project Assistant
- 2010-2014 Investigation toxic effects of Cobalt Ferrite and Iron Oxide nanoparticles in breast cancer cell lines-METU BAP-07-02-2011-004. Project Assistant
- 2010-2014, Research Project, “Assessing the human health risks from exposure of arsenic in drinking water through molecular epidemiological approaches” The Scientific and Technological Research Council of Turkey (TUBITAK). Project Assistant

ATTENDANCE AT CONFERENCES AND WORKSHOPS

- 9-10 September 2014 Illuminating Genomic Dark Matter "ncRNA in Disease and Cancer, MD Anderson Cancer Center, Houston, Texas
- 12-14 September 2011 Advanced Molecular Cell Biology Practical Training Course- TUBITAK-GEBİ

- 21-22 September 2011 Basic Cell Culture Training Course- Ege University-Department of Bioengineering
- 20 November 2009 nanopharmaceutical; Developments and applications, Gazi University, Faculty of Pharmacy
- 06-07 May 2006 Advanced Light Microscopy Certification, Ankara University, Department of Biotechnology
- 10-11 May 2006 Genomics Certification, Ankara University , Department of Biotechnology

PUBLICATIONS (Papers prepared & to be submitted soon)

Asik E, Aslan TN, Güray T, Volkan M. “2-amino-2-deoxy-glucose conjugated cobalt ferrite magnetic nanoparticle (2DG-MNP) as a targeting agent for breast cancer cells.” Environmental toxicology and pharmacology (Accepted)

Aslan TN, **Asik E**, Güray TN, Volkan M. Preparation and evaluation of cytotoxic effect of deoxyglucose labeled and gold loaded apoferritin protein cages in breast cancer cell lines.

Asik E, Akpınar Y, Volkan M, Güray T, Iscan M, Demircigil G. Cobalt Ferrite Magnetic Nanoparticles Assessed by Uptake, Cytotoxicity and Genotoxicity

Aslan TN, **Asik E**, Volkan M, “Preparation and radiolabeling of surface-modified magnetoferritin protein cages with rhenium (I) carbonyl complex for magnetic targeted radiotherapy”. (RSC Advances, accepted)

Asik E, Güray T, Volkan M, Ozpolat B. Silencing of Eukaryotic Elongation Factor 2 Kinase inhibits BRCA1 + mutated Breast Cancer invasion and tumorigenesis.

Aslan TN, **Asik E**, Güray TN, Volkan M. Cytotoxic effect of rhenium labeled magnetic protein cages in breast cancer cell lines.

ACADEMIC POSTER PRESENTATIONS

- Ela Kadioglu, N. Deniz Hisarli, **Elif Asik**, Gonca Cakmak Demircigil, Usama Alshana, Nusret Ertas, Celalettin R. Celebi, Esref Atabey, O. Yavuz Ataman, Hakan Serce, Nazmi Bilir, A. Murat Tuncer, Sema Burgaz Arsenic (+3) Methyltransferase, and Glutathione S-Transferase Omega Genetic Variants Associated with Arsenic Susceptibility: Influences on As metabolism and skin lesions SOT Annual Meeting San Diego California 2015
- S. Burgaz, N. Ertař, U. Alshana, B. Altun, N. D. Hisarlı, **E. Ařık**, G. Ç. Demircigil, E. Kadiođlu, C. R. Çelebi, E. Atabey, O. Y. Ataman, H. Serçe, N. Bilir, A. M. Tuncer. Arsenic levels of residents of Nevřehir province, Turkey. The 5 International Congress on Arsenic in the Environment (As2014) (Buenos Aires, Argentina: 11-16 May 2014).
- N. Ertař, U. Alshana, B. Altun, N. D. Hisarlı, **E. Ařık**, G. Ç. Demircigil, E. Kadiođlu, C. R. Çelebi, E. Atabey, O. Y. Ataman, H. Serçe, N. Bilir, A. M. Tuncer, S. Burgaz. Total arsenic determination in hair and urine samples from residents of Nevřehir Province, Turkey. Speciation studies in urine samples. IMA 2013-Instrumental Methods of Analysis-Modern Trends and Applications (Thessaloniki, Greece: 15-19 September 2013)
- B. Altun, N. Ertař, U. Alshana, N. D. Hisarlı, **E. Ařık**, G. Ç. Demircigil, E. Kadiođlu, C. R. Çelebi, E. Atabey, O. Y. Ataman, H. Serçe, N. Bilir, A. M. Tuncer, S. Burgaz. Hair arsenic concentrations of residents living in Nevřehir province, Turkey. EUROTOX 2013 (Interlaken, Switzerland: 01-04 September 2013).
- Ela Kadiođlu.N.Deniz Hisarli , **Elif Ařık**, Gonca cakmak demircigil, Usama Alshana, Nusret Ertas, Celalettin R.Celebi, Esref Atabey, Yavuz Ataman, Hakan Serce, Nazmi Bilir, Murat Tuncer, Sema Burgaz-AS3MT gene polymorphism in residents exposed to inorganic arsenic

via drinking water. Abstracts of the 48th Eurotox, Stockholm Sweden,17th-20th 2012, Toxicology Letters, Vol.211S,P11-44,

- Gonca Cakmak Demircigil, **Elif Asik**, Murat Kaya, Tuba Nur Alp,Murvet Volkan,Mesude Iscan .Genotoxicity of cobalt ferrite nanoparticlea on MDA-231 cells using Comet Assay Abstracts of 48th Eurotox ,Stockholm Sweden,17th-20th June 2012 ,Toxicology Letters, Vol.211S,P33-28,
- **Elif Asik**, Murat Kaya, Tuba Nur Alp,Murvet Volkan,Mesude Iscan- Cytotoxicity of cobalt ferrite nanoparticles on breast cancer cell lines Abstracts of 48th Eurotox , Stockholm Sweden,17th-20th June 2012,Toxicology Letters, Vol.211S,P33-29,
- Usama Alshana, Nusret Ertas, Kadioğlu, Gonca cakmak demircigil **Elif Aşık**, N.Deniz Hisarlı, Celalettin R.Celebi, Esref Atabey, Yavuz Ataman, Hakan Serce, Nazmi Bilir, Murat Tuncer, Sema Burgaz Urinary Arsenic Speciation of in Residents of Nevşehir Area,Turkey,by High Performance Liquid Chromatography Coupled to Hydride-Generation Atomic Fluorescence Spectrometry 8th Aegean Analytical Chemistry Days Op25,35 16-20 September 2012,İzmir Turkey

LANGUAGES

- Native: Turkish
- Advanced: English

IT SKILLS

- Photoshop,
- Adobe Illustrator
- Graph pad